4-10

SANDIA REPORT

SAND96–0810 • UC–706
Unlimited Release
Printed April 1996

RECEIVED
APR 18 1996
OSTI

Development of Structural Health Monitoring Techniques Using Dynamics Testing

George H. James III

Prepared by
Sandia National Laboratories
Albuquerque, New Mexico 87185 and Livermore, California 94550
for the United States Department of Energy
under Contract DE-AC04-94AL85000

Approved for public release; distribution is unlimited.

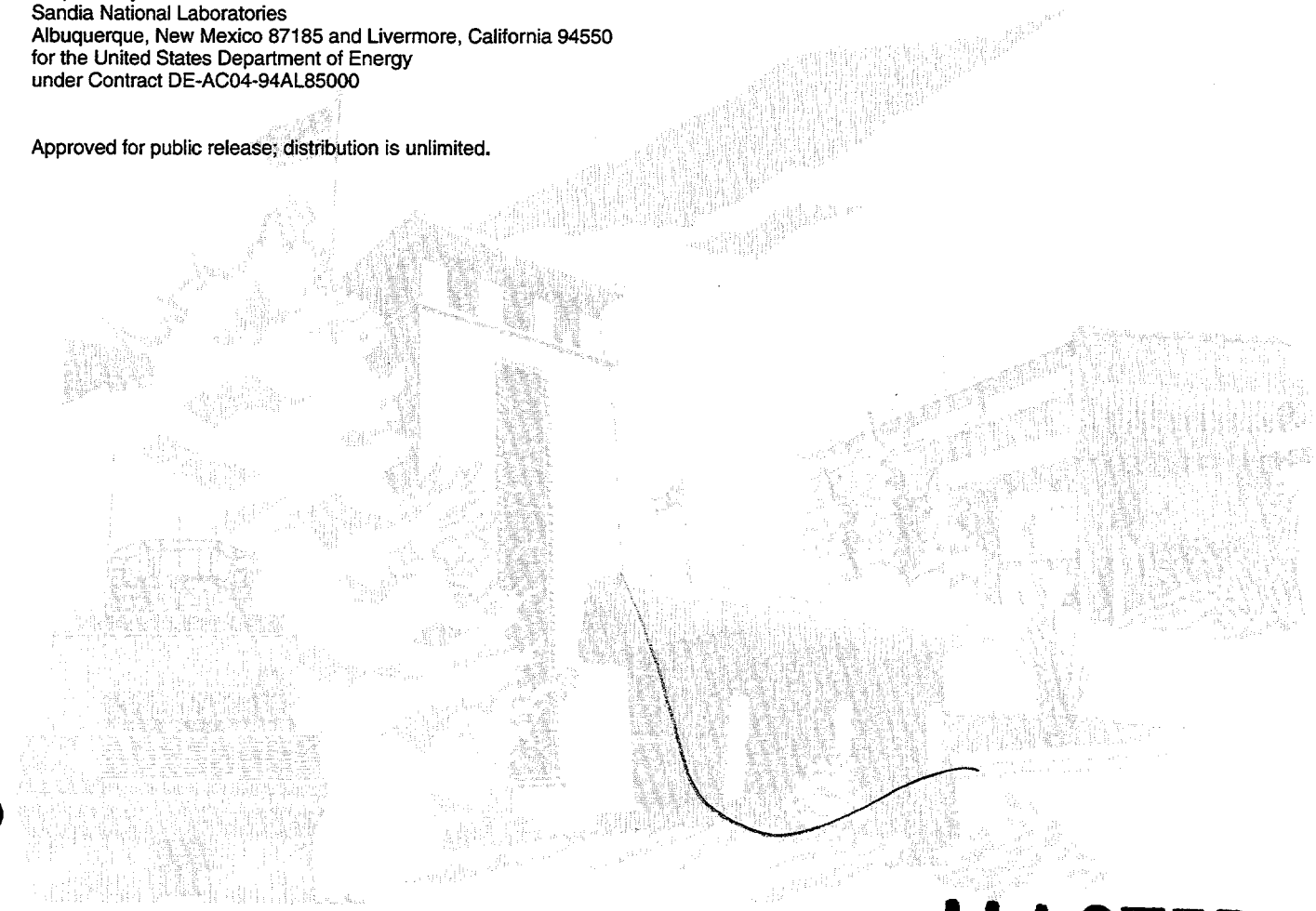

SF2900Q(8-81)

DISTRIBUTION OF THIS DOCUMENT IS UNLIMITED

MASTER

Issued by Sandia National Laboratories, operated for the United States Department of Energy by Sandia Corporation.

NOTICE: This report was prepared as an account of work sponsored by an agency of the United States Government. Neither the United States Government nor any agency thereof, nor any of their employees, nor any of their contractors, subcontractors, or their employees, makes any warranty, express or implied, or assumes any legal liability or responsibility for the accuracy, completeness, or usefulness of any information, apparatus, product, or process disclosed, or represents that its use would not infringe privately owned rights. Reference herein to any specific commercial product, process, or service by trade name, trademark, manufacturer, or otherwise, does not necessarily constitute or imply its endorsement, recommendation, or favoring by the United States Government, any agency thereof or any of their contractors or subcontractors. The views and opinions expressed herein do not necessarily state or reflect those of the United States Government, any agency thereof or any of their contractors.

Printed in the United States of America. This report has been reproduced directly from the best available copy.

Available to DOE and DOE contractors from
Office of Scientific and Technical Information
PO Box 62
Oak Ridge, TN 37831

Prices available from (615) 576-8401, FTS 626-8401

Available to the public from
National Technical Information Service
US Department of Commerce
5285 Port Royal Rd
Springfield, VA 22161

NTIS price codes
Printed copy: A14
Microfiche copy: A01

DISCLAIMER

Portions of this document may be illegible in electronic image products. Images are produced from the best available original document.

SAND96-0810
Unlimited Release
Printed March 1996

Distribution
Category UC-706

DEVELOPMENT OF STRUCTURAL HEALTH MONITORING TECHNIQUES USING DYNAMICS TESTING

George H. James III
Experimental Structural Dynamics Department
Sandia National Laboratories
Albuquerque, NM 87185-0557

ABSTRACT

Today's society depends upon many structures (such as aircraft, bridges, wind turbines, offshore platforms, buildings, and nuclear weapons) which are nearing the end of their design lifetime. Since these structures cannot be economically replaced, techniques for structural health monitoring must be developed and implemented. Modal and structural dynamics measurements hold promise for the global non-destructive inspection of a variety of structures since surface measurements of a vibrating structure can provide information about the health of the internal members without costly (or impossible) dismantling of the structure. In order to develop structural health monitoring for application to operational structures, developments in four areas have been undertaken within this project: operational evaluation, diagnostic measurements, information condensation, and damage identification. The developments in each of these four aspects of structural health monitoring have been exercised on a broad range of experimental data. This experimental data has been extracted from structures from several application areas which include aging aircraft, wind energy, aging bridges, offshore structures, structural supports, and mechanical parts. As a result of these advances, Sandia National Laboratories is in a position to perform further advanced development, operational implementation, and technical consulting for a broad class of the nation's aging infrastructure problems.

ACKNOWLEDGMENTS

There are four groups which made this project successful.

The **principal investigators and project engineers** formed a distributed leadership team for this project: Ken Alvin, Tom Ashwill, Tom Baca, Al Beattie, Tom Carne, John Gieske, Jim Goodding, Dan Gregory, Bruce Hansche, David Martinez, Randy Mayes, Tom Paez, K.C. Park, Lee Peterson, Garth Reese, Tom Rice, Dennis Roach, Ron Rodeman, Bill Shurtleff, and Paul Veers

The **university students** performed much of the ground-breaking work and were critical to the success of many aspects of this project: Scott Doebling, Todd Simmermacher, Chris Doktor, Nikki Robinson, Raul Meza, and Elizabeth Smith

The **internal and external collaborators** provided much perspective, professional interaction, and joint developments: David Zimmerman (University of Houston); Bob West (Virginia Tech); Roberto Osegueda and Carlos Ferregut (University of Texas at El Paso); David Allen and Norris Stubbs (Texas A&M University); Ken White and colleagues (New Mexico State University); Ward Turner and Brad Campbell (Exxon); Kris Digre and Denby Morrison (Shell); Dan Doling (PMB Engineering); John Webster and colleagues (Holographics, Inc.); Ben Bell and Rory Davis (FloWind, Inc.); Chuck Farrar, Norm Hunter, David Jauregui, Mike Prime, Dan Shevitz, and Scott Doebling (Los Alamos National Laboratory); Jack Allread and Walt Musial (National Renewable Energy Laboratory); David Andaleon, Lupe Arguello, Diane Hurtado, Scott Klenke, David Lo, John Red-Horse, and Dan Segalman (Sandia National Laboratories)

The **support personnel** were instrumental in maintaining the infrastructure which allowed this complicated project to proceed: John Ball, Barry Bronkema, Lucille Chacon, Ron Coleman, Larry Dorrell, Gene Koenig, Ken Harmon, Peggy Malone, Craig Shierling, and Seyfred Toledo

This work was supported by the United States Department of Energy under Contract DE-AC04-94AL85000.

CONTENTS

CONTENTS
(cont.)

CONTENTS
(cont.)

ACRONYMS

AANC	Airworthiness Assurance and NDI Validation Center
AASHTO	American Association for State Highway and Transportation Officials
ACTI	Advanced Computational Technology Initiative
AFOSR	Air Force Office of Scientific Research
AIAA	American Institute of Aeronautics and Astronautics
ARPA	Advanced Research Projects Administration
ASCE	American Society of Civil Engineers
ASME	American Society of Mechanical Engineers
ATR	Alliance for Transportation Research
B737	A passenger transport aircraft manufactured by Boeing
CU	University of Colorado at Boulder
DC9	A passenger transport aircraft manufactured by McDonnell Douglas
DOF	Degrees-Of-Freedom
ERA	Eigensystem Realization Algorithm
ESPI	Electronic Speckle Pattern Interferometry
FAA	Federal Aviation Administration
FAST	Future Aerospace Science and Technology center
FEM	Finite Element Model
FRF	Frequency Response Function
HAWT	Horizontal Axis Wind Turbine
I40	Interstate Highway 40
ID	IDentification
IMAC	International Modal Analysis Conference
LANL	Los Alamos National Laboratory
LDRD	Laboratory Directed Research and Development project
LDV	Laser Doppler Vibrometer
LSI	A user interface for LDV testing
MAC	Modal Assurance Criteria
MAXCON	MAtriX COmpletioN
MMS	Minerals Management Service
MRPT	Minimum Rank Pertubation Theory
MURI	Multidisiplinary Research Program of the University Research Initiative
NASA	National Aeronautics and Space Administration
NDE	NonDestructive Evaluation
NDI	NonDestructive Inspection
NExT	Natural Excitation Technique
NREL	National Renewable Energy Laboratory
OSSP	Outstanding Student Summer Program
OTC	Offshore Technology Conference
PVP	Pressure Vessels and Piping Conference
QNDE	Quanatitative Non Destructive Evaluation Conference

ACRONYMS
(cont.)

SBIR	Small Buisness Innovation and Research project
SDM	Structures, Structural Dynamics, and Materials Conference
SEM	Society of Experimental Mechanics
SNL	Sandia National Laboratories
SPIE	The International Society for Optical Engineering
STIFTEST	A damage identification algorithm
STRECH	Structural Translation and Rotation Error Checking
SVD	Singular Value Decomposition
TAMU	Texas A&M University
UH	University of Houston
UNM	University of New Mexico
USAF	United States Air Force
UTEP	University of Texas at El Paso
VAWT	Vertical Axis Wind Turbine
VPI	Virginia Tech
ZETA	Zonic Engineering Test Analysis software

DEVELOPMENT OF STRUCTURAL HEALTH MONITORING TECHNIQUES USING DYNAMICS TESTING

EXECUTIVE SUMMARY

Introduction

Today's society depends upon many structures (such as aircraft, bridges, wind turbines, offshore platforms, buildings, and nuclear weapons) which are nearing the end of their design lifetime. Since these structures cannot be economically replaced, techniques for structural health monitoring must be developed and implemented. Modal and structural dynamics measurements hold promise for the global non-destructive inspection of a variety of structures since surface measurements of a vibrating structure can provide information about the health of the internal members without costly (or impossible) dismantling of the structure. In order to develop structural health monitoring for application to operational structures, developments in four areas have been undertaken within this project: operational evaluation, diagnostic measurements, information condensation, and damage identification. The developments in each of these four aspects of structural health monitoring have been exercised on a broad range of experimental data. This experimental data has been extracted from structures from several application areas which include aging aircraft, wind energy, aging bridges, offshore structures, structural supports, and mechanical parts.

The project directly supported the efforts of over 25 individuals working on over 20 sub-projects and interacting with over 30 additional internal and external collaborators. As a result of these advances and interactions, Sandia National Laboratories is in a position to perform further advanced development, operational implementation, and technical consulting for a broad class of the nation's aging infrastructure problems.

Summary of Operational Evaluation Advances

As a result of the access to a generalized base of technologies and applications, Sandia National Laboratories has approached the problem of structural health monitoring from a unique perspective. This LDRD project has produced a broader understanding of the structural health monitoring problem and its application to operational structures. One of the most important advances to result from this aspect of the study was the development of a process (engineered flaw specimen, damage accumulation testing, operational implementation) to perform operational evaluation of a structure's health or damage state. Each aspect of this process was exercised for a variety of structures. The experience is invaluable.

Engineered Flaw Specimens
The simulated aircraft panel tests proved the worth of a non-contact sensor to avoid mass-loading of the structure. Also, the need to control boundary conditions, and torque levels were seen. Also, the utility of standard test object with interchangeable parts to simulate damage produced an effective means of performing such tests. The simulated guy anchor showed the worth of a carefully controlled experiment to study specific damage scenarios. This allows the proper understanding and possible modeling to be developed for the final operational structure of interest. The damaged composite plates provided a well-planned series of tests to study several dissimilar damage scenarios.

Damage Accumulation Testing
The wind turbine quasi-static fatigue test showed that damage accumulation tests must be carefully controlled and monitored. Discrepancies due to fixture and test condition alterations must be recorded and/or minimized. However, this test showed that unexpected changes in the structures may occur which would not be present in a simpler engineered flaw specimen test. The wind turbine blade root fatigue test continued development of the damage accumulation testing concept. This test produced a new type of fatigue test, the resonance fatigue test, which allowed more rapid testing and less specialized equipment. However, the right excitation source is must (typically this means longer strokes than traditional electro-dynamic shakers provide). The wind turbine blade fatigue test again showed the usefulness of non-contact sensing and the proper excitation source. Much experience in the design of load transfer devices was gained from this test.

Operational Implementation
The Rio Grande/I40 bridge test provided a wealth of insight into the implementation of structural health monitoring techniques in large civil structures. The usefulness of ambient vibration testing was seen. The DC9 stringer tests provided important experience in complex geometry testing with a non-contact transducer. Experience in dealing with noisy data and environmental changes was realized.

Summary of Diagnostic Measurements Advances

Large-Area Measurements
Techniques for applying large-scale non-contacting measurement systems in the field have been developed and exercised. This technology produces high spatial density and high modal density data sets with localized information. The series of activities devoted to developing large-area measurements (Simulated Aircraft Panel Test, First DC9 Stringer Test, Composite Patch Tests, Aluminum Beam Development Test, Second DC9 Stringer Test, and Damaged Composite Plate Tests) produced a system which can be used effectively for large-area non-contacting measurements. The noteworthy developments include the following:

1. For large structures broad-band excitation is most effective below 2000 Hz;
2. Actively cooling the laser head appears to aid in reducing noise issues;
3. A covering of dye penetrant is useful in acquiring clean data;

4. A test with up to a few thousand data points can be performed with the system;
5. New resection procedures allow better spatial calibration of the laser head;
6. A driving point accelerometer should be used and is important in the subsequent analysis;
7. The laser system seems to produce more random errors with free-free structures; and
8. The coherence function can be acquired and integrated to produce a scalar metric for checking the fidelity of the data.

Sensor Fusion

The series of activities devoted to developing sensor fusion techniques (First DC9 stringer test, damaged air compressor tests, wind turbine blade root fatigue test, and wind turbine blade fatigue Test) attempted to combine traditional or large-area diagnostic measurements with laser holography, ultrasonic inspection, and acoustic emissions testing. No conclusive results were obtained from these attempts. However, important experience and directions for future work were obtained. A natural link between laser holography and scanning laser vibrometer measurements can be envisioned. This work spawned a follow-on LDRD proposal to develop such a combined system. The fatigue test environment appears to hold promise for developing structural dynamics/ultrasonics sensor fusion concepts. However, this activity was not possible on this project due to premature failure of the test specimen. The fatigue environment also appears to hold promise for developing structural dynamics/acoustic emissions sensor fusion concepts. However, a composite test article does not appear to be amenable to acoustic emissions testing. A homogeneous structure would be a better development structure.

Summary of Information Condensation Advances

A set of tools for condensing the information into sensitive and robust mathematical constructions based on static flexibility shapes and experimental matrices (such as flexibility, stiffness, and mass) have been developed. Seven major advances resulted from the information condensation aspects of this work:

1. The estimation of rotational DOF can provide enhanced sensitivity in some cases;
2. The collection of mode shapes into static flexibility shapes increases robustness and sensitivity of some damage identification schemes;
3. Estimating static flexibility information from structural dynamics data provides a much more effective means of obtaining static information;
4. Flexibility matrices are dominated by low frequency information which is typically easier to measure;
5. Driving point flexibilities can be used as an enhanced visual tool;
6. Experimental structural dynamics matrices can replace reduced FEM models to maintain localized information; and
7. An approach to producing experimental matrices is to scale the null space of the measured modes to drive the resulting matrices toward an assumed connectivity.

Summary of Damage Identification Advances

The damage identification advances performed on the Structural Health Monitoring LDRD centered around the development of procedures which effectively utilize advances in the other areas, specifically diagnostic measurements and information condensation. STRECH has been expanded to operate on static flexibility shapes. This not only created a localization tool but also a scalar damage detection tool. Work on a characteristic shape analysis did not prove successful on the data set it was applied to. However, this effort fueled later work on a non-LDRD project developed a successful neural network based damage identification procedure which also used static flexibility. Novel procedures to perform disassembly have proven to be successful on small experimental data sets. More advanced disassembly algorithms are currently under study with larger data sets. The MRPT approach has been enhanced using experimentally-derived structural matrices and disassembly and has proven extremely successful in the limited application to two data sets. A model-based dynamic force residual method and novel mode projection algorithm were also developed.

Recommendations

Several recommendations for follow-on efforts are suggested by this work:

1. The resonant fatigue test concept is a novel method for damage accumulation testing and should be further developed and operationally implemented at Sandia;
2. Since most operational implementations will be in-situ, continued work on the use of ambient response analysis should be undertaken;
3. Embedded, miniature, cost-effective, and self-contained sensor packages should be developed and made available commercially for external and internal markets;
4. A more robust scanning laser vibrometer package which can extract three dimensional information, perform sensor fusion with laser holography and laser ranging, and measure higher frequency information (especially for composite materials) should be developed;
5. Techniques for information condensation which are hybrid experimental/analytical should be developed which retain localized information of experimental data without the numerical rank limitations should be developed;
6. To complete the structural health monitoring technology base, work on the fourth stage of lifetime prediction should be initiated, which will require developing a link between the damage identification procedures and damage mechanics modeling; and
7. A National Aging Infrastructure Center which would include the AANC, the Structural Health Monitoring tools developed on this project, and other structural health diagnostic techniques, should be established at Sandia. This center would attack a broad range of aging infrastructure issues to provide "exceptional service in the national interest".

INTRODUCTION

Today's society depends upon many structures (such as aircraft, bridges, wind turbines, offshore platforms, buildings, and nuclear weapons) which are nearing the end of their design lifetime. Since these structures cannot be economically replaced, techniques for **structural health monitoring** must be developed and implemented. **Modal and structural dynamics measurements** hold promise for the global non-destructive inspection of a variety of structures since surface measurements of a vibrating structure can provide information about the health of the internal members without costly (or impossible) dismantling of the structure. Advanced signal processing, non-contacting and embedded sensors, and analysis/test correlation technologies combine to make this a promising approach for the health monitoring of **operational structures**.

An **operational structure** is defined to be one which can perform, is performing, or has performed its intended function as opposed to a laboratory test article or a computer model. Operational structures are often geometrically complex and may be too large to test in a laboratory. These structures are rarely truss-like and in fact tend to be more plate-like. Also, the boundary conditions associated with such structures are not known as well as a laboratory test structure or a computer model. And finally, the environment associated with an operational structure (e.g. weather, traffic patterns, or location) is usually changing and has a serious impact on the measured structural response. Therefore, it is desirable to perform health monitoring research and development on structures possessing such characteristics. A unique aspect of the work reported herein is that the focus is on operational structures.

Modal testing and structural dynamics measurements are a set of technologies which determine a subset of structural characteristics such as modal frequencies, modal damping, modal mass, and mode shapes. These characteristics range from being extremely global in nature (typically at the lower frequencies) to being extremely local in nature (typically at the higher frequencies). Changes in these characteristics can be related to aging, damage accumulation, and manufacturing flaws since the modal parameters are related to global structural properties of stiffness, mass distribution, energy dissipation, and non-linearity sources. This global nature of the modal parameters provides a very powerful tool for inspecting large areas of aging structures. Structural health monitoring is one obvious application of modal techniques and has been the focus of a Laboratory Directed Research and Development (LDRD) project at Sandia for the past two years. The results of this project are the subject of this report.

Structural Health Monitoring is the process of monitoring a structure over a period of time using periodically spaced measurements. The output of this technique is periodically updated information regarding the ability of the structure to continue to perform its desired function in light of the inevitable aging resulting from the operational environments. Structural Health Monitoring is usually described as a four step process which answers the following questions at each step:

1. Is there damage in the structure (detection)?;
2. Where is the damage in the structure (localization)?;
3. What is the extent of the damage (extent)?; and
4. How much useful life remains in the structure (prediction)?

Experimental modal and structural dynamics techniques are most useful for the first two steps and the Sandia work over the last two years has focused on these steps. Development work has been performed in four areas (which will be defined and discussed extensively in a later section) : operational evaluation, diagnostic measurements, information condensation, and damage identification. Analytical structural dynamics techniques and/or traditional NDE techniques must be included to answer the question associated with step three. The answer to the step four question is the most elusive and requires material constitutive information on a local level. Work in materials aging studies, damage mechanics, and high-performance computing are attacking this task. Combining these studies with the structural health monitoring technologies under development will create a powerful tool for effectively monitoring and maintaining the nation's aging infrastructure.

This report begins by providing a **historical background** of the structural health monitoring work at Sandia. The purpose of this section is to give the reader a perspective on complex interactions and technical culture that gave rise to structural health monitoring at Sandia. The next section will be a **literature review** of the relevant publications that influenced the Sandia work. This includes the literature that resulted from this project. Many of these memos, reports, and publications which resulted from this work are provided in an extensive set of appendices. The next section summarizes the **technical activities** which resulted from this work. The technical details are provided in the papers which are included as appendices. The technical activities section is organized around the four development areas listed above: operational evaluation, diagnostic measurements, information condensation, and damage identification. The **recommendations and conclusions** section summarizes the technical advances, research conclusions, and recommendations for further work. The final section is devoted to the **references**. An extensive set of appendices follow which provide copies of most publications funded by this work.

HISTORICAL BACKGROUND

Initial Efforts

The idea of using structural dynamics testing as a method for monitoring the health of structures is a natural extension of structural system identification techniques. The joint work performed in system ID work by Experimental Structural Dynamics Department (9741 or Modal group) and the Structural Dynamics Department (9234 or Analysis group) in the past several years has provided the framework for research into structural health monitoring which has occurred in the last three years. The close proximity (organizationally) of the Modal group to the Aging Aircraft Project Department (9757) and the Non-Destructive Evaluation Department (9752 or NDE group) as well as the Modal group's long term support of the Wind Energy Technology Department (6214 or Wind Energy Group) have also been catalysts for the development of this technology.

Early indications of external interest in structural health monitoring were seen at the 1990 NASA/Air Force System ID and Health Monitoring Workshop by Ron Rodeman (9741), George James (9741), and John Red-Horse (9234). Ron Rodeman produced the first proposal to Sandia management in April of 1990 to pursue structural health monitoring using ER&D, NASA, or Air Force funds. Tom Carne (9741), George James (9741), and David Martinez (9234) visited NASA Johnson Space Center in January of 1991 and learned of the interest in structural health monitoring within the civilian space program. Also in 1991, Ron Rodeman had initial contact with the American Association of Railroads in which it was learned that a significant problem existed in the health monitoring of the nation's railroad bridges. Internal planning activities within the Modal group resulted in Dennis Roach (9752), George James, and John Red-Horse making contacts with the offshore drilling industry in early 1992.

LDRD Proposal Efforts

Dennis Roach took the lead role in writing and submitting an LDRD proposal in March of 1992 entitled "Health Monitoring of Structures Using Dynamic Analysis". The proposal included studying health monitoring as related to aging aircraft, offshore structures, and aging bridges. His proposal team included personnel from the Modal group and the Analysis group. The proposal received a very high score technically and was to be funded if additional LDRD funds became available. Unfortunately, this did not happen. Dennis transferred to the Aging Aircraft Project Department and continued to push development of this technology.

George James and Tom Carne took on the task of resubmitting the Health Monitoring LDRD. The proposal entitled "Health Monitoring of Structures Using Dynamic Testing" included team members from the Modal group, the Analysis group, the Aging Aircraft Project, and the Wind Energy Group. The LDRD was subsequently funded for $380K in FY94 (a $57K increase in FY94 budget was later granted) and $400K in FY95. A $16K

reduction in funding was later seen in FY95. This SAND report covers work performed under this LDRD project as well as some on-going efforts.

Increased awareness of the nation's infrastructure deterioration, a better understanding of the LDRD process, and more involvement by management aided in the selection of the 1993 proposal for funding. The focus on the offshore oil industry was dropped from the 1993 LDRD proposal and replaced with a focus on fatigue in wind turbine blades. This change was instituted for several reasons: (1) Sandia is one of the technological leaders in the development of wind energy in the country, (2) health monitoring of wind structures is a critical issue, (3) engineers at Sandia have an in-depth understanding of wind energy structures, and (4) the Wind Energy group has been using NDT group expertise and engineers for several years which further broadened the base of technical knowledge to apply to this problem.

During the FY94 LDRD proposal process George James participated in an proposal lead by David Andaleon (8111 or the Exploratory Systems Department) to study rapid inspection and/or monitoring of buildings after an earthquake. Bruce Hansche and George James submitted an FY94 proposal to further develop the scanning laser vibrometer to obtain three-dimensional information. During the FY95 LDRD proposal process George James and Diane Hurtado (6121 or Repository Isolation Systems Department) led a team that included Ken Alvin, David Lo (9118), and David Allen (Texas A&M University or TAMU). This team produced a proposal for studying the correlation between micro-mechanical models of corrosion and fatigue and global measurements such as structural dynamics and acoustic emissions. Dan Segalman (9234) and George James also produced a proposal covering research which would lead to non-intrusive sensor systems for performing structural health monitoring on weapon systems. None of these proposals were successful.

University of Colorado at Boulder Collaboration

Jim Lauffer (9741) brought in Scott Doebling, a Ph.D. student from the University of Colorado at Boulder (CU), on the OSSP program for the summer of 1993. Scott provided the Modal group with first hand insight into the modal parameter estimation and health monitoring work at CU by the group led by Lee Peterson and K.C. Park. Early in 1994, George James with 9741's Health Monitoring LDRD funds and John Red-Horse with 9234's System ID LDRD funds placed a contract with CU to further this work of joint interest. In July of 1994, K.C. Park of CU formed a team consisting of CU, Sandia, University of Houston (UH), Virginia Tech (VPI), Stanford University (Stanford), and Howard University (Howard) to produce a proposal to the DOD Multidisiplinary Research Program of the University Research Initiative (MURI). This proposal, entitled "Integrated Diagnostics for Maintenance and Operational Safety of Structural and Machinery Systems", represented an important integration of Sandia's effort into the nationwide research effort to study structural health monitoring. A further strengthening of the Sandia/CU ties resulted when a major contributor to the Sandia contract, Ken Alvin of CU, was offered a visiting scientist position at Sandia by David Martinez (9234). Scott

Doebling accepted a post-doctoral research position at Los Alamos National Laboratories in the summer of 1995. Also during the summer of 1995, Nikki Robinson, an M.S. student from CU came to Sandia on the OSSP program. She performed modal testing and analysis on aging aircraft related structures. She continued to be funded at CU on follow-on work from the LDRD into 1996. The CU collaboration fueled many creative and innovative advances produced by the LDRD and continues to produce results.

Diagnostic Measurements Efforts

Before leaving the Modal Group, Dennis Roach submitted a capital equipment request for a scanning laser vibrometer for use in health monitoring studies. The request was approved in January of 1993 and George James subsequently purchased such a system. Bruce Hansche of the NDT group was enlisted early in the LDRD project to work on Aging Aircraft testing and a variety of non-contact measurement issues. His work to further understand and extend the use of the scanning laser vibrometer has been jointly funded by the Health Monitoring LDRD and by Dan Gregory (2741) using 9741 funds for advanced manufacturing development. Bruce's work on the Health Monitoring LDRD prompted the addition of his name as a principal investigator on the renewal proposal of the Health Monitoring LDRD. Bruce subsequently became a member of the Modal group and is expanding the group's use of non-contact sensing systems. His access to and work with an Electronic Speckle Pattern Interferometer (ESPI) system added the capability for rapid operating shape visualization to the diagnostic measurement tools available for health monitoring research.

Scott Gray (while a member of 9741) and later Scott Klenke (9741) began joint work with Bob West of Virginia Tech (VPI) on the Virtual Test LDRD. Bob is a member of a research group at VPI which specializes in applying laser vibrometer technology to structural dynamics testing. A student of Bob's, Chris Doktor, was at Sandia during the summer of 1994 to perform work to allow Sandia to measure full 3D strain and velocity fields with the scanning laser vibrometer. To facilitate this work the contract with VPI had to be increased. This increase was funded jointly by the Health Monitoring LDRD, the Virtual Test LDRD, and Dan Gregory's Advanced Manufacturing LDRD. Bruce Hansche was instrumental in maintaining and expanding the VPI work at Sandia.

During an early literature survey, it was discovered that Roberto Osegueda of the Civil Engineering Department at The University of Texas at El Paso had performed structural health monitoring work with a scanning laser vibrometer. A technical relationship was established with UTEP which has proven advantageous to both parties.

Aging Aircraft Efforts

In August 1991, a major center with emphasis on validation of NonDestructive Inspection (NDI) techniques for aging aircraft was established at Sandia National Laboratories (SNL) by the Federal Aviation Administation (FAA). The main element of this center was the Airworthiness Assurance and NDI Validation Center (AANC). It supports the inspection

portion of the FAA's National Aging Aircraft Program through validation and reliability projects as well as technology development initiatives. To support these goals, the AANC has set up a hanger facility at the Albuquerque International Airport which contains a series of hardware specimens including complete transport and commuter aircraft. The facility replicates a working maintenance environment by incorporating both physical inspection difficulties as well as the environmental factors which influence inspection reliability. In 1994, the FAA expanded Sandia's charter to include a wide array of technical disciplines such as structural mechanics, computer science, fire safety, and corrosion. In its existing role with the FAA, Sandia'a AANC works with all aircraft manufacturers and airlines to foster new technologies associated with civil aircraft maintenance and structural repair.

Dennis Roach's association with the AANC prompted the first experiments in structural health monitoring using modal testing techniques. Dennis produced a plate which simulated an aircraft skin and allowed him to inflict simulated damage. He performed these tests in early 1992. This work became an instrumental example in the initial health monitoring LDRD proposal. Additionally, this work prompted Dennis and Norris Stubbs of Texas A&M University (TAMU) to submit a proposal to the FAA to further pursue manipulating the stiffness matrix as a damage diagnostic. Scott Doebling became the first user of the scanning laser vibrometer system as he performed health monitoring studies that simulated aircraft skin plate during the summer of 1993.

Bruce Hansche, Dennis Roach, and George James performed a series of aging aircraft tests for the Health Monitoring LDRD in conjunction with a small company, Holographics, Inc., using similar optical techniques for aircraft damage detection. This resulted in Sandia's participation in a Holographics, Inc. proposal to ARPA for additional work on aircraft damage detection using laser vibrometer technology. The proposal was successful; however, Sandia's role and funding were minimal. These tests, which were performed in November of 1993 and March of 1994, used the scanning laser vibrometer to extract frequency response information at 2233 locations on a McDonnell-Douglas DC9 aircraft fuselage. This is an order of magnitude increase in the number of feasible locations to extract structural dynamics information. An induced damage test was performed in which an aircraft stringer was sequentially cut. Modal tests were performed initially and after each cut. The data was also sent to the University of Colorado at Boulder for additional analysis. The size of the data base prompted researchers at Sandia and CU to develop procedures to condense the information into a usable set of important parameters.

During this same test, a composite patch attached to the DC9 was tested with the scanning laser vibrometer and electrodynamic shaker input. At the same time, a composite patch attached to a Boeing 737 with known flaws was tested. The scans included over 1600 points with a frequency band of 0 to 5000 Hz. However, noise problems in the vibrometer invalidated the results.

During November of 1994, George James, Bruce Hansche, and Tom Paez supported Roberto Osegueda of UTEP in the preparation of a proposal to the Air Force Office of

Scientific Research (AFOSR) for the Future Aerospace Science and Technology (FAST) center. These Sandia researchers were provided with significant collaborative activities in the program. The FAST center at UTEP was funded and began work in October of 1995. Heinze Schmidt (2000), Tom Baca, Tom Paez, and George James attended the kick-off meeting in October of 1995.

The DC9 test article was revisited during the summer of 1995 by Nikki Robinson (CU) and Raul Meza (UTEP). Both of these M.S. students were with the OSSP program at the time. Raul had responsibility for the laser vibrometer while Nikki performed the data reduction. The induced damage test was reconstructed using a simple bolted repair joint on the stringer. Also during the summer of 1995, Dennis Roach designed and acquired a set of five composite plates which simulated aircraft control surfaces and typical flaws seen in aircraft composites. Raul and Nikki also tested these plates. Follow-on work with the plates has been performed at UTEP with FAST Center funds. Also during the summer of 1995, George James and Dennis Roach assisted Tim Hasselman of ACTA, Inc. in the preparation of an SBIR proposal to perform research on the creation of a structural health monitoring system for military aircraft.

Bridge Efforts

Tom Paez (9741) was contacted by Chuck Farrar of Los Alamos National Laboratories (LANL) in the spring of 1993. The intent of this contact was to involve Tom in a study of Bridge Scour, a non-structural aspect of bridge aging. Through this interaction, Sandia learned of an upcoming set of tests to be performed as the I40/Rio Grande bridge was being razed. As the lead engineer on the project, Chuck Farrar hosted Tom Paez, Tom Carne, and George James at the bridge site. The Modal group provided LANL with information on the Natural Excitation Technique (NExT) which allowed modal data to be extracted from the bridge during traffic excitation. The Sandia engineers subsequently approached Stephen Roehrig of the Advanced Transportation Programs (9604 or Transportation group) for funds to support a Sandia participation on the tests. The transportation group did provide seed money for this participation.

Through an unrelated channel, Tom Carne was contacted by New Mexico State University (the lead institution for the I40 bridge tests), to provide the shaker excitation for the bridge tests. Randy Mayes (9741) agreed to lead the task of designing and operating the shaker during the test. Mike Nusser and Ron Hollingshead of the Mechanical & Climatic Testing Department (9742) completed Randy's design team. The team performed a superb job of designing and operating the shaker for the bridge tests. The transportation group funds and internal 9741 funds provided by Tom Baca (9741) allowed Randy to participate in the modal tests on the bridge and to provide LANL with additional sensors for the test. Randy was able to apply a technique he developed for localizing the errors in finite element models, called STRECH, to the bridge data using LDRD funds. His success prompted him to organize a session at the 1995 International Modal Analysis Conference (IMAC) covering the I40 Bridge tests and involving the major participants. Randy has subsequently worked with the Transportation group, New Mexico State, and New

Mexico's Alliance for Transportation Research (ATR) to propose a follow-on project to design and build a portable device to test bridges. Randy spent November 11, 1994 manning an Alliance for Transportation Research Exhibit at the American Association for State Highway and Transportation Officials (AASHTO) conference in Albuquerque, NM. This provided a unique opportunity to promote the work performed on the Rio Grande/I40 bridge test to individuals who are tasked with maintaining and monitoring bridges all across the country.

Todd Simmermacher, a student of David Zimmerman (UH), was brought in by the Health Monitoring LDRD on the OSSP program during the summer of 1994. Todd utilized health monitoring techniques in use at UH with the I40 bridge data. Garth Reese (9234), Randy Mayes, and George James worked with Todd during the summer. He and Garth provided the first analytical model-based damage detection work supported by the Health Monitoring LDRD. Todd's work also strengthened the relationship between Sandia and UH.

Several other bridge activities have been carried out during the course of the LDRD work. Early in the LDRD project communication was established with Brian Hornbeck of the U.S. Army. His interest is in the Structural Health Monitoring of mobile bridges. Correspondance has been maintained as the LDRD progressed. In late 1994, a bridge collapsed in South Korea. The Rio Grande/I40 bridge work was used as the basis for a proposal to produce a health monitoring system for similar bridges in Korea. Eventually, both Sandia and Los Alamos had to withdraw from the team. During the spring of 1995, Vern Gabbard (9719 or Tonapah Test Range) proposed using a bridge at the test range for additional testing. One of the most interesting applications would be explosive excitation to simulate earthquake inputs. This was proposed both to the Alliance for Transportation Research and the 1995 LDRD process without success to date. During the summer of 1995, Randy Mayes, George James, and Chuck Farrar (LANL) were invited to a workshop on bridge health monitoring at the University of Cincinnati. This meeting clearly identified the national reputation of the bridge health monitoring work in New Mexico.

Wind Energy Efforts

During the summer of 1993, Tom Carne and Anthony Gomez (9741) provided engineers at the National Renewable Energy Laboratory (NREL) with equipment and expertise to perform modal tests at subsequent stages during the quasi-static fatigue test of a composite Horizontal Axis Wind Turbine (HAWT) blade. This fatigue test was performed over a five month period. The data was subsequently provided to Sandia for analysis. Jim Goodding of CSA Engineering (under contract to 9741) performed the modal analysis of this data. George James then performed damage identification research using the data.

Paul Veers of the Wind Energy group coordinated a series of fatigue tests of a Vertical Axis Wind Turbine (VAWT) blade and blade/root joint. The tests were of joint interest to the Health Monitoring LDRD and the manufacturer, FloWind, Inc. FloWind initially

provided a blade section and root joint to test while Sandia performed the test and subsequently obtained a data set for health monitoring research. The lead test engineer was Ron Rodeman and Tom Ashwill (6214) performed the structural analysis. Dan Gregory and Ron Coleman (9742) worked with Ron to perform the resonant fatigue test in which the structure was excited near a modal frequency. Similar tests were performed during the 1980's by Dan for the Wind Energy group.

John Gieskie (9752 or the NDE group) performed an ultrasonic inspection of the adhesive in the root joint. David Reedy and Kurt Metzinger (both from 9118 or the Material and Structural Mechanics Department) participated in the test to determine the load transfer characteristics of the adhesive. The fatigue test uncovered a design flaw in the root joint which was subsequently corrected by the manufacturer. Tom Paez performed an analysis of the data using probabilistic neural network techniques. The data was also provided to Norm Hunter (LANL) to exercise other advanced damage detection procedures.

FloWind provided a 16 foot section of a redesigned blade without the blade/root joint in March of 1995. A resonant fatigue test was performed on this specimen in a free configuration by Tom Rice (9741). Tom Carne, Jim Goodding, and Gene Koenig (9741) assisted with this test. A significant effort was required to produce load transfer devices (shaker connection, stingers, blade clamps, and rotation isolation) for the test. AL Beattie (9752) performed some initial work to exercise acoustic emission testing on the blade. The fatigue test continued into FY96 and was subsequently funded from other sources. Appendix L contains a set of presentation aids covering this activity.

Offshore Oil Industry Activities

Although the offshore structure was dropped from the FY1993 LDRD proposal, significant communication developed between the Sandia health monitoring project and the offshore oil industry. At the suggestion of David Martinez (9234), George James began investigating DOE's Advanced Computational Technology Initiative (ACTI) as a source of funding for joint work with the offshore oil industry. During the 63rd Shock and Vibration Symposium in October of 1992, Tom Baca met Charles Smith of the Minerals Management Service (MMS) who is responsible for federal government programs relating to the structural health monitoring of offshore structures. George James contacted Charles Smith in September of 1994 and was provided with a list of five key industry engineers who work in this field.

George James, John Red-Horse, Randy Mayes, and Tom Carne contacted these individuals and discussed the status of the offshore oil industry and the possibility of generating an ASCI proposal. One of these individuals, Kris Digre of Shell Oil, was chairman of an industry panel assessing the technology for recertifying aging offshore structures (denoted as API Task Group 92-5 - Assessment of Existing Platforms to Demonstrate Fitness for Purpose). Kris provided a list of his committee members and corresponding members. A letter and pre-proposal was drafted by George James, John Red-Horse and Chuck Farrar (LANL) and sent to all API 92-5 committee members. One

respondent to the letter was Dan Dolan of PMB Engineering. Dan agreed to act as the industry partner for the ACTI proposal which was prepared and submitted by November 1 1994. The team included George James representing 9741, John Red-Horse representing 9234, Chuck Farrar of Los Alamos National Laboratories, David Zimmerman of the University of Houston (UH), Norris Stubbs of Texas A&M University (TAMU), Lee Peterson and K.C. Park of the University of Colorado at Boulder, and Dan Dolan of PMB Engineering. The proposal was not funded, however significant interactions continued with the industry.

Charles Smith (MMS) visited Sandia for an unrelated contract review on November 11, 1994. Tom Carne, George James, and Keith Ortiz (5167) met with Charles for more detailed discussions on the aging offshore structure problem. Dan Dolan invited the ACTI proposal team to Houston, Texas for a PMB presentation to the API 92-5 task group on November 14, 1994. George James, John Red-Horse, Chuck Farrar, and David Zimmerman (UH) attended this meeting. These team members and Todd Simmermacher (UH) met with Denby Morrison of Shell Oil on the same trip. Denby related some of the historical work with structural health monitoring on offshore structures. Denby also agreed to provide Sandia with ambient excitation data from a large offshore structure during Hurricane Frederick. The intent of this exchange was to apply Sandia's Natural Excitation Technique (NExT) to the data for an initial understanding of the technique's applicability. Initial analysis of this data was performed by Elizabeth Smith, a student intern from the University of New Mexico (UNM) in the Modal Group during September of 1995.

Ward Turner of Exxon continued to push for continued communication between the National Laboratories and the offshore industry to solidify a mutual understanding capabilities and needs. This prompted Kris Digre to invite the ACTI proposal team to attend and present at the March 2, 1995 API 92-5 Task Group meeting. John Red-Horse, George James, and Chuck Farrar delivered a presentation at this meeting. As a follow-on, a select group of industry representatives were invited to Sandia for more detailed presentations on National Laboratory capabilities and discussions of future collaborative efforts. Ward Turner and Brad Campbell of Exxon and Denby Morrison of Shell attended this meeting on July 11-12, 1995. A set of "next steps" and potential projects were defined. However, continued collaboration was dependent on government support of the national laboratories. The meeting summary was prepared by Ward Turner and is provided as APPENDIX K.

Weapon System Activities

Weapon systems comprise another class of structures prone to aging which require health monitoring. Also, given the direction of the national laboratories, weapons are the most likely application to fund further development and application of Structural Health Monitoring Technologies. The development of weapon system health monitoring methodologies was initiated when the Defense Programs Division (5000) at Sandia called upon 9741 to provide "Revolutionary Concepts for Stockpile Stewardship" in relation to

the design and maintenance of future weapon systems. A brainstorming session, led by Dan Gregory (9741), was held in January of 1994 to provide such concepts. Health monitoring of weapon systems was listed as one of the most mature technologies available to revolutionize stockpile stewardship. Tom Baca (9741) resubmitted this concept to 5000 for further consideration during August of 1994. Tom Paez (9741) submitted a proposal for FY95 1206 development funds to study the use of probabilistic neural networks to perform structural health monitoring on weapon systems. The proposal was funded and began work in October of 1994. This was a highly successful project which utilized information condensation technologies developed by the Structural Health Monitoring LDRD. A special session at the October 1995 Structural Health Monitoring Workshop at Los Alamos was devoted to weapon system applications. The staff and management of 9741 continued to pursue weapon applications for structural health monitoring into FY96.

Miscellaneous Activities

Roller Coaster Inspections

Walt Disney World and the Alliance for Transportation Research (ATR) developed a set of potential cooperative projects with the national labs during June of 1993. Structural Health Monitoring of roller coaster structures was listed as one potential topic. The I40/Rio Grande Bridge project was used as an example of the technology.

Reusable Launch Vehicles

A group of engineers from NASA Marshall Space Center visited Sandia in early 1994. They were very interested in the Sandia Structural Health Monitoring work as it applied to reusable launch vehicles. Over the next two years Sandia had some interaction each of the companies developing reusable launch vehicle concepts. Tom Baca discussed the Structural Health Monitoring activities at Sandia with Chuck Larson of Rockwell International in June of 1994. His primary interest is in monitoring of fuel tanks for reusable launch vehicles. Sandia engineers visited Rockwell's Downey, California plant in October of 1994 for a more detailed interchange of technical needs and capabilities. During the 1995 Adaptive Structures Forum, George James made initial contact with Lisa Emery of Martin Marietta Manned Space Systems. Her responsibility is development of structural health monitoring tools for reusable launch vehicle fuel tanks. Ed White of McDonnell Douglas Aerospace visited Sandia in August of 1995. His visit was to learn about the Structural Health Monitoring Activities at Sandia. Ed's work is in the area of health monitoring of military aircraft and reusable launch vehicles.

Nuclear Power Plants

On November 1, 1994, George James and Rod May (9706 or Business Development Department) briefed engineers from the Advanced Nuclear Power Technology Department (6471) on 9700 structural Health Monitoring Activities. During FY96, Tom Paez and Scott Klenke were funded to perform some initial work on Nuclear Power Plant Structural Monitoring.

Tower Guy Anchors

During January of 1995, a meteorological tower in a remote Sandia location collapsed onto a building. The health monitoring team took this opportunity to perform some scoping studies for structural health monitoring. Tom Rice, with input from Tom Carne and Randy Mayes, performed a series of laboratory tests in which the towers failed guy anchor was simulated. Tom showed that thinning of the rod could be detected experimentally. A set of tests were then performed on a guy anchor which was still embedded in the ground. The structural configuration was sufficiently different from the laboratory tests to render the results inconclusive.

Air Compressor Blades

During the course of the LDRD, Sandia acquired a pair of air compressor blades which were identical except for a visible flaw. Bruce Hansche used Laser Holography (ESPI system) to study the vibratory response of the blades. The work proved the utility of the ESPI system for mode shape visualization but was inconclusive at detecting the damage.

Major Technical Interchanges

The LDRD funding allowed several important technical interchanges to be planned and/or attended by the researchers. An initial kick-off meeting occurred on November 10, 1993. The meeting was attended by the diverse principle investigators and other individuals who would contribute significantly to the project. Randy Mayes and George James traveled to New Mexico State University on February 15, 1994. Randy presented his damage detection results using the I40 bridge data. Future collaborative efforts were discussed as well. The kick-off meeting for the second year occurred on October 17-18, 1994. This meeting included two days of presentations by the primary researchers and collaborators. As mentioned above, significant technical interchanges occurred during discussions with the offshore oil industry including the November 14, 1994 meeting in Houston, the March 2, 1995 meeting in New Orleans, and the July 11-12, 1995 meeting at Sandia. The summer meeting also included a large cross-section of the researchers and collaborators. The July 18-20, 1995 North American Workshop on Instrumentation and Vibration Analysis of Highway Bridges for Condition Assessment was attended by Randy Mayes and George James. The most significant meeting attended by the researchers and collaborators on this project was the Los Alamos Structural Health Monitoring Workshop in September of 1995. In fact Sandia researchers were instrumental in the planning and execution of the workshop. A diverse cross section of developers and users of structural health monitoring technology attended this workshop. The FAST center kick-off meeting at UTEP in October of 1995 was not directly funded by the LDRD, but the preliminary interactions with the UTEP researchers were.

LDRD work was also presented at several professional conferences. Bruce Hansche, George James, and Scott Doebling manned a poster exhibit at the Quantitative Nondestructive Evaluation Conference in Snowmass, CO on August 2, 1994. This was the first presentation of the Aging Aircraft work. George James presented work in several areas of study at the November 1994 ASME Winter Annual Meeting. Randy Mayes

presented the I40/Rio Grande bridge work at both the 13th International Modal Analysis Conference (IMAC) in February of 1995 and the March 1995 North American Conference on Smart Structures and Materials. Four papers were presented at the April 1995 Structures, Structural Dynamics, and Materials (SDM) conference by Lee Peterson, Scott Doebling, Todd Simmermacher, and George James. Ken Alvin presented his model-based damage identification results at the 1995 International Adaptive Structures Conference in November of 1995. Tom Rice presented the resonant fatigue testing results at the January 1996 Wind Energy Symposium. Nikki Robinson will be presenting the DC9 Aging Aircraft Test results at the February 1996 IMAC conference and the April 1996 SDM conference. George James will be presenting the composite plate results at the June 1996 SPACE' 96 conference.

LITERATURE REVIEW

The following literature survey is by no means an exhaustive compilation of the relevant work. It does represent a collection of authors and their works which have influenced the work performed at Sandia National Laboratories either directly of indirectly. This review also includes the literature produced by this LDRD project.

Early Works

Reference [1] is one of the earliest publication to discuss using changes in dynamic response to track damage. Vandiver draws on modal testing of buildings to propose his technique. He also uses Statistical Energy Analysis to analyze the response of the structure. No experimental data was reported in this presentation.

Reference [2] also is a classic publication in the damage detection work using vibrational frequencies on offshore structures. An offshore platform (West Sole WE) was removed from the North Sea in 1978. An induced damage test was performed on an underwater member. Above and below water level accelerometer measurements were taken using ambient wave excitation. Frequencies and shapes appear to have been determined using peak picking on auto spectra and relative phasing on cross-spectra. Above water measurements contained 15 to 20 peaks between 0 and 10 Hz. Six modes below 4 Hz were studied in detail and tracked as the platform was damaged. The frequencies of these global modes were estimated to have been determined to within 1%. Above water measurements were taken for 45 minutes. Underwater measurements were taken for 20 minutes and showed the global modes as well as several highly damped local modes. Data was acquired for modes up to 20 Hz with five modes between 4 and 10 Hz being studied in detail. The confidence in these modes was estimated at 2 to 3% Finite element models were used to assist in the modal extraction and to verify the results. The general conclusions were that above-water measurements of the lowest global modes could be used to determine the complete failure of a member, while local measurements (requiring underwater accelerometers) could be used to determine partial member failures.

Reference [3] contains experimental data only to correlate a finite element model. Some fine work was performed to estimate confidence levels due to several effects and to determine detectability thresholds. A general framework for determining detectability is developed. Earlier work by the authors is reported which verifies that ambient measurements are acceptable for determining modal parameters.

Crohas and Lepert discuss in reference [4] the idea of continuously monitoring frequency domain information from forced response testing to determine the health of an offshore platform. Although experimental measurements are shown, no health monitoring/damage detection results are provided. They did report measuring up to 40 modes of the structure and reported the local modes of the members starting at 15 Hz.

Stubbs and Others

Reference [5] is the initial presentation of Stubbs' approach. The co-author is Roberto Osegueda whose later work will be discussed in the next sub-section. The approach utilizes modal frequency changes before and after damage as well as analytically calculated sensitivities of the modal frequencies with respect to the structural parameters at the possible locations of damage. A finite element model is typically used to develop the sensitivity matrices and the approach requires that the frequencies be matched before and after damage. Changes in mass and damping (as well as the sensitivities) are assumed known. A numerical example using a simply supported beam is also provided. The results are favorable for this simple example. The technique as presented iterates to adapt to the regions expected to damage (this is done by setting to zero all positive stiffness changes which are considered non-physical).

Reference [6] is a companion to reference [5] in which Stubbs' technique is applied to a simple cantilever beam. Although better modal testing techniques could have been used, the experiment appears to have been relatively complete. The results were successful even though the structure was extremely simple. It was common to see light damage predicted in other areas besides that of the known location. This reference cites four earlier numerical studies in the development of Stubb's method from 1985 to 1990.

Reference [7] reports on Stubbs' recent work utilizing experimental data from a scale model of a pier deck for health monitoring work. The work reported successful results for these laboratory-based test. Reference [8] reports on Stubbs, Kim, and Farrar's work on the Rio Grande I40 bridge. Although Stubbs used a different data set, the I40 experiment was a critical aspect of the Sandia LDRD work reported herein.

Osegueda, Ferregut, and Others

Osegueda's thrust in reference [9] is to prepare for a probabilistic formulation for damage detection. A laboratory experiment is described as well as experimental results. Standard deviations on measured frequencies are provided. A good overview of previous work is provided. An important note is that Osegueda has upgraded Stubbs' method to include changes in mode shapes as well as frequencies, although no results were included in this publication. Reference [10] is the appropriate reference for these results.

Reference [11] contains a summary of Osegueda's research at the University of Texas at El Paso (UTEP) using an Ometron VPI 9000 Scanning Velocimeter and several different damage detection schemes. Stubbs' method (called the eigenvalue sensitivity method in this work) was the first one and required an analytical model to generate the sensitivities. This method worked best when only eigenvalue measurements were available, however the resolution was limited by the number of resonant frequencies. The eigenvalue-eigenvector sensitivity method (developed by Osegueda) allows changes in mode shapes to be used as well. This technique works well, but requires extremely accurate measures of the mode shapes. The exact eigenvalue method (also developed at UTEP) incorporates

changes in modal orthogonality into the problem. This method requires a pairing of damaged and undamaged mode shape and works very well with analytical data. These techniques were exercised analytically as well as experimentally. A modal strain energy approach was also applied experimentally and worked well with some of the higher modes.

Reference [12] continues Ferregut and Osegueda's efforts to place damage detection within a probabilistic framework. The effects of uncertainties in the damage detection process are studied and a method for predicting the statistics on the final damage parameters is exercised. Also, the probability of detecting various levels of damage is examined. Reference [13] discusses a thrust by the same researchers to develop artificial neural networks for damage detection. This work later was expanded to include collaboration with Sandia National Laboratories.

Smith and Others

Some of Smith's early work in damage detection of large space structures is presented in reference [14]. An extensive structural identification algorithm developed by Smith and others is applied to the damage detection problem. Smith's method is an optimal update method which maintains the sparsity of the original finite element model. The method requires a finite element model of the structure, but does use changes in frequency and shape for the system identification problem. Six modes of a simple truss structure were used in this example. A 120 Degrees-Of-Freedom (DOF) model was used, although only 14 measurement locations were available. Some experimental results (obtained with good modal test procedures and equipment) are presented, however no damage detection results are presented. A technique for expanding the measured mode shapes to the full model DOF is required. This expansion process did not provide full modes with the proper orthogonality for the system identification technique. Hence, expansion was reported as an area of needed work.

Reference [15] provides the next installment of Smith's work. An expansion/orthoganalization scheme has been developed by Smith & Beattie [16] to correct the orthoganlization problems seen in reference [14]. Also measurements at all 120 locations or any subset of sensors were available. Only three modes (selected differently for each damage case) were used for each damage detection experiment. Tests using analytical data were only successful when all 120 sensors were used. Li and Smith's latest work [17] has produced a hybrid technique which draws from both model sensitivity and optimal matrix update approaches for system identification.

Zimmerman, Simmermacher, Kaouk, and Others

Zimmerman and Widengren provide a technique in reference [18] which uses control theory techniques to modify structural models. An eigenvalue assignment algorithm is used to calculate a simulated feedback control system which updates a subset of the analytical modes corresponding to the measured modes. Symmetric damping and stiffness

matrix updates are calculated. These update matrices will not necessarily maintain the proper connectivity.

Zimmerman and Kaouk [19] refine the method of reference [18] to attack the damage detection problem more effectively. A subspace rotation algorithm is used to enhance eigenvector assignability. A simple iterative scheme is provided to maintain sparsity. The upgraded algorithm is shown to work well as long as the proper eigenvector entries are chosen.

Reference [20] builds on the reference [18] and reference [19] work and adds a damage location pre-processor damage detection problem. Several numerical tests are shown with and without added noise. The technique is shown to work well in this situation. However, all the tests included simulated measurements at every DOF

Kaouk and Zimmerman expand their method to calculate the extent of damage using a perturbation of the original analytical model possessing a minimum rank [21]. They also allow damage in mass and damping properties. Any two matrices can be allowed to change. A simulated example of a 50 bay truss with incomplete eigenvector measurements is used. An experimental example of a mass-loaded cantilever beam is also used. The Minimum Rank Perturbation Theory (MRPT) is further expanded to remove the need to have an original Finite Element Model (FEM) [22]. MRPT is further expanded to utilize a variety of test data types including static data [23].

And finally, three groups of damage detection researchers including Zimmerman, Smith, and McDonnell Douglas Aerospace jointly studied the most troubling problem in health monitoring, the incomplete measurements problem [24]. The test structures were truss type objects in this work. However, there were several useful points to consider when performing reduction/expansion which arose from this work. Simmermacher's work using the Rio Grande/I40 bridge data produced evidence that model order reduction is one of the primary reasons that current model-based damage detection schemes are difficult to exercise [25]. This work was funded by the Structural Health Monitoring LDRD as part of the Outstanding Student Summer Program (OSSP) and is included as APPENDIX G of this report.

Zimmerman, Kaouk, and Simmermacher provided several techniques to allow engineering insight and judgment into the application of MRPT [26]. In references [27] and [28], Kaouk and Zimmerman provide a technique in which MRPT can be applied to different partitions of a structural model to reduce the number of measured modes required for damage detection. Zimmerman, Simmermacher, and Kaouk provide a technique which utilizes Frequency Response Function (FRF) information instead of modal parameters to perform damage identification using MRPT [29,30]. This is an important capability for two reasons. First, errors associated with modal truncation are reduced. And second, the procedure becomes more automated since a highly technical modal analysis does not have to be performed for each damage case.

Peterson, Alvin, Doebling, Park, and Robinson

A series of experiments to support damage detection by model updating is reported in references [31,32] by University of Colorado-Boulder researchers. It was found that selection of the appropriate modal parameters was critical to the success of such an approach. Also, the truss structure utilized for these tests exhibited a multitude of localized modes. This further complicated modal selection and modal data reduction.

Reference [33] is largely concerned with producing normal modes from complex modes generated by ERA however, a number of important issues relating damage detection are addressed by this work. A multiple step process is provided, however the last step requires a non-linear minimum norm solution for the case of more modes than sensors. The techniques also require driving point measurements to allow for the proper mass normalization.

An extension of this is the production of mass, damping, and stiffness matrices directly from data [33,34]. The procedure is based on a Guyan reduction, however the reduced matrices (using physical coordinates) are augmented with a set of generalized coordinates to model the extra modes of the system. There is some connection between this procedure and Craig-Bampton component mode synthesis. A damage detection method for truss structures was presented based on these procedures. It required a model order of 500 with fairly automatic modal testing. The results were not conclusive for damage detection, but could hold promise for an iterative procedure. Further application of the experimentally calculated mass and stiffness matrices to damage detection by the University of Colorado-Boulder researchers is reported in reference [35]. The experimental application of these techniques to a truss structure has shown that the extraction of modal vectors for the higher modal frequencies is important. A further direction of research at UC-Boulder which is driven by the work mentioned above, is in the analysis of high-modal density data sets [36].

Techniques to calculate and use the flexibility matrix were developed at the University of Colorado Boulder and found to be extremely robust and sensitive to changes in the structural system [37]. The estimation of stiffness and flexibility properties is greatly enhanced by accounting for out-of-band modes [38,39]. Doebling's work in this area was funded by the Structural Health Monitoring LDRD and reference [38] is included as APPENDIX H of this report. A unique method for assessing local stiffness properties was developed by Peterson in which the stiffness matrix is disassembled along an assumed connectivity pattern [40]. This work was also funded by the Structural Health Monitoring LDRD and is provided in APPENDIX I. Robinson's work has been focused on the development of structural health monitoring tools for aircraft applications such as structural member connection [41,42] and composite material monitoring [42]. Reference [41] is included as APPENDIX N of this report.

West and Others

Researchers at Virginia Tech are developing the tools to perform laser velocimeter-based structural imaging [43-47]. This technology promises to allow a high-spatial density grid of 3-D measurements to be acquired in a non-contacting fashion. The highly localized effects of damage tend to require such measurements. It should be noted that the work reported in [47] was partially supported by the Structural Health Monitoring LDRD.

Sandia and Los Alamos National Laboratories

A technique for localizing damage in a finite element model using experimental data was developed at Sandia [48] and has been named the Structural Translation and Rotation Error CHecking algorithm or STRECH. The technique has recently been expanded to perform damage detection using an undamaged data set [49,50]. The algorithm first compared the ratio of difference between two sensor location measurements of a damaged mode shape to an undamaged mode shape. It has since been discovered that the static flexibility shape is more sensitive on the Rio Grande/I-40 bridge data. Reference [49] is provided as APPENDIX E of this report. Another approach used at Sandia was MAtriX COmpletioN (MAXCON) which produced experimental mass and stiffness matrices coupled with a simple form of disassembly. This approach worked extremely well on the bridge data [51]. This work is included as APPENDIX J. The two previous works listed above compared damaged experimental data to undamaged experimental data. Reference [52] details a procedure to compare to an undamaged analytical model. The procedure incorporates the variance of the experimental data in the localization indicator. The method can utilize a mix of mode shape projection and model reduction. In fact, a new mode projection algorithm is provided which incorporates statistical measures to reduce the bias caused by imperfect experimental data. This work is included as APPENDIX L.

Another development at Sandia National Laboratories was the Natural Excitation Technique (NExT) [53]. This technique has allowed the modal parameters to be extracted from a variety of structures in their operation environment including wind turbines, transportation systems, missiles [54], and bridges [55].

Los Alamos National Labs performed the dynamics testing of the I-40 bridge [56]. This work included modal testing to support model correlation and damage detection, sine dwell testing to verify new non-contact sensor concepts, and ambient testing using NExT. Sandia Labs provided the excitation source and logistics support for these tests [57]. The data was used at Los Alamos to study damage identification algorithms [58,59].

Reference [60] describes a recent test to failure of a composite wind turbine blade. The blade was failed using quasi-static loading. Two nondestructive testing techniques, acoustic emission and electronic shearography were used to monitor the blade during the test. This same approach was adopted for a fatigue test to failure of a similar blade which also included a number of modal tests during the course of the test. MAXCON was also applied to this data set with good results [51].

Reference [61] details a set of experiments performed at Sandia Labs on a simulated aircraft panel. Accelerometers and a scanning laser vibrometer were used to study the damage detection using STRECH and techniques developed at UC-Boulder. Although this work preceded the initiation of the LDRD project, it had a great influence on the direction of the Structural Health Monitoring LDRD. Therefore, it is included as APPENDIX A of this report. This work was followed by later experiments in the FAA Aging Aircraft NDI Validation Center at Sandia [62] (also APPENDIX B of this report). An induced damage test was performed on the forward fuselage of a DC-9 aircraft. A stringer was cut in four stages and modal tests were performed using a scanning laser vibrometer after each cut. An extremely dense grid of measurements points was utilized which included over 2000 measurement points. The frequency band of the measurements was from 0 to 2000 Hz with the excitation from 500 to 1500 Hz. The tests also included laser holography measurements. The improvement in resolution was seen when modal decomposition was used on the data [63]. Reference [63] is provided as APPENDIX D of this report. Later tests and analysis showed the additional resolution and ease of application which results from flexibility calculations [41,42]. Four composite panels with various types of damage were produced to simulate the situation commonly seen in damaged control surfaces. These panels were tested with the scanning laser vibrometer (529 points, 0 to 2000 Hz) and submitted to flexibility analysis [42,64]. The results reiterate the sensitivity and ease of application of the flexibility analyses. Reference [64] is provided as APPENDIX O of this report.

TECHNICAL ACTIVITIES

As mentioned in the introduction, development work has been performed in four areas: operational evaluation, diagnostic measurements, information condensation, and damage identification. A subsection will be devoted to each of these development areas.

Operational Evaluation

The operational evaluation development has centered around techniques needed to answer two questions in the implementation of a structural health monitoring system:

1. what data needs to be acquired to track important structural changes; and
2. how is this data to be collected in the operational environment.

The answer to these questions was found to require a three step process. The first step utilizes **engineered flaw specimens** to develop an initial understanding of which parameters are sensitive to the expected damage and to validate the diagnostic measurements. This initial step draws heavily from work performed in the AANC. The use of analytical tools such as experimentally-validated Finite Element Models (FEMs) can be a great asset in this process.

The next step utilizes **damage accumulation testing** during which significant structural components of the structure under study are subjected to a realistic accumulation of damage. This may require induced-damage testing, fatigue testing, corrosion growth, temperature cycling, etc. to accumulate certain types of damage in an accelerated fashion. Hence a study of the relationship between damage level and measured parameters is possible as well as initial information concerning sensor placement, data acquisition interval, and possibly environmental effects. As with the initial step, a verified analytical model is extremely useful as the available information is multiplied.

The final step is **operational implementation**. This step in the process is concerned with the final selection of sensors, data acquisition, monitoring intervals, excitation sources, and baseline data set. This step deals with the full structure in its actual environment and may require a verified analytical model. Aspects of all three steps in the operational evaluation development process have been studied in this work and represent the unique contributions a national laboratory can make in a research community composed of government, university, and industry. However, the scope of this work was not to produce a complete structural health monitoring system for any particular structure and this was not attempted.

There were three activities which dealt with engineered flaw specimens: the simulated aircraft panel tests, the simulated guy anchor tests, and the damaged composite plate tests. Likewise, there were three damage accumulation testing activities: analysis of the wind turbine quasi-static fatigue test data, the wind turbine blade root resonant fatigue test, and the wind turbine blade resonant fatigue test. There were also five operational

implementation activities: analysis of the Rio Grande/I40 test data, the first DC9 tests, field tests of guy anchor, the second DC9 tests, and the NExT analysis of offshore structure response data. These ten activities will be discussed briefly.

Simulated Aircraft Panel - Engineered Flaw Specimen
Although this activity was not funded by the LDRD it was an important precursor and is included for completeness. The structure used for this experiment was an aluminum plate with three parallel L-brackets running horizontally across it. It is a representation of a typical section of aircraft skin. Each bracket was held in place by a row of bolts, spaced at 1 inch increments across the plate. The middle bracket was replaced with a shorter one to simulate damage. Sixteen accelerometers and the scanning laser vibrometer (49 points) were used to acquire data. Comparisons between damaged and undamaged and between traditional and non-contact measurements were possible. Although the torque levels on the bolts were not tightly controlled, this test article represented the first engineered flaw specimen used for health monitoring work. Diagnostic measurements and damage ID developments accompanied this test and will be discussed in the appropriate sections. The report on this work is available as APPENDIX A.

Simulated Guy Anchor - Engineered Flaw Specimen
A 17 year old meteorological tower in a remote area of Sandia National Laboratories collapsed in January of 1995 when a guy anchor failed underground. The structural health monitoring LDRD funded a one week scoping study to determine the validity of structural dynamics techniques to monitor underground guy anchors. Each guy anchor has two rods embedded in the ground and terminating in a concrete block. The rods are susceptible to corrosion which causes the diameter to neck down in the affected region. One of these rods was simulated with a 72 inch long, 7/8 inch diameter aluminum bar. Five inches of the rod was cantilevered axially while the other end was supported laterally by a foam pad. An accelerometer was placed on the end of the bar. Impulse excitation was applied to the end of the bar. Measurements of FRF and time history of the impulse were made. The rod was then necked down to .3 inches over a 2 inch section to simulate corrosion. Another set of measurements were performed. The necked rod clearly shows changes in the dynamic properties. APPENDIX F provides a set of presentation aids related to this work.

Damaged Composite Plates - Engineered Flaw Specimen
For this work, five plates were designed and built with a series of flaws engineered into the construction. The effects of these flaws were then be studied by comparing the response of different plates. The plates were 24 inches by 24 inches constructed of a .5 inch thick Nomex honeycomb core sandwiched between four ply T300 plain weave graphite cloth panels. The graphite lay-up was [-45,0,90,45]. A layer of hysol film adhesive bonded the graphite panels to the honeycomb core. Plate #1 had no engineered flaw and was considered the undamaged specimen. Plate #2 had a four inch diameter disbond (created with a teflon disk) in the geometric center of one graphite panel. Plate #3 had a four inch diameter region of the honeycomb core (located in the geometric center of the plate) filled with fluid. The individual honeycomb cells surrounding the fluid were

potted to contain it. Plate #4 used a teflon insert to produce a four inch diameter delamination between plies 2 and 3 at the geometric center of one graphite panel. Plate #5 contained two of the four inch diameter disbonds located at the geometric centers of opposing quadrants of a graphite panel. A four inch diameter delamination, and a four inch diameter fluid ingress section were at the geometric centers of the two remaining quadrants. These three types of flaws represent common flaws seen in composite aerospace structures. The design of these plates was heavily influenced by Sandia's interation with the commercial aircraft industry through the AANC. This aspect of the LDRD targeted Structural Health Monitoring R&D with application to a current technology gap in aircraft industry.

These plates were tested in a free-free configuration with the scanning laser vibrometer and shaker input. The test data produced traditional plate modes as would be expected from such a set-up. The paper provided in APPENDIX O provides a useful write-up of the test and initial results.

Wind Turbine Quasi-static Fatigue Test Data - Damage Accumulation Testing
A fatigue test to failure of a composite wind turbine blade was performed at the National Renewable Energy Laboratory. Periodic modal tests were performed during this test as well as acoustic emissions tests. This data was utilized to study the application of health monitoring techniques in a damage accumulation environment. When coupled with a non-contact transducer such as a scanning laser vibrometer, this technology could be applied in the field to periodically monitor a field of wind turbines. Ideally, the data would be combined with analytical tools to estimate remaining life in the blades.

The blade was constructed of fiberglass and included a tapered fiberglass airfoil on a tapered fiberglass spar. The blade was bonded to a short steel rod used to cantilever the blade to a stifback. The final visible failure was a bond failure between the fiberglass blade and the steel connecting rod. A hydraulic actuator was used to fatigue the specimen at 1 Hz. As mentioned above, the fatigue test was periodically stopped to allow modal testing. The hydraulic actuator was removed and impact excitation with a three pound instrumented mallet was used for the modal tests. Accelerometers were placed at 30 locations on the 32 foot long blade and data was acquired to 64 Hz. Approximately eleven modal frequencies are consistently present in this band. National Renewable Energy Laboratory personnel performed the modal tests using Sandia Lab equipment and consulting. There were 51 days of testing and 32 modal tests spread over a four month period.

The test data included some unexpected phenomena. Following an initial drastic drop in all modal frequencies, most of the modal frequencies stayed constant until failure. At failure, most of the frequencies increased. The static stiffness also seemed to increase. One would expect the stiffness and therefore the frequencies to decrease with damage. An explanation for these phenomena has not been found. However, the test fixture was reoriented and hydraulic actuators changed at least three times during the test. Also during the four months of testing, a broad range of environmental changes were seen.

These changes may have contributed to the unexplained phenomena seen in the data. The paper in APPENDIX J is a good reference for this work.

Wind Turbine Blade Root Fatigue Test - Damage Accumulation Testing
A FloWind Corporation blade joint from the 17EHD Vertical Axis Wind Turbine (VAWT) was fatigue tested as part of the Structural Health Monitoring LDRD. The test specimen was a 14-foot long section of pultruded fiberglass blade bonded to steel attachment hardware that would bolt to the tower on the actual turbine. Strain gauges were placed at 20 locations to monitor stress concentrations and load transfer characteristics. 34 accelerometers were also used for the structural health monitoring study.

A modal test was performed to obtain an initial damping estimate. A difficult task in performing the resonant fatigue test was the selection of a proper excitation source. The final configuration had the blade mounted on a vibration slip table and driven by an UnHoltz-Dickie Model T-4000 electrodynamic shaker. The test article was excited at the first resonant frequency (initially at 4.3 Hz). This allowed a faster test with lower input forces when compared to a traditional quasi-static fatigue test. Failure occurred after 22,000 cycles as opposed to the 100,000 estimated. A design flaw was found to be contributing to the premature failure. This was subsequently corrected by the company. APPENDIX C contains a detailed memo describing the test and results.

Wind Turbine Blade Fatigue Test - Damage Accumulation Testing
A second pultruded fiberglass VAWT blade was obtained from FloWind. This 16 foot blade was of a newer and lighter design and did not include the root joint. A resonant fatigue test was planned and performed on this specimen. A free-free configuration was used on this test. The difficult issue in the design of this test was the load transfer fixture. The blade was instrumented at seven strain gauge locations and with 70 accelerometers. The excitation frequency of 25 Hz resonated the blade in its first bending mode of vibration. During the course of the test it became obvious that a large-area non-contacting transducer such as a scanning laser vibrometer would have been much more efficient than traditional accelerometers which tended to break-off of the structure during resonance. The blade failed after 15.5 hours of testing and 1.325 million cycles. APPENDIX M contains a set of presentation aids which cover this test.

Rio Grande/I40 Bridge Test - Operational Implementation
The Rio Grande/I40 bridge tests were a set of induced damage tests performed on the decommissioned structure. Before demolition of the bridge, a series of progressively more serious cuts were made in one support beam of the bridge. A series of four cuts were made in the plate girder after the bridge was closed to all traffic. The fourth cut completely cut half of the lower flange and half of the chosen plate girder. Modal tests were performed in the initial condition and after each cut. Random excitation was provided from 2-12 Hz with a peak input of 500 lbs. Uniaxial sensors at 26 locations were used as the primary instrumentation set. All sensors and the force input were in the vertical direction. This allowed the extraction of six modes in this direction.

These tests were useful from an operational implementation point-of-view since they were performed on an actual bridge in the field. Environmental conditions and most boundary conditions were actual and not simulated. Neither were the logistical or scheduling issues contrived. Before closure of the bridge, ambient excitation testing was performed with great success [55]. There were three issues that were not representative of an actual bridge health monitoring system. First, construction crews were razing the other spans of the bridge during construction, which may have affected the boundary conditions. Second, traffic was removed from the bridge during all induced damage testing. Interestingly enough, there was sufficient excitation from vehicular traffic on other nearby bridges to excite the bridge-under-test [56]. And finally, the cuts were not necessarily representative of actual damage that a bridge might see. However, the test was extremely successful in allowing several institutions to gain insight into actual bridge monitoring. APPENDIX E and reference [56] are the best references for this work.

First DC9 Stringer Test - Operational Implementation

An induced damage test was performed on the front fuselage of a decommissioned DC-9 transport aircraft (which was a specimen at the AANC). A stringer was cut in four stages to simulate various levels of sub-surface damage. A non-contacting laser velocimeter was used to acquire broad-band frequency response functions using a dense grid of spatial measurement points. Details on the instrumentation will be provided in the diagnostic measurements section. An electrodynamic shaker provided the excitation. The shaker was attached directly to the aircraft skin using suction cups. While convenient for field conditions, this configuration made it difficult to measure the force input. Random input between 500 and 1500 Hz was used with a two pound maximum amplitude. Data was acquired from 0 to 2000 Hz.

These tests contained many aspects of an operational environment. The physical dimensions were realistic since the structure was an actual fuselage section. Structural non-linearities from cable and fixture rattling were present as would be seen on an operational aircraft. There were several environmental changes in the structure throughout the course of the test since data was taken in March and November in an actual hanger. However, this test series differed from the operational environment in several ways. The front fuselage of the aircraft was disconnected from the rest of the aircraft, which did alter the boundary conditions. As a result, accessibility to the interior was not restricted. The operational aircraft includes insulation that would have covered the interior surface of the region of interest. Therefore, the damping properties would have been greater on an operational aircraft. Also, there were no time constraints or other activity-related disturbances as would have been seen in an actual aircraft maintenance facility. In spite of these deviations, this test series was excellent in understanding the types of data, testing techniques, and processing methods which are required for monitoring the structural health of an operational aircraft.

For this application, Structural Health Monitoring is intended to fill an important gap in the current aircraft inspection tools. Namely, the lack of robust and efficient **global**

inspection procedures. It should be noted that a variety high-fidelity **local** inspection procedures do exist but are time and labor intensive. More information will be provided on this test series in the following sections. Also, APPENDIX B and APPENDIX D contain more detailed descriptions of the tests.

Guy Anchor Field Test - Operational Implementation

A set of experiments were performed on a guy anchor of the same construction as the failed anchor as mentioned above. The intent was to determine if the laboratory tests of the simulated guy anchor could easily produce a structural health monitoring procedure for the field. The field configuration had two of the rods mounted in the ground which were fused together at several locations and were supporting guy wires. The only difference between this test and an operational test would be the absence of guy wires (since the tower had already collapsed!). However, the other boundary, environmental, and logistic conditions were identical to an operational configuration. The results were inconclusive due to the lack of damage accumulation testing which would have utilized a more representative substructure than the engineered flaw tests. APPENDIX F contains a set of figures relevant to this work.

Second DC9 Stringer Test - Operational Implementation

The DC9 test article was revisited during the summer of 1996. The damaged stringer was "repaired" using metal plates which could be replaced with a split set of mass mock-ups to simulate the damage. Several changes were made in the test set-up which resulted from the experience of the first set of DC9 tests. The most significant change was in the input. A 50lb. shaker was supported independently from the aircraft skin, and excited the structure via a stinger. The stinger was attached to the aircraft using an aluminum pad and dental cement. Maximum inputs were less than five pounds and covered the region from 0 to 1250 Hz. This configuration is less likely to be implementable on an operational system, but provided a more robust input for the experiments. The results of this test series will also be reported later, although APPENDIX N is a good reference.

NExT Analysis of Offshore Structure Response Data - Operational Implementation

A set of ambient responses from a large offshore structure undergoing hurricane loading was acquired as part of the LDRD work. The data set included accelerations, strain, and displacement measurements over a nine hour period. Initial processing of this data using NExT [53] was performed on this project. Although this aspect of the work was not completed, valuable insights were obtained in the application of ambient vibration testing to the implementation of structural health monitoring.

Summary of Operational Evaluation Advances

One of the most important advances to result from this aspect of the study was the development of a process (engineered flaw specimen, damage accumulation testing, operational implementation) to perform operational evaluation of a structure's health or damage state. Each aspect of this process was exercised for a variety of structures. The experience is invaluable.

More specifically, the **simulated aircraft panel** tests proved the worth of a non-contact sensor to avoid mass-loading of the structure. Also, the need to control boundary conditions, and torque levels were seen. Also, the utility of standard test object with interchangeable parts to simulate damage produced an effective means of performing such tests. The **simulated guy anchor** showed the worth of a carefully controlled experiment to study specific damage scenarios. This allows the proper understanding and possible modeling to be developed for the final operational structure of interest. The **damaged composite plates** provided a well-planned series of tests to study several dissimilar damage scenarios. However, the underlying uncertainty associated with manufacturing differences between the plates is ever present.

The **wind turbine quasi-static fatigue test** showed that damage accumulation tests must be carefully controlled and monitored. Discrepancies due to fixture and test condition alterations must be recorded and/or minimized. However, this test showed that unexpected changes in the structures may occur which would not be present in a simpler engineered flaw specimen test. The **wind turbine blade root fatigue test** continued development of the damage accumulation testing concept. This test produced a new type of fatigue test, the resonance fatigue test, which allowed more rapid testing and less specialized equipment. However, the right excitation source is must (typically this means longer strokes than traditional electro-dynamic shakers provide). **The wind turbine blade fatigue test** again showed the usefulness of non-contact sensing and the proper excitation source. Much experience in the design of load transfer devices was gained from this test.

The **Rio Grande/I40 bridge test** provided a wealth of insight into the implementation of structural health monitoring techniques in large civil structures. The usefulness of ambient vibration testing was seen. The **DC9 stringer tests** provided important experience in complex geometry testing with a non-contact transducer. Experience in dealing with noisy data and environmental changes was realized. These experiences influenced other developments which will be discussed in the following subsections.

Diagnostic Measurements

Structural health monitoring is a more rigorous application for structural dynamics measurements than most applications to date. As a result, developments in the area of diagnostic measurements were important aspects of the current study. The implementations of structural health monitoring as envisioned in this work suggested developments in four types of measurement technologies: discrete, embedded, large-area, and sensor fusion. Discrete sensors are traditional measurement devices such as accelerometers or strain gauges which are mounted to the external surfaces of the structure under study. Embedded sensors are attached permanently (or embedded in) the structure under study and may be traditional, miniaturized, or large-area contact sensors (such as piezo-film or fiber optic strain gauges). Large-area sensors are typically optical and non-contacting in nature (such as scanning laser Doppler velocimetery, laser holography, or video). Sensor fusion is defined as the coupling of structural dynamics

information with advanced NDE tools such as laser holography or shearography, acoustic emissions, ultrasonic inspection, or x-ray. The current work focused on the developments in large-area sensors (although limited work in sensor fusion was performed) and provided important contributions to the research community. These two areas, large-area and sensor fusion, will be critical in the development of techniques which relate structural dynamics measurements to material damage mechanics parameters, which is a proposed follow-on activity to this work. There were nine activities in the diagnostic measurements area which will be discussed next.

Simulated Aircraft Panel Test - Large-Area
The simulated aircraft panel test was the first use of the scanning laser vibrometer at Sandia. The panel was suspended free-free with shaker excitation up to 100 Hz. Accelerometers and the scanning laser were used to acquire data at 49 locations. This allowed a comparison between the two systems. The frequency information was extracted well using both types of sensors. However, the laser signal dropped-out often which produced shape results containing more measurement error than those produced with accelerometer data. APPENDIX A is the necessary reference for this work.

First DC9 Stringer Test - Large-Area and Sensor Fusion
All measurements were acquired with a scanning laser vibrometer on the exterior skin of the aircraft. Two data sets were obtained for each modal test. One data set covered the 38" by 14" area with only 53 measurement points. Measurements were concentrated on the major structural members and around the damage area. A driving point accelerometer FRF was saved for each laser FRF. Fifty averages were used for the 2048 point FRFs. The second data set took a measurement every .5" to produce a measurement grid of 2233 points. Driving point information was not saved. The FRF's were calculated with 10 averages and 1024 frequency lines. The time required to take this large data set was 3 hours and 45 minutes.

Future tests should include shaker excitation on major structural members of the fuselage. Also, the excitation should include the lower frequencies of the spectrum. There appears to be useful information in the lower frequencies of the structure. The laser vibrometer outputs contained a great deal of noise especially when the measurement bandwidth was large. This test series also pointed out deficiencies in the registration (or spatial calibration) of the scanning laser vibrometer which drove later collaborative work to produce more robust algorithms.

These tests were performed in conjunction with Holographics, Inc. and their laser holography based procedures. The intent of this collaboration was to compare laser holography and scanning laser vibrometer technologies and assess complimentary uses. Qualitative comparisons were made which provided the development of concepts for joint application of the technologies. However a quantitative comparison was not possible since the incomplete DC9 test article contained artificial boundary conditions which were not amenable to Holographics technology. APPENDIX B contains a write-up of the experimental aspects of these tests.

Composite Patch Tests - Large-Area

Personnel from the AANC facility are interested in studying the use of composite materials to perform structural repair on commercial aircraft. The development of techniques to verify the installation and monitor the repair is an important aspect of this work. In order to further this study, several boron/epoxy test patches were applied to different structures in the AANC facility. Researchers from the Structural Health Monitoring LDRD used two of these test patches to gain further experience and insight into the use of the scanning laser vibrometer for diagnostic measurements. Scans with 1682 locations and up to 5000 Hz measurement bandwidth (using an electromagnetic/piezo-electric shaker) were attempted on two patches which measured approximately eight inches by eight inches. One patch was a proper installation on the skin of the DC9 test article. The other patch had known flaws and was applied to the B737 test article. In both cases, the noise characteristics of the vibrometer and the high modal density prevented a reasonable interpretation of the data. The patch inspection problem requires a measurement device with a large bandwidth (up to 10,000 Hz) and high spatial resolution. This is different than the stringer inspection problem studied above which requires a large stand-off distance and less bandwidth (up to 2,000 Hz). In fact, laser holography would be an excellent candidate for sensor fusion with scanning laser vibrometer measurements for this work. These data sets may still provide useful information given the advances in information condensation which this LDRD project subsequently provided.

Aluminum Beam Development Test - Large-Area

The two activities mentioned above pointed out the need to develop more robust spatial calibration and data analysis techniques for the scanning laser vibrometer. The Structural Health Monitoring LDRD then collaborated with Virginia Tech (VPI) and two other Sandia LDRD projects to develop the appropriate algorithms. A VPI student, Chris Doktor, performed a series of development tests at Sandia during the summer of 1994. The primary test article was a one meter long aluminum beam. References [43-47] provide technical details which formed the basis for this work. The resulting resection algorithms were then available for later tests at Sandia using the scanning laser vibrometer.

Second DC9 Stringer Test - Large-Area

During the summer of 1995, a second round of tests were performed on the DC9 test article. Experience, hardware changes, and new algorithms were used to improve the quality of the experimental data from the scanning laser vibrometer. The scan pattern was one half the density of the original data. By using one inch centers on the scan locations the number of points was decreased by a factor of four. This allowed decreased testing time and an increased number of points to be acquired. Also, coherence functions were saved to allow checks of data quality. The driving point accelerometer data was acquired separately to reduce the size of the data set. New resection techniques and algorithms provided enhanced spatial calibration of the system. Hardware changes and actively cooling the laser head improved the noise situation and the resulting data. Preliminary analysis of the data was performed immediately following testing as well. Also, it has been found extremely useful to analyze the driving point accelerometer signal to obtain

frequency and damping information. The laser vibrometer measurements are then used to estimate shape information. APPENDIX N provides information on these tests and the subsequent analysis.

Damaged Composite Plates - Large-Area

Also during the summer and fall of 1995, the tests were performed on the damaged composite plates as was mentioned earlier. The tests procedures continued to develop large-area sensor technologies and drew heavily from the 2nd DC9 Stringer tests with a few exceptions. First, the structure was free-free and could undergo pendulum type motions except when constrained by the shaker attachment. Second, the laser head was not actively cooled, although the room was temperature controlled at 68° F. Third, the gross surface was flat as opposed to the curved aircraft fuselage. And finally, the fine surface texture was much rougher than the aircraft skin since it was of composite construction. These differences become important as a unique problem developed during these tests. The data would randomly and without warning produce an averaged measurement that was completely noise with extremely low coherence. This is similar to the problem seen in the simulated aircraft panel tests. An explanation for this effect has not been fully verified, but it is quite probable that laser speckle is the problem. However, a procedure to temporarily avoid the problem was developed. A set of four identical measurement data sets are acquired for each plate. The coherence for each measurement point is integrated to produce a scalar metric for comparison. The data with the highest integrated coherence is retained in a final composite data set. It is possible for one or two points to still be useless in all four data sets. In these rare cases, the neighboring points FRFs are averaged to estimate the missing data. It should be noted that an algorithm could be developed to automatically perform this check and reacquire the data on-the-fly. APPENDIX O provides more detail on these tests.

Damaged Air Compressor Tests - Sensor Fusion

The Structural Health Monitoring LDRD investigators had access to a pair of air compressor impellers with a base radius of six inches. The impellers were identical except one had a known flaw. Tests were performed with traditional accelerometers and **laser holography** using the ESPI system. Although it was not possible to detect the flaw, important concepts for combining laser holography and traditional of large-area sensors were developed. In summary, the ESPI system can provide rapid visualization of operating shapes. This would then allow the scanning laser vibrometer to be used with narrow band excitation to acquire quantitative data on the dynamics. This is the most efficient procedure for using the scanning system. A follow-on development project has been proposed to combine the ESPI visualization and the scanning laser vibrometer resection algorithms into one software/hardware system.

Wind Turbine Blade Root Fatigue Test - Sensor Fusion

Initial attempts were made to combine traditional discrete sensors with NDE **ultrasonics testing** during the Blade/Root Joint test. Before the fatigue test was performed, an ultrasonic inspection was made of the metal/fiberglass bond of the test article. The intent was to perform other inspections during and after the fatigue test to allow comparisons

between the structural health monitoring information from accelerometer data and the ultrasonics inspection results. However, the test specimen failed prematurely in a non-bonded area making such a comparison impossible.

Wind Turbine Blade Fatigue Test - Sensor Fusion

Initial attempts were also made to combine traditional discrete sensors with NDE **acoustic emissions** testing during the fatigue test of the composite blade. The intent was to monitor acoustic emissions during the fatigue test and correlate the results with information from the structural health monitoring studies. An array of acoustic emission sensors was placed on the test object during initial modal testing of the specimen. However, the test article was not conducive to acoustic emissions testing to the high-amplitude (and therefore noisy) resonant fatigue testing. Also, the fibers were good reflectors of the sound waves which further complicated the results.

Summary of Diagnostic Measurements Advances

The series of activities devoted to developing **large-area** measurements (Simulated Aircraft Panel Test, First DC9 Stringer Test, Composite Patch Tests, Aluminum Beam Development Test, Second DC9 Stringer Test, and Damaged Composite Plate Tests) produced a system which can be used effectively for large-area non-contacting measurements. The noteworthy developments include the following:

1. For large structures broad-band excitation is most effective below 2000 Hz;
2. Actively cooling the laser head appears to aid in reducing noise issues;
3. A covering of dye penetrant is useful in acquiring clean data;
4. A test with up to a few thousand data points can be performed with the system;
5. New resection procedures allow better spatial calibration of the laser head;
6. A driving point accelerometer should be used and is important in the subsequent analysis;
7. The laser system seems to produce more random errors with free-free structures; and
8. The coherence function can be acquired and integrated to produce a scalar metric for checking the fidelity of the data.

The series of activities devoted to developing **sensor fusion** techniques (First DC9 stringer test, damaged air compressor tests, wind turbine blade root fatigue test, and wind turbine blade fatigue Test) attempted to combine traditional or large-area diagnostic measurements with laser holography, ultrasonic inspection, and acoustic emissions testing. No conclusive results were obtained from these attempts. However, important experience and directions for future work were obtained. A natural link between laser holography and scanning laser vibrometer measurements can be envisioned. This work spawned a follow-on LDRD proposal to develop such a combined system. The fatigue test environment appears to hold promise for developing structural dynamics/ultrasonics sensor fusion concepts. However, this activity was not possible on this project due to premature failure of the test specimen. The fatigue environment also appears to hold promise for developing structural dynamics/acoustic emissions sensor fusion concepts.

However, a composite test article does not appear to be amenable to acoustic emissions testing. A homogeneous structure would be a better development structure.

Information Condensation

The diagnostic measurement technologies envisioned (and currently under study) to perform structural health monitoring produce at least an order of magnitude more data than more traditional uses of structural dynamics information. A condensation of the data is advantageous and necessary since comparisons to many data sets over the lifetime of the structure are envisioned. Also, since data will be acquired from a structure over an extended period of time and in an operational environment, robust data reduction techniques must be developed to retain sensitivity to the structural changes of interest in the presence of environmental noise. And finally, the intent of structural health monitoring is to augment and/or replace scheduled maintenance and inspections. Therefore, more automatic data reduction procedures are required as the envisioned customers tend to want to use less highly-trained personnel. To operate within these constraints such mathematical constructions as experimental mass, damping, stiffness, and flexibility matrices were found to be powerful tools. The information condensation developments of this project comprise the most unique and important contributions to the structural health monitoring research community. There were four activities which were performed in the area of information condensation which will be discussed.

Static Flexibility Shapes

Early in the project, it was realized that combining mode shape information into a static flexibility shape enhanced damage detection procedures by providing expanded sensitivity and robustness. Additionally, estimating rotations with curve-fitting to neighboring points was seen to provide even greater sensitivity. This approach was exercised on the Rio Grande/I40 Bridge data and the wind turbine quasi-static fatigue data. The results of these studies are provided in APPENDIX E and APPENDIX J. An additional advantage from this development is in the ability to estimate static information from structural dynamics data. A structural dynamics test has several advantages over a statics test: it is much easier to perform, it has much more fidelity in the data, it requires lower input forces, and it may be performed in-situ.

Flexibility Matrix

An improvement over the static flexibility shape is the flexibility matrix which collects all the flexibility information into one mathematical entity. The interesting characteristic of flexibility information is the fact that the lower modes dominate. This is advantageous since these are the modes commonly measured in structural dynamics testing. Another extremely important feature of the flexibility matrix is its robustness in the presence of parameter estimation errors such as split or noise modes. This means that data sets with high modal density can be quickly analyzed in a semi-automated fashion. APPENDIX H and APPENDIX I provide more information on the estimation and use of flexibility information.

Driving Point Flexibilities

A further refinement in the use of flexibility information is the use of the diagonal values or the driving point flexibilities. This subset of the flexibility information allows a rapid and robust indication of the full flexibility properties of the structure. In some cases, the driving point flexibilities can be used to graphically depict damage without an undamaged comparison case. In this manner, an enhanced visual inspection tool is created. It should be remembered that much additional information is available in the off-diagonal flexibility terms which must be mathematically analyzed using damage identification techniques as will be discussed in the next sub-section. APPENDIX N and APPENDIX O provide examples of applying driving point flexibilities to aerospace-type structures.

Experimental Mass & Stiffness Matrices - MAXCON

Modal information can also be condensed into experimental mass and stiffness matrices [33,35]. These are inverse properties to the flexibility matrices and hence do not have the property of being dominated by the lower modal frequencies. However, these mathematical entities can be directly related to analytical FEM models. In fact they can replace reduced FEM models which mask changes in local properties by reduction [24]. The primary issue in creating experimental structural dynamics models is the question of how to complete the rank of the system (which means estimating unmeasured modes). A procedure, which scales the null space of the measured modes to drive the system to an assumed connectivity pattern, was developed in this work and is called MAtriX COmpletioN (MAXCON). Using the experimental matrices which result from MAXCON and coupling to other damage identification tools and an assumed connectivity has been shown to be a powerful tool. APPENDIX J provides the reference for MAXCON.

Summary of Information Condensation Advances

Seven major advances have resulted from this work:

1. The estimation of rotational DOF can provide enhanced sensitivity in some cases;
2. The collection of mode shapes into static flexibility shapes increases robustness and sensitivity of some damage identification schemes;
3. Estimating static flexibility information from structural dynamics data provides a much more effective means of obtaining static information;
4. Flexibility matrices are dominated by low frequency information which is typically easier to measure;
5. Driving point flexibilities can be used as an enhanced visual tool;
6. Experimental structural dynamics matrices can replace reduced FEM models to maintain localized information; and
7. An approach to producing experimental matrices is to scale the null space of the measured modes to drive the resulting matrices toward an assumed connectivity.

Damage Identification

The damage identification development has been associated with producing algorithms to operate on the condensed data to determine if damage has occurred and, if so, to locate

and determine the extent of the damage. Most of the effort in the LDRD project reported herein has been focused on detection and location. The Sandia contributions in the damage identification area have focused on procedures which take advantage of the unique work in diagnostic measurements and information condensation. There are six damage identification activities which will be discussed.

STIFTEST

STIFTEST was developed at the University of Colorado [35] and is a damage identification procedure which evaluates the effective stiffness between two measurement points. This stiffness is calculated mode-by-mode for any two measurement points and then summed over the number of modes. This procedure was used on the simulated aircraft panel test with good success. The procedure formed the conceptual framework for later efforts in the use of experimental mass and stiffness matrices and disassembly. APPENDIX A contains information on the application of STIFTEST to the simulated aircraft panel data.

STRECH

STRECH or Structural Translation or Rotation Error Checking was initially developed at Sandia as a simple tool to locate errors in FEM models with experimental data. STRECH is a procedure which compares the differences between two mode shape (or static flexibility shape) degrees-of-freedom for damaged and undamaged cases. For damage identification, STRECH is especially powerful when used with flexibility data. SRETCH is the only tool developed on the LDRD project which has successfully provided a scalar indicator of global damage (which directly attacks the problem of damage detection). STRECH has also successfully been used to localize damage using data from the simulated aircraft panel, the Rio Grande/I40 bridge, and the wind turbine quasi-static fatigue test. APPENDIX A, APPENDIX E, and APPENDIX J contain information on these applications and background of STRECH.

Characteristic Shape Analysis

Characteristic shapes are the primary deformation shapes seen in a structure undergoing sinusoidal vibration. The Singular Value Decomposition (SVD) is performed on the a data matrix containing deformation information at several time steps during the test. The singular vectors are the characteristic shapes and the singular values are the amplitudes of the characteristic shapes. This type of processing is conducive to resonant fatigue testing which is a sinusoidally excited test. By comparing the characteristic shape data periodically during the test to the initial shapes, a damage identification procedure was expected. This was performed on the wind turbine blade root test data as part of the LDRD studies. The results proved to be inconclusive since the failure occurred outside the instrumented section of the blade. However, the experience gained from this work was useful in later development of a neural network damage identification procedure at Sandia.

Neural Networks

The Structural Health Monitoring LDRD did not fund the development of a neural network based damage identification procedure. However, significant aspects of the LDRD work were used as part of a spin-off effort which did successfully develop this capability. Specifically, the development of static flexibility information condensation and the characteristic shape analysis concepts fed into this neural network development project.

Dynamic Force Residual - MRPT

The Minimum Rank Perturbation Theory (MRPT) is a procedure which traditionally uses reduced FEM matrices of the undamaged structure and modal data from the damaged structure to calculate a dynamic force residual [21]. This residual is processed to determine location and extent of damage. MRPT was used to study the size of FEM as it relates to damage identification. It was found that less refined FEM models had the advantage of requiring less model order reduction, which in turn enhanced the damage identification of the Rio Grande/I40 bridge data. These results can be seen in APPENDIX G. An extension of MRPT was developed at Sandia which used experimentally based models (MAXCON) and matrix disassembly to replace the reduced FEM matrices. This procedure was successfully applied to the wind turbine quasi-static fatigue test data and the Rio Grande/I40 bridge data. APPENDIX J provides the results of this study.

Dynamic Force Residual - Model-based

A new method for identifying the location of structural damage given an initial FEM, experimental frequencies, and experimental mode shapes was developed in this work [52]. This method builds on the concept of the modal force error vector, which is the undamped impedance of the given FEM at each identified frequency multiplied by the corresponding identified mode shape. In order to mitigate the problems associated with reducing analytical models to the set of measurement DOF, a mode shape projection algorithm is utilized. The projection algorithm is a linear least-squares method which can be controlled to minimize bias caused by model errors. The localization indicator is then defined by the modal force error and a DOF-dependent normalization based on the variance of the identified frequencies and mode shapes. The performance of the method in localizing structural damage is examined using experimental data from the Rio Grande/I40 bridge. This work is provided in APPENDIX L.

Disassembly

The development of a novel damage identification procedure based on structural matrix disassembly was also performed on the Structural Health Monitoring LDRD. Disassembly uses a structural matrix (flexibility, stiffness, mass, or damping) and decomposes or disassembles it into local elements. This allows the local properties of the structure to be monitored using experimental matrices composed of modal parameters from the structure of interest. A simplified form of this procedure using simple spring elements has found to be successful in small experimental data sets as seen in APPENDIX J. References [39,40] and APPENDIX N show advanced developments of disassembly. This damage identification procedure is still actively under study using Sandia follow-on funds.

Summary of Damage Identification Advances

The damage identification advances performed on the Structural Health Monitoring LDRD centered around the development of procedures which effectively utilize advances in the other areas, specifically diagnostic measurements and information condensation. STRECH has been expanded to operate on static flexibility shapes. This not only created a localization tool but also a scalar damage detection tool. Work on a characteristic shape analysis did not prove successful on the data set it was applied to. However, this effort fueled later work on a non-LDRD project developed a successful neural network based damage identification procedure which also used static flexibility. Novel procedures to perform disassembly have proven to be successful on small experimental data sets. More advanced disassembly algorithms are currently under study with larger data sets. The MRPT approach has been enhanced using experimentally-derived structural matrices and disassembly and has proven extremely successful in the application to two data sets. A model-based dynamic force residual method and novel mode projection algorithm were also developed.

RECOMMENDATIONS

The work performed on this project points to several recommendations for follow-on efforts:

1. The **resonant fatigue test** concept is a novel method for damage accumulation testing and should be further developed and operationally implemented at Sandia;
2. Since most operational implementations will be in-situ, continued work on the use of **ambient response analysis** should be undertaken;
3. Embedded, miniature, cost-effective, and self-contained **sensor packages** should be developed and made available commercially for external and internal markets;
4. A more **robust scanning laser vibrometer** package which can extract three dimensional information, perform sensor fusion with laser holography and laser ranging, and measure higher frequency information (especially for composite materials) should be developed;
5. Techniques for information condensation which are **hybrid experimental/analytical** should be developed which retain localized information of experimental data without the numerical rank limitations should be developed;
6. To complete the structural health monitoring technology base, work on the fourth stage of lifetime prediction should be initiated, which will require developing a link between the damage identification procedures and **damage mechanics modeling**; and
7. A **National Aging Infrastructure Center** which would include the AANC, the Structural Health Monitoring tools developed on this project, and other structural health diagnostic techniques, should be established at Sandia. This center would attack a broad range of aging infrastructure issues to provide "exceptional service in the national interest".

CONCLUSIONS

As a result of the access to a generalized base of technologies and applications, Sandia National Laboratories has approached the problem of structural health monitoring from a unique perspective. This LDRD project has produced a broader understanding of the structural health monitoring problem and its application to operational structures (**operational evaluation**). Techniques for applying large-scale non-contacting measurement systems in the field (**diagnostic measurements**) have been developed and exercised. This technology produces high spatial density and high modal density data sets with localized information. A set of tools for condensing this localized information into sensitive and robust mathematical constructions based on static flexibility shapes and experimental matrices (such as flexibility, stiffness, and mass) have been developed (**information condensation**). And finally a set of damage identification tools which are tailored to condensed data have been produced (**damage identification**). Each of the four aspects of structural health monitoring have been exercised on a broad range of experimental data. This experimental data has been extracted from structures from several application areas which include aging aircraft, wind energy, aging bridges, offshore structures, structural supports, and mechanical parts. Therefore, Sandia National Laboratories is in a position to capitalize on these unique developments and understanding with further advanced development, operational implementation, and technical consulting for a broad class of the nation's aging infrastructure problems.

REFERENCES

1. Vandiver, J. Kim, "Detection of Structural Failure on Fixed Platforms by Measurement of Dynamic Response", paper OTC 2267, proceedings of the 7th Offshore Technology Conference, Houston, TX, May 5-8, 1975.

2. Kenley, Richard M. and Dodds, Colin J., "West Sole WE Platform: Detection of Damage by Structural Response Measurements", paper OTC 3866, proceedings of the 12th Offshore Technology Conference, Houston, TX, May 5-8, 1980.

3. Coppolino, R. N. and Rubin, Sheldon, "Detectability of Structural Failures in Offshore Platforms by Ambient Vibration Monitoring", paper OTC 3865, proceedings of the 12th Offshore Technology Conference, Houston, TX, May 5-8, 1980.

4. Crohas, H. and Lepert, P., "Damage-Detection Monitoring Method for Offshore Platform is Field Tested", Oil and Gas Journal, February 22, 1982, pp. 94-103.

5. Stubbs, Norris and Osegueda, Roberto, "Global Non-Destructive Damage Evaluation in Solids", International Journal of Analytical and Experimental Modal Analysis, Vol. 5, Number 2, April, 1990, pp. 67-79.

6. Stubbs, Norris and Osegueda, Roberto, "Global Damage Detection in Solids - Experimental Verification", International Journal of Analytical and Experimental Modal Analysis, Vol. 5, Number 2, April, 1990, pp. 81-97.

7. Eggers, David W. and Stubbs, Norris, "Structural Assessment Using Modal Analysis Techniques", proceedings of the 12th International Modal Analysis Conference, Honolulu, Hawaii, January 31 - February 3, 1994.

8. Stubbs, Norris, Kim, Jeong-Tae, and Farrar, Charles R., "Field Verification of a Nondestructive Damage Localization and Severity Estimation Algorithm", proceedings of the 13th International Modal Analysis Conference, Nashville, TN., February 13-16, 1995.

9. Osegueda, Roberto. A.; DSouza, Paul. D.; and Qiang, Yijie., "Damage Evaluation of Offshore Structures Using Resonant Frequency Shifts", PVP-Vol. 239/MPC-Vol. 33, Serviceability of Petroleum, Process, and Power Equipment, presented at the 1992 ASME Pressure Vessels and Piping Conference, New Orleans, LA, June 21-25, 1992.

10. Osegueda, Roberto A.; Vila, Martin; and Mahajan, S. K., "A Modal Analysis Method for Locating Stiffness and Mass Changes in Structures", Developments in Theoretical and Applied Mechanics, Volume XV, Edited by S. V. Hanagud; M. P.

Kamat; and C.E. Ueng, College of Engineering, Georgia Tech University, pp. 333-340.

11. Osegueda, Roberto, "Damage Evaluation of Structures Using Frequencies and Mode Shapes Extracted From Laser Interferometry", Shock & Vibration Information Analysis Center, AD A260119, Nov., 1992.

12. Ferregut, Carlos, Osegueda, Roberto A., and Stephenson, Thomas, "Probabilistic Detectability of Structural Damage Using Frequency Sensitivity Methods", proceedings of the SPIE Smart Systems for Bridges, Structures, and Highways Conference of the 1995 Smart Structures and Materials Conference, San Diego, CA, February 28 - March 3, 1995.

13. Ferregut, Carlos, Osegueda, Roberto A., and Ortiz, Jaime, "Artificial Neural Networks for Structural Damage Detection and Classification", proceedings of the SPIE Smart Systems for Bridges, Structures, and Highways Conference of the 1995 Smart Structures and Materials Conference, San Diego, CA, February 28 - March 3, 1995.

14. Smith, Suzanne W. and McGowan, Paul E., "Locating Damage Members in a Truss Structure Using Modal Test Data: A Demonstration Experiment", AIAA-89-1291, presented at the 30th AIAA Structures, Structural Dynamics, and Materials Conference, Mobile, Alabama, April 3-5, 1989.

15. McGowan, Paul E.; Smith, Suzanne W.; and Javeed, Mehzad, "Experiments for Locating Damaged members in a Truss Structure", presented at the 2nd USAF/NASA Workshop on System Identification and Health Monitoring of Precision Space Structures, California Institute of Technology, Pasedena, CA, March 27-29, 1990.

16. Smith, Suzanne W. and Beattie, C. A., "Simultaneous Expansion and Orthogonalization of Measured Modes for Structural Identification", AIAA-90-1218, presented at the AIAA SDM Dynamics Specialists Conference, Long Beach, CA, April, 1990.

17. Li, Cuiping and Smith, Suzanne W., "A Hybrid Approach for Damage Detection in Flexible Structures", AIAA-94-1710-CP, presented at the AIAA SDM Dynamics Specialists Conference, Hilton Head, SC, April 21-22, 1994.

18. Zimmerman, D. C. and Widengren, M., "Correcting Finite Element Models Using a Symmetric Eigenstructure Assignment Technique", AIAA Journal, Vol. 28, No. 9, September 1990, pp. 1670-1676.

19. Zimmerman, D. C. and Kaouk, "An Eigenstructure Assignment Approach For Structural Damage Detection", AIAA Journal, Vol. 30, No. 7, July 1992, pp. 1848-1857.

20. Zimmerman, David C. and Kaouk, M., "Structural Damage Detection using a Subspace Rotation Algorithm.", AIAA-92-2521-CP, presented at the 33rd Structures, Structural Dynamics, and Materials Conference, Dallas, Texas, April, 1992.

21. Kaouk, Mohamed and Zimmerman, David C., "Structural Damage Assessment Using a Generalized Minimum Rank Perturbation Theory", AIAA-93-1483-CP, presented at the 34th Structures, Structural Dynamics, and Materials Conference, La Jolla, CA, April, 1993.

22. Kaouk, Mohamed and Zimmerman, David C., "Structural Damage Detection Using Measured Modal Data and No Original Analytical Model", presented at the 12th International Modal Analysis Conference, Honolulu, Hawaii, January 31 - February 3, 1994.

23. Zimmerman, David C. and Simmermacher, Todd, "Model Refinement and System Health Monitoring Using Data From Multiple Static Loads and Vibration Tests", AIAA-94-1714-CP, presented at the AIAA SDM Dynamics Specialists Conference, Hilton Head, SC, April 21-22, 1994.

24. Zimmerman, D. C.; Smith, S. W.; Kim, H. M.; and Bartkowicz, T. J.; "An Experimental Study of Structural Damage Detection Using Incomplete Measurements", AIAA-94-1712-CP, presented at the AIAA SDM Dynamics Specialists Conference, Hilton Head, SC, April 21-22, 1994.

25. Simmermacher, Todd; Zimmerman, D. C.; Mayes, R. L.; Reese, G. M.; and James, G. H.; "The Effects of Finite Element Grid Density on Model Correlation and Damage Detection of a Bridge", proceedings of the 1995 AIAA Adaptive Structures Forum in conjunction with the 1995 Structures, Structural Dynamics, and Materials Conference, New Orleans, LA., April 10-13, 1995.

26. Zimmerman, David C.; Kaouk, Mohamed; and Simmermacher, Todd; "On the Role of Engineering Insight and Judgment in Structural Damage Detection", proceedings of the 13th SEM International Modal Analysis Conference, Nashville TN, February 13-16, 1995.

27. Kaouk, Mohamed and Zimmerman, David C., "Structural Health Assessment Using A Partition Model Update Technique", proceedings of the 1995 AIAA Adaptive Structures Forum in conjunction with the 1995 Structures, Structural Dynamics, and Materials Conference, New Orleans, LA., April 10-13, 1995.

28. Kaouk, Mohamed and Zimmerman, David C., "Reducing the Required Number of Modes for Structural Damage Assessment", proceedings of the 1995 AIAA Adaptive Structures Forum in conjunction with the 1995 Structures, Structural Dynamics, and Materials Conference, New Orleans, LA., April 10-13, 1995.

29. Zimmerman, David C.; Simmermacher, Todd; and Kaouk, Mohamed; "Structural Damage Detection Using Frequency Response Functions", proceedings of the 13th SEM International Modal Analysis Conference, Nashville TN, February 13-16, 1995.

30. Zimmerman, David C.; Simmermacher, Todd; and Kaouk, Mohamed; "Model Correlation and System Health Monitoring Using Frequency Domain Measurements", proceedings of the 1995 AIAA Adaptive Structures Forum in conjunction with the 1995 Structures, Structural Dynamics, and Materials Conference, New Orleans, LA., April 10-13, 1995.

31. Doebling, S. W.; Hemez, F. M.; Barlow, M. S.; Peterson, L. D.; and Farhat, C., "Damage Detection in a Suspended Scale Model via Model Update", proceedings of the 11th IMAC conference, Kissimmee Florida, February 1-4, 1993.

32. Doebling, S. W.; Hemez, F. M.; Barlow, M. S.; Peterson, L. D.; and Farhat, C., "Selection of Experimental Modal Data Sets for Damage Detection via Model Update", paper AIAA-93-1481-CP, proceedings of the 34th SDM conference, La Jolla, CA, April 1993.

33. Alvin, Kenneth F., "Second-Order Structural Identification Via State Space-Based System Realizations," CU-CSSC-93-09, Center for Space Structures and Controls, University of Colorado, Boulder, Colorado, April 1993.

34. Alvin, K. F.; Peterson, L. D.; and Park, K. C., "A Method for Determining Minimum-Order Mass and Stiffness Matrices from Modal Test Data", proceedings of the 11th IMAC conference, Kissimmee Florida, February 1-4, 1993.

35. Peterson, L. D.; Alvin, K. F.; Doebling, S. W.; and Park, K. C., "Damage Detection Using Experimentally Measured Mass and Stiffness Matrices", paper AIAA-93-1482-CP, proceedings of the 34th SDM conference, La Jolla, CA, April 1993.

36. Doebling, Scott W., Alvin, Kenneth F., and Peterson, Lee D., "Limitations of State-Space System Identification Algorithms for Structures with High Modal Density", presented at the 12th International Modal Analysis Conference, Honolulu, Hawaii, January 31 - February 3, 1994.

37. Hinkle, Jason D.; Doebling, Scott W.; and Peterson, Lee D., "The Effects of Gravity Preload on the Flexibilities of a Precision Deployable Structure", proceedings of the

1995 AIAA Structures, Structural Dynamics, and Materials Conference, New Orleans, LA, April, 1995.

38. Doebling, S., Alvin, K., and Peterson, L., "Improved Convergence of Estimated Stiffness Parameters for Experiments with Incomplete Reciprocity", proceedings of the 1995 AIAA Adaptive Structures Forum in conjunction with the 1995 Structures, Structural Dynamics, and Materials Conference, New Orleans, LA., April 10-13, 1995.

39. Doebling, S. W., "Measurement of Structural Flexibility Matrices for Experiments with Incomplete Reciprocity", CU-CAS-95-10, Ph.D. Dissertation, Aerospace Engineering Sciences, University of Colorado at Boulder, Boulder, CO, April, 1995.

40. Peterson, L., Alvin, K., and Doebling, S., "Experimental Determination of Local Structural Stiffness by Disassembly of Measured Stiffness Matrices", proceedings of the 1995 AIAA Adaptive Structures Forum in conjunction with the 1995 Structures, Structural Dynamics, and Materials Conference, New Orleans, LA., April 10-13, 1995.

41. Robinson, Nikki A.; Peterson, Lee D.; James, George H.; and Doebling, Scott W.; "Damage Detection in Aircraft Structures Using Dynamically Measured Static Flexibility Matrices", to appear in the proceedings of the 14th SEM International Modal Analysis Conference, Dearborn, MI, February 12-15, 1996.

42. Robinson, Nikki A.; Peterson, Lee D.; James, George H.; and Meza, Raul; "Health Monitoring Studies for Aircraft Applications", to appear in the proceedings of the 1996 AIAA Adaptive Structures Forum in conjunction with the 1996 Structures, Structural Dynamics, and Materials Conference, Salt Lake City, UT., April 18-19, 1996.

43. Doktor, Christopher A. and West, Robert L., "The Extraction of Longitudinal Strain Fields From the Dynamic Response of a Vibrating Beam", presented at the 12th International Modal Analysis Conference, Honolulu, Hawaii, January 31 - February 3, 1994.

44. Montgomery, David E. and West, Robert L., "Modeling of 2-D and 3-D Velocity Response Fields Using a Nonlinear Optimization Formulation", presented at the 12th International Modal Analysis Conference, Honolulu, Hawaii, January 31 - February 3, 1994.

45. Montgomery, David E. West, Robert L., and Wicks, Alfred L. "Estimation of In-Plane Motion Using Multiple Laser Doppler Vibrometer Scans", presented at the 12th International Modal Analysis Conference, Honolulu, Hawaii, January 31 - February 3, 1994.

46. Montgomery, David E. and West, Robert L.; "Identification of Estimated Error Variance in Time Signal Coefficients of Laser Doppler Vibrometer Data", proceedings of the 13th SEM International Modal Analysis Conference, Nashville TN, February 13-16, 1995.

47. Doktor, C. A., "Development of a Statistical Method for Validating ESDM Strain-Field Output," M.S. Thesis, Virginia Polytechnic Institute and State University, Department of Mechanical Engineering, Blacksburg, Virginia, December 1995.

48. Mayes, Randy L., "Error Localization Using Mode Shapes - An Application to a Two Link Robot Arm", presented at the 10th International Modal Analysis Conference, San Diego, CA, February 3-7, 1992.

49. Mayes, R. L., "An Experimental Algorithm for Detecting Damage Applied to the I40 Bridge over the Rio Grande", proceedings of the 13th SEM International Modal Analysis Conference, Nashville, TN, January 31, 1995.

50. Mayes, R. L., "An Experimental Algorithm for Detecting Damage Applied to the I40 Bridge over the Rio Grande", proceedings of the Smart Structures for Bridges, Structures, and Highway Systems Symposium of the 1995 North American Conference on Smart Structures and Materials, SPIE, San Diego, CA, February 26-March 3, 1995.

51. James, G., Carne, T., Hansche, B., Mayes, R., Reese, G., and Simmermacher, T., "Health Monitoring of Operational Structures - Initial Results", proceedings of the 1995 AIAA Adaptive Structures Forum in conjunction with the 1995 Structures, Structural Dynamics, and Materials Conference, New Orleans, LA., April 10-13, 1995.

52. Alvin, Kenneth F., "Robust Model Error Localization For Damage Detection and Finite Element Model Update", proceedings of the 1995 International Adaptive Structures Conference, November, 1995.

53. James, George H., Carne, Thomas G., and Lauffer, James P., "The Natural Excitation Technique (NExT) for Modal Parameter Extraction from Operating Wind Turbines", SAND92-1666, Sandia National Laboratories, Albuquerque, NM, 1993.

54. James, George H., Carne Thomas G., and Marek, Edward L., "In-Situ Modal Analysis of STARS Missile Flight Data and Comparison to Pre-Flight Predictions from Test-Reconciled Models," to appear in Proceedings of the 15th IES Aerospace Testing Seminar, Manhattan Beach, CA, October 11-13, 1994.

55. Farrar, Charles R. and James, George H., "Identification of Dynamic Properties from Ambient Vibration Measurements", proceedings of the Pacific Conference on Earthquake Engineering, Melbourne, Australia, November, 1995.

56. Farrar, C. R., Baker, W. E., Bell, T. M., Cone, K. M., Darling, T. W., Duffey, T. A., Eklund, A., and Migliori, A., "Dynamic Characterization and Damage Detection in the I-40 Bridge over the Rio Grande", LA-12767-MS, Los Alamos National Laboratories, Los Alamos, NM, June 1994.

57. Mayes, Randy L. and Nusser, Michael A., "The Interstate-40 Bridge Shaker Project", SAND 94-0228, Sandia National Laboratories, Albuquerque, NM, April 1994.

58. Jauregui, David V. and Farrar, Charles R., "Comparison of Damage Identification Algorithms on Experimental Modal Data from a Bridge", to appear in the proceedings of the 14th SEM International Modal Analysis Conference, Dearborn, MI, February 12-15, 1996.

59. Jauregui, David V. and Farrar, Charles R., "Damage Identification Algorithms Applied to Numerical Modal Data from a Bridge", to appear in the proceedings of the 14th SEM International Modal Analysis Conference, Dearborn, MI, February 12-15, 1996.

60. Sutherland, H., Beattie, A., Hansche, B., Musial, W., Allread, J., Johnson, J., and Summers, M., "The Application of Non-Destructive Techniques to the Testing of a Wind Turbine Blade", SAND93-1380, Sandia National Laboratories, Albuquerque, NM, June 1994.

61. Doebling, Scott, "Report on Development of a Laser Doppler Velocimeter System", final report for Outstanding Student Summer Program at Sandia National Laboratories, Experimental Structural Dynamics Department, August 1993.

62. Hansche, B., James, G., Pride, N., Roach, D., Schmidt, T., and Webster, J., "Initial Studies on the Use of Laser Velocimetry, in the Inspection and Health Monitoring of Aircraft", Proceedings of the Quantitative Nondestructive Evaluation Conference", Snowmass, CO, August 2, 1994.

63. James, G., Carne, T., Mayes, R., and Reese, G., "Damage Detection and Health Monitoring of Operational Structures", proceedings of the Adaptive Structures and Material Systems Symposium of the 1994 ASME Winter Annual Meeting, Chicago, IL, November 6-11, 1994.

64. James, G.; Roach, D.; Hansche, B.; Meza, R.; and Robinson, N.; "Health Monitoring Studies on Composite Structures for Aerospace Applications", to appear in the proceedings of the 5th ASCE International Conference on Engineering, Construction, and Operations in Space - SPACE '96, Albuquerque, NM, June 1-6, 1996.

APPENDIX A

REPORT ON DEVELOPMENT OF A LASER DOPPLER VELOCIMETER SYSTEM

Scott Doebling

Final Report for Sandia National Laboratories OSSP Program
Albuquerque, NM

August 1993

Intentionally Left Blank

Evaluation of a Laser Doppler Measurement System and Techniques for Damage Detection

Scott W. Doebling
Department of Aerospace Engineering Sciences
University of Colorado at Boulder
Boulder, CO 80309

Abstract

This report contains the details of a study evaluating the use of a laser Doppler velocimeter (LDV) system to acquire modal data. The ability of the LDV to make non-contact measurements in an automated manner makes it attractive as a data acquisition tool. The accuracy of the LDV is assessed relative to measurements from contacting accelerometers, and the LDV is used to measure the mass loading effects of the accelerometers. Additionally, the structure is 'damaged' and retested so that the effectiveness of using the LDV with two damage detection algorithms can be evaluated.

Introduction

Structural damage detection is the process of finding discrepancies between two sets of dynamic response data for the same structure, and then attributing the differences to changes in particular physical parameters of the structure. One way to study damage detection is to conduct a modal survey of the structure in its nominal configuration, then compare the mass and stiffness parameters of the identified model to those obtained from a later test. Such a comparison can be made by using a finite element model (FEM) updating scheme, where the changes in mass and stiffness are inferred by matching the modal behavior of the FEM to the identified modal parameters, or by using a direct comparison between identified mass and stiffness parameters.

Generally, a modal survey is conducted by instrumenting the structure with accelerometers, and then measuring the response of the structure to a known impact or driving force. In the context of damage detection, however, the traditional method introduces some questions about the modal data. First, the mass loading of the accelerometers has an effect on the behavior of the structure, and the effect will be different for two data sets if the sensors are removed between tests. This is true in any modal survey, of course, but is especially important in damage detection because in general the changes in structural characteristics due to damage effects are very small, and are thus likely to go undetected if other factors cause changes in the test results. Second, detecting the damage may require data from a large number of sensor locations, which may be impractical due to testing constraints and the previously mentioned loading effects. Although, if one knew the approximate location of the damage, one could concentrate the sensors in that region of the structure. Thus, a possible strategy is to do a sparse survey of the structure to estimate the general location of the damage, then to do a more detailed survey of the region in question to get a more precise location of the damage. But again, this method is faced with practical limitations and the adverse effects of accelerometer mass loading.

An alternative to the traditional accelerometer survey which may help to alleviate some of these problems is the use of a standoff measurement system, such as the laser Doppler velocimeter (LDV). This type of system allows measurements to be made without loading the structure in any way, and provides sufficient spatial resolution for a very high number of measurement points (typically up to ~16,000,000) within a particular field of view. Such a system can be automated to scan a number of measurement locations and acquire velocity response data at each one. However, the systems are sometimes limited to measuring data at sets of coplanar points, which limits the level of automation of the test. The use of a scanning standoff measurement system thus alleviates the problems of mass loading and provides the possibility of measurements with a high level of spatial density.

This report contains the results of a study done comparing the modal survey results of a traditional accelerometer test and a laser Doppler velocimeter system. The frequencies and mode shapes obtained via each method are compared. The velocimeter data was obtained both with and

without the mass loading of the accelerometers, so that this effect can be studied independently by direct comparison of the identified frequencies. The utility of each method for damage detection was also investigated, by comparing the results using two damage detection algorithms: *STIFTEST* [1] and *STRECH* [2]. The first section of the report gives an overview of the operation of the LDV system. The second section contains a description of the experiments performed. The third section contains the analysis of the test results, including the accelerometer loading effects and the results of the damage detection study.

Overview of the Laser Doppler Velocimeter Measurement System

The velocity sensing apparatus in the laser head is based on the theory of the Michelson interferometer (see Figure 1). [3] In this device, the laser beam is divided into two beams: one reference beam and one signal beam. The signal beam travels out of the laser housing and onto the surface of the test structure. The reflected part of the signal beam travels back into the housing, where it is recombined with the reference beam. When the test structure vibrates, the path length traveled by the signal beam changes, resulting in a modulation in the intensity of the recombined beam. A complete cycle of the intensity modulation corresponds to one-half the wavelength of the signal beam, $\lambda/2$. Therefore, the frequency of the modulation corresponding to a surface velocity ,v, is given by $F_d = 2v/\lambda$. This modulation is known as the Doppler effect, and thus F_d is the Doppler frequency. The recombined beam is sent to two independent detection channels, which have a differing path length such that there is an apparent 90° phase difference between the signals seen by the detection channels. The direction of motion of the surface is indicated by which signal is leading in phase. These signals are modulated by internally generated signals, which are also 90° out of phase, and which have a common carrier frequency of F_c. When the two resulting signals are summed, the result is a single output with frequency $F_c \pm F_d$. A frequency tracking circuit then generates an analog frequency proportional to the velocity of the test surface. The capabilities of the LDV system are summarized here [3]:

Velocity Range: ± 1 μm/s to ± 1 m/s
Frequency Range: DC to 300kHz
Standoff Distance: 200 m (depending on surface properties)

The primary sets of hardware used to acquire test data with the Lazon system are shown in Figure 2. The laser head contains the laser source, the Doppler conversion system and the rotating mirrors which position the laser beam at the appropriate test point. The Lazon laser driver unit converts two analog input voltages into servo commands for the position mirrors, and provides power for the mirrors and the Doppler conversion system. The Zonic System 7000 Front End is used as the A/D and D/A unit for testing with the Lazon system, although any front end could theoretically be used. Four analog output channels are used: Two send command voltages to the positioning mirrors, and two send command voltages to the modal shakers. Three analog inputs are used: One carries the velocity signal from the laser head, and the other two carry the force signals from the load cells. (Note that when only one shaker is used, the other analog input can be used for another measurement, such as a driving point accelerometer.)

Control of the Lazon system is accomplished using the LSI software package, which generates System 7000 commands using Zonic Engineering Test Analysis software (ZETA). ZETA is the command-driven, interpreted language which can issue commands directly to the System 7000 to control actions such as excitation, data acquisition, signal conditioning and signal processing. When the user runs the LSI software package, ZETA runs underneath it and is essentially invisible, although LSI does allow the user to issue ZETA commands directly (e.g. to set up channels to accept ICP inputs). LSI generates a list of points on the structure to scan using a universal group file and a universal geometry file. The user chooses four 'registration points' on the structure and manually positions the beam at each of these four locations. Based on the mirror command voltages which define these four locations, LSI generates a coordinate transformation between the local structure coordinates and the reference frame of the laser head. Then LSI interpolates the locations of the points in the group file using this coordinate transformation and the information in the geometry file. The user can then set up the data acquisition parameters and choose the TDAS storage functions. This sensor works like a 'roving accelerometer', acquiring data for

the full sequence at one measurement location, and then moving to the next one. LSI is equipped to handle four analog outputs from the System 7000 (two of which position the laser mirrors) and four analog inputs (one of which is the velocity signal from the laser head). The flexibility of ZETA would allow the user to write a batch routine to simultaneously acquire LDV and accelerometer data.

Experimental Testbed and Procedure

The structure used for this experiment is an aluminum plate with three parallel L-brackets running horizontally across it. It is a representation of a typical section of aircraft skin. Each bracket is held on by a row of bolts, spaced at 1" increments across the plate. The plate is suspended for the tests with a nylon cord through a hole in the center of the top stringer where the bolt has been removed. For the accelerometer portion of the test, the measurements were made in a four-by-four grid as shown in Figure 3. For the LDV portion of the test, the measurements were made in a seven-by-seven grid as shown in Figure 4. The driving point is indicated by an 'x' in both of these figures. The data was acquired using a modal shaker with continuous random excitation for 20 averages of about 4 seconds each, using a Hanning window with 25% overlap.

There are three variables present in the test matrix for this experiment. The first is the measurement device - either the LDV or the accelerometers. The second is the loading of the structure due to the attached accelerometers. The third is the damage level of the structure - either damaged or undamaged. The combinations of these variables which were assessed are listed in Table 1. The damage was inflicted to the structure by replacing the center stringer with one which is 8" shorter on one end, as shown in Figure 5. It should be noted that the torque levels of the bolts were not controlled, which could have caused some additional variation in the response of the structure.

For case 1 (undamaged, accelerometers), eight modes were extracted from the data in the frequency range 0 - 100 Hz. The frequencies and damping ratios for these modes are shown in Table 2. The normal mode shapes are shown in Figure 6. These mode shapes follow a classical bending-torsion

pattern, with the stiffening effect of the stringers changing the response somewhat from what would be expected of a simple plate.

Two main problems were encountered during the acquisition of this data. First, a primary mode was missed because the driving point was aligned with the node line. This mode is a 'saddle mode' where the diagonally opposite corners move in phase with each other, and the adjoining corners move opposite each other. Second, a suspected misalignment in the LDV optics caused the amplitude of the Doppler signal to drop out quite frequently, which put a high variation on the measured velocity. This variation, which changed the magnitudes of the response peaks greatly from one ensemble to the next, totally erased any consistency between peak magnitudes. Thus, the mode shape information from the LDV was totally unreliable. However, there was still a sufficient increase in response magnitude at the modes to allow extraction of the modal frequencies.

Analysis of Results

One of the effects that can be examined using the LDV is the shift of measured frequencies due to the mass loading effect of the accelerometers. When accelerometers are mounted to a structure, it is generally assumed that their effect on the response of the structure is negligible, or at least reproducible in the model, since there is no way to measure the effect. However, the response of the structure can be measured with the LDV both before and after the accelerometers are attached, allowing the changes in response due to the loading to be assessed. To do this, we compare the frequencies of the measured modes in cases 2 and 6, as shown in Figure 7. Case 2 represents the measurements made by the LDV with the loading present, and case 6 is the LDV measurements without loading. It can be seen that for each mode on the chart, the value of the frequency is reduced slightly by the effects of the loading. The average reduction in frequency due to the loading is 3.30%.

Another issue that can be addressed by analyzing the frequency information is the difference in accuracy of the LDV and the accelerometers. This can be examined by comparing the frequencies of cases 1 and 2, as shown in Figure 8. Case 1 is the accelerometer measurement, and case 2 is the loaded

LDV measurement. It can be seen in the figure that the frequencies are consistently even for the first eight modes. The average frequency difference is 0.21%, which would be considered acceptable for most applications. Therefore, the relative accuracy of the LDV is the same as that of the accelerometers.

In order to assess the changes in the structure due to damage, the first things to look at are the changes in mode shapes and modal frequencies. The mode shapes can be compared using a linear Modal Assurance Criteria (MAC) plot of the damaged and undamaged mode shapes, as shown in Figure 9. The entries in the matrix which have values close to unity indicate mode shapes that correspond to each other. The values along the left axis are the modes from the undamaged structure, and the values along the right axis are the modes from the damaged structure. It can be seen that the first five modes of the undamaged case correlate well, but that the remainder fail to produce strong correlation with any modes from the damaged case. This is an example of how the structural response can change enough that it is difficult to locate two modes which 'correspond' to each other. This can cause a problem with many model update and damage detection techniques, which often depend on analyzing the frequency shifts for a particular mode. When a mode disappears or when a new mode shape appears after damage, tracking frequency shifts becomes difficult to impossible. Figure 10 shows the changes in modal frequency for each mode extracted from the accelerometer data. It is interesting to note that most of the lower modes undergo an increase in frequency after the damage due to the reduction in mass, but some higher modes undergo a decrease in frequency due to the reduction in stiffness.

Two damage detection algorithms are used in this study. The first is STIFTEST [1], which arose out of Alvin's work in extraction of second-order mass and stiffness matrices from state-space (ERA-type) realizations. This method evaluates the effective stiffness value between two points on the structure using the normal mode shapes and the modal frequencies. The effective stiffness is calculated mode by mode for a particular DOF pair, and then the values for all modes are summed. By calculating the stiffnesses for two different data sets, the differences between the effective stiffness of each element can be obtained. These differences can be interpreted in terms of damage along that element. Since it sums the differences over all modes

before making the comparison, this method can easily incorporate information from higher frequency modes.

The second damage detection algorithm is STRECH. [2] STRECH was first developed to assess the differences between experimental and analytical models. Here, the concept is extended by comparing two experimental models, one damaged and one undamaged. STRECH determines a 'stretch factor' between two locations based on the displacement and rotation mode shapes. By taking the ratios of the corresponding stretch factors between two cases, the change in stiffness between those two DOF can be assessed. Experience has shown that this method seems to work very well on lower frequency modes, but not as well on higher frequency modes. The primary difference between these two methods is the way in which the model comparison is made: STIFTEST sums over all the modes, then compares; STRECH compares, then can sum over the modes for a superposition of the solutions. Both methods are applied to the FEM solution and the experimental data in the following sections. The results of the damage detection analyses are presented as color plots of the elements between each of the accelerometer locations. The colors represent the magnitude of the difference of the indicator values (element stiffnesses in the case of STIFTEST, and stretch values in the case of STRECH), with red representing the elements with the most change and blue representing the elements with the least change. These element connectivity plots are oriented the same as the structural diagrams in Figure 3.

The first damage detection analysis uses the modes from the FEM solution. The results from the STRECH analysis, which used the first flexible mode, are shown in Figure 11. The result shows a high stretch factor for the element parallel to and just above the middle of the center stringer. The STRECH result is rather vague, but it should be noted that the rotational DOF were not included in the STRECH analysis. Additional work by Mayes has shown that these rotational responses can be critical, and this result tends to support that conclusion. Therefore, it is thought that including the rotations would greatly improve the result. Including translational DOF from additional modes did not significantly improve the solution. The results from STIFTEST are shown in Figure 12. The STIFTEST analysis was performed using the first 10 flexible modes, and shows high stiffness reductions in the the four members parallel to the middle stringer which are

the closest to the damage area. The STIFTEST result reflects the reduction in lateral bending stiffness due to the damaged stringer. This result benefits greatly from the ability to incorporate information from all of the available modes. It should be noted that there are no reductions in stiffness in any of the diagonal elements, indicating that only a small amount of strain energy was stored in these elements for the given modes. Perhaps higher frequency modes would have contributed more information about these elements.

The second damage detection analysis uses the measured modes. The results from STRECH are shown in Figure 13. This STRECH analysis is a superposition of STRECH ratios from undamaged modes 1, 2 and 3, and damaged modes 2, 3 and 4. In this case, STRECH identifies reduced stiffness in the diagonal elements across the area of the damaged stringer. This indicates that sufficient information is contained in the measured modes to identify the reduction in stiffness in these elements. The results from STIFTEST are shown in Figure 14. The STIFTEST analysis was performed using the first 8 modes in the undamaged case and the first 9 modes in the damaged case. STIFTEST also locates the reduced stiffness in the diagonal elements across the area of the damaged stringer. Additionally, STIFTEST incorrectly locates a reduction in a diagonal element in the area which is directly opposite the damaged stringer. This apparent reduction is due to the symmetry of the identified mode shapes, and is a common effect in damage detection analysis. It is suspected that adding higher frequency modes will eventually contribute enough information to discriminate between the ends of the stringer. The ability of STIFTEST to use a large number of modes is quite advantageous in this type of situation.

Conclusions

The laser Doppler velocimeter is theoretically capable of making accurate, high bandwidth measurements with large standoff distances. The data acquired has confirmed that the LDV produces accurate frequency information (relative to the accelerometers), but the accuracy of the mode shapes cannot be confirmed until the optics have been repaired. In terms of the practical aspects of employing the LDV for modal testing, there is a trade-off between using the LDV or traditional accelerometers. The accelerometers

generally have a longer set up time and add a loading effect to the structure (shown in this case to shift frequencies by about 3.3 %). However, the LDV requires line-of-sight to a coplanar set of points, and requires more data acquisition time since measurements are made one location at a time.

The two damage detection algorithms performed better on the measured data than they did on the FEM solution. Overall, STIFTEST seemed more accommodating to higher frequency modes, and the STRECH results could probably be improved by incorporating into the mode shapes the rotational degrees of freedom.

Further Research

To further develop the utility of the LDV as a tool for modal data acquisition and damage detection, the following studies are suggested:

- Re-acquire the data from the damaged structure when the LDV has been repaired, and see how the higher spatial resolution of the LDV measurements improves the damage detection results.
- Assess the robustness of the LDV system by using it in a field environment.
- Develop methods for using modal data from the LDV in conjunction with non-destructive inspection (NDI) techniques for the inspection of aircraft structures.

Acknowledgments

This work was performed while the author was an OSSP Summer Intern in Department 2741, Experimental Structural Dynamics, of Sandia National Laboratories in Albuquerque, NM. The author wishes to thank George James and Randy Mayes of Sandia for their contributions to the data acquisition and damage detection phases of this report, and Garth Reese, of Sandia Department 1434, for performing the finite element analysis.

References

1. Alvin, Peterson, Doebling, Park, "Damage Detection using Experimentally Measured Mass and Stiffness Matrices," 34th AIAA Structures, Structural Dynamics and Materials Conference, April, 1993

2. Mayes, R., "Error Localization Using Mode Shapes - An Application to a Two-Link Robot Arm," 10th International Modal Analysis Conference, February 1992.

3. *Lazon User Manual*, Zonic Corporation, Milford, OH, 1993

Table 1: Test Cases

Case Number	Meas. Type	Loading Condition	Damage Level
Case 1	Accel	Loaded	Undamaged
Case 2	LDV	Loaded	Undamaged
Case 3	LDV	Loaded	Damaged
Case 4	Accel	Loaded	Damaged
Case 5	LDV	Unloaded	Damaged
Case 6	LDV	Unloaded	Undamaged

Table 2: Extracted Frequencies and Damping Ratios

Mode Number	Frequency (Hz)	Damping Ratio (%)
1	8.92	2.20
2	16.14	0.86
3	29.69	0.82
4	52.92	0.52
5	56.81	0.51
6	75.27	0.95
7	77.02	0.85
8	82.53	1.43

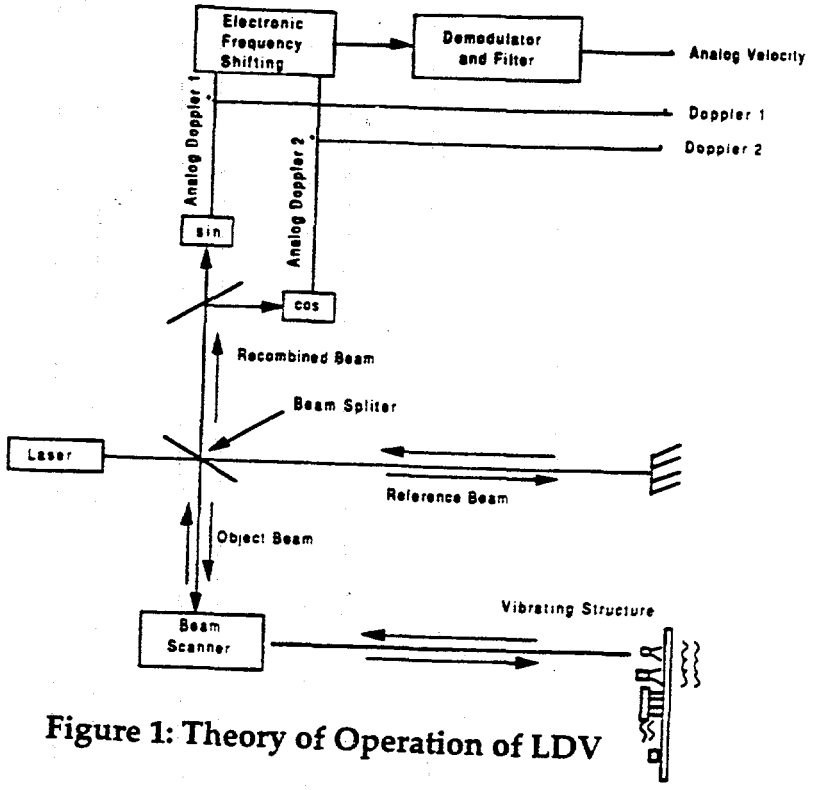

Figure 1: Theory of Operation of LDV

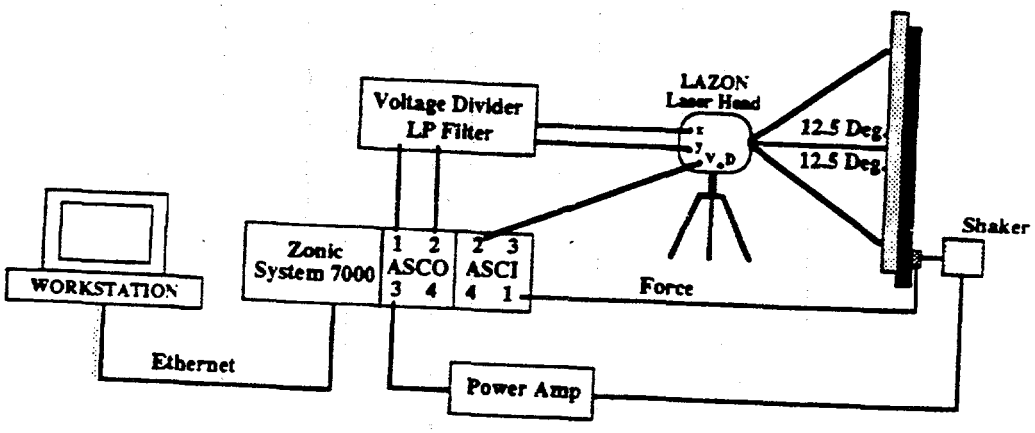

Figure 2: Operational Configuration of LDV

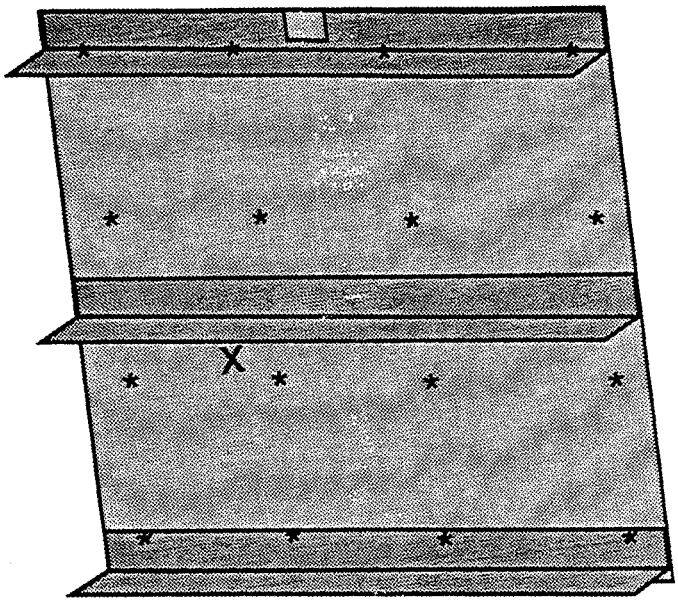

Figure 3: Measurement Locations for Accelerometers

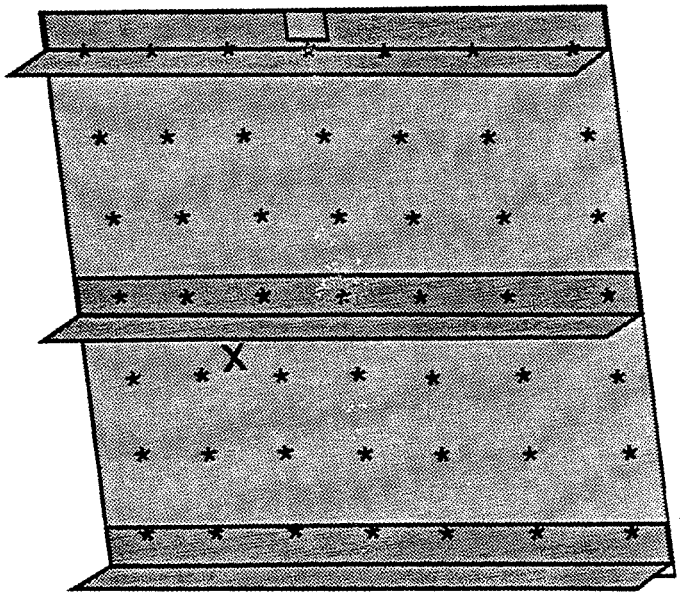

Figure 4: Measurement Locations for LDV

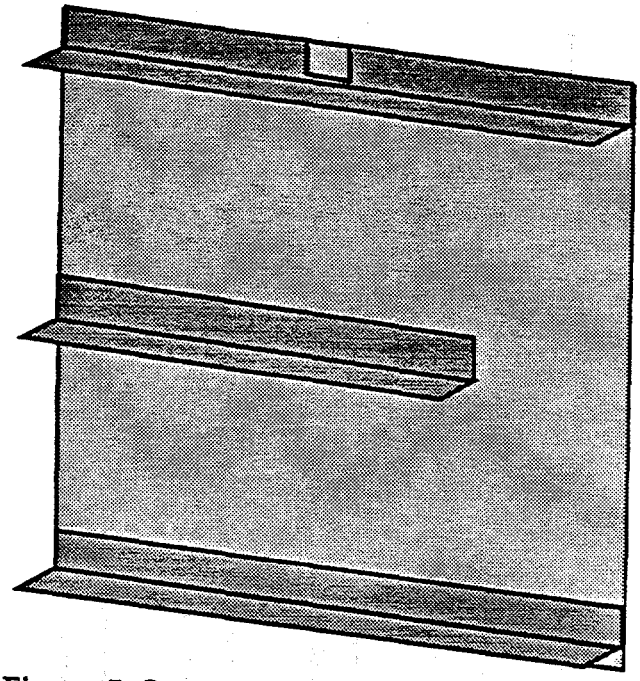

Figure 5: Structure with Damaged Stringer

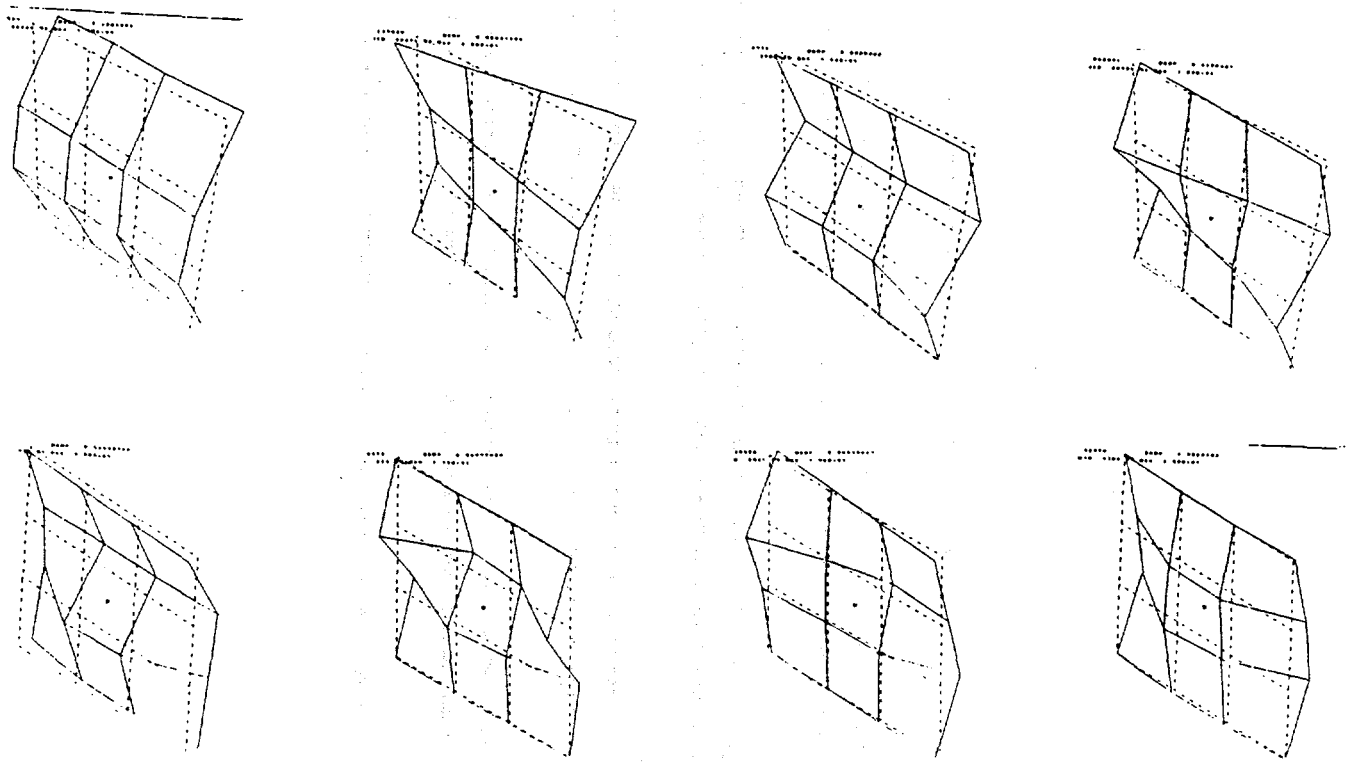

Figure 6: Measured Mode Shapes

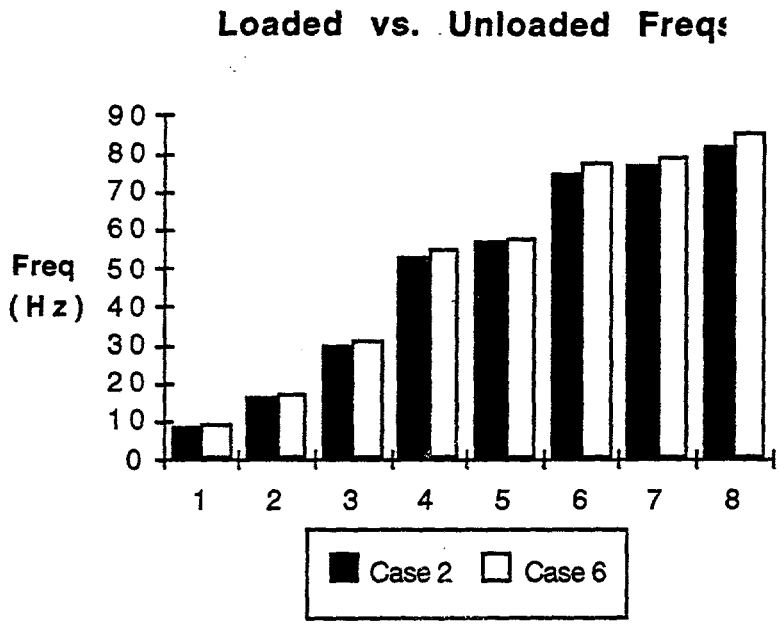

Case2: Loaded
Case 6: Unloaded

Figure 7: Comparison of Frequencies for Loading Effects

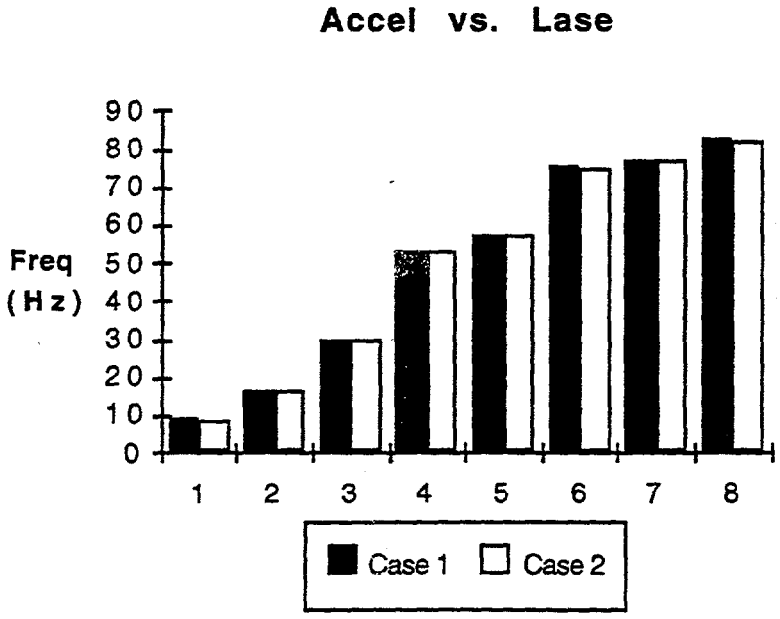

Case 1: Accelerometers

Case 2: Loaded, LDV

Figure 8: Comparison of Frequencies for Accuracy

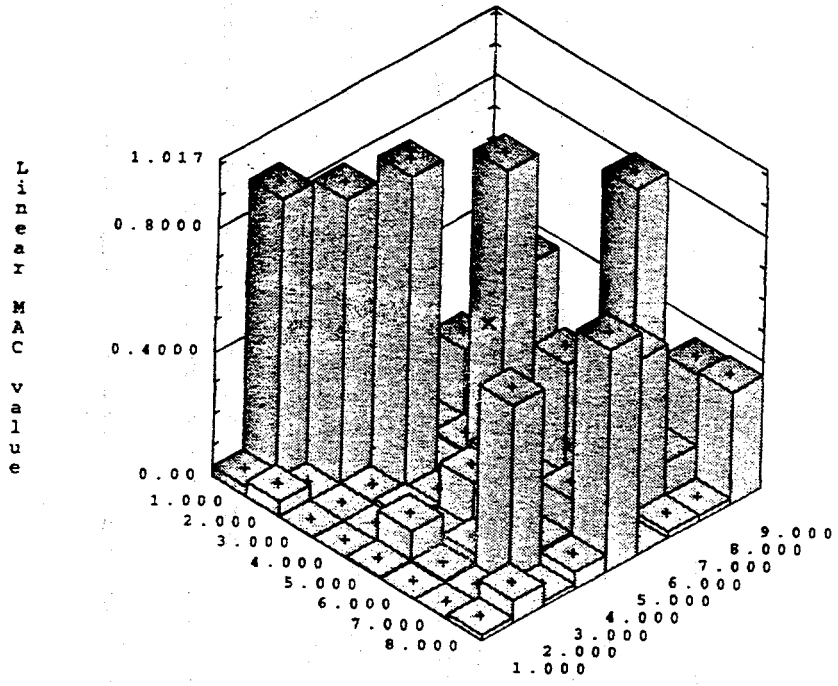

Figure 9: MAC Plot for Undamaged and Damaged Modes

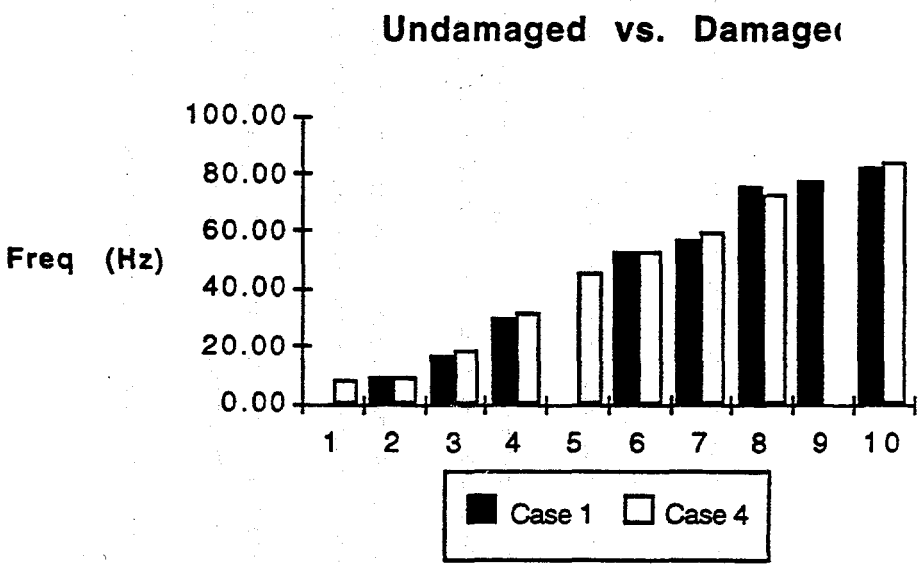

Case 1: Undamaged

Case 4: Damaged

Figure 10: Frequency Comparison for Damage Effects

Figure 11: STRECH Results for FEM Solution

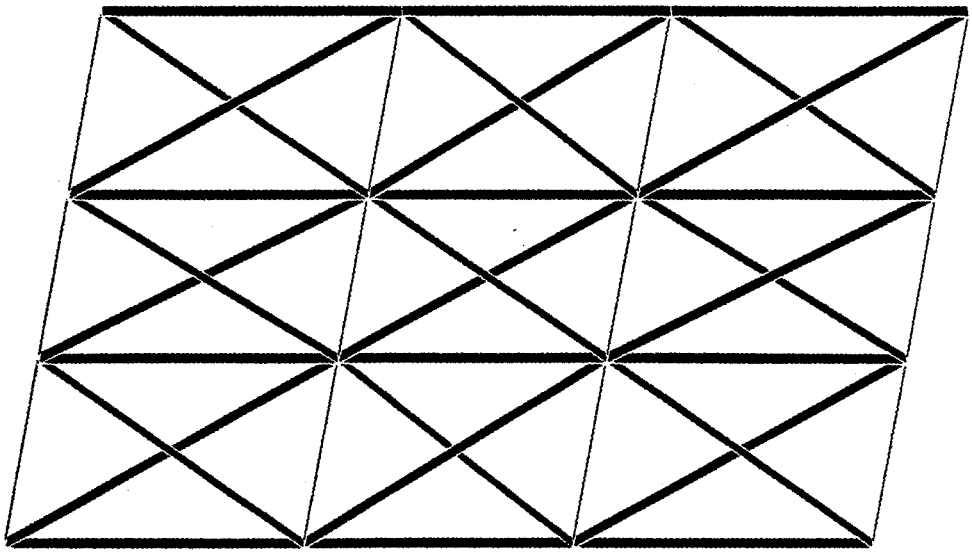

Figure 12: STIFTEST Results from FEM Solution

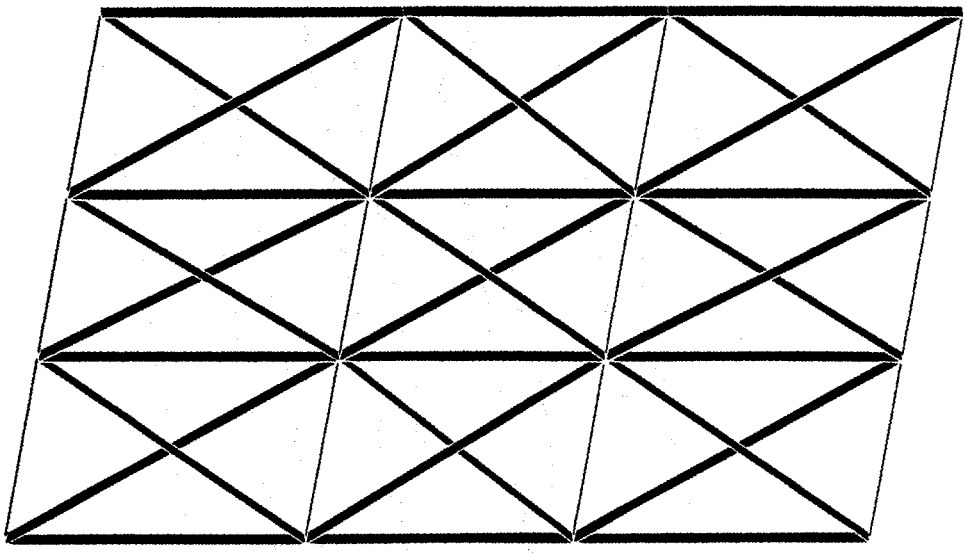

Figure 13: STRECH Results from Measured Modes

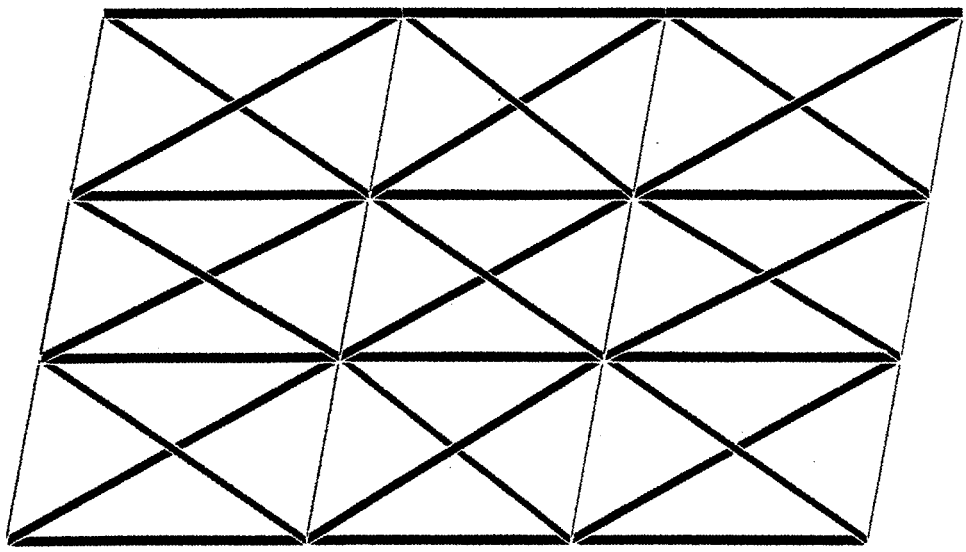

Figure 14: STIFTEST Results from Measured Modes

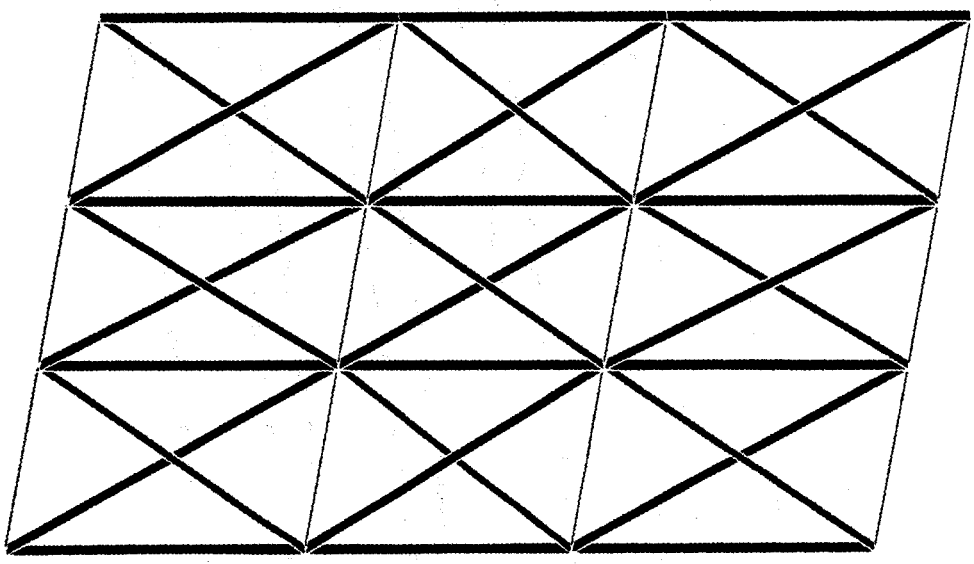

APPENDIX B

INITIAL STUDIES ON THE USE OF LASER VELOCIMETRY IN THE INSPECTION AND HEALTH MONITORING OF AIRCRAFT

Bruce Hansche, George James, Nathan Pride, Dennis Roach, Tim Schmidt, and John Webster

Proceedings of the Quantitative Nondestructive Evaluation Conference Snowmass, CO

August 2, 1994

Intentionally Left Blank

INITIAL STUDIES ON THE USE OF LASER VELOCIMETRY IN THE INSPECTION AND HEALTH MONITORING OF AIRCRAFT

Bruce Hansche, George James, and Dennis Roach
Sandia National Laboratories
Albuquerque, NM 87185

Nathan Pride, Tim Schmidt, and John Webster
Holographics Inc.
Long Island City, NY 11101

ABSTRACT

During routine inspections of commercial aircraft, various forms of surface corrosion, or other surface defects, are often encountered. However, it is difficult to assess the need for structural repair without a complete knowledge of the corresponding damage to the subsurface structure. Therefore, it is important for inspection techniques to be able to quickly assess the health of a structure, including subsurface damage, with only access to the external inspection surface. Modal and structural dynamics measurements hold promise for the global non-destructive inspection of a variety of structures including aircraft. Surface measurements of a vibrating structure can provide information about the internal members without costly - or sometimes impossible - dismantling of the object. However, there are limitations with the traditional measurement techniques for these parameters (modal frequencies, modal damping, mode shapes, and frequency response functions). Modal testing techniques can cover a broad frequency band and have a large array of mathematical tools for signal processing and data analyses. Modal testing is normally characterized by contact sensors, low spatial density, and low frequencies (less than 1 kHz). These limitations severely restrict the ability of modal techniques to locate the type of damage seen in aircraft. Full-field techniques, such as laser holographic interferometry, provide high frequency, high spatial density measurements in a non-contact fashion. However, laser imaging techniques like holographic interferometry operate on a single vibration frequency at a time, and do not have the same level of mathematical processing support as modal techniques.

Laser velocimetry provides a "best of both worlds" approach with some additional advantages not found in either modal or coherent optics techniques. With laser velocimetry, full-field, high-frequency, high spatial density measurements can be obtained in a non-contact fashion. Quantitative data, in the form of frequency response functions are available for mathematical analyses. In addition, laser velocimetry can acquire broad-band frequency information and spatial sampling positions can be controlled through data acquisition software.

This paper discusses the application of laser velocimetry based measurements to the inspection of metallic and composite aircraft structures. An initial induced flaw experiment, where an aircraft stringer was damaged in successive stages, provided an opportunity to prove the

viability of this technology in aircraft health monitoring. Initial studies on aircraft composite structures have shown that this approach can detect adhesive debonds and delaminations in the composite patch lay-up. An acoustically coupled, broad area excitation technique has been developed to support the composite work. Within the constraints of spatial resolution requirements, areas of up to one square meter can be covered in a single scan producing a quasi real-time result.

INTRODUCTION

A major portion of the structure of a modern transport aircraft consists of a relatively thin skin fastened to underlying elements such as stringers, frames, and ribs. All of these structural elements are critical, and flaws such as corrosion, cracks, and fastener or bond failure must be detected at an early stage. Flaws like cracks or failed fasteners in substructure (stringers, frames, etc.) are currently detected by a painstaking internal visual inspection, which requires complete teardown of the aircraft. Some flaws, such as corrosion, may manifest on the surface of the aircraft and can be detected by an external visual inspection. Even in this case, the internal extent of the flaw cannot be easily determined, and inspectors must determine whether to remove the skin for further inspection. These expensive disassembly and inspection processes create a great interest in nondestructive inspection techniques which can detect subsurface defects by observations made on the surface of the aircraft.

In this paper, we describe some initial verification experiments applying modal analysis techniques to detect some typical aircraft structural flaws. Conventional modal data is taken by fastening an array of sensors (typically accelerometers) to a structure, mechanically driving the structure, and recording the response at each sensor. Application of the sensors is itself time consuming, and for a thin-skinned structure such as an aircraft, the mass loading of the sensors may significantly affect the results. Hence, in this study we have used laser Doppler velocimetry (also known as laser Doppler vibrometry, or LDV) instead of accelerometers to measure surface response to the driving signal.

We begin by discussing some of the aspects of system health monitoring by modal techniques. We give a brief description of the LDV technique and compare it to conventional modal data taking. We describe two preliminary experiments using LDV and modal analysis for flaw detection, and conclude by suggesting what the next steps might be.

HEALTH MONITORING VIA MODAL TECHNIQUES

Today's society depends upon many structures (such as aircraft, bridges, wind turbines, offshore platforms, and buildings) which are nearing the end of their design lifetime. Since many of these structures cannot be economically replaced, techniques for damage detection and health monitoring must be developed and implemented. Modal and structural dynamics measurements hold promise for the global non-destructive inspection of a variety of structures since surface measurements of a vibrating structure can provide information about the health of the internal members without costly (or impossible) dismantling of the structure. Advanced signal processing, non-contacting and embedded sensors, and analysis/test correlation technologies combine to make this a promising approach for the health monitoring of operational structures.

At Sandia, we have a research and development program underway to investigate health monitoring via modal techniques. Reference [1] describes this program, gives a review of related work at other institutions, and briefly describes three experiments conducted so far: a highway bridge, a wind turbine blade, and the aircraft experiments we cover in this paper. The basic idea is that flaws of interest will affect the stiffness of the structure, which will in turn affect its modal

response. The major questions we are trying to answer are: will detectable changes in modal properties occur before the flaw becomes critical; what modal parameters are most sensitive to a particular flaw type; and how can we analyze the data to most readily and conveniently detect these parameter changes?

Excitation Techniques

To conduct a modal test, the structure is typically excited with a known or measurable input which is stronger, in the frequency range of interest, than the ambient mechanical noise. Mechanically driving the structure at a point, as with an electromagnetic shaker or impact hammer, provides good energy transfer into the structure. The driving energy is spatially nonuniform, however, and the area over which the signal has sufficient amplitude may be limited. Air coupled excitation, as with a speaker or point noise source, can provide more uniform excitation, but the energy transferred to the structure is significantly less, the actual signal delivered to the structure is hard to quantify, and the sound may be sufficiently loud to cause personnel hazards. For either driving method, waveforms may be constant-frequency sinusoidal, swept sinusoidal, broad band random, or pulsed, depending on the test. We have used various combinations, as will be described below.

Measurement Techniques

The usual means of collecting modal data is by an array of transducers (typically accelerometers) attached to the structure. Disadvantages of this technique include the time consumed in placing the transducers, and the mass loading they contribute to the structure. The sensor array is typically spatially sparse, with a maximum of a few hundred sample points. Advantages are that the sensors can be mounted for sensitivity to either in-plane or out-of-plane motion, so by mounting three accelerometers per sample location, vector information can be obtained. Also, the sensors provide information in parallel, so that within the limitation of the sampling/multiplexing electronics, measurements are taken simultaneously at each location.

The scanning LDV is a non-contact optical "transducer" sensitive to surface velocity. Its major advantages over accelerometers are versatility in selecting spatial sample points, and its noncontact nature. Its main disadvantages include sequential (as opposed to parallel) data taking, and possibly its scalar (as opposed to vector) sensitivity. Note that the LDV reads velocity as opposed to acceleration.

Another optical technique useful for surface displacement measurements, which we mention here for completeness, is holographic interferometry or holometry. Holometry can be used to measure surface displacements on the order of microns, either in a time-average or double exposure mode. It is an imaging technique, so the sample grid can be very dense, typically 512 by 512 points taken simultaneously. For modal analysis, it can be used in a sine-dwell mode, allowing rapid visualization of operating shapes at a particular frequency. Several images can be made at various frequencies, and the results used to aid in positioning accelerometers or LDV sample points, which can then get time-resolved broad band information for further modal analysis. We are currently working on integration of holographic and LDV instruments at Sandia.

Analysis Techniques

The core question in the modal health monitoring project is "can we detect flaws?" The two major subsets to this question are "what data shall we take?", and "what do we do with the data once we have it?". Ideally, we can develop analysis techniques that are sufficiently straightforward or automatic to be fieldable in the sense that they can be applied by a technician in a rote manner. Currently, we are in the mode of trying various analysis techniques on known flaws to see which works best. In all cases, this is a comparison technique. Ideally, we could

compare our results with a theoretical prediction from, for example, a finite element mechanical model based on as-designed information. For structures as complex as aircraft, this is probably an unachievable goal-- as-designed information of sufficient detail is difficult or impossible to obtain, and even with it, we believe it would be extremely difficult to sort out acceptable variations in response from actual flaw indications. For now, we are concentrating on before-after comparisons, which require a set of baseline data on the actual structure.

The raw data from these tests is a set of amplitude signals representing either acceleration or velocity at each sample point. Standard modal data acquisition hardware provides rapid Fourier transform capabilities, so for broad band excitation functions such as random or impulse, the frequency response functions (FRF's) can be calculated and stored for each sample point. Of course, if a single frequency (sine-dwell) excitation is used, the raw data consists of structural response at that frequency only. Before-after comparisons of various parameters, such as mode frequency, response amplitude at a particular frequency, and damping can be made on a point-by point basis. One attractive analysis technique is to plot amplitudes of one of these parameters as an image, and use the eye-brain system of the observer to correlate the data spatially and do the global before-after comparison.

Even if the flaw is not readily evident in the parameter comparisons described above, sufficient information may be contained in the entire data set to detect it. A modal extraction on the full data set can be performed, and mode amplitudes (as opposed to the operating shapes described above) can be plotted as an image. Other more sophisticated analysis algorithms, such as the modified STRECH technique [2] are also being considered. At the Center for Aerospace Structures, U. of Colorado algorithms are being developed around the extraction of second-order structural parameters (mass and stiffness) directly from modal data. These could result in plots of structural stiffness similar to the velocity and mode amplitude plots presented here.

LASER DOPPLER VELOCIMETRY

The Doppler effect is the shift in frequency seen when a periodic wave (monochromatic laser light in this case) scatters from a moving object (the surface under test). In most practical cases, the light used to sense velocity v is that which is scattered back in the direction of illumination--in this case, the frequency shift is $\Delta F = 2v/\lambda$. A laser Doppler velocimeter (LDV) instrument contains an optical interferometer which interferes the scattered light with an internal reference beam to detect the frequency F, and usually electronics to convert this frequency to an output voltage proportional to F. Thus, the instrument appears to be a noncontact transducer which has a voltage output proportional to instantaneous surface velocity. These instruments have a large dynamic range. Depending on frequency, commercial LDV instruments can measure from one micron per second to about one meter per second, which translates to amplitudes of .001 micron to one meter. Other LDV models are commercially available that extend these ranges. The instruments we used contained programmable scanning mirrors to direct the laser beam, allowing interrogation of a large number of data points. Reference [3] covers optical Doppler signal processing in some detail.

The LDV has several advantages over mechanical transducers for modal testing. It produces no mass loading, so it can be used on very light objects or in hostile environments. The number and location of the sample points are software programmable, so not only can a moderately dense array of points be sampled (perhaps several thousand points per test), but the sample locations can be changed easily, even dynamically during the test. The scanning LDV also has some disadvantages. The data is read one point at a time, and the integration time may be many

seconds per point, depending on signal bandwidth and noise. This means that the drive signal must be stationary or repeatable, perhaps for hours. Also, the coherent light interacts with the diffuse test surface to produce a speckle pattern, which is a random intensity variation in the scattered light. At a particular sample point, the intensity reaching the detector can be zero, producing a signal dropout. The data taking algorithm may need to sense these dropouts and repeat the measurement at a few points. Naturally, optical access is required to the test surface, either by line-of-sight, relay optics, or fiber optics.

By using a triaxial installation, accelerometers can read true vector information at each sample point. With the LDV, only one scalar measurement is made per sample point: velocity in the direction of the laser beam. This means that the sensitivity to a particular motion vector (such as out-of-plane, normal to the surface) may vary as the angle of incidence of the interrogating beam changes for each sample point. Also, to get vector information, the LDV head must be positioned at three separate locations, samples taken at the same set of points, and the data merged. This makes both data taking and analysis quite complex--practical solutions to this problem are the subject of current research.

EXPERIMENTS

DC-9 Controlled Damage Experiment

An induced damage test was performed on the front fuselage of a decommissioned DC-9 transport aircraft, which is one of the samples in Sandia's Aging Aircraft Test Specimen Library. A Zonic LAZON system was used to acquire broad-band frequency response functions using a dense grid of spatial measurement points. Figure 1 shows a schematic of the induced damage test. Stringer S21R forward of frame BS256 on the DC-9 was cut in four stages. An electrodynamic shaker was attached to the skin of the aircraft to provide dynamic input. Random input between 500 and 1500 Hz was used with a two pound maximum amplitude. Data was acquired from 0 to 2000 Hz.

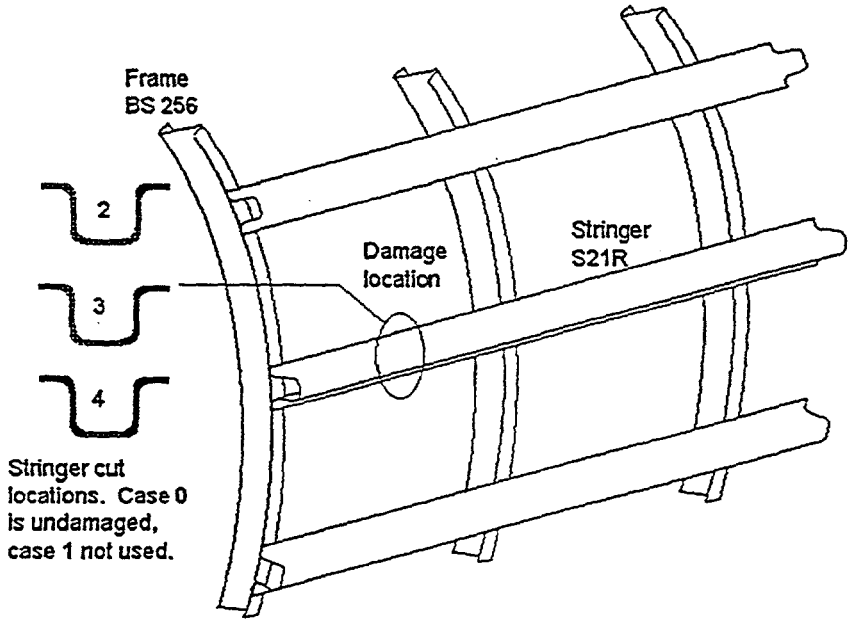

Figure 1. Schematic of DC-9 structure and induced damage. The amplitude plots in figures 2 and 3 cover the left half of this diagram--essentially two rectangular skin panels. Note damage case 1 data is not considered here.

All measurements were acquired with a scanning laser vibrometer on the exterior skin of the aircraft. Two data sets were obtained for each modal test. One data set covered the 38" by 14" area with only 53 measurement points. Measurements were concentrated on the major structural members and around the damage area. A driving point accelerometer FRF was saved for each laser FRF. To reduce noise and problems with signal dropouts, fifty averages were used for the 2048 point FRF's. The second data set took data on a 0.5 inch square grid to produce a measurement set of 2233 points. Driving point information was not saved. The FRF's were calculated with 10 averages and 1024 frequency lines. The time required to take this large data set was 3 hours and 45 minutes.

Data analysis from this test is ongoing. The results presented here were generated in the following manner: First, several FRF's were displayed, mainly those from the known damage location. From these, several resonance frequencies were selected. For each of the selected frequencies, an image was created representing response amplitude at that frequency as a function of position on the surface–this image is the "operating shape" at that frequency. Figure 2 shows one of these image sets for each of the 4 damage cases at 1062 Hz. The damaged stringer runs horizontally in the center of these images, with the damage location in the center of the image. The skin is constrained by the stringer, so we expect much greater amplitude of motion within the panels defined by the substructure. As the level of damage increases, we expect to see motion along the stringer as well. In these images, damage is evident only for case 4–the worst damage.

The next step was to do a full modal analysis of the data set. The nearest modes to the above were displayed as true mode shape images, as shown in Figure 3. In this case, the damage begins to appear at case 3, which is an indication (admittedly a preliminary one) that extended data analysis, in this case the extraction of mode shapes, might increase the sensitivity of this technique.

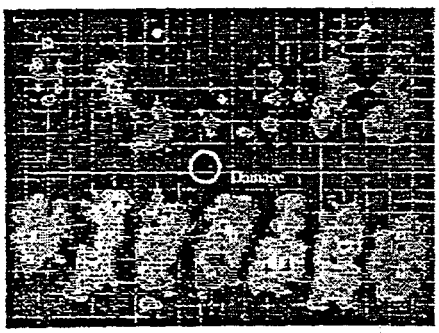

Figure 2a. Damage 0

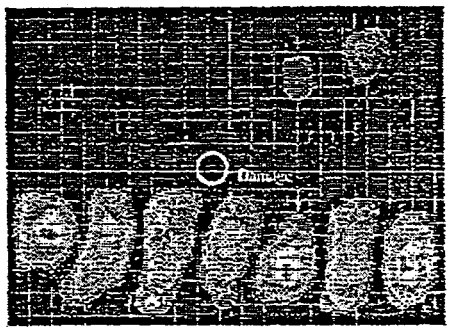

Figure 2b. Damage 2

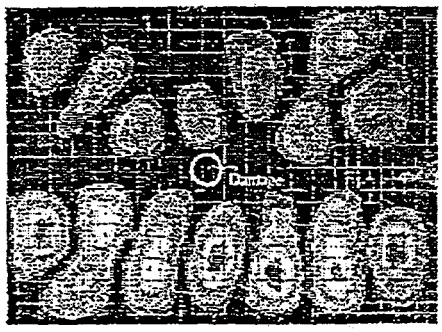

Figure 2c. Damage 3

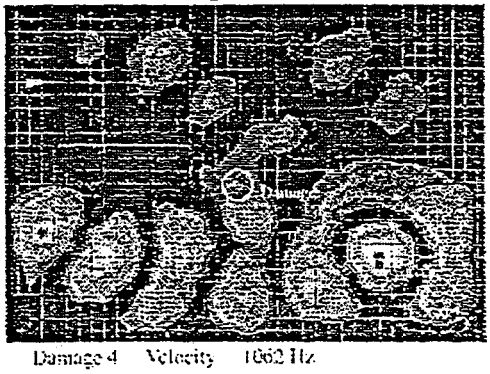

Figure 2d. Damage 4

Figure 2. FRF amplitude ("operating shapes") at 1062 Hz for the four damage cases, DC-9.

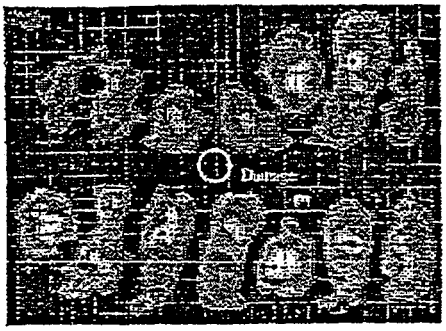

Figure 3a. Damage 0, 1065 Hz.

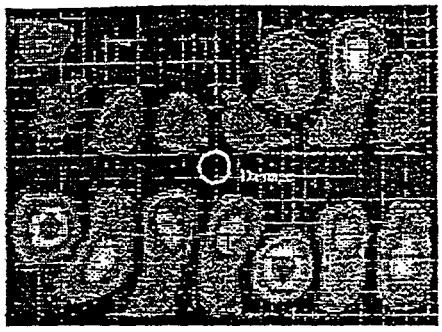

Figure 3b. Damage 2, 1062 Hz.

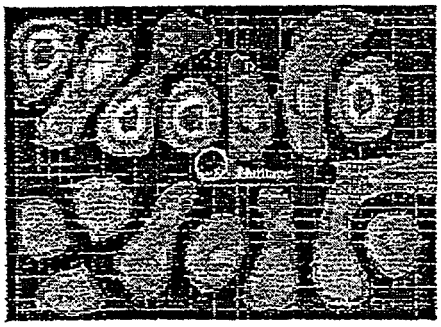

Figure 3c. Damage 3, 1054 Hz.

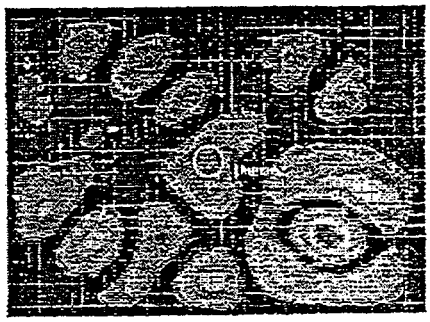

Figure 3d. Damage 4, 1059 Hz.

Figure 3. Mode amplitude of the mode nearest 1062 Hz for the four damage cases, DC-9.

The Composite Patch Experiment

The sample for this experiment was a boron/epoxy composite repair with programmed debond flaws. The sample is 9 by 12 inches, with zones of 2, 4, 6, and 8 composite plies. The debonds are at various depths. In this case, the excitation was an air coupled rapid rise time pulse, applied once per sample point. The LDV instrument used was a Polytec scanning laser vibrometer, model OFV-50 with OFV-3000S. To conduct the test, sample FRF's were first displayed. Eight likely "relaxation frequencies" were selected, and the instrument programmed to record response amplitude at these frequencies for each sample point. Data was taken on a 16 by 32 point sample grid, and the total time to take one data set was 8.5 minutes, limited by the repetition rate of the acoustic pulse generator. Figure 4 shows a representative result--the motion of the surface is greatest over the debonds, as might be expected. Further development on this technique is ongoing.

CONCLUSIONS

This study was motivated by a need for rapid, wide area, nonintrusive damage detection methods for structures such as aircraft. These experiments are preliminary, but the results are encouraging. We nave demonstrated that the LDV can be used to collect modal data of sufficient quality to detect damage. Clearly, further research is needed on technique sensitivity, and data analysis methods. There are several techniques under study for damage detection which are available for numerical processing. Global stiffness metrics (static shapes, experimental stiffness matrices, analytical model comparisons) which do not require a one-to-one comparison of modes appear to hold promise.

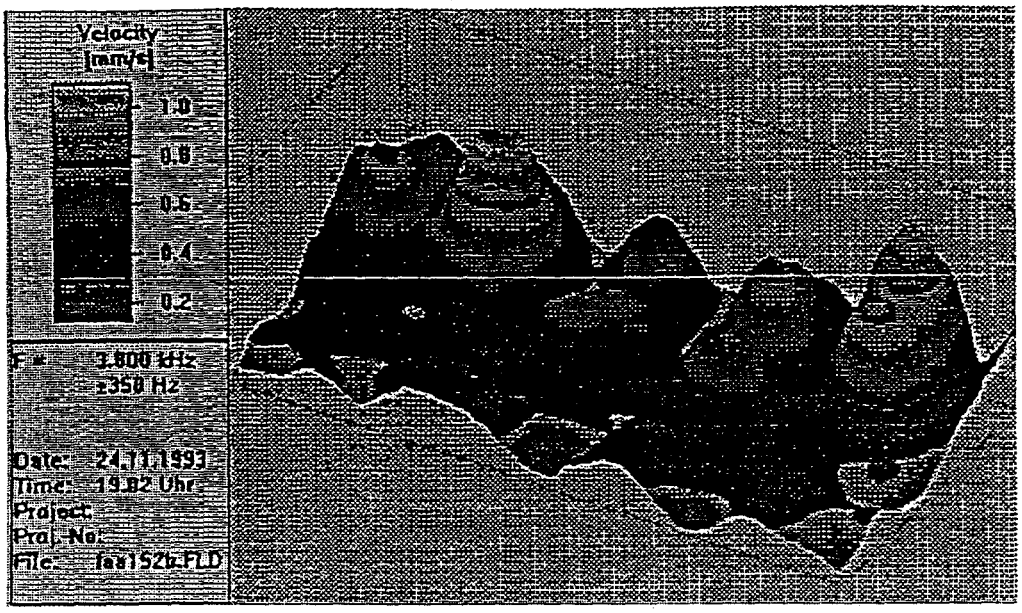

Figure 4. Response amplitude at 3.8 kHz for the composite repair sample with air coupled acoustic impulse loading.

ACKNOWLEDGMENTS

This work was supported by the United States Department of Energy under Contract DE-AC04-94AL85000, and by the Federal Aviation Administration Technical Center under US Department of Transportation Contract DTFA-03-91-A-0018.

REFERENCES

1. G. James, R. Mayes, T. Carne, and G. Reese, "Damage Detection and Health Monitoring of Operational Structures", Proceedings of ASME Winter Annual Meeting, Chicago, IL, November 1994.

2. R. L Mayes, "Error Localization Using Mode Shapes - An Application to a Two Link Robot Arm", presented at the 10th International modal Analysis Conference, San Diego, CA, February 3-7, 1992.

3. L. E. Drain, *The Laser Doppler Technique*, (Wiley, New York, 1980).

APPENDIX C

WIND TURBINE BLADE JOINT FATIGUE TEST

Ron Rodeman and Dan Gregory

Sandia National Laboratories Internal Memo to Paul Veers, 6214
Albuquerque, NM

September 12, 1994

Intentionally Left Blank

Sandia National Laboratories

Albuquerque, New Mexico 87185-5800

date: September 14, 1994

to: Paul S. Veers,MS0708, 6214

from: Ronald Rodeman, 2741 and Dan Gregory, 2741

subject: Wind Turbine Blade Joint Fatigue Test

On August 26 and 27, 1994 the fatigue test of the wind turbine blade was run in Area 3 at Bldg. 6610. The configuration of the test is as shown in Fig. 1. There it is depicted that the slip table is translated back and forth at the first natural frequency of the blade in an attempt to produce the required strain (1180με) at the root of the blade. The UnHoltz-Dickie Model T-4000 electrodynamic vibration table that was used is capable of a peak force of 40000#s and a maximum displacement of .4" zero to peak.

From low level modal tests done in Bldg. 860 we had determined that the blade had a damping of approximately 1%. In addition we had estimated that we would need a tip deflection on the order of 5" zero to peak, as the structure was driven at resonance at 3.8 Hz., to achieve the required strain. For a single degree of freedom system driven at resonance from the base the amplification of the motion at the mass is given as

$$\frac{x}{y} = \frac{1}{2\beta}$$

where x is the mass motion, y is the base motion and ß is the damping. For the level of damping that we measured we would then predict an amplification of 50, i.e. (Q = 50). Extending this simple model to the wind turbine blade driven at the base at the first mode resonance it appeared that we would have considerable margin in being able to run the test on the slip table.

Initial bare table runs were made at 6610 at 3.8 Hz; these runs indicated that the slip table had near maximum capability at this frequency. We then proceeded to ship and mount the blade on the table in preparation for testing. Our initial low-level runs indicated that our damping was consistent with what we had measured in Bldg. 860. However as we attempted to run the table at higher levels we observed a marked increase in damping. We found that we were unable to achieve a root strain of 1180με even with maximum table motion. In addition the natural frequency of the blade was seen to be a function of input level.

We did notice something that was unusual. In attempting to achieve the required strain we happened to see that we were getting a localized heating right at the base of the tines of the steel "tuning fork" that is used with the clamshell to hold the fiberglass blade. We measured this temperature during maximum level testing and found it to be 150°F. We had observed that there seemed to be a small amount of relative motion

between the clamshell and the tuning fork right at the base of the tines. However, this apparent motion was not noticeable along the clamshell as we moved up the tines.

Since we were faced with being unable to achieve the required strain with the available equipment we looked at the effect of shortening the blade. An approximate analysis indicated that we might achieve nearly a 25% increase in strain while increasing our first mode frequency by 40%. Based on this we decided to shorten the blade by two feet. We did get an increase in natural frequency, (4.3Hz.), however, once again the damping went up with increased level. We found that the maximum strain that we could achieve at the root was on the order of 850με; this strain was achieved in a fifteen minute maximum level test. We noticed that the measured strains on the clamshell were of the order of 1900με. We made the decision to run the test by controlling the root strain to be 650με; this would cause a strain of approximately 1250με in the clamshell. Since this strain was greater than the analytically predicted maximum strain to attain failure in 100,000 cycles we felt that the test would be representative.

The blade was instrumented with 34 Endevco 7751 accelerometers with the approximate locations depicted in Fig. 2; the thicker section represents the clamshell and the thinner section the blade. In addition the 20 original strain channels were also used. The strain gauges are in the locations shown in Fig. 3; the channel designation of the gauges is given in Table 1. We performed an initial modal test to baseline the structure; that data is available but has not yet been reduced.

We then proceeded to run the fatigue test by driving the structure at a nominal frequency of 4.3 Hz. while maintaining root strain at 650με. All data were continuously recorded at 50 Hz. We were anticipating that the fatigue life would be of the order of 100,000 cycles which would imply that we would be running the test in excess of seven hours. As the test progressed (≈20 mins.) we noticed that the control system was having difficulty maintaining the root strain. The control system had been configured to change the amplitude of table motion, while maintaining a fixed frequency, to achieve the required root strain. After nearly one hour of testing it became apparent that we would be unable to maintain required level at 4.3 Hz. The drive frequency was changed to 3.95 Hz. The frequency was changed again to 3.52 Hz. fifteen minutes later.

After one hour and twenty-five minutes a crack was observed in the left tine of the steel structure. It appeared to be emanating laterally outward from the last bolthole where the clamshell bolted to the tine. At the time the crack was observed it was already 1.5" in length. The test was continued for five more minutes; during this time the crack progressed all the way to the edge and through the thickness of the steel. This crack appeared right in the area where we had observed the localized heating.

As indicated all channels were continuously recorded during the test. Since each trace has over 180,000 points only the envelopes of the responses are displayed. The envelopes are given in Figs. 4- 17. From the plot of strain of gauge 19 we can see the strain amplitude start to roll off from the initial level of 650με at around 3000 secs. At that time the drive frequency was changed and the control system once again attempts to maintain the root strain at 650με. Notice from the plot how quickly the level rolls off until the frequency is lowered to 3.5Hz. One other interesting plot is Accelerometer 123; that accelerometer is nearest the point of observed failure. Even though the drive

level is dropping off the acceleration at 123 is increasing; when the drive frequency was reduced to 3.9 Hz. the acceleration at 123 began to decrease.

Strain channels 13-16 exhibit a pronounced asymmetry after the frequency change at 3000 seconds. These strain gauges are on the clamshell nearest the point where failure initiated.

After we found that the structure had failed much earlier than predicted we realized that our 15 minute test where we sought to achieve the desired strain level at the root might have contributed to the damage of the blade. Only five channels were recorded for that test. The envelopes of four of the data channels are presented in Figs. 18 -21. From the envelope of the root strain gauge data it can be seen that we were still well below the initial desired root strain level.

At this point we are preparing to do ultrasonic inspection of the clamshell to blade bond to determine if we initiated any failures in the bond. The unit will be disassembled after this inspection.

Gauge	Channel No.
1	1
2	2
3	3
4	4
5	5
6	6
7	7
8	8
A	9
B	10
C	11
D	12
E	13
F	14
G	15
H	16
I	17
J	18
K&L	19
M&N	20

Table 1.

RR:2741

Distribution:
MS0557 Baca, T. J.,2741
MS0557 Carne,T. G., 2741
MS0557 James,George,2741
MS0555 Garcia, John R.,2742
MS0708 Dodd, Henry, 6214
MS0708 Ashwill, Tom, 6214
MS0708 Berg, Dale, 6214
Bell, Ben
Davis Rory

Copy to:

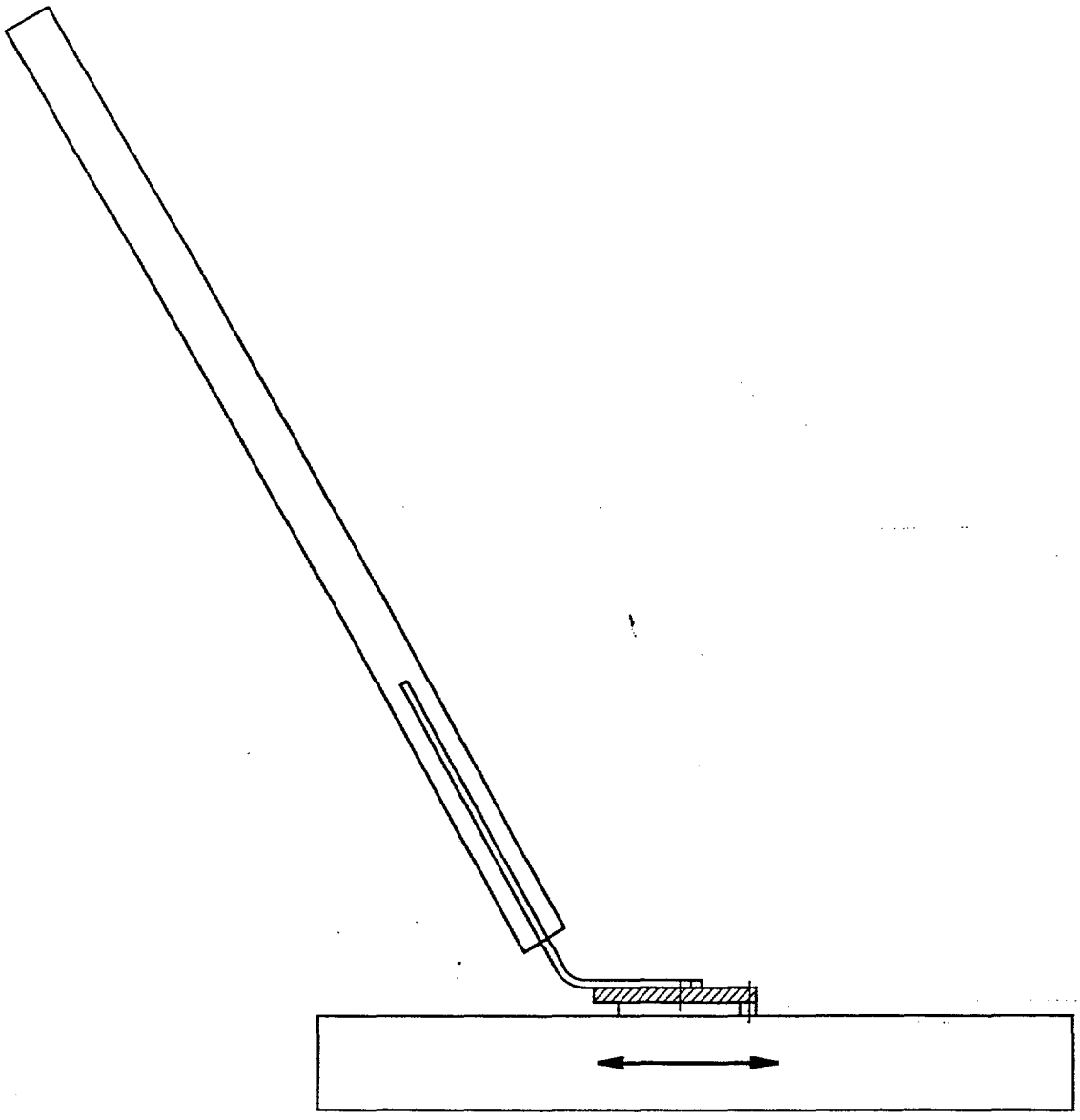

Fig. 1

Fig. 2

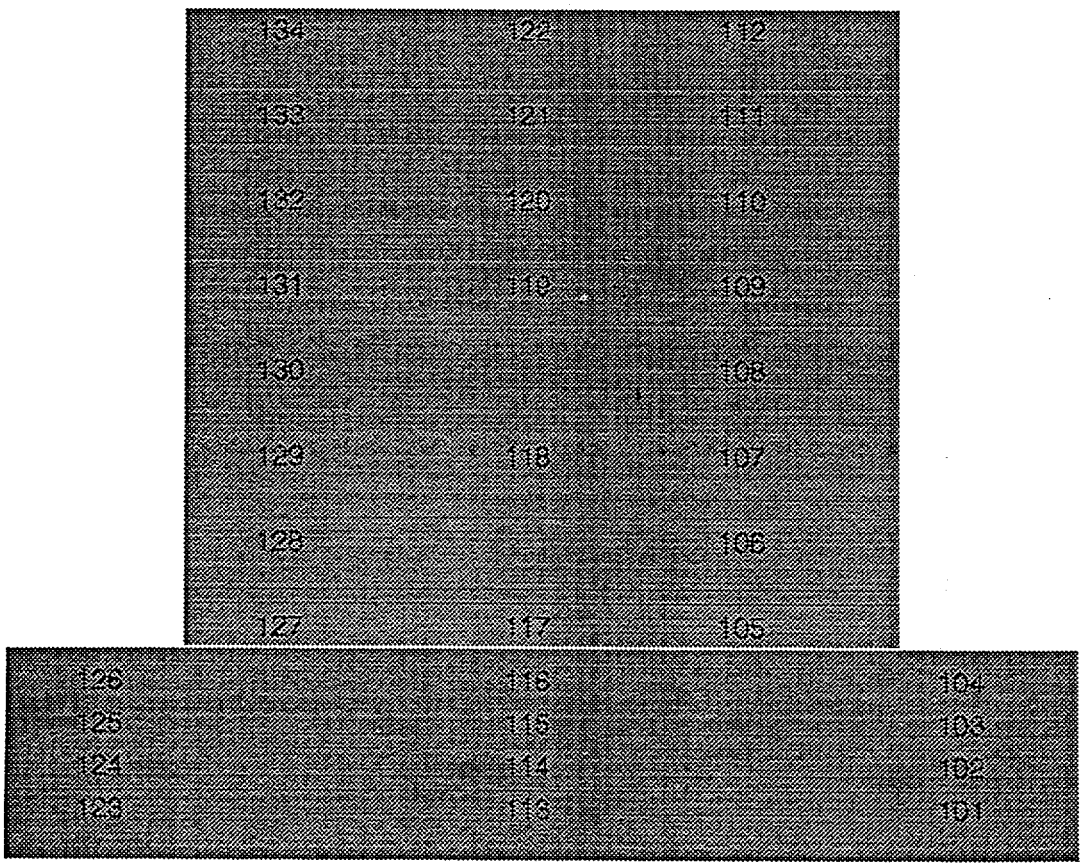
134
133
132
131
130
129
128
127
122
121
120
119
118
117
112
111
110
109
108
107
106
105
126
125
124
123
116
115
114
113
104
103
102
101

FIGURE 3. STRAIN GAGES

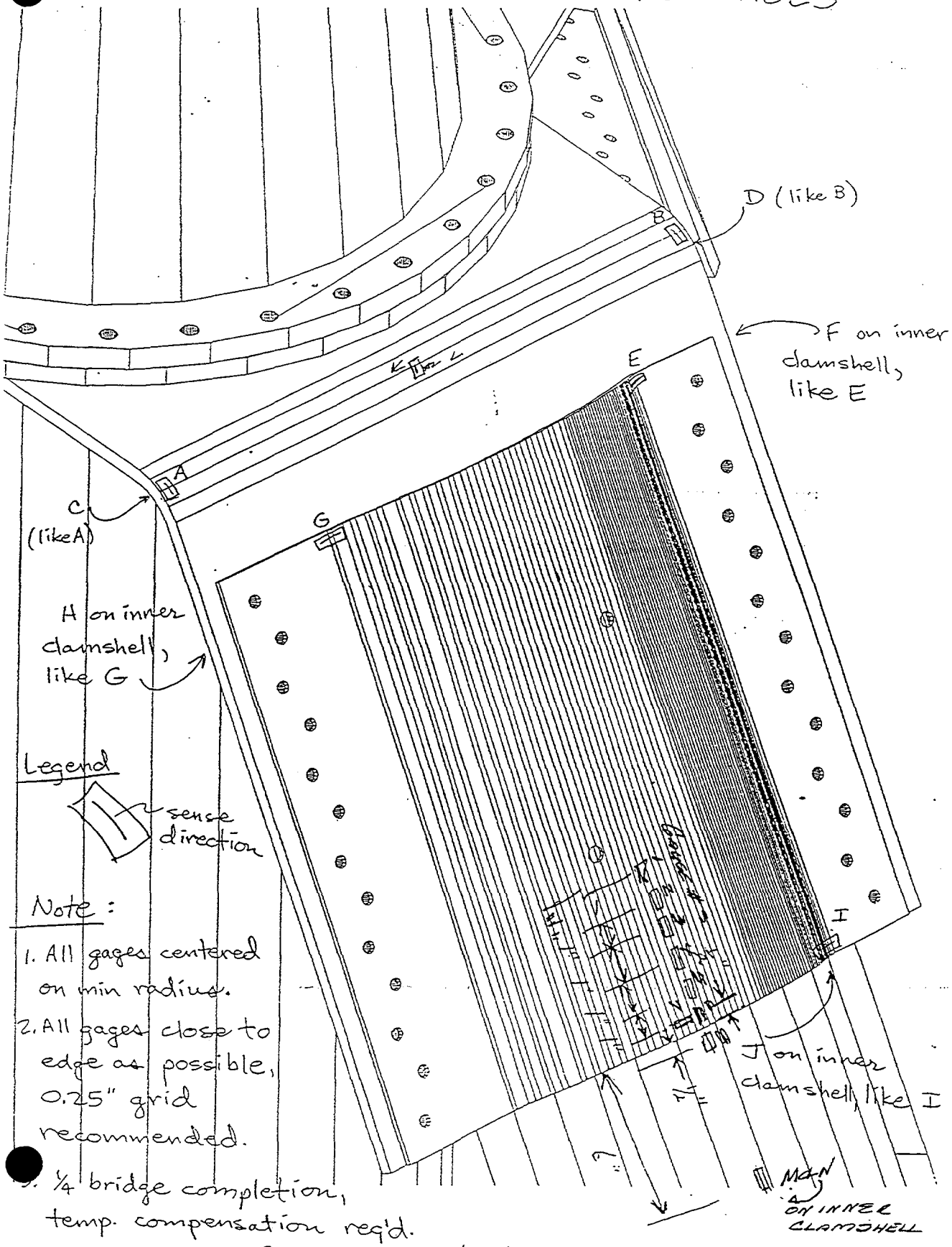

Note:

1. All gages centered on min radius.
2. All gages close to edge as possible, 0.25" grid recommended.
3. ¼ bridge completion, temp. compensation req'd.
4. I.T not req'd for long term tests.

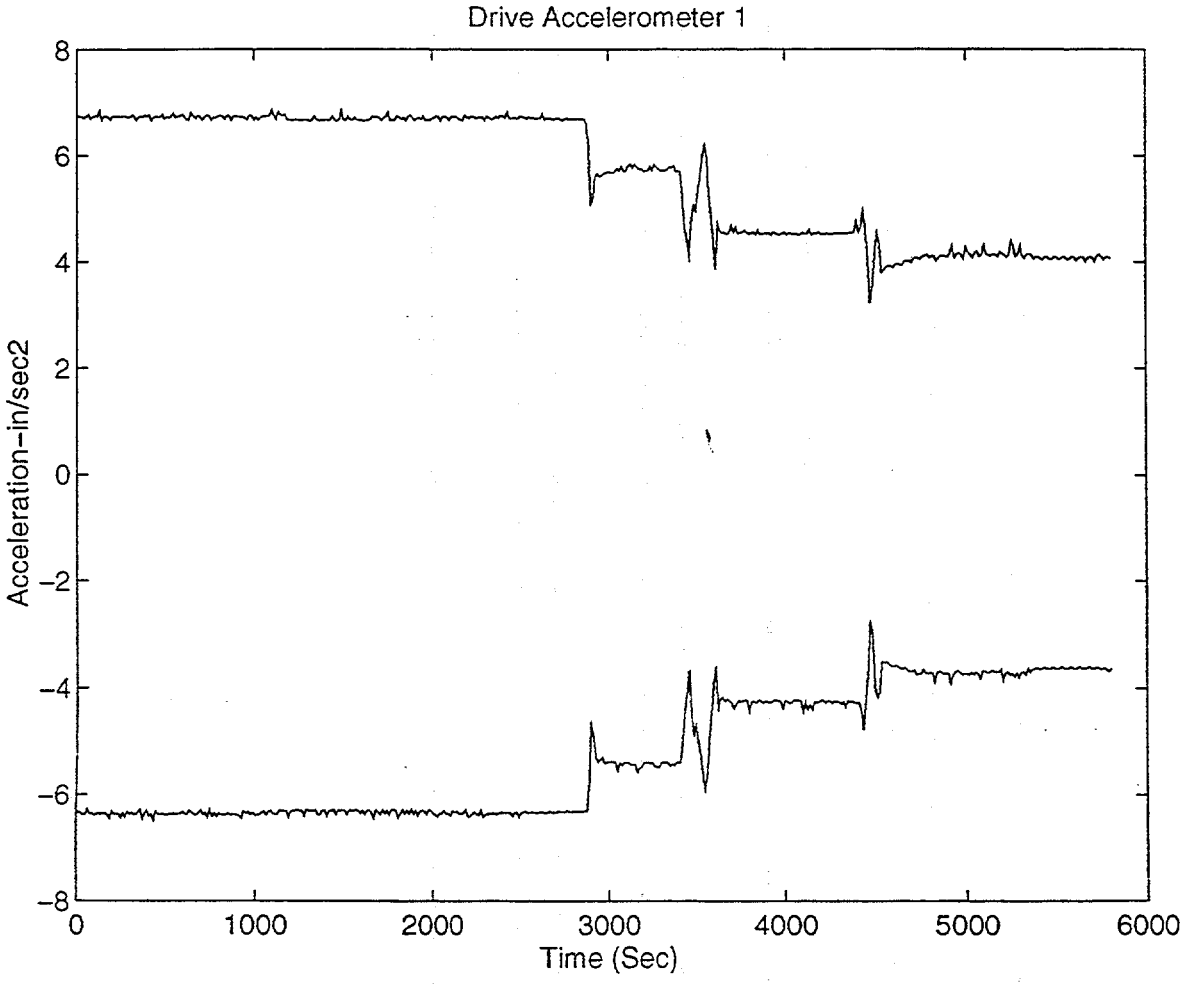
Drive Accelerometer 1
Acceleration-in/sec2
Time (Sec)
8
6
4
2
0
-2
-4
-6
-8
0
1000
2000
3000
4000
5000
6000

FIGURE 4

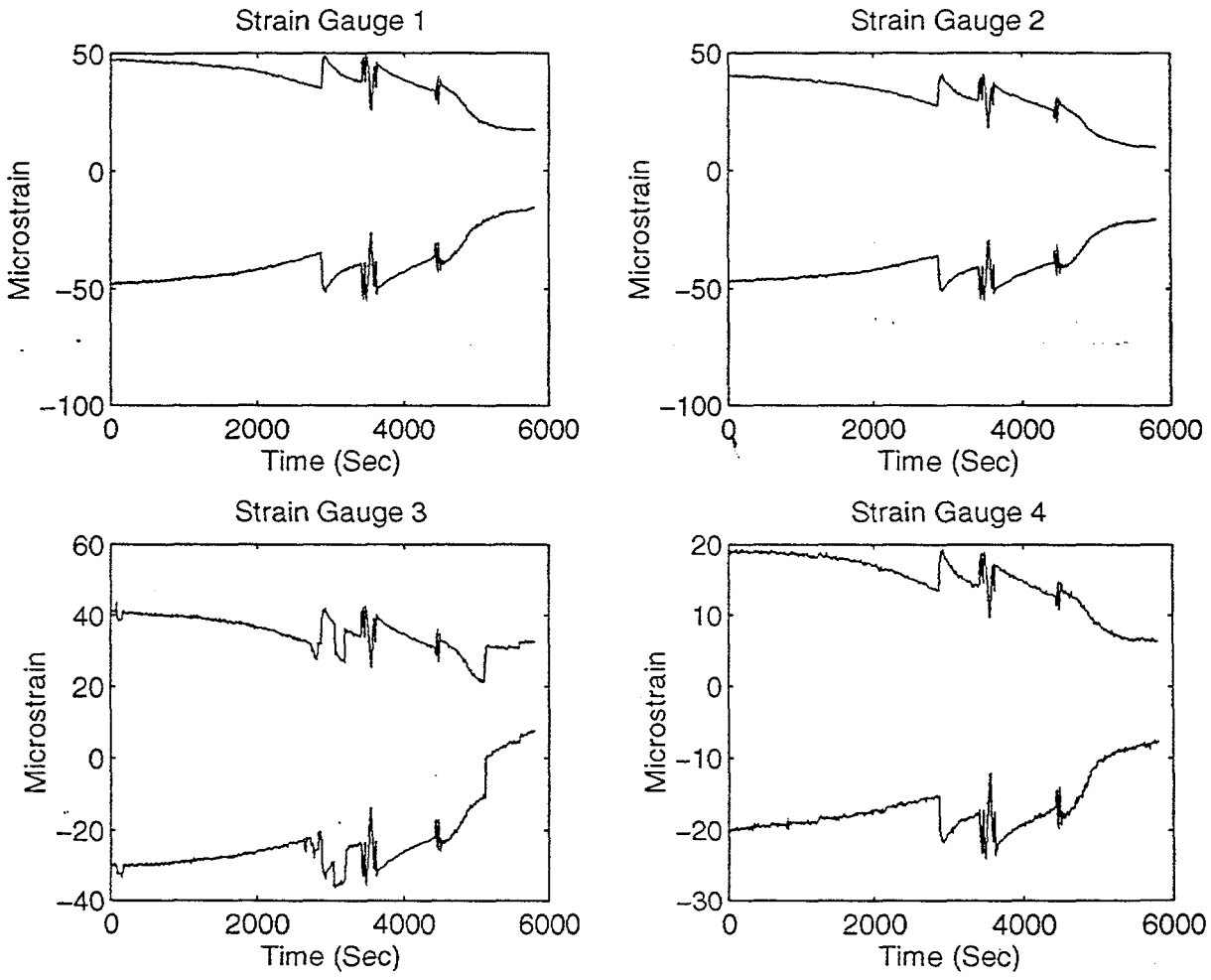
Strain Gauge 1
Microstrain
50
0
−50
−100
0
2000
4000
6000
Time (Sec)
Strain Gauge 2
Microstrain
50
0
−50
−100
0
2000
4000
6000
Time (Sec)
Strain Gauge 3
Microstrain
60
40
20
0
−20
−40
0
2000
4000
6000
Time (Sec)
Strain Gauge 4
Microstrain
20
10
0
−10
−20
−30
0
2000
4000
6000
Time (Sec)

FIGURE 5

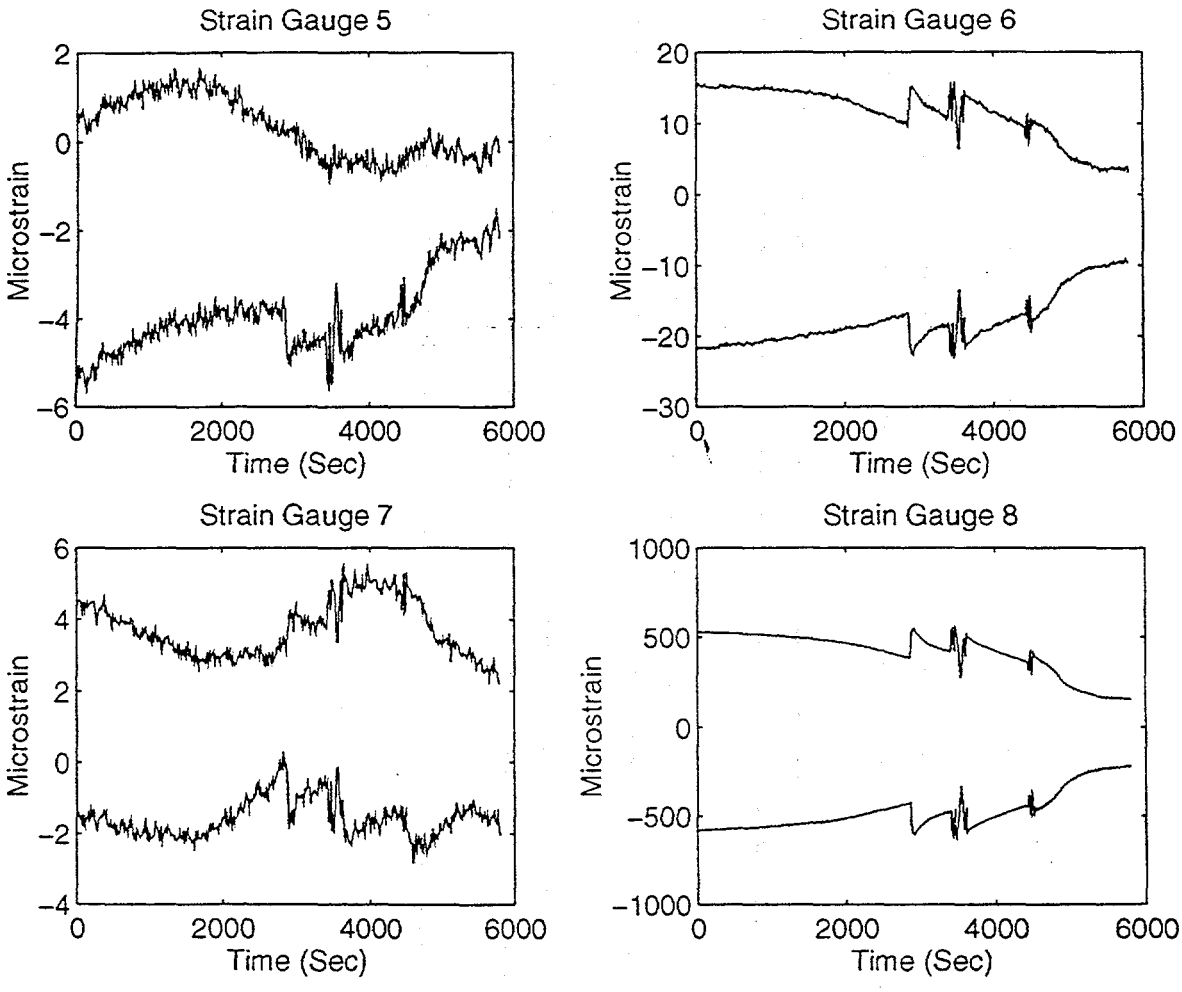
Strain Gauge 5
Microstrain
Time (Sec)
Strain Gauge 6
Microstrain
Time (Sec)
Strain Gauge 7
Microstrain
Time (Sec)
Strain Gauge 8
Microstrain
Time (Sec)

FIGURE 6

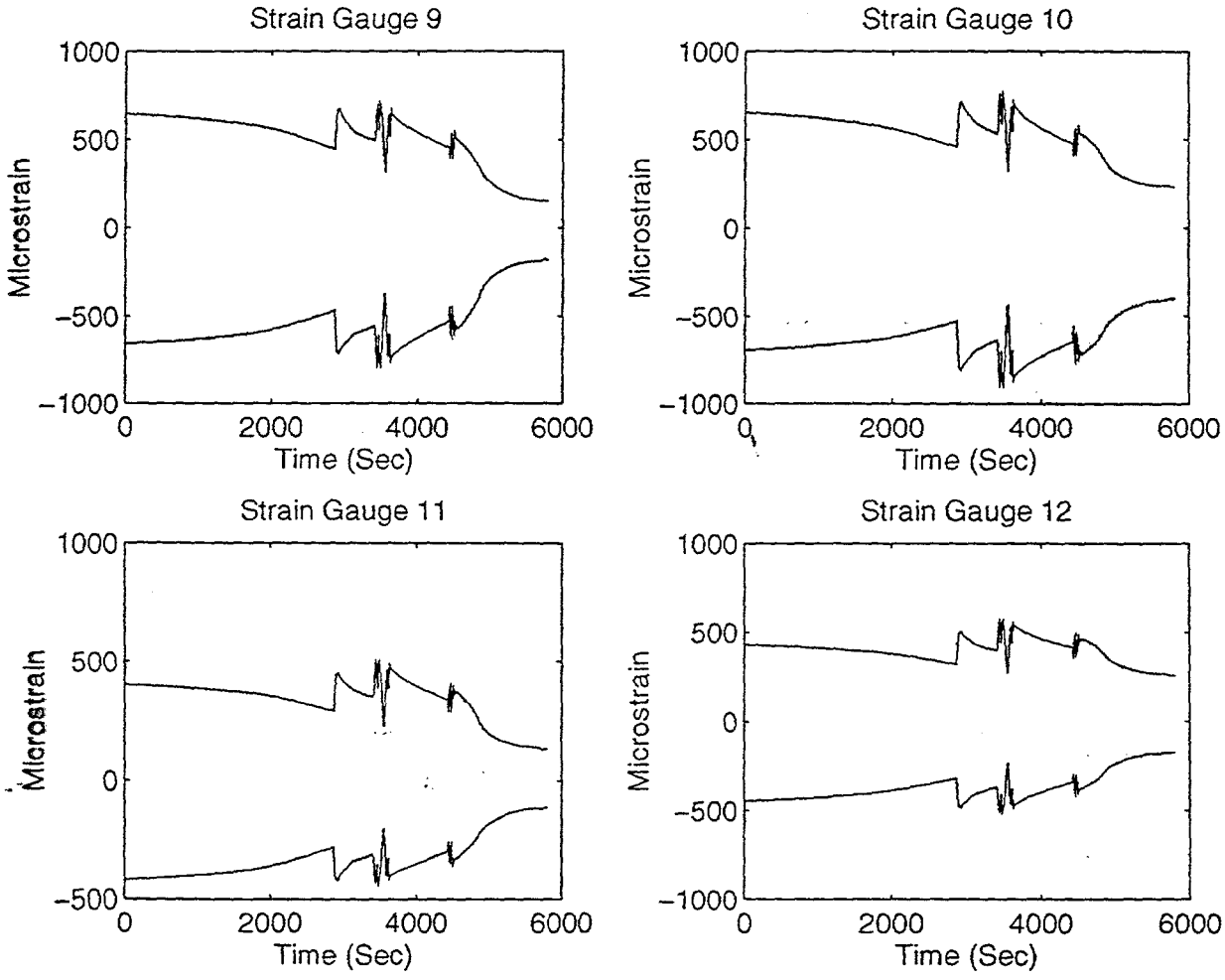
Strain Gauge 9
Strain Gauge 10
Strain Gauge 11
Strain Gauge 12
Microstrain
Time (Sec)
1000
500
0
-500
-1000
0
2000
4000
6000

FIGURE 7

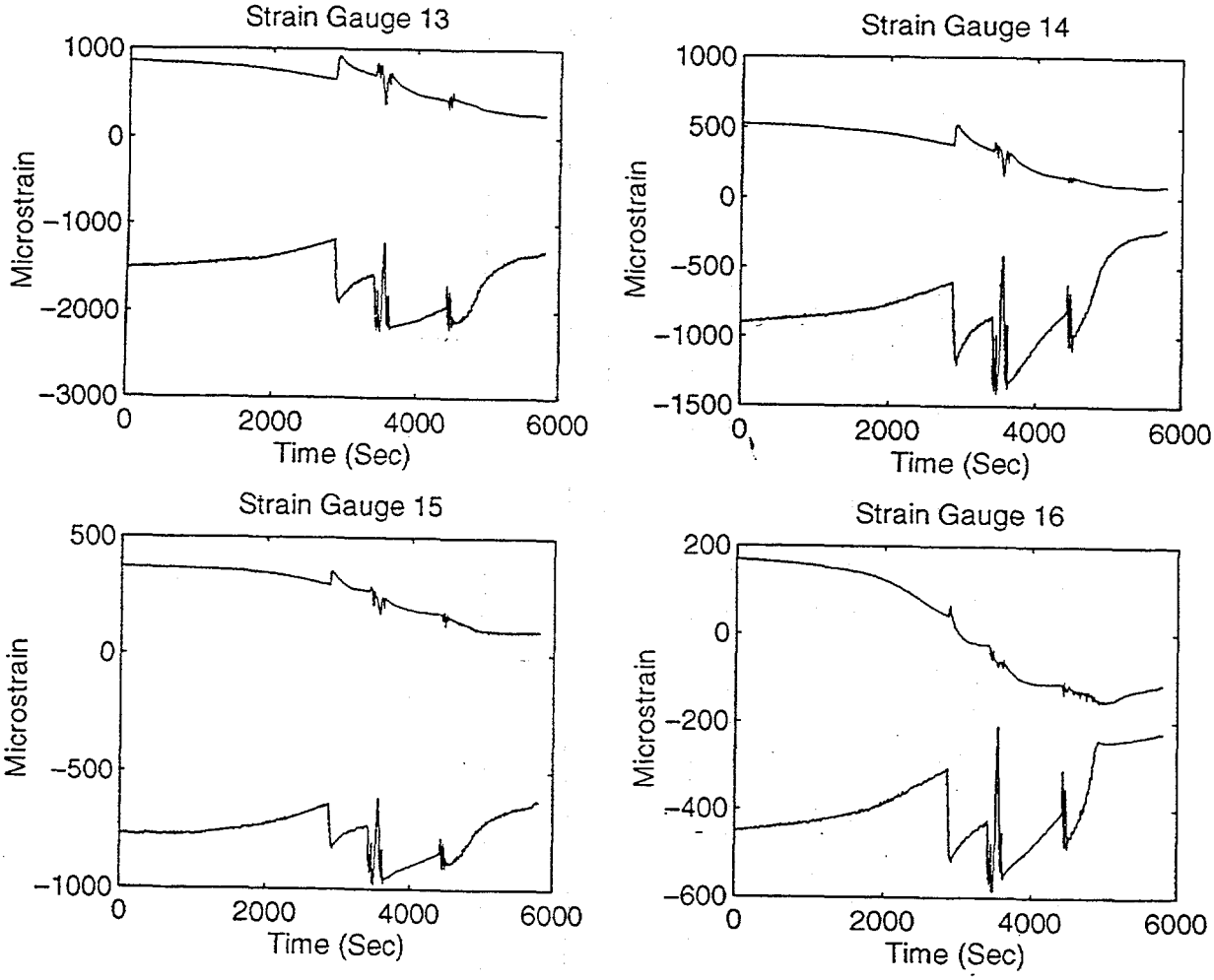
Strain Gauge 13
Microstrain
1000
0
-1000
-2000
-3000
0
2000
4000
6000
Time (Sec)
Strain Gauge 14
Microstrain
1000
500
0
-500
-1000
-1500
0
2000
4000
6000
Time (Sec)
Strain Gauge 15
Microstrain
500
0
-500
-1000
0
2000
4000
6000
Time (Sec)
Strain Gauge 16
Microstrain
200
0
-200
-400
-600
0
2000
4000
6000
Time (Sec)

FIGURE 8

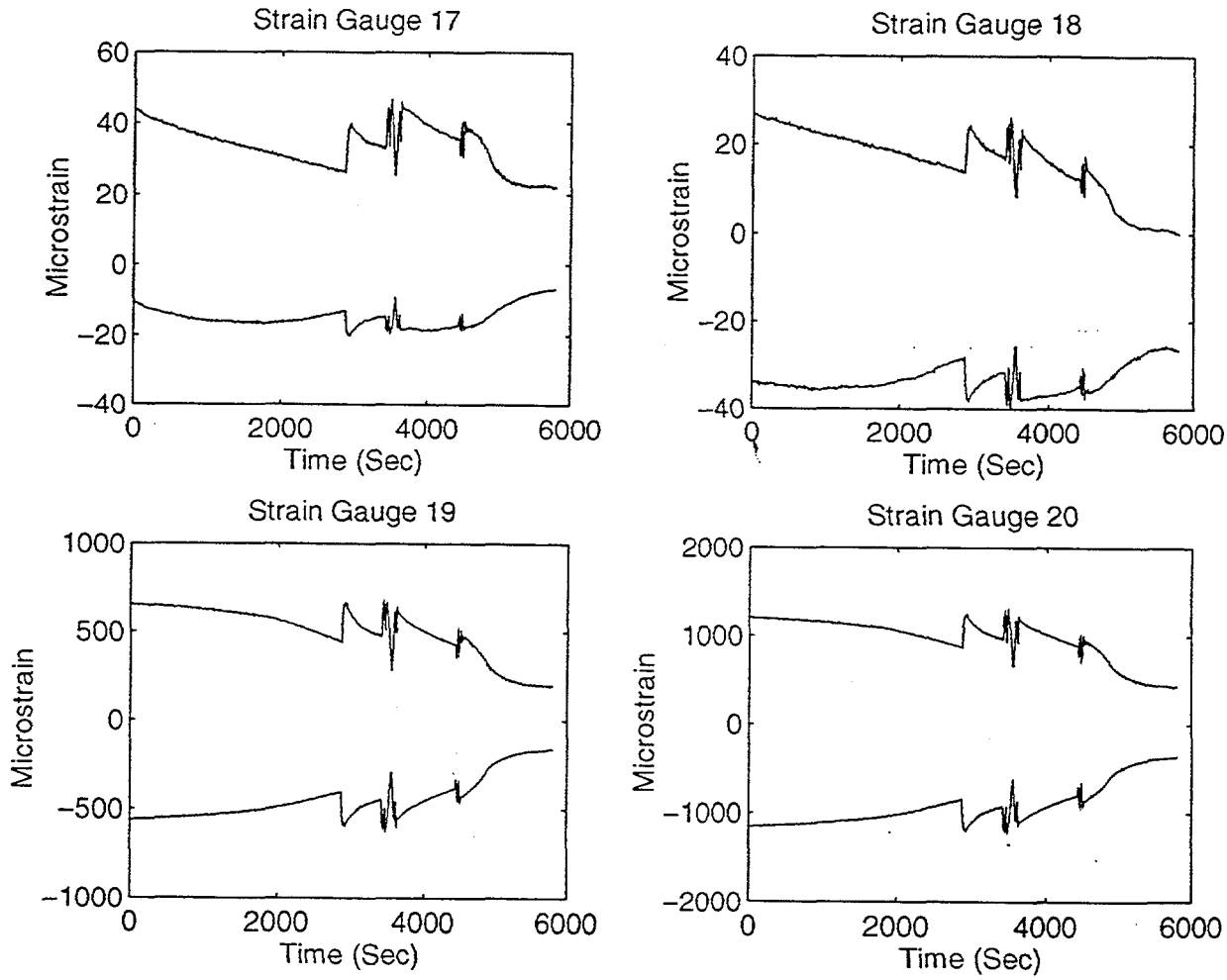
Strain Gauge 17
Microstrain
60
40
20
0
−20
−40
0
2000
4000
6000
Time (Sec)
Strain Gauge 18
Microstrain
40
20
0
−20
−40
0
2000
4000
6000
Time (Sec)
Strain Gauge 19
Microstrain
1000
500
0
−500
−1000
0
2000
4000
6000
Time (Sec)
Strain Gauge 20
Microstrain
2000
1000
0
−1000
−2000
0
2000
4000
6000
Time (Sec)

FIGURE 9

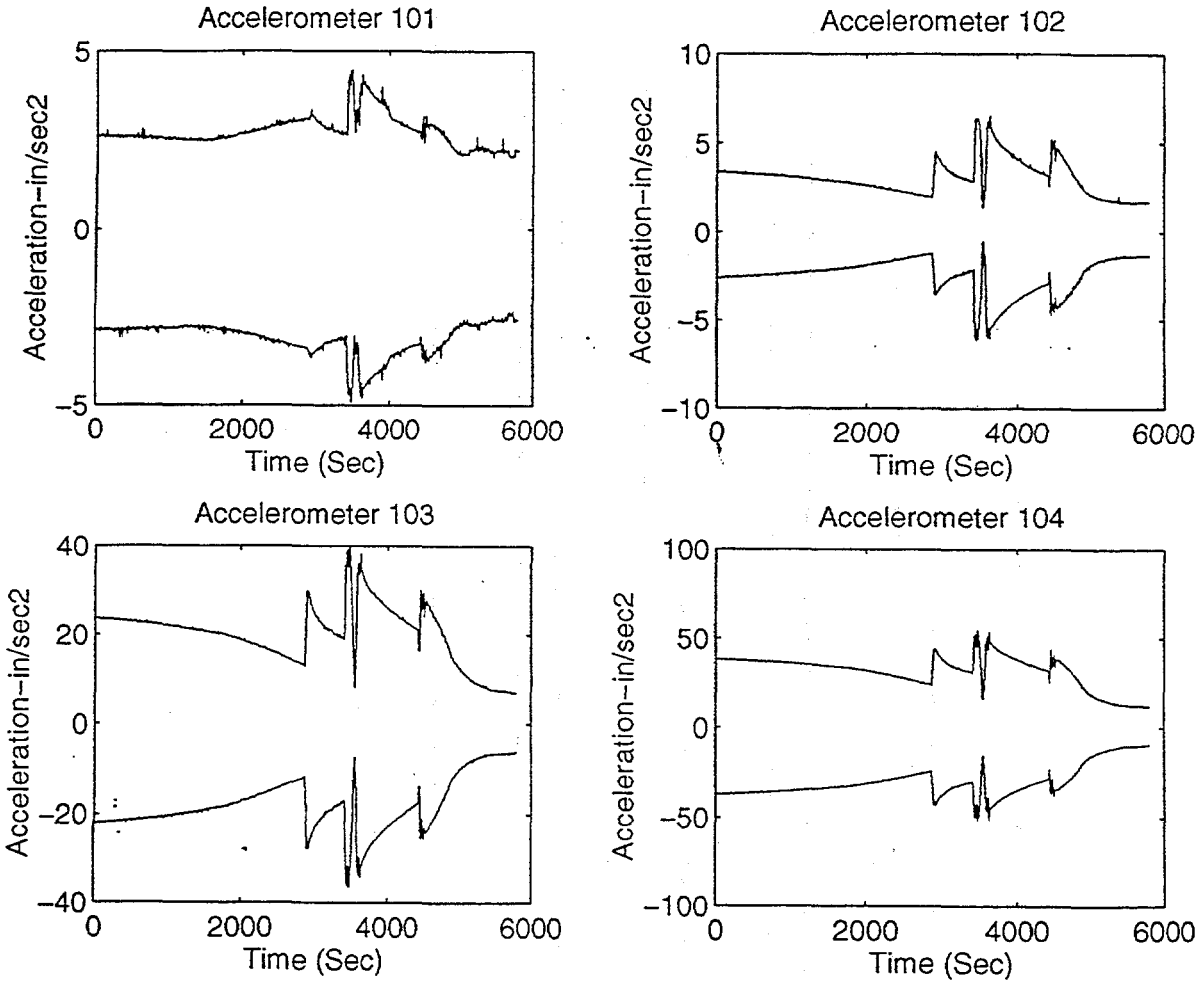
Accelerometer 101
Acceleration-in/sec2
Time (Sec)
Accelerometer 102
Acceleration-in/sec2
Time (Sec)
Accelerometer 103
Acceleration-in/sec2
Time (Sec)
Accelerometer 104
Acceleration-in/sec2
Time (Sec)

FIGURE 10

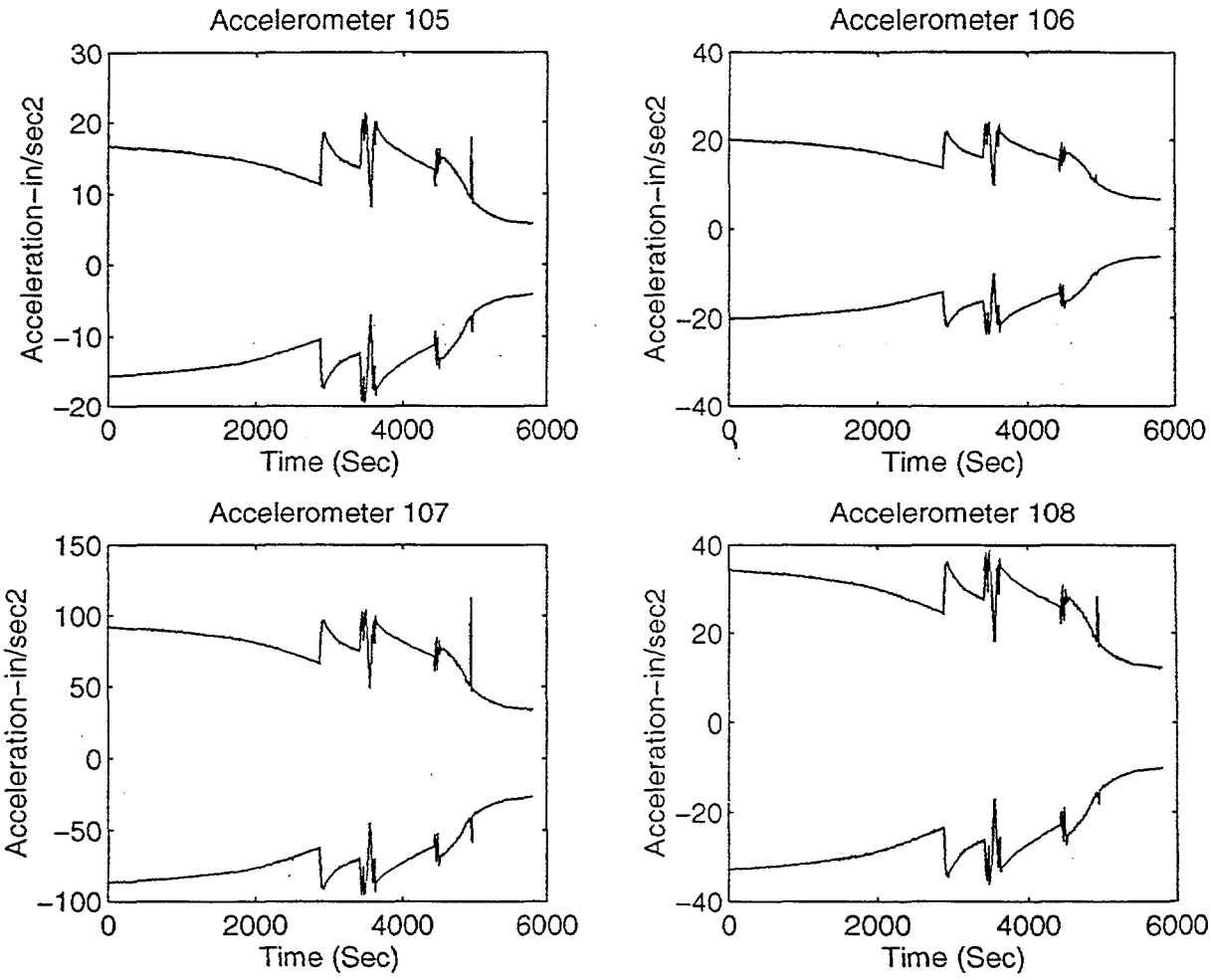
Accelerometer 105
Acceleration-in/sec2
Time (Sec)
Accelerometer 106
Acceleration-in/sec2
Time (Sec)
Accelerometer 107
Acceleration-in/sec2
Time (Sec)
Accelerometer 108
Acceleration-in/sec2
Time (Sec)

FIGURE 11

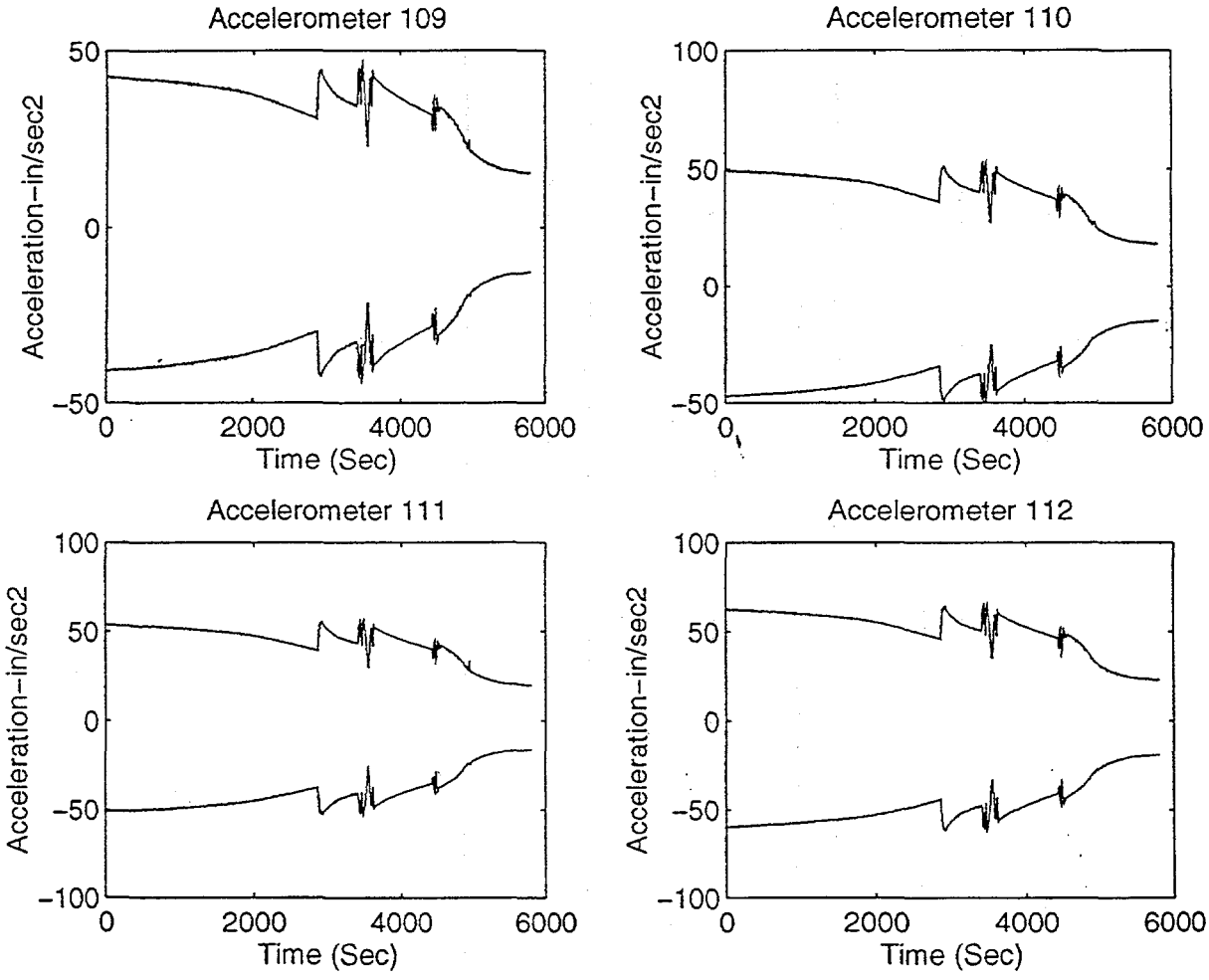
Accelerometer 109
Acceleration-in/sec2
50
0
-50
0
2000
4000
6000
Time (Sec)
Accelerometer 110
Acceleration-in/sec2
100
50
0
-50
0
2000
4000
6000
Time (Sec)
Accelerometer 111
Acceleration-in/sec2
100
50
0
-50
-100
0
2000
4000
6000
Time (Sec)
Accelerometer 112
Acceleration-in/sec2
100
50
0
-50
-100
0
2000
4000
6000
Time (Sec)

FIGURE 12

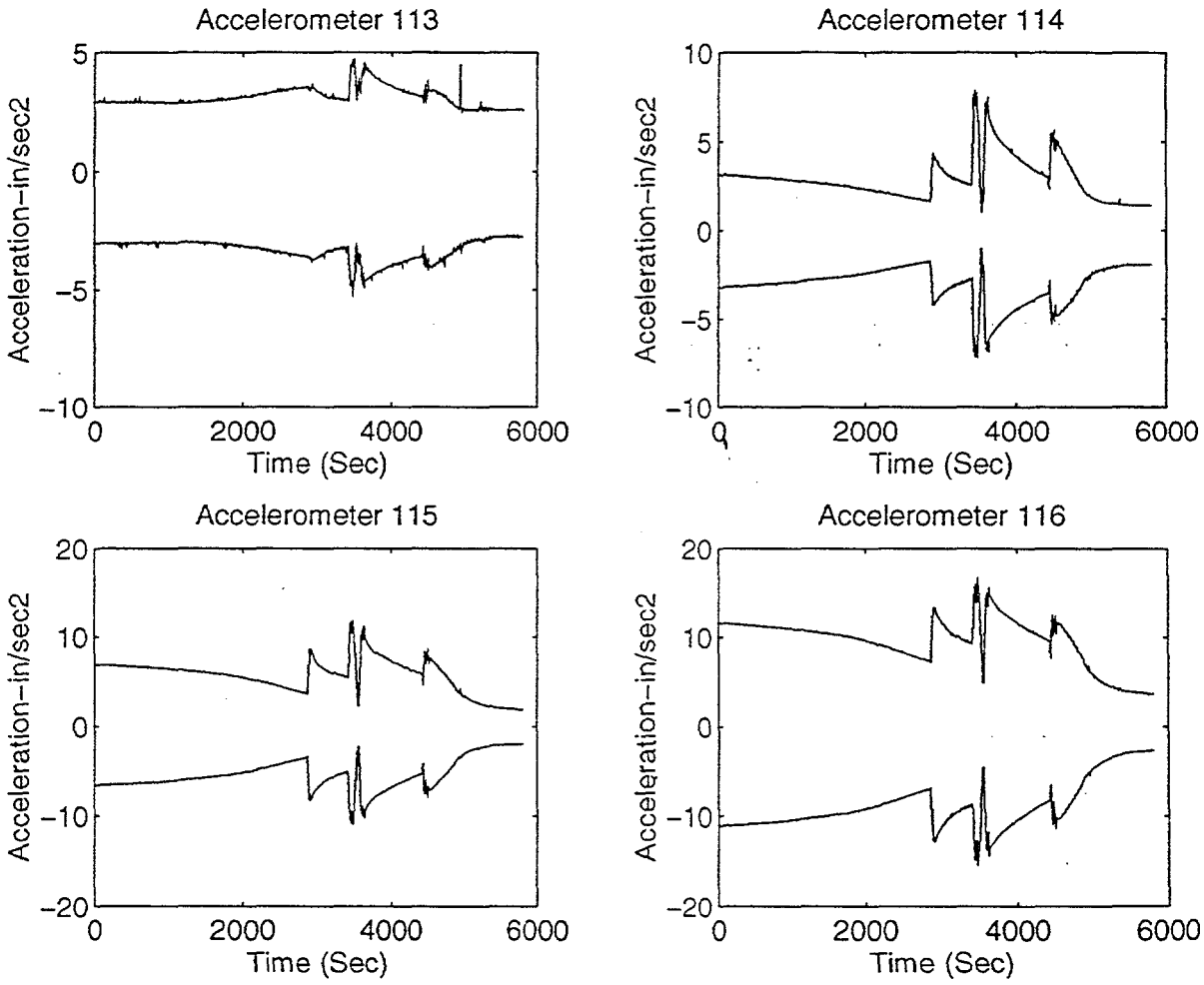
Accelerometer 113
Acceleration-in/sec2
5
0
-5
-10
0
2000
4000
6000
Time (Sec)
Accelerometer 114
Acceleration-in/sec2
10
5
0
-5
-10
0
2000
4000
6000
Time (Sec)
Accelerometer 115
Acceleration-in/sec2
20
10
0
-10
-20
0
2000
4000
6000
Time (Sec)
Accelerometer 116
Acceleration-in/sec2
20
10
0
-10
-20
0
2000
4000
6000
Time (Sec)

FIGURE 13

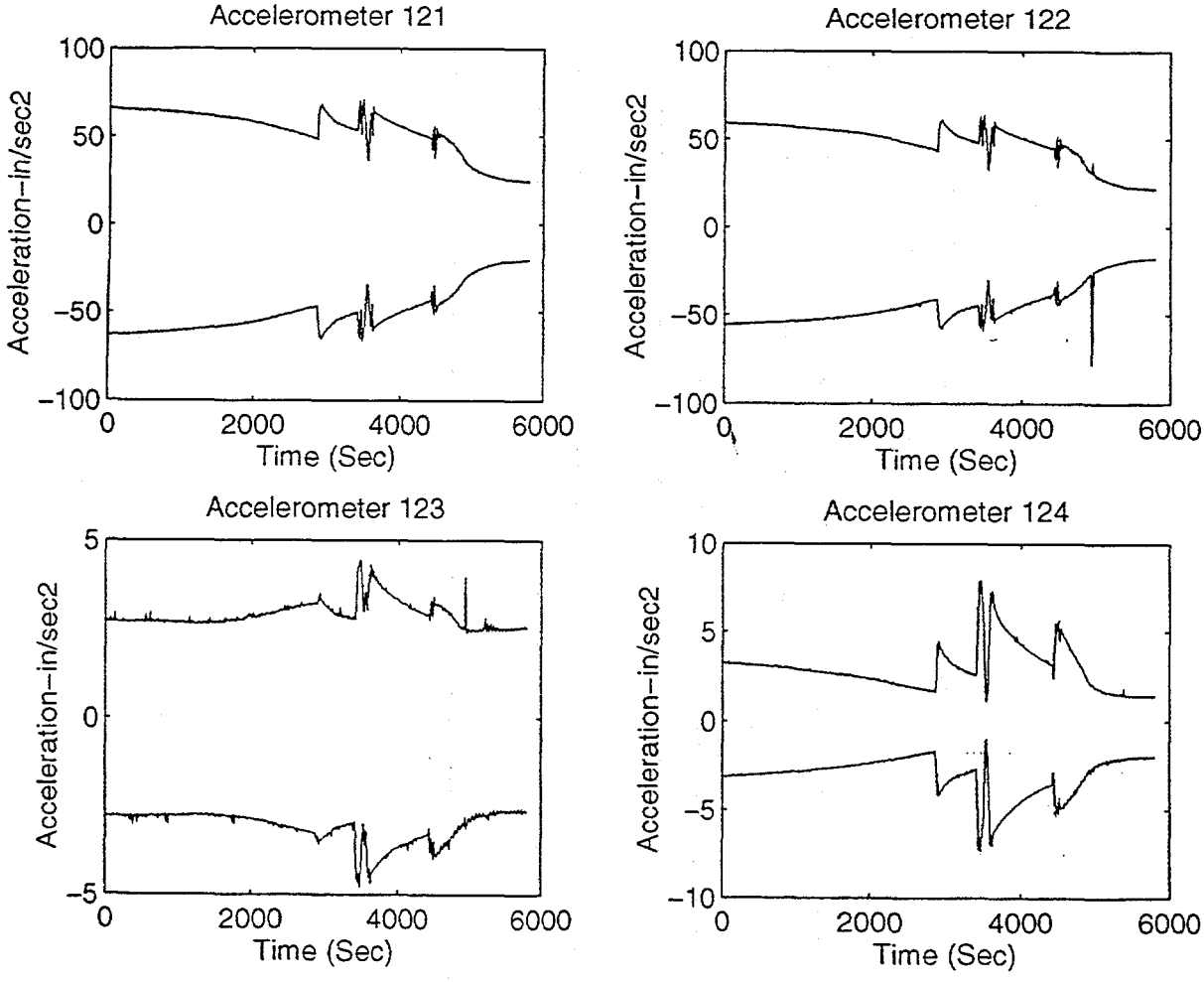
Accelerometer 121
Acceleration-in/sec2
100
50
0
-50
-100
0
2000
4000
6000
Time (Sec)
Accelerometer 122
Acceleration-in/sec2
100
50
0
-50
-100
0
2000
4000
6000
Time (Sec)
Accelerometer 123
Acceleration-in/sec2
5
0
-5
0
2000
4000
6000
Time (Sec)
Accelerometer 124
Acceleration-in/sec2
10
5
0
-5
-10
0
2000
4000
6000
Time (Sec)

FIGURE 14

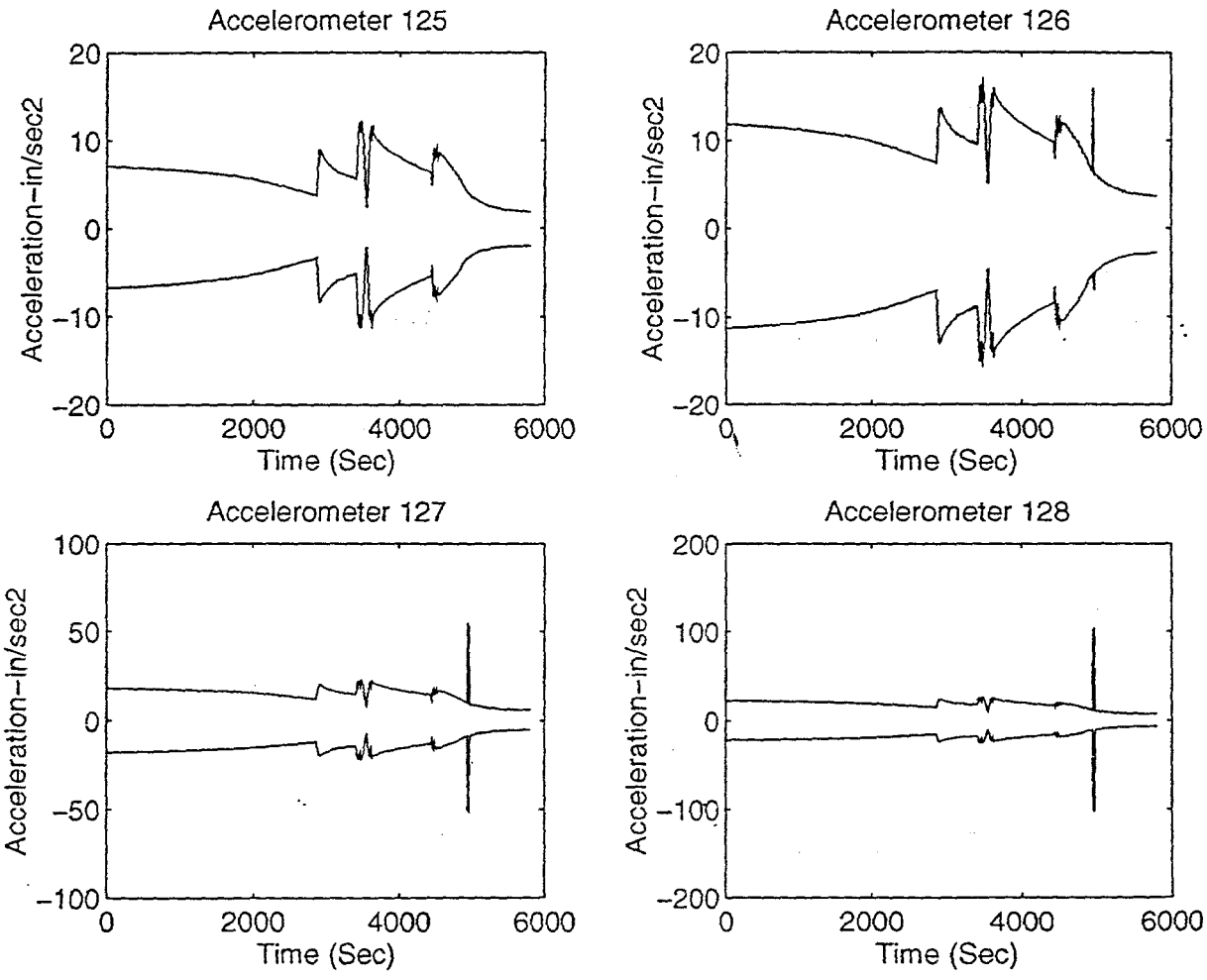
Accelerometer 125
Acceleration-in/sec2
20
10
0
-10
-20
0
2000
4000
6000
Time (Sec)
Accelerometer 126
Acceleration-in/sec2
20
10
0
-10
-20
0
2000
4000
6000
Time (Sec)
Accelerometer 127
Acceleration-in/sec2
100
50
0
-50
-100
0
2000
4000
6000
Time (Sec)
Accelerometer 128
Acceleration-in/sec2
200
100
0
-100
-200
0
2000
4000
6000
Time (Sec)

FIGURE 15

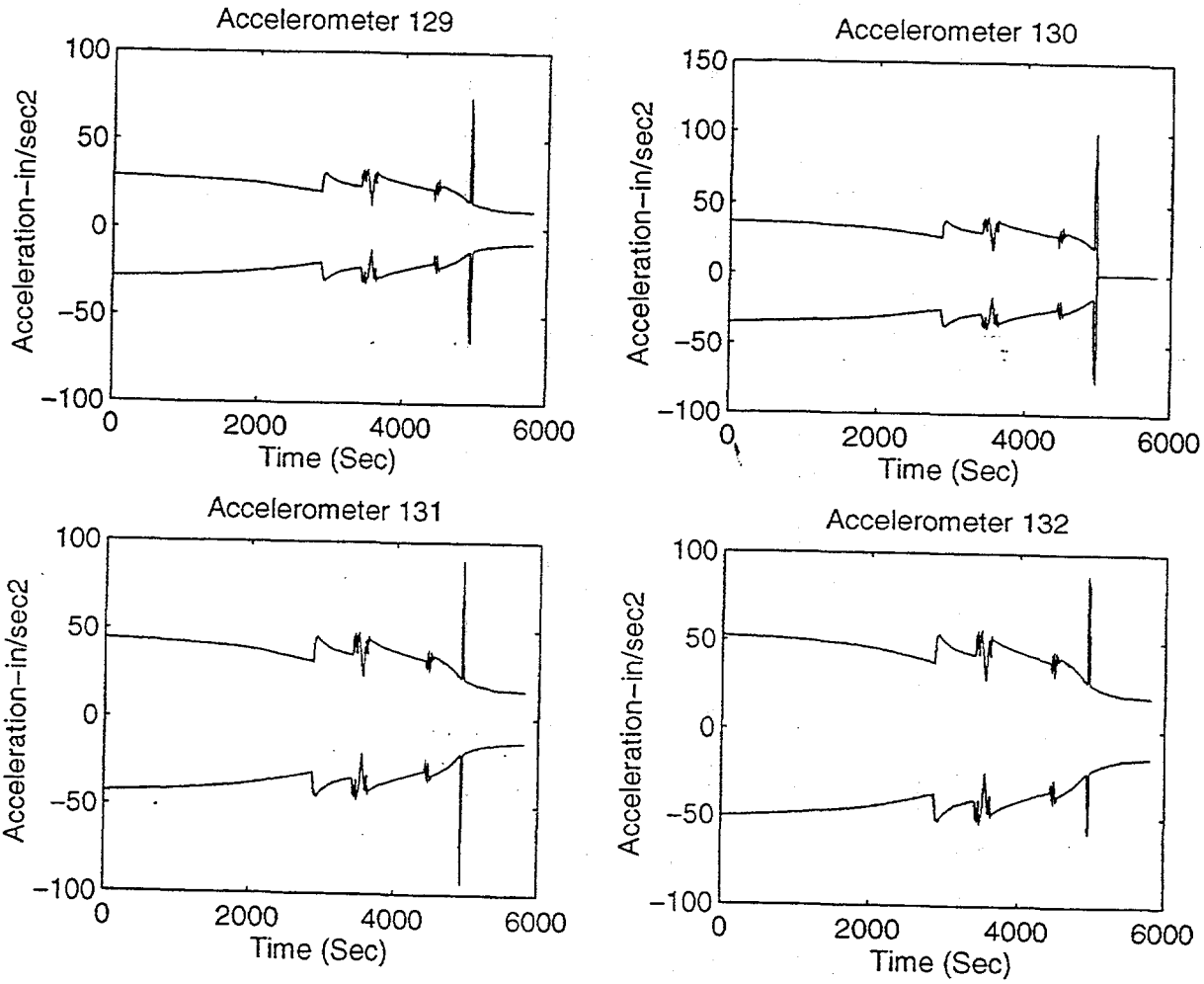
Accelerometer 129
Acceleration-in/sec2
100
50
0
-50
-100
0
2000
4000
6000
Time (Sec)
Accelerometer 130
Acceleration-in/sec2
150
100
50
0
-50
-100
0
2000
4000
6000
Time (Sec)
Accelerometer 131
Acceleration-in/sec2
100
50
0
-50
-100
0
2000
4000
6000
Time (Sec)
Accelerometer 132
Acceleration-in/sec2
100
50
0
-50
-100
0
2000
4000
6000
Time (Sec)

FIGURE 16

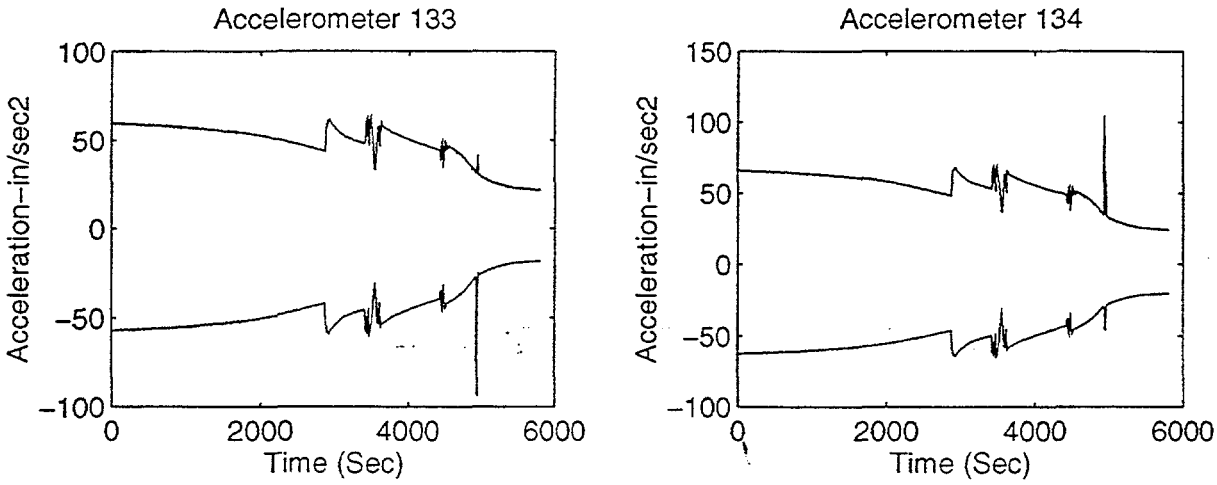
Accelerometer 133
Acceleration–in/sec2
100
50
0
−50
−100
0
2000
4000
6000
Time (Sec)
Accelerometer 134
Acceleration–in/sec2
150
100
50
0
−50
−100
0
2000
4000
6000
Time (Sec)

FIGURE 17

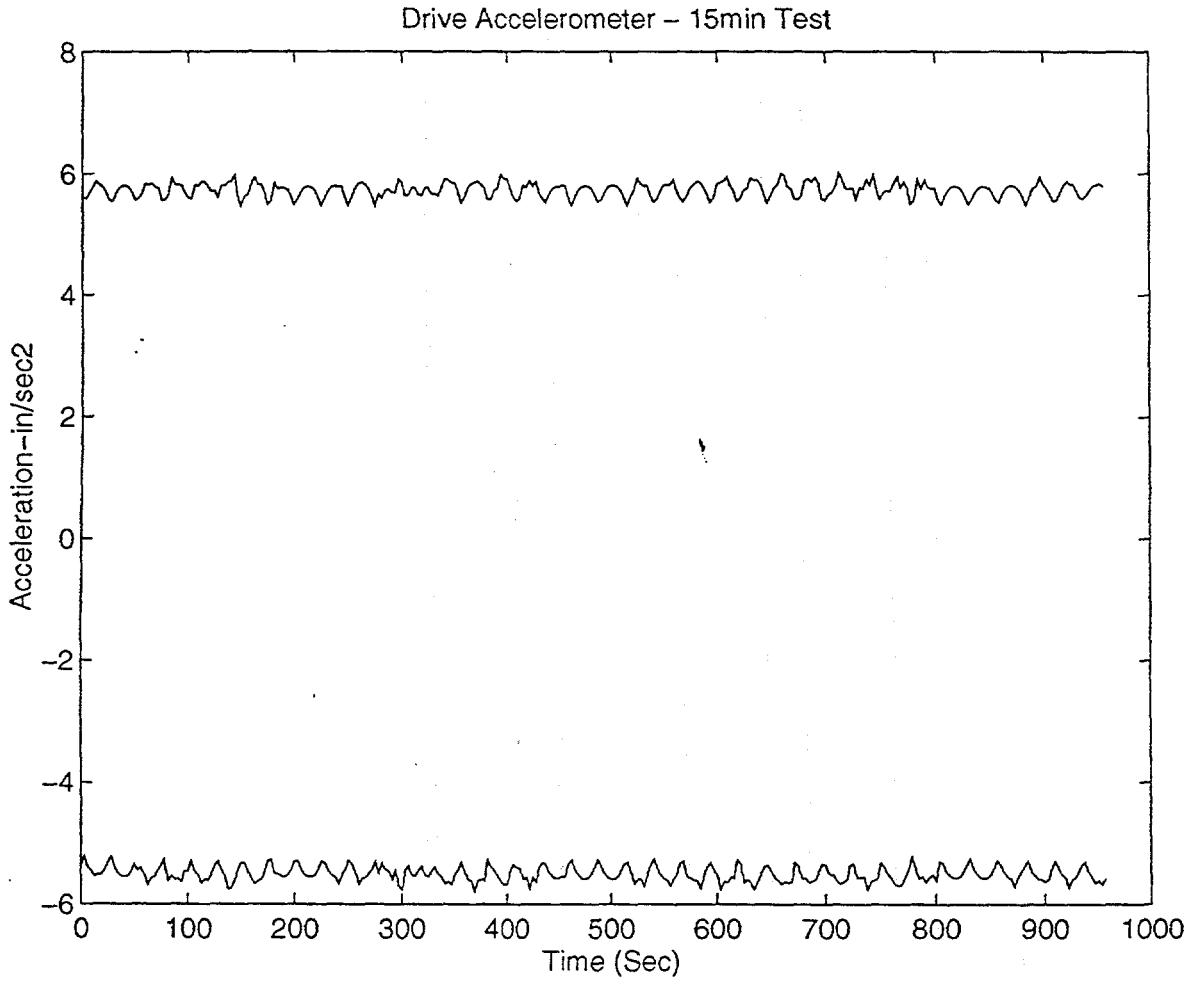
Drive Accelerometer – 15min Test
Acceleration-in/sec2
8
6
4
2
0
-2
-4
-6
0
100
200
300
400
500
600
700
800
900
1000
Time (Sec)

FIGURE 18

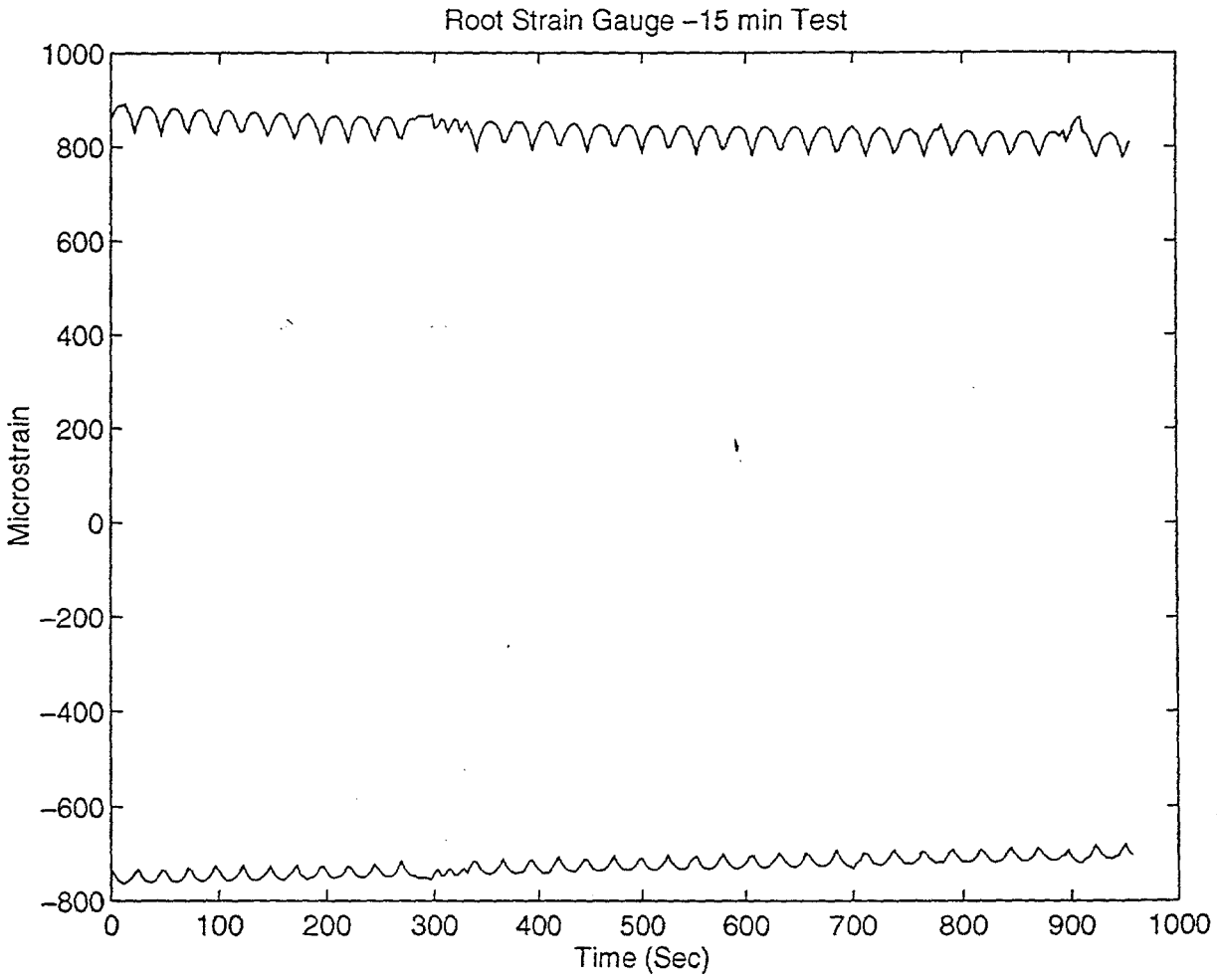
Root Strain Gauge –15 min Test
1000
800
600
400
200
0
–200
–400
–600
–800
Microstrain
0
100
200
300
400
500
600
700
800
900
1000
Time (Sec)

FIGURE 19

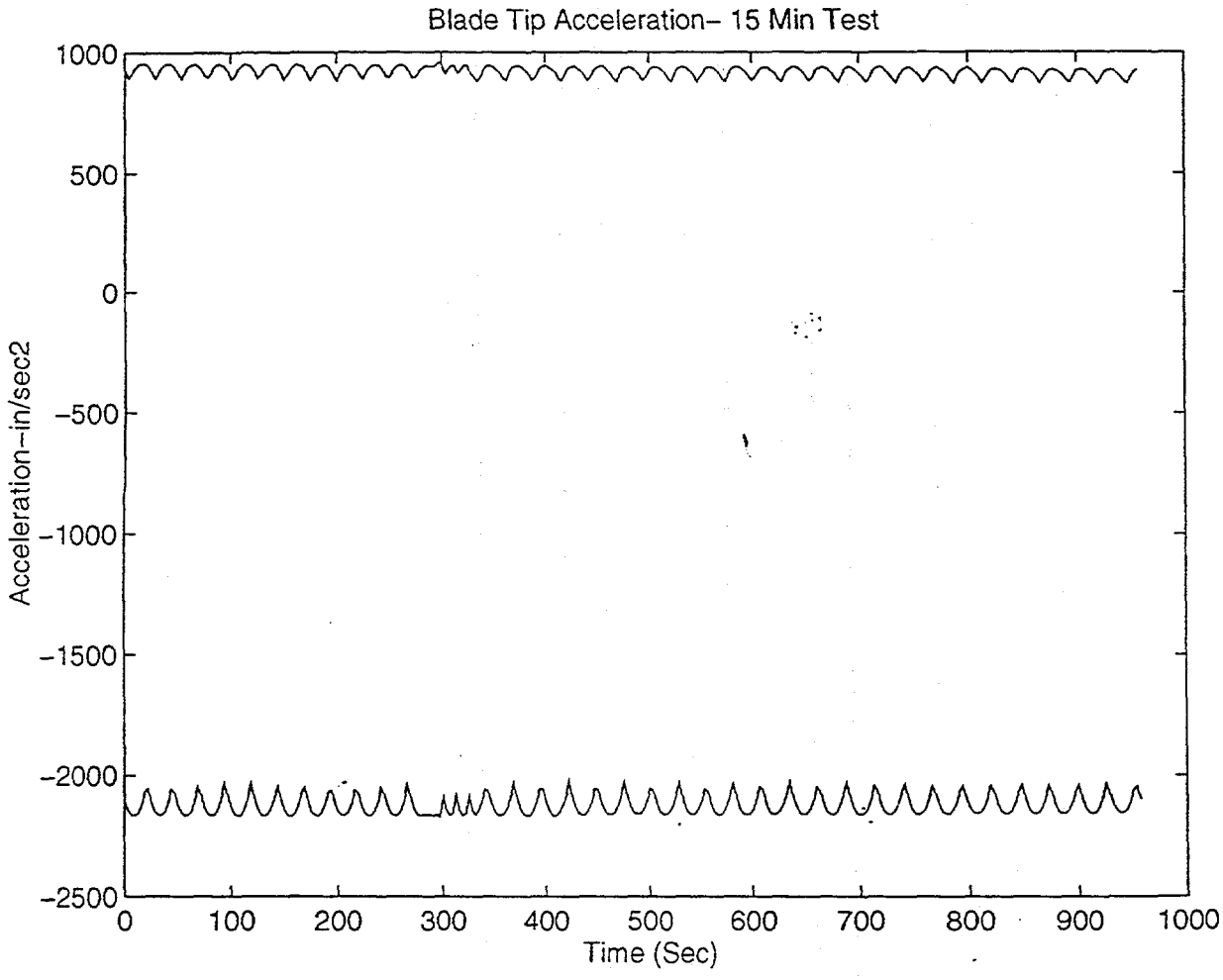
Blade Tip Acceleration– 15 Min Test
1000
500
0
−500
−1000
−1500
−2000
−2500
Acceleration–in/sec2
0
100
200
300
400
500
600
700
800
900
1000
Time (Sec)

FIGURE 20

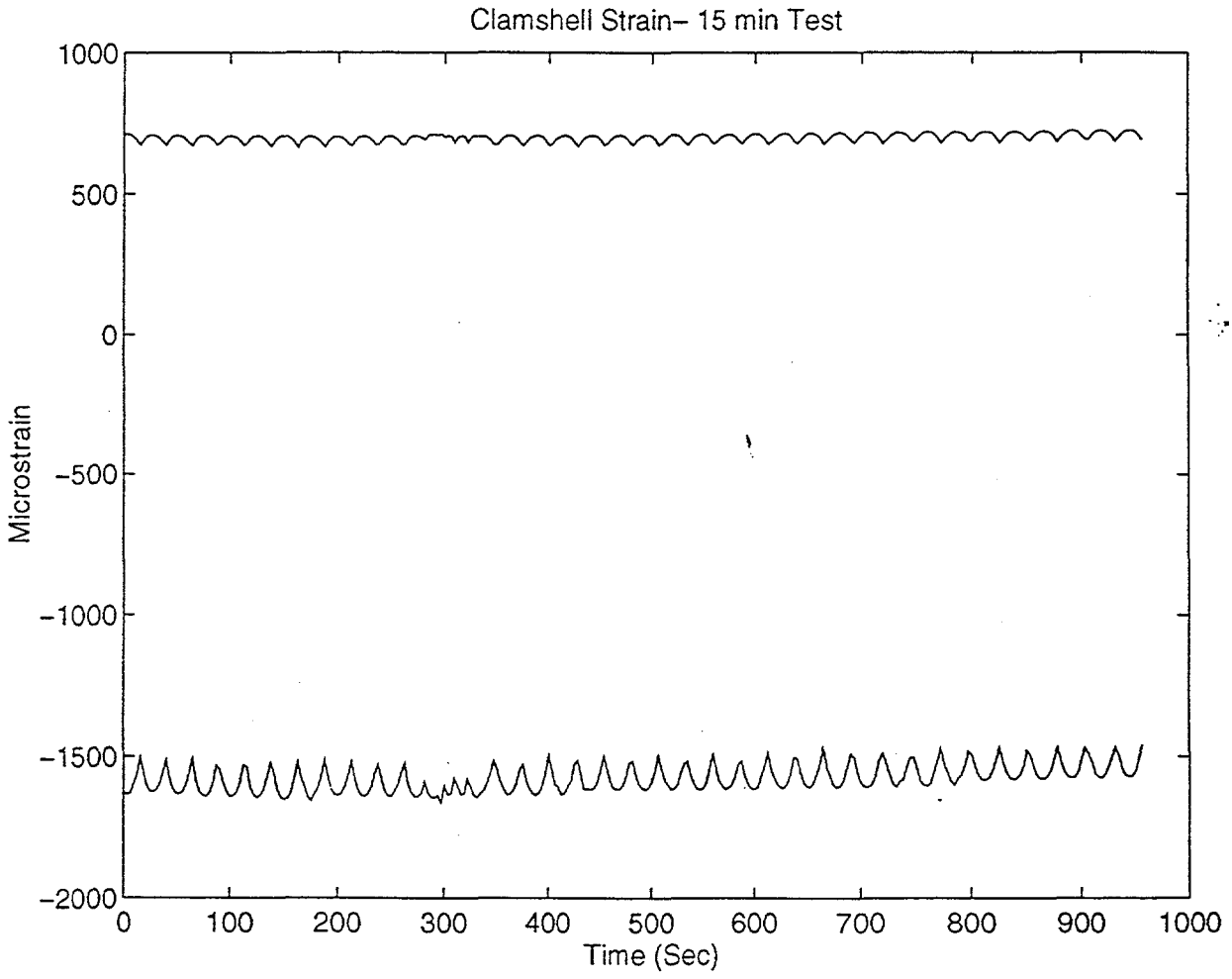
Clamshell Strain– 15 min Test
1000
500
0
-500
-1000
-1500
-2000
Microstrain
0
100
200
300
400
500
600
700
800
900
1000
Time (Sec)

FIGURE 21

Intentionally Left Blank

APPENDIX D

DAMAGE DETECTION AND HEALTH MONITORING OF OPERATIONAL STRUCTURES

George James, Tom Carne, Randy Mayes, and Garth Reese

Proceedings of the Adaptive Structures and Material Systems Symposium of the 1994 ASME Winter Annual Meeting
Chicago, IL

November 6-11, 1994

Intentionally Left Blank

DAMAGE DETECTION AND HEALTH MONITORING OF OPERATIONAL STRUCTURES

George James, Randy Mayes, Thomas Carne, and Garth Reese
Experimental Structural Dynamics Department
Sandia National Laboratories
Albuquerque, NM 87185-0557

ABSTRACT

Initial damage detection/health monitoring experiments have been performed on three different operational structures: a fracture critical bridge, a composite wind turbine blade, and an aging aircraft. An induced damage test was performed on the Rio Grande/I40 bridge before its demolition. The composite wind turbine test was fatigued to failure with periodic modal testing performed throughout the testing. The front fuselage of a DC-9 aircraft was used as the testbed for an induced damage test. These tests have yielded important insights into techniques for experimental damage detection on real structures. Additionally, the data are currently being used with current damage detection algorithms to further develop the numerical technology. State of the art testing technologies such as, high density modal testing, scanning laser vibrometry and natural excitation testing have also been utilized for these tests.

INTRODUCTION

Today's society depends upon many structures (such as aircraft, bridges, wind turbines, offshore platforms, and buildings) which are nearing the end of their design lifetime. Since these structures cannot be economically replaced, techniques for damage detection and health monitoring must be developed and implemented. Modal and structural dynamics measurements hold promise for the global non-destructive inspection of a variety of structures since surface measurements of a vibrating structure can provide information about the health of the internal members without costly (or impossible) dismantling of the structure. Advanced signal processing, non-contacting and embedded sensors, and analysis/test correlation technologies combine to make this a promising approach for the health monitoring of operational structures.

An operational structure is defined to be one which can perform, is performing, or has performed its intended function as opposed to a laboratory test article or a computer model. Operational structures are often geometrically complex and may be too large to test in a laboratory. These structures are rarely truss-like and in fact tend to be more plate-like. Also, the boundary conditions associated with such structures are not known as well as a laboratory test structure or a computer model. And finally, the environment associated with an operational structure (e.g. weather, traffic patterns, or location) is usually changing and has a serious impact on the measured structural response. Therefore, it is desirable to perform health monitoring research and development on structures possessing such characteristics. This work discusses damage detection studies using three different operational structures.

This report begins by providing a literature review of some of the relevant damage detection/health monitoring research. Three specific tests will then be discussed. The first will be an induced damage test on a decommissioned bridge. The second will be a fatigue test of a wind turbine blade. The final test will an induced damage test on the forward fuselage of an aircraft. All of these tests are still under analysis and no final damage detection results will be presented. A description of each test, representative data, lessons learned, and on-going analyses will be presented followed by a summary and conclusions section.

LITERATURE REVIEW

The following literature survey is by no means an exhaustive compilation of the relevant work. It does represent a collection of authors and their works which have influenced the work performed at Sandia National Laboratories either directly of indirectly.

Early Works

Reference [1] is one of the earliest publication to discuss using changes in dynamic response to track damage. Vandiver draws on modal testing of buildings to propose his technique. He also uses Statistical Energy Analysis to analyze the response of the structure. No experimental data was reported in this presentation.

Reference [2] also is a classic publication in the damage detection work using vibrational frequencies on offshore structures. An offshore platform (West Sole WE) was removed from the North Sea in 1978. An induced damage test was performed on an underwater member. Above and below water level accelerometer measurements were taken using ambient wave excitation. Frequencies and shapes appear to have been determined using peak picking on auto spectra and relative phasing on cross-spectra. Above water measurements contained 15 to 20 peaks between 0 and 10 Hz. Six modes below 4 Hz were studied in detail and tracked as the platform was damaged. The frequencies of these global modes were estimated to have been determined to within 1%. Above water measurements were taken for 45 minutes. Underwater measurements were taken for 20 minutes and showed the global modes as well as several highly damped local modes. Data was acquired for modes up to 20 Hz with five modes between 4 and 10 Hz being studied in detail. The confidence in these modes was estimated at 2 to 3% Finite element models were used to assist in the modal extraction and to verify the results. The general conclusions were that above-water measurements of the lowest global modes could be used to determine the complete failure of a member, while local measurements (requiring underwater accelerometers) could be used to determine partial member failures.

Reference [3] contains experimental data only to correlate a finite element model. Some fine work was performed to estimate confidence levels due to several effects and to determine detectability thresholds. A general framework for determining detectability is developed. Earlier work by the authors is reported which verifies that ambient measurements are acceptable for determining modal parameters.

Crohas and Lepert discuss in reference [4] the idea of continuously monitoring frequency domain information from forced response testing to determine the health of an offshore platform. Although experimental measurements are shown, no health monitoring/damage detection results are provided. They did report measuring up to 40 modes of the structure and reported the local modes of the members starting at 15 Hz.

Stubbs, Osegueda, and Others

Reference [5] is the initial presentation of Stubbs approach. The approach utilizes modal frequency changes before and after damage as well as analytically calculated sensitivities of the modal frequencies w.r.t. the structural parameters at the possible locations of damage. A finite element model is typically used to develop the sensitivity matrices and the approach requires that the frequencies be matched before and after damage. Changes in mass and damping (as well as the sensitivities) are assumed known. A numerical example using a simply supported beam is also provided. The results are favorable for this simple example. The technique as presented iterates to adapt to the regions expected to damage (this is done by setting to zero all positive stiffness changes which are considered non-physical).

Reference [6] is a companion to reference [5] in which Stubb's technique is applied to a simple cantilever beam. Although better modal testing techniques could have been used, the experiment appears to have been relatively complete. The results were successful even though the structure was extremely simple. It was common to see light damage predicted in other areas besides that of the known location. This reference cites four earlier numerical studies in the development of Stubb's method from 1985 to 1990.

Osegueda's thrust in reference [7] is to prepare for a probabilistic formulation for damage detection. A laboratory experiment is described as well as experimental results. Standard deviations on measured frequencies are provided. A good overview of previous work is provided. An important note is that Osegueda has upgraded Stubbs method to include changes in mode shapes as well as frequencies, although no results were included in this publication. Reference [8] is the appropriate reference for these results.

Reference [9] contains a very non-technical summary of Osegueda's research at the University of Texas at El Paso (UTEP) research using an Ometron VPI 9000 Scanning Velocimeter and several different damage detection schemes. Stubbs method (called the eigenvalue sensitivity method in this work) was the first one and required an analytical model to generate the sensitivities. This method worked best when only eigenvalue measurements were available, however the resolution was limited by the number of resonant frequencies. The eigenvalue-eigenvector sensitivity method (developed by Osegueda) allows changes in mode shapes to be used as well. This technique works well, but requires extremely accurate measures of the mode shapes. The exact eigenvalue method (also developed at UTEP) incorporates changes in modal orthogonality into the problem. This method requires a pairing of damaged and undamaged mode shape and works very well with analytical data. These techniques were exercised analytically as well as experimentally. A modal strain energy approach was also applied experimentally and worked well with some of the higher modes.

Reference [10] reports on Stubb's recent work utilizing experimental data from a scale model of a pier deck for health monitoring work. The work reported successful results for these laboratory-based test Reference [11] reports on Stubbs work on the Rio Grande I40 bridge.

Smith and Others

Some of Smith's early work in damage detection of large space structures is presented in reference [12]. An extensive structural identification algorithm developed by Smith and

others is applied to the damage detection problem. Smith's method is an optimal update method which maintains the sparcity of the original finite element model. The method requires a finite element model of the structure, but does use changes in frequency and shape for the system identification problem. Six modes of a simple truss structure were used in this example. A 120 d.o.f. model was used, although only 14 measurement locations were available. Some experimental results (obtained with good modal test procedures and equipment) are presented, however no damage detection results are presented. A technique for expanding the measured mode shapes to the full model d.o.f.s is required. This expansion process did not provide full modes with the proper orthoganality for the system identification technique. Hence, expansion was reported as an area of needed work.

Reference [13] provides the next installment of Smith's work. An expansion/orthoganalization scheme has been developed by Smith & Beattie [14] to correct the orthoganlization problems seen in reference [12]. Also measurements at all 120 locations or any subset of sensors were available. Only three modes (selected differently for each damage case) were used for each damage detection experiment. Tests using analytical data were only successful when all 120 sensors were used. Li and Smith's latest work [15] has produced a hybrid technique which draws from both model sensitivity and optimal matrix update approaches for system identification.

Zimmerman and Others

Zimmerman and Widengren provide a technique in reference [16] which uses control theory techniques to modify structural models. An eigenvalue assignment algorithm is used to calculate a simulated feedback control system which updates a subset of the analytical modes corresponding to the measured modes. Symmetric damping and stiffness matrix updates are calculated. These update matrices will not necessarily maintain the proper connectivity.

Zimmerman and Kaouk [17] refine the method of reference [16] to attack the damage detection problem more effectively. A subspace rotation algorithm is used to enhance eigenvector assignability. A simple iterative scheme is provided to maintain sparcity. The upgraded algorithm is shown to work well as long as the proper eigenvector entries are chosen.

Reference [18] builds on the reference [16] and reference [17] work and adds a damage location pre-processor damage detection problem. Several numerical tests are shown with and without added noise. The technique is shown to work well in this situation. However, all the tests included simulated measurements at every d.o.f.

Kaouk and Zimmerman expand their method to calculate the extent of damage using a perturbation of the original analytical model possessing a minimum rank. They also allow damage in mass and damping properties. Any two matrices can be allowed to change. A simulated example of a 50 bay truss with incomplete eigenvector measurements is used. An experimental example of a mass-loaded cantilever beam is also used. The Minimum Rank Perturbation Theory (MRPT) is further expanded to allow remove the need to have an original Finite Element Model (FEM) [20]. MRPT is further expanded to utilize a variety of test data types including static data [21].

And finally, three groups of damage detection researchers including Zimmerman, Smith, and McDonnell Douglas Aerospace jointly studied the most troubling problem in health monitoring, the incomplete measurements problem [22]. The test structures were truss type objects in this work. However, there were several useful points to consider when performing reduction/expansion which arose from this work.

Peterson, Alvin, Doebling, Park, and Others

A series of experiments to support damage detection by model updating is reported in references [23,24] by University of Colorado-Boulder researchers. It was found that selection of the appropriate modal parameters was critical to the success of such an approach. Also, the truss structure utilized for these tests exhibited a multitude of localized modes. This further complicated modal selection and modal data reduction.

Reference [25] is largely concerned with producing normal modes from complex modes generated by ERA however, a number of important issues relating damage detection are addressed by this work. A multiple step process is provided, however the last step requires a non-linear minimum norm solution for the case of more modes than sensors. The techniques also require driving point measurements to allow for the proper mass normalization.

An extension of this is the production of mass, damping, and stiffness matrices directly from data [25,26]. The procedure is based on a Guyan reduction, however the reduced matrices (using physical coordinates) are augmented with a set of generalized coordinates to model the extra modes of the system. There is some connection between this procedure and Craig-Bampton component mode synthesis. A damage detection method for truss structures was presented based on these procedures. It required a model order of 500 with fairly automatic modal testing. The results were not conclusive for damage detection, but could hold promise for an iterative procedure. Further application of the experimentally calculated mass and stiffness matrices to damage detection by the University of Colorado-Boulder researchers is reported in reference [27]. The experimental application of these techniques to a truss structure has shown that the extraction of modal vectors for the higher modal frequencies is important. A further direction of research at UC-Boulder which is driven by the work mentioned above, is in the analysis of high-modal density data sets [28].

West and Others

Researchers at Virginia Tech are developing the tools to perform laser velocimeter-based structural imaging [29-31]. This technology promises to allow a high-spatial density grid of 3-D measurements to be acquired in a non-contacting fashion.

The highly localized effects of damage tend to require such measurements.

Sandia and Los Alamos National Laboratories

A technique for localizing damage in a finite element model using experimental data was developed at Sandia [32] and has been named the Structural Translation and Rotation Error CHecking algorithm or STRECH. The technique has recently been expanded to perform damage detection using an undamaged data set [33]. The algorithm first compared the ratio of difference between two sensor location measurements of a damaged mode shape to an undamaged mode shape. It has since been discovered that the static flexibility shape is more sensitive on the Rio Grande/I-40 bridge data.

Another development at Sandia National Laboratories was the Natural Excitation Technique (NExT) [34]. This technique has allowed the modal parameters to be extracted from a variety of structures in their operation environment including wind turbines, transportation systems, missiles [35], and bridges [36].

Los Alamos National Labs performed the dynamics testing of the I-40 bridge [36]. This work included modal testing to support model correlation and damage detection, sine dwell testing to verify new non-contact sensor concepts, and ambient testing using NExT. Sandia Labs provided the excitation source and logistics support for these tests [37]. Recently, the data was used to study the effects of finite element grid density on model correlation and damage detection [38].

Reference [39] describes a recent test to failure of a composite wind turbine blade. The blade was failed using quasi-static loading. Two nondestructive testing techniques, acoustic emission and electronic shearography were used to monitor the blade during the test. This same approach was adopted for a fatigue test to failure of a similar blade which also included a number of modal tests during the course of the test. Initial results from this test will be provided in this report.

Reference [40] details a set of experiments performed at Sandia Labs on a simulated aircraft panel. Accelerometers and a scanning laser vibrometer were used to study the damage detection using STRECH and techniques developed at UC-Boulder. This work was followed by later experiments in the FAA Aging Aircraft NDI Validation Center at Sandia [41]. An induced damage test was performed on the forward fuselage of a DC-9 aircraft. A stringer was cut in four stages and modal tests were performed using a scanning laser vibrometer after each cut. An extremely dense grid of measurements points was utilized which included over 2000 measurement points. The frequency band of the measurements was from 0 to 2000 Hz with the excitation from 500 to 1500 Hz. The tests also included laser holography measurements.

I40 BRIDGE TEST

The Interstate 40 bridge over the Rio Grande in Albuquerque, New Mexico was a fracture critical bridge which means it was constructed without structural redundancy. Figure 1 provides a schematic of this structure. The primary structural members were two 10' deep plate girders which ran the length of the bridge. If one of these members failed, the bridge could be expected to collapse. Since many similar bridges are still in operation, the Federal Highway Administration and the National Science Foundation provided funds to New Mexico State University (NMSU) to develop and test new nondestructive inspection techniques. NMSU was supported by both Los Alamos [36] and Sandia National Laboratories [37] as well as Texas A&M University [11]. All three support institutions have performed some form of damage detection on the data [11, 33, 36].

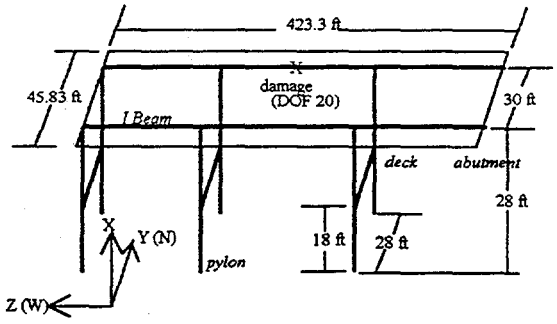

Figure 1. Bridge Model Schematic

Description of Test

The Rio Grande/I40 bridge tests were a set of induced damage tests performed on the decommissioned structure. Before demolition of the bridge, a series of progressively more serious cuts were made in one support beam of the bridge [36]. Los Alamos performed a series of modal tests on the bridge as well as extensive modeling. Modal tests were performed in the initial condition and after each cut. Los Alamos personnel also applied the Sandia-developed Natural Excitation Technique (NExT) [34] to the bridge data which allowed extraction of modal parameters during traffic excitation. A new type of non-contact sensor based on microwave interferometry was also used on the bridge by Los Alamos personnel. Sandia designed and operated the exciter system for the dynamics tests. Sandia personnel also acted as consultants for the application of NExT and provided some logistics support during the modal tests.

A series of four cuts were made in the plate girder after the bridge was closed to all traffic. The fourth cut completely cut half of the lower flange and half of the chosen plate girder. Random excitation was provided from 2-12 Hz with a peak input of 500 lbs. Uniaxial sensors at 26 locations were used as the primary instrumentation set. All sensors and the force input were in the vertical direction. This allowed the extraction of six modes in this direction. Power spectral density data from 10 additional sensor locations for the Texas A&M work were also acquired. Also, sine dwell testing was provided for the Los Alamos microwave sensors.

Representative Results

Figure 2 provides the driving point frequency response function before damage . Table 1 lists the modal frequencies for the first six modes after each cut. Notice the slight increase in frequency after the first cut. This inconsistency is believed to be due to mass being removed from an adjacent bridge which shares the same pillar. In general the changes in frequency become obvious only after the fourth cut.

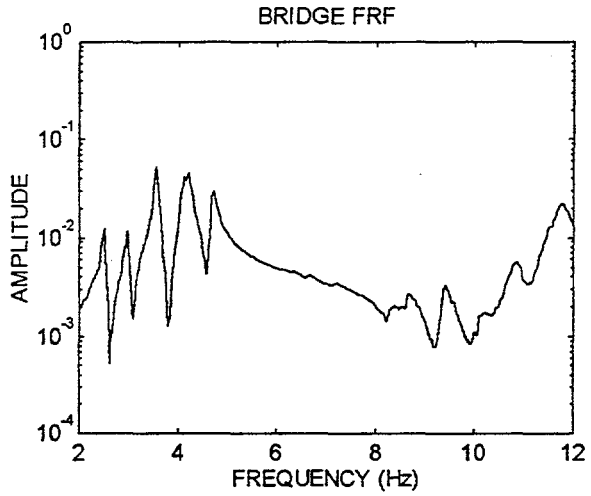

Figure 2. Bridge FRFs Before & After Damage

Table 1. Modal Frequencies (Hz) vs. Damage Case

	DAMAGE CASE				
MODE	0	1	2	3	4
1	2.48	2.51	2.52	2.46	2.29
2	2.96	2.99	2.99	2.94	2.84
3	3.54	3.57	3.52	3.48	3.49
4	4.09	4.12	4.10	4.04	3.99
5	4.16	4.21	4.19	4.14	4.15
6	4.64	4.67	4.66	4.58	4.52

Lessons Learned

The excitation system used on the I40 bridge tests was required to perform both random and sine dwell testing to meet all of Los Alamos' requirements. However, for modal testing specific applications, an impact type exciter would be more useful. such a device would put more energy in at the lower end of the frequency spectrum. This would aid in the estimation of static stiffness. Also, such a device would be more portable and hence have more field applicability.

The spatial proximity of the sensors is critical to the ability to resolve damage location. Therefore, a larger number of sensor locations would have been useful. Also, for model based techniques of damage detection the reduction of unmeasured degrees of freedom (d.o.f.) is a great source of error. Therefore, measuring more d.o.f. is useful. Also, accelerometers with lower frequency response would improve the results of such tests. Alternatively, displacement or velocity based sensors could be considered. The utility of a software driven measurement device such as a scanning laser vibrometer should be studied for field applications.

Certain inconsistencies resulted in the data which were suspected to be caused by traffic on adjacent bridges and demolition of other bridges nearby. The ability to measure or otherwise quantify these effects is useful.

A important outcome of the Los Alamos tests is that NExT works well on these type of structures. Further developments of health monitoring using NExT data can greatly increase the applicability to operational structures. The ideal health monitoring system would include non-contact or embedded measurements taken from a structure undergoing in-situ excitation in its operating environment coupled with automated or semi-automated signal processing.

On-Going Analysis

The Structural Translation and Rotational Error CHecking algorithm (STRECH) was a tool originally developed for test/analysis correlation by comparing deflection changes between adjacent measurement points in measured and analytical mode shapes. STRECH is currently being used to compare experimental shape information before and after damage to the bridge. Analytical sensitivity studies on STRECH using the finite element method are also underway utilizing this bridge data. Other damage detection methods are also currently being used on this data. A study of various modeling issues which affect correlation and damage detection is also underway.

WIND TURBINE BLADE TEST

A fatigue test to failure of a composite wind turbine blade was performed at the National Renewable Energy Laboratory. Periodic modal tests were performed during this test as well as acoustic emissions tests. This data will be utilized to further study the application of health monitoring techniques. When coupled with a non-contact transducer such as a scanning laser vibrometer, this technology could be applied in the field to periodically monitor a field of wind turbines and estimate remaining life in the blades.

Description of Test

The fatigue test of the blade was periodically stopped to allow modal testing to be performed. Accelerometers were placed at 30 locations on the blade and data was acquired to 64 Hz. Approximately nine modal frequencies are present in this band. Impact excitation with a three pound instrumented mallet was used. National Renewable Energy Laboratory personnel performed the modal tests using Sandia Lab equipment and consulting. There were 51 days of testing and 32 modal tests spread over a four month period.

Representative Results

Figure 3 provides a comparison between the initial FRF (solid line) measured at the end of the blade before the test and after the test (dashed line). Visible changes in the FRF's can be seen. Figure 4 is a plot of the real part of the same FRF at 3 Hz for each of the 32 modal tests. As the value of the FRF goes up at the low end the stiffness is dropping. As seen in Figure 4, this trend continues until day 40. The straight line is a linear fit to the data up to this point and serves to reinforce this trend. After day 40, the stiffness begins to increase (FRF value decreases). This is contrary to intuition and is receiving further study. It should be noted that this method for estimating static stiffness is a quick-look approach and not considered the final results.

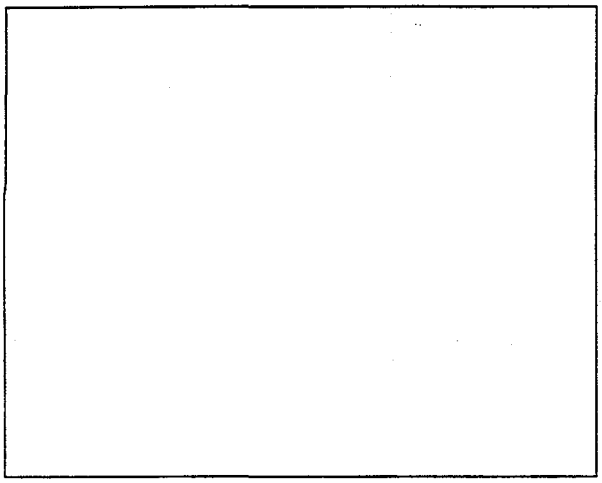

Figure 3. Blade FRF's Before & After

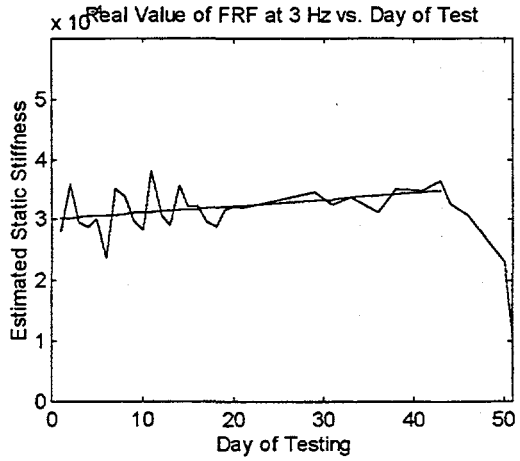

Figure 4. Real Value of FRF's at 3 Hz

Lessons Learned

The data analysis of this test is currently underway and no final results are available. However, the need for consistent and high-quality modal data is apparent. The appearance of such anomalies as increasing stiffness at the end of the test require doubts about the testing procedure to be cleared up.

On-Going Analysis

Modal data analysis is underway. Part of this process is to estimate static stiffness from modal measurements. This is expected to provide higher quality results than those presented in Figure 4. Damage detection techniques including STRECH will be applied to this data set after modal analysis. The results can then be compared to acoustic emissions results.

AGING AIRCRAFT TEST

Modal and structural dynamics measurements hold promise for the global non-destructive inspection of a variety of structures including aging aircraft. Surface measurements of a vibrating structure can provide information about the health of the internal members without costly (or impossible) dismantling of the object. However, there are limitations with the traditional measurement techniques for these parameters (modal frequencies, modal damping, mode shapes, operating shapes, and frequency response functions). Modal testing techniques can cover a broad frequency band and have a large suite of mathematical tools for signal processing. However, modal testing is characterized by contact sensors, low spatial density, and low frequencies (less than 1kHz). These limitations severely restrict the ability of modal techniques to locate the type of damage seen in aging aircraft. Full-field techniques, such as laser holography, provide high frequency, high spatial density measurements in a non-contact fashion. However, laser imaging techniques operate on a single frequency at a time and do not have the same level of mathematical processing support as modal techniques. Laser velocimetry provides a "best of both worlds" approach with some extra advantages not found in modal or full-field techniques. High-frequency, high spatial density measurements can be obtained in a non-contact fashion. Quantitative mathematical results are available as with modal techniques. Laser velocimetry can acquire broad-band frequency information and spatial position can be controlled through software.

Description of Test

An induced damage test was performed on the front fuselage of a decommissioned DC-9 transport aircraft. A non-contacting laser velocimeter was used to acquire broad-band frequency response functions using a dense grid of spatial measurement points. Figure 5 shows a schematic of the induced damage test. Stringer S21R forward of frame BS256 on the DC-9 was cut in four stages as shown in Figure 5. A complete data set was not taken at cut 1 and this cut is not shown. An electrodynamic shaker was attached to the skin of the aircraft to provide dynamic input. Random input between 500 and 1500 Hz was used with a two pound maximum amplitude. Data was acquired from 0 to 2000 Hz.

All measurements were acquired with a scanning laser vibrometer on the exterior skin of the aircraft. Two data sets were obtained for each modal test. One data set covered the 38" by 14" area with only 53 measurement points. Measurements were concentrated on the major structural members and around the damage area. A driving point accelerometer FRF was saved for each laser FRF. Fifty averages were used for the 2048 point FRFs. The second data set took a measurement every .5" to produce a measurement grid of 2233 points. Driving point information was not saved. The FRF's were calculated with 10 averages and 1024 frequency lines. The time required to take this large data set was 3 hours and 45 minutes.

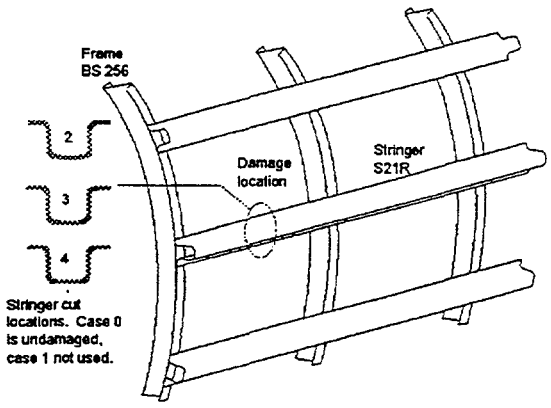

Figure 5. Schematic of Aging Aircraft Test

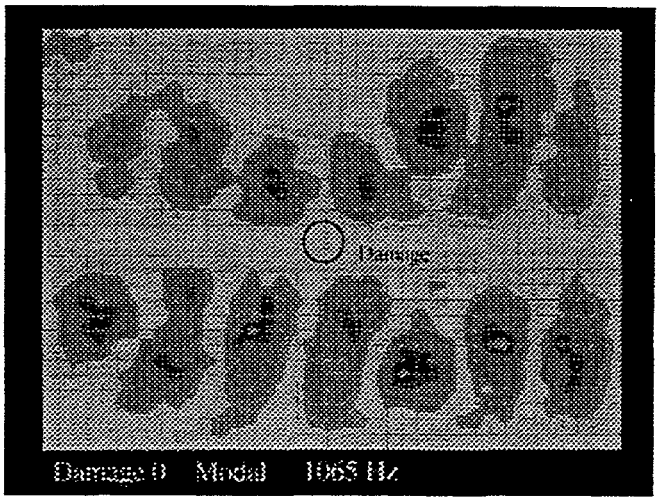

Figure 6. 1065 Hz Mode Damage Case 0

Representative Results

Figure 6 provides a contour plot of the amplitude of a mode at 1065 Hz. The dark regions denote highest amplitude of vibration. This plot includes the region between two frames with the damage in the center of the plot. Figure 5 provides a reference for this. The light band across the center of the plot is the area constrained by the stringer to be damaged. It can be seen that the motion is a seven lobed mode in the lower bay.

Figure 7. provides a similar mode at 1062 Hz after the second cut. The pattern is roughly the same as seen in Figure 6 although the mode shows less noise. Figure 8. provides the results from the mode at 1051 Hz after the third cut. The character of this mode is different than the undamaged mode. There is motion on the actual stringer. Figure 9 provides the mode at 1059 Hz after the fourth cut. The character of the mode is significantly different with much more motion on the stringer.

Lessons Learned

Future tests should include shaker excitation on a major structural members of the fuselage. Also, the excitation should include the lower frequencies of the spectrum. There appears to be useful information in the lower frequencies of the structure. The laser vibrometer outputs were contained a great deal of noise. This problem is currently under study and should be rectified before future testing is carried out.

There were several environmental changes in the structure throughout the course of the test. This should be studied carefully since such a situation will exist in reality. Damage detection techniques which are robust or can detect environmental changes should be developed.

On-Going Analysis

The results presented above show that the measurement technique can detect damage. However to be useful, single mode comparisons are not feasible. Global stiffness metrics such as static mode shapes or experimental stiffness matrices should be used to avoid these problems. These techniques are currently being applied to this data set. Another test similar to this one is currently being planned to incorporate information gained from this test.

SUMMARY AND CONCLUSIONS

Initial studies on damage detection and health monitoring have been performed on three operational structures. The data from these tests are still under analysis, however the results appear encouraging. In general, the collection of consistent and quality modal data is at the heart of this work. There are several techniques for damage detection which are available for numerical processing which are under study. Global stiffness metrics (static shapes, experimental stiffness matrices, analytical model comparisons) which do not require a one-to-one comparison of modes appear to hold promise. Non-contact measurement techniques are useful for high spatial density and non-intrusive testing as well as rapid application in the field.

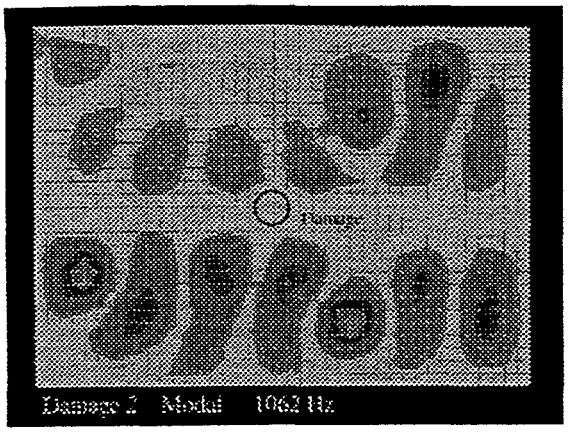

Figure 7. 1062 Hz Mode - Damage Case 2

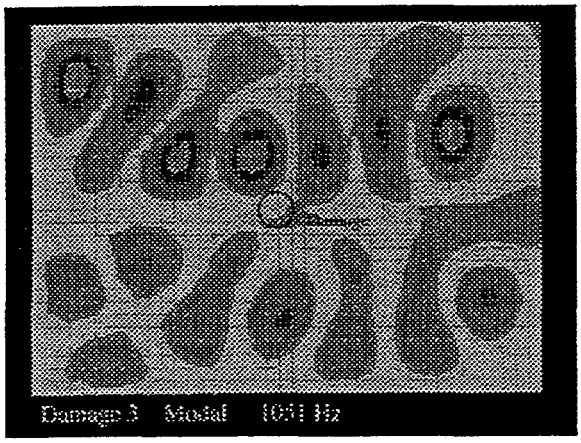

Figure 8. 1051 Hz Mode - Damage Case 3

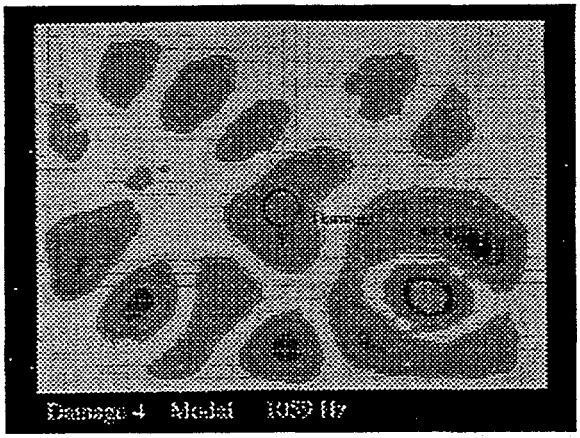

Figure 9. 1059 Hz Mode - Damage Case 4

ACKNOWLEDGMENTS

The authors greatly appreciate the work of Bruce Hansche and Todd Simmermacher, who were instrumental in this work. Our appreciation goes out to Chuck Farrar at Los Alamos National Labs and the Civil Engineering Department of New Mexico State University for allowing us to participate in the I40 bridge test. Engineers at the National Renewable Energy Lab were largely responsible for performing the wind turbine blade modal tests. And finally, the staff of the FAA-AANC and at Holographic, Inc. were critical participants in the aging aircraft tests. This work was supported by the United States Department of Energy under Contract DE-AC04-94AL85000.

REFERENCES

1. Vandiver, J. Kim, "Detection of Structural Failure on Fixed Platforms by Measurement of Dynamic Response", paper OTC 2267, proceedings of the 7th Offshore Technology Conference, Houston, TX, May 5-8, 1975.

2. Kenley, Richard M. and Dodds, Colin J., "West Sole WE Platform: Detection of Damage by Structural Response Measurements", paper OTC 3866, proceedings of the 12th Offshore Technology Conference, Houston, TX, May 5-8, 1980.

3. Coppolino, R. N. and Rubin, Sheldon, "Detectability of Structural Failures in Offshore Platforms by Ambient Vibration Monitoring", paper OTC 3865, proceedings of the 12th Offshore Technology Conference, Houston, TX, May 5-8, 1980.

4. Crohas, H. and Lepert, P., "Damage-Detection Monitoring Method for Offshore Platform is Field Tested", Oil and Gas Journal, February 22, 1982, pp. 94-103.

5. Stubbs, Norris and Osegueda, Roberto, "Global Non-Destructive Damage Evaluation in Solids", International Journal of Analytical and Experimental Modal Analysis, Vol. 5, Number 2, April, 1990, pp. 67-79.

6. Stubbs, Norris and Osegueda, Roberto, "Global Damage Detection in Solids - Experimental Verification", International Journal of Analytical and Experimental Modal Analysis, Vol. 5, Number 2, April, 1990, pp. 81-97.

7. Osegueda, Roberto. A.; DSouza, Paul. D.; and Qiang, Yijie., "Damage Evaluation of Offshore Structures Using Resonant Frequency Shifts", PVP-Vol. 239/MPC-Vol. 33, Serviceability of Petroleum, Process, and Power Equipment, presented at the 1992 ASME Pressure Vessels and Piping Conference, New Orleans, LA, June 21-25, 1992.

8. Osegueda, Roberto A.; Vila, Martin; and Mahajan, S. K., "A Modal Analysis Method for Locating Stiffness and Mass Changes in Structures", Developments in Theoretical and Applied Mechanics, Volume XV, Edited by S. V. Hanagud; M. P. Kamat; and C.E. Ueng, College of Engineering, Georgia Tech University, pp. 333-340.

9. Osegueda, Roberto, "Damage Evaluation of Structures Using Frequencies and Mode Shapes Extracted From Laser Interferometry", Shock & Vibration Information Analysis Center, AD A260119, Nov., 1992.

10. Eggers, David W. and Stubbs, Norris, "Structural Assessment Using Modal Analysis Techniques", proceedings of the 12th International Modal Analysis Conference, Honolulu, Hawaii, January 31 - February 3, 1994.

11. Stubbs, Norris and Kim, Jeong-Tae, "Field Verification of a Nondestructive Damage Localization and Severity Estimation Algorithm", a final report prepared for New Mexico State University under agreement No. 01-3-4439X1, Department of Civil Engineering, Texas A&M University, March 31, 1994.

12. Smith, Suzanne W. and McGowan, Paul E., "Locating Damage Members in a Truss Structure Using Modal Test Data: A Demonstration Experiment", AIAA-89-1291, presented at the 30th AIAA Structures, Structural Dynamics, and Materials Conference, Mobile, Alabama, April 3-5, 1989.

13. McGowan, Paul E.; Smith, Suzanne W.; and Javeed, Mehzad, "Experiments for Locating Damaged members in a Truss Structure", presneted at the 2nd USAF/NASA Workshop on System Identification and Health Monitoring of Precision Space Structures, California Institute of Technology, Pasedena, CA, March 27-29, 1990.

14. Smith, Suzanne W. and Beattie, C. A., "Simultaneous Expansion and Orthogonalization of Measured Modes for Structural Identification", AIAA-90-1218, presented at the AIAA SDM Dynamics Specialists Conference, Long Beach, CA, April, 1990.

15. Li, Cuiping and Smith, Suzanne W., "A Hybrid Approach for Damage Detection in Flexible Structures", AIAA-94-1710-CP, presented at the the AIAA SDM Dynamics Specialists Conference, Hilton Head, SC, April 21-22, 1994.

16. Zimmerman, D. C. and Widengren, M., "Correcting Finite Element Models Using a Symmetric Eigenstructure Assignment Technique", AIAA Journal, Vol. 28, No. 9, September 1990, pp. 1670-1676.

17. Zimmerman, D. C. and Kaouk, "An Eigenstructure [illegible] Assignment Approach For Structural Damage Detection", AIAA Journal, Vol. 30, No. 7, July 1992, pp. 1848-1857.

18. Zimmerman, David C. and Kaouk, M., "Structural Damage Detection using a Subspace Rotation Algorithm.", AIAA-92-2521-CP, presented at the 33rd Structures, Structural Dynamics, and Materials Conference, Dallas, Texas, April, 1992.

19. Kaouk, Mohamed and Zimmerman, David C., "Structural Damage Assessment Using a Generalized Minimum Rank Pertubation Theory", AIAA-93-1483-CP, presented at the 34th Structures, Structural Dynamics, and Materials Conference, La Jolla, CA, April, 1993.

20. Kaouk, Mohamed and Zimmerman, David C., "Structural Damage Detection Using Measured Modal Data and No Original Analytical Model", presented at the 12th International Modal Analysis Conference, Honolulu, Hawaii, January 31 - February 3, 1994.

21. Zimmerman, David C. and Simmermacher, Todd, "Model Refinement and System Health Monitoring Using Data From Multiple Static Loads and Vibration Tests", AIAA-94-1714-CP, presented at the the AIAA SDM Dynamics Specialists Conference, Hilton Head, SC, April 21-22, 1994.

22. Zimmerman, D. C., Smith, S. W., Kim, H. M., and Bartkowicz, T. J., "An Experimental Study of Structural Damage Detection Using Incomplete Measurements", AIAA-94-1712-CP, presented at the the AIAA SDM Dynamics Specialists Conference, Hilton Head, SC, April 21-22, 1994.

23. Doebling, S. W.; Hemez, F. M.; Barlow, M. S.; Peterson, L. D.; and Farhat, C., "Damage Detection in a Suspended Scale Model via Model Update", proceedings of the 11th IMAC conference, Kissimmee Florida, February 1-4, 1993.

24. Doebling, S. W.; Hemez, F. M.; Barlow, M. S.; Peterson, L. D.; and Farhat, C., "Selection of Experimental Modal Data Sets for Damage Detection via Model Update", paper AIAA-93-1481-CP, proceedings of the 34th SDM conference, La Jolla, CA, April 1993.

25. Alvin, Kenneth F., "Second-Order Structural Identification Via State Space-Based System Realizations," CU-CSSC-93-09, Center for Space Structures and Controls, University of Colorado, Boulder, Colorado, April 1993.

26. Alvin, K. F.; Peterson, L. D.; and Park, K. C., "A Method for Determining Minimum-Order Mass and Stiffness Matrices from Modal Test Data", proceedings of the

11th IMAC conference, Kissimmee Florida, February 1-4, 1993.

27. Peterson, L. D.; Alvin, K. F.; Doebling, S. W.; and Park, K. C., "Damage Detection Using Experimentally Measured Mass and Stiffness Matrices", paper AIAA-93-1482-CP, proceedings of the 34th SDM conference, La Jolla, CA, April 1993.

28. Doebling, Scott W., Alvin, Kenneth F., and Peterson, Lee D., "Limitations of State-Space System Identification Algorithms for Structures with High Modal Density", presented at the 12th International Modal Analysis Conference, Honolulu, Hawaii, January 31 - February 3, 1994.

29. Doktor, Christopher A. and West, Robert L., "The Extraction of Longitudinal Strain Fields From the Dynamic Response of a Vibrating Beam", presented at the 12th International Modal Analysis Conference, Honolulu, Hawaii, January 31 - February 3, 1994.

30. Montgomery, David E. and West, Robert L., "Modeling of 2-D and 3-D Velocity Response Fields Using a Nonlinear Optimization Formulation", presented at the 12th International Modal Analysis Conference, Honolulu, Hawaii, January 31 - February 3, 1994.

31. Montgomery, David E. West, Robert L., and Wicks, Alfred L. "Estimation of In-Plane Motion Using Multiple Laser Doppler Vibrometer Scans", presented at the 12th International Modal Analysis Conference, Honolulu, Hawaii, January 31 - February 3, 1994.

32. Mayes, Randy L., "Error Localization Using Mode Shapes - An Application to a Two Link Robot Arm", presented at the 10th International modal Analysis Conference, San Diego, CA, February 3-7, 1992.

33. Mayes, Randy L., "Damage Detection on the I-40 Bridge Using STRECH and Static Flexibility", a Sandia National Laboratories memo to John Minor of the Civil Engineering Department at New Mexico State University, Los Cruces, NM, March 30, 1994.

34. James, George H., Carne, Thomas G., and Lauffer, James P., "The Natural Excitation Technique (NExT) for Modal Parameter Extraction from Operating Wind Turbines", SAND92-1666, Sandia National Laboratories, Albuquerque, NM, 1993.

35. James, George H., Carne Thomas G., and Marek, Edward L., "In-Situ Modal Analysis of STARS Missile Flight Data and Comparison to Pre-Flight Predictions from Test-Reconciled Models," to appear in Proceedings of the 15th IES Aerospace Testing Seminar, Manhattan Beach, CA, October 11-13, 1994.

36. Farrar, C. R., Baker, W. E., Bell, T. M., Cone, K. M., Darling, T. W., Duffey, T. A., Eklund, A., and Migliori, A., "Dynamic Characterization and Damage Detection in the I-40 Bridge over the Rio Grande", LA-12767-MS, Los Alamos National Laboratories, Los Alamos, NM, June 1994.

37. Mayes, Randy L. and Nusser, Michael A., "The Interstate-40 Bridge Shaker Project", SAND 94-0228, Sandia National Laboratories, Albuquerque, NM, April 1994.

38. Simmermacher, Todd, "The Effects of Finite Element Grid Density on Model Correlation and Damage Detection of a Bridge", final report for Outstanding Student Summer Program at Sandia National Laboratories, Experimental Structural Dynamics Department, August 1994.

39. Sutherland, H., Beattie, A., Hansche, B., Musial, W., Allread, J., Johnson, J., and Summers, M., "The Application of Non-Destructive Techniques to the Testing of a Wind Turbine Blade", SAND93-1380, Sandia National Laboratories, Albuquerque, NM, June 1994.

40. Doebling, Scott, "Report on Development of a Laser Doppler Velocimeter System", final report for Outstanding Student Summer Program at Sandia National Laboratories, Experimental Structural Dynamics Department, August 1993.

41. James, G., Hansche, B., Pride, N., Roach, D., Schmidt, T., and Webster, J., "Initial Studies on the Use of Laser Velocimetry, in the Inspection and Health Monitoring of Aircraft", Proceedings of the Quantitative Nondestructive Evaluation Conference", Snowmass, CO, August 2, 1994.

APPENDIX E

An Experimental Algorithm for Detecting Damage Applied to the I40 Bridge over the Rio Grande

Randy Mayes

Proceedings of the 13th SEM International Modal Analysis Conference
Nashville, TN

January 31, 1995

Intentionally Left Blank

An Experimental Algorithm for Detecting Damage Applied to the I-40 Bridge Over the Rio Grande

Randall L. Mayes
Sandia National Laboratories
Experimental Structural Dynamics Department
Albuquerque, New Mexico, USA

ABSTRACT

An algorithm originally used to locate errors in finite element models is applied to a full scale bridge damage detection experiment. The method requires experimental frequency response function data measured at discrete locations along the major bridge load paths. In the bridge damage application the algorithm is most effective when applied to static flexibility shapes estimated with a truncated set of six mode shapes rather than individual mode shapes. The algorithm compares "before damage" and "after damage" data to locate physical areas where significant stiffness changes have occurred. A damage indicator shows whether damage is detectable. Damage is correctly located in the two most significant damage cases using the driving point static flexibility estimates. Limitations of the technique are addressed. The damage detection experiment was performed on a three span steel girder bridge that was 425 feet long. This bridge was part of Interstate 40 across the Rio Grande. The New Mexico State University Department of Civil Engineering organized the experiment. The frequency response functions were collected by Los Alamos National Laboratories personnel. The bridge excitation was provided by Sandia National Laboratories.

NOMENCLATURE

FRF	Frequency response function
x	Displacement scalar
f	Force scalar
SR	STRECH ratio
M	Moment
z	Coordinate in direction of beam axis
E	Young's modulus
I	Area moment of inertia of a beam
θ	Rotation displacement
l	Beam span length between to sensors
Ψ_i^r	Mode shape at point i for rth mode
m_r	Modal mass of rth mode
ω_r	Modal frequency
ω	Frequency
ζ_r	Critical damping ratio
DI	Damage indicator

This work was performed at Sandia National Laboratories and supported by the U.S. Department of Energy under contract DE-AC04-94AL85000.

INTRODUCTION

At the end of the summer in 1993, New Mexico State University directed a series of experiments on a full scale bridge designed to provide a data base for bridge health monitoring algorithms. Sandia National Laboratories participated with Los Alamos National Laboratories in the acquisition of dynamic measurements on the bridge. Sandia furnished and operated a shaker to provide both sinusoidal and random force inputs to the bridge while Los Alamos acquired the dynamic measurements. The modal test was originally designed for use in updating a finite element model of the bridge. However, subsequent to the testing, Sandia obtained the frequency response functions (FRFs) from Los Alamos to attempt to apply some damage detection algorithms to the data. These algorithms were based on a system identification algorithm originally applied in comparing modal test data to a finite element model to physically locate differences between the experimentally derived and analytically derived modal models[1]. This work was performed using funding from a laboratory directed research and development project in health monitoring at Sandia National Laboratories.

Many techniques using modal quantities have been used to attempt to locate damage, assuming that it is basically manifested as a local change in stiffness from the original structure. Frequency comparisons, global mode shape comparisons, and damping comparisons have often been disappointing in determining and locating damage[5]. It is this author's contention that global shape comparisons or even point to point comparisons are not the correct quantities to evaluate. If there is a change in stiffness, then there should be a change in displacement difference *across* that stiffness due to some forcing function. Damage detection techniques that assume a change in stiffness should consider displacement gradient type quantities. This approach is applied in this work.

DESCRIPTION OF EXPERIMENT

Two papers in this conference [2],[3] describe the experiments in detail. A description for the purposes of this paper will now be given. Figure 1 shows a schematic view of the three span bridge that was tested. It was about 425 feet long and was one of three bridges that carried east-bound traffic across the Rio Grande in Albuquerque, New Mexico. The bridge was replaced by a new bridge immediately after the testing , which provided the opportunity to induce significant damage as well as test without traffic on the bridge. Two main steel plate girders (running the entire length) support the bridge, one on either side. This bridge is a fracture critical bridge, meaning that if one of the main plate girders was to fail, there is no redundant support to prevent catastrophic failure. Twenty-six vertical accelerometers were mounted near the neutral axis of the plate girders, 13 along each girder. They were evenly distributed along the length of each span. Damage was induced with a cutting torch just west of center on the north plate girder. There was a series of five tests performed. The first test was performed on the as-used condition. The other tests were performed after each of four progressively severe vertical cuts were induced in the plate girder. The I shaped cross section of the girder is shown in Figure 2. The first cut was in the web centered about the neutral axis, and was two feet long . The second cut extended down to, but not into, the bottom flange. The third cut was halfway through the bottom flange. The final cut severed the bottom flange. Modal tests were performed at each stage using a random force input from the Sandia shaker mounted on the south side of the bridge in the center of the east span as shown in Figure 1. Los Alamos collected data from all sensors simultaneously. New Mexico State University directed the dynamic testing and performed all the static testing as well (not discussed in this paper).

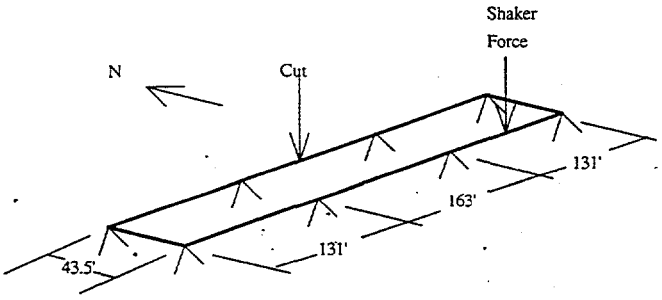

Figure 1 - Schematic of Three Span Bridge

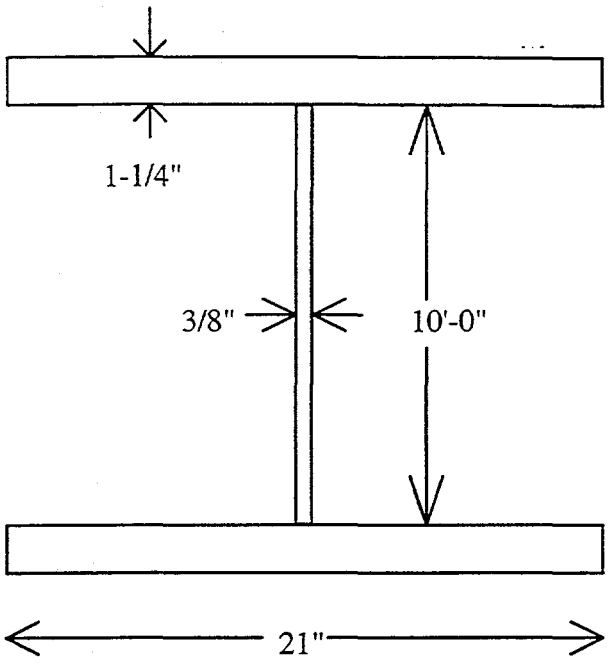

Figure 2 - Cross Section of the Steel Plate Girder (Not to Scale)

STRECH CONCEPT

As stated in the introduction, an algorithm for error localization in a finite element model was published in an earlier IMAC[1]. The algorithm has been named with an acronym, Structural Translation and Rotation Error CHecking or STRECH. STRECH is basically a static concept that has been applied successfully to locate soft or stiff areas of a finite element model by comparing the lowest cantilevered mode shapes from a modal test with the finite element model. A description of the algorithm will be given here utilizing static displacements from a two degree of freedom system as shown in Figure 3. The top figure would represent displacements in a "healthy" structure. The bottom figure would represent the displacements after spring 23 was damaged, that is, reduced in stiffness. For the purpose of this example, assume there is no damage to spring 12.

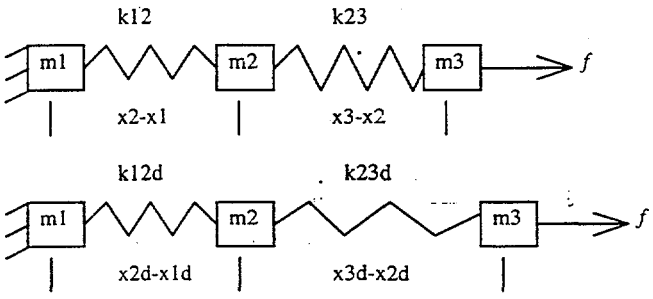

Figure 3 - Demonstration of the STRECH Concept

The simple static force displacement relations from the undamaged case are

$$f = k_{12} \bullet x_{12} = k_{23} \bullet x_{23} \qquad (1)$$

where x_{12} is displacement $x2$-$x1$ and f is the applied force. For the damaged case (superscript d)

$$f = k_{12}^{d} \bullet x_{12}^{d} = k_{23}^{d} \bullet x_{23}^{d} \qquad (2)$$

By equating the right hand sides of (1) and (2)

$$k_{23} \bullet x_{23} = k_{23}^{d} \bullet x_{23}^{d} \qquad (3)$$

which can be rearranged as

$$\frac{x_{23}^{d}}{x_{23}} = \frac{k_{23}}{k_{23}^{d}} > 1 \qquad (4)$$

Similarly, a relationship for spring 12 can be written

$$\frac{x_{12}^{d}}{x_{12}} = \frac{k_{12}}{k_{12}^{d}} = 1 \qquad (5)$$

Theoretically, it would be easy to tell if there were damage to the springs and the extent of damage by applying a known force to both systems and measuring the displacements. In this case equation 4 would show that spring 23 had been damaged. This is the basic concept behind STRECH. The displacements can obviously be rotations and the forces in each element can be moments (which is how the relations will be used for the applications in this paper to the I-40 bridge). The displacement quotients given in equations (4) and (5) are known as the STRECH ratios. In general, additional degrees of freedom, constraints and load paths (i.e. parallel springs) may be included in real physical systems so that extent of damage to an individual spring may not be calculated, but the general trend of being able to detect damage and locate relative soft or stiff areas across the structure has been viable.

Although this concept is a static one, success has been realized by applying this to the first cantilevered mode shape when the mode shape looks a great deal like the static displacement shape. This has been utilized on a cantilevered robot arm, a cantilevered missile payload and a cantilevered third stage of a missile with payload. In each case significant stiffness differences between a finite element model and a modal test mode shape were identified, enabling the analyst to identify critical parameters to update in the finite element model.

NORMALIZATION AND DENOMINATOR FILTER

The realities of acquiring and fitting experimental data from a structure can cause some problems in the interpretation of the results of the STRECH ratios. One problem can occur if experimental data is accidentally taken with an incorrect global scale factor applied. To eliminate some of the confusion that might be caused by such a problem, a normalization has been applied. The STRECH ratio between two sensors are calculated

$$\mathrm{SR}_{ij} = \frac{x_{ij}^{d}}{x_{ij}} \bullet \frac{\sum_{kl} x_{kl}}{\sum_{kl} x_{kl}^{d}} \qquad (6)$$

The superscript d indicates data from the potentially damaged state. Data with no superscript is the baseline data which is considered undamaged. The summations are for all displacement differences defined along the load paths by the engineer. This basically defines the displacement difference x_{ij} as a fraction of the sum of all displacement differences measured for the structure's specific state. Although the average SR is not always exactly equal to one, it is generally very near one. This makes the interpretation of the data much easier, as a value much greater than one will indicate an area of the structure that has been significantly reduced in stiffness (i.e. damaged). The highest SR should correspond to the part of the structure most likely to be damaged. In practice, x is usually a displacement difference between two points on the structure, each of which has three coordinates. The algorithm calculates the square root of the sum of the squares of the three coordinate displacement differences, so that all x quantities shown in equation 6 are positive values. In this application, only vertical accelerations were measured, so the accelerations in the other two coordinate directions were considered zero.

From equation 6 it can be seen that if x_{ij} is very small, the SR can become very uncertain. Since all experimental data has noise associated with it, and data fitting algorithms are not perfect either, a false SR that is very large (because of a small denominator corrupted significantly by noise) may be calculated. A small value of x_{ij} in the denominator means that the structure is not being exercised between points i and j in the baseline structure. If this is the case, the true response should be insensitive to damage between those two points. Therefore, the engineer establishes a minimum denominator value for x_{ij} below which the SR is not calculated at all. In the algorithm, the minimum denominator value is set as a percentage of the largest displacement difference for the baseline structure.

APPLICATION TO THE I-40 BRIDGE

In this paper, the application is health monitoring with experimental data only. Processed experimental data for the I-40 bridge in its as used condition was the baseline data information (undamaged). Processed experimental data from four different

damage cases were the comparison data which were examined for evidence of softening between the sensor locations.

USE OF ROTATIONS

The SRs were calculated based on differences in rotation. The field measurements were accelerations in the vertical direction. Estimates of the rotations were obtained from displacement shape data by passing a parabola through three adjacent displacements on one of the plate girders. The slope of the parabola at the middle point was utilized as the estimate for the rotation of that point. The use of the rotation is justified based on force displacement relations of a beam.

$$M = EI\frac{\partial\theta}{\partial z} \tag{7}$$

where θ is the rotation of the plate girder in the plane of the web and z is in the direction of the neutral axis of the plate girder. M is moment, E is the modulus of elasticity, and I is the area moment of inertia. The partial can be approximated as a finite difference so that equation 7 now takes a form similar to equation 1.

$$M = \frac{EI}{l}\bullet\theta_{ij} \tag{8}$$

θ_{ij} is θ_j-θ_i and l is the distance between two sensors. Two load paths were chosen, one from one end to the other of each plate girder. SRs were calculated between each pair of adjacent accelerometer locations.

STRECH RATIOS USING MODE SHAPES

Initially, SRs were calculated comparing rotation differences for the first mode shape of the damaged and undamaged data. The modal frequency and damping were extracted with the Polyreference technique while real mode shapes were extracted using a technique devised by the author[4]. Six modes were extracted. The SR calculations were marginally successful when applied to the first mode for the third and fourth (most severe) cuts. Calculations applied to higher modes failed miserably. The comparisons for the third and fourth cuts had the worst indications of damage in members adjacent to the four inner pylons, with secondary indications in the damaged area. If the minimum denominator value was raised enough (20 percent or more of the maximum rotation difference in the undamaged bridge), the damaged member showed worst damage because all elements adjacent to pylons were excluded from calculations.

STRECH RATIOS USING STATIC FLEXIBILITY

Since the SR calculations were not extremely successful in detecting the location of damage with the first mode shape, another approach was utilized. Because the STRECH ratio is a static concept, a static deflection should work better for comparisons than a dynamic mode shape. An estimate of the static flexibility (the static deflection shape due to a unit load) can be obtained from the modal parameters by use of the following well known formula for the frequency response function based on real modes.

$$\frac{x(\omega)}{f(\omega)} = \sum_{r=1}^{\infty}\frac{\Psi_i^r\Psi_k^r}{m_r(\omega_r^2 - \omega^2 + 2j\varsigma_r\omega\omega_r)} \tag{9}$$

where $x(\omega)$ is displacement as a function of frequency, $f(\omega)$ is an applied point force as a function of frequency, Ψ_i^r is the mode shape at the response point for the rth mode, Ψ_k^r is the mode shape at the driving point for the rth mode, m_r is the modal mass, ζ_r is the damping ratio, ω is the frequency in radians/second, ω_r is the rth natural frequency and the summation is for all modes. An estimate of the static flexibility is achieved by evaluating equation 9 at zero frequency. In this case a truncation was made using only 6 modes.

$$\frac{x(0)}{f(0)} = \sum_{r=1}^{6}\frac{\Psi_i^r\Psi_k^r}{m_r\omega_r^2} \tag{10}$$

Theoretically any driving point can be chosen, but the actual driving point appeared most accurate in this work. Figure 4 shows the estimate of the static flexibility shape for the undamaged bridge. The maximum displacement is at the point where the shaker was located. Recall that the damage was induced on the opposite side of the bridge from the shaker in the middle span. Although, this is far from the optimum location for the applied static force in terms of exercising the damaged portion of the bridge, the results were encouraging as compared to the calculations performed with individual mode shapes.

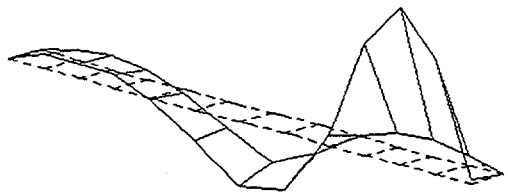

Figure 4 - Static Flexibility Shape of Undamaged Bridge

TRUNCATED STATIC FLEXIBILITY AS A DAMAGE INDICATOR

Figures 5 through 8 give the reader an intuitive feel for the value of the truncated static flexibility as an indicator of damage. The figures show an elevation view of the static flexibility shape of each of the main plate girders. The dashed lines are the undamaged plot. The solid lines are the damaged plot. The damaged girder is offset slightly above the other girder to separate the two. It is easier to separate the two by looking at the left side. The places where it appears there is very little deflection are where the girder ties into the pinned joints at the pylons. These

greatly exaggerated plots show the estimated static deflection as calculated from the modal parameters using equation 10. Notice how the damaged static flexibility shape progressively deviates from the undamaged (dashed) plot. For the most sever damage shown in Figure 8, the differences become very localized, but very pronounced in the center span on the damaged side. The very localized area moment of inertia was reduced by about 1 percent in cut 1, 13 percent in cut 2, 45 percent in cut 3 and 93 percent in cut 4. Remember that the effect is smeared over a significant distance as well. After these figures were obtained, the author attended the '94 IMAC where Aktan and others[5] presented convincing results that identified the static flexibility as a viable indicator of damage. They used 18 modes to increase the accuracy of the static flexibility estimate. The figures indicate that a less accurate static flexibility calculated with only 6 modes provides useful information for this case. This seems plausible, since the damage was introduced in a place that is exercised strongly by four of the first six modes.

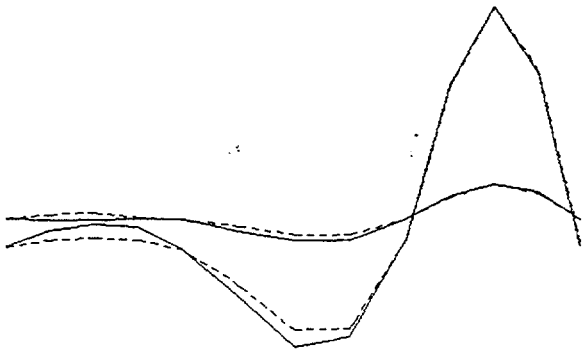

Figure 5 - Static Flexibility Comparisons for Both Main Plate Girders after Cut 1 (Dashed is undamaged - Solid is Damaged)

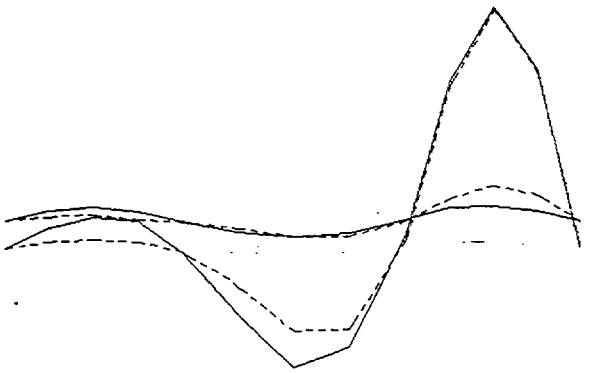

Figure 6 - Static Flexibility Comparisons for Both Main Plate Girders after Cut 2 (Dashed is undamaged - Solid is Damaged)

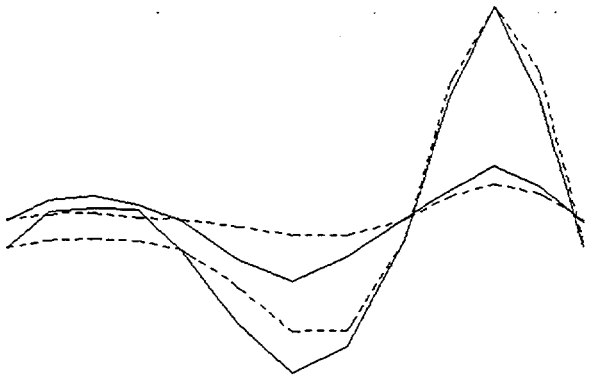

Figure 7 - Static Flexibility Comparisons for Both Main Plate Girders after Cut 3 (Dashed is undamaged - Solid is Damaged)

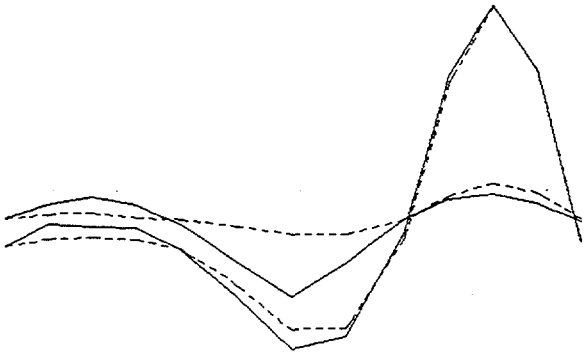

Figure 8 - Static Flexibility Comparisons for Both Main Plate Girders after Cut 4 (Dashed is undamaged - Solid is Damaged)

DAMAGE INDICATOR

Although the previous figures give some intuition into the progression of damage, a close examination would reveal at least the possibility that there is some noise or bias in the shapes. A quantity is needed that can be calculated to indicate the onset of recognizable damage. A threshold value for that quantity needs to be established which is high enough to discount the effects of noise, but low enough to sense significant damage. A quantity is proposed here using terms within the SR calculation as given below.

$$\text{Damage Indicator (DI)} = \frac{\sum_{ij} \left| x_{ij} - x_{ij}^{d} \right|}{\sum_{ij} x_{ij}} \qquad (11)$$

where the terminology is the same as in equation 6. The damage indicator was calculated for each damage case using rotation differences. In addition, the modal parameters were extracted two more times on the undamaged bridge by two other common methods. Static flexibilities for the undamaged bridge were computed, and the damage indicator was also calculated for these two cases in which there was no damage to get a feel for the

effects of variation in modal extraction techniques on the damage estimates. The first extraction of undamaged modal parameters was used as the baseline. These results are printed in Table 1. The first two rows are the damage indicators for the undamaged bridge where the same data was used, but different modal extraction techniques were utilized to form the static flexibility. Then the damage indicators are calculated for each cut. Although this is not a statistically conclusive study, it appears that the damage indicator begins to rise significantly enough at cut 2 to indicate the presence of damage.

Table 1 - Damage Indicators

Case	Damage Indicator
Undamaged - Extraction Method 2	9%
Undamaged - Extraction Method 3	8%
Cut 1	14 %
Cut 2	28%
Cut 3	40 %
Cut 4	33%

DAMAGE LOCATION USING STRECH RATIOS ON STATIC FLEXIBILITY

The SR calculations were much more successful when applied to the static flexibility calculations, even though the damaged part of the structure was not exercised well. Using a minimum denominator value of only one percent (of the maximum rotation difference in the undamaged case) to filter the most noisy calculations, the location of damage was correctly identified for the two worst damage cases, cuts 3 and 4. For cut 1 the damaged location was the second choice of the algorithm. For cut 2 the damaged location was the fourth choice. Why does the calculation appear more successful for cut 1, where the damage was so minimal, than for cut 2? The answer may be in the fidelity of the data. Results from Los Alamos' report [6] show that the input force level was much higher for cuts 1 and 3 than for cuts 2 and 4. This would provide a better signal to noise ratio in the FRFs which could lead to a more accurate static flexibility shape for cut 1 than for cut 2. Even though the signal to noise ratio might not have been as good for cut 4, the damage was so significant that the noise did not matter so much. Note that the SR increases with increasing level of damage in the actual damaged element (number 107-108). Table 2 lists the results.

Table 2 - Predicted Damage Locations for Static Flexibility

Case/Element No.	STRECH Ratio	Comment
Cut 4/ Element 107-108	**13.2**	Correct 1st choice
Cut 3/ Element 107-108	**10.5**	Correct 1st choice
Cut 2/ Element 4-5	7. 07	Wrong 1st choice
Cut 2/ Element 10-11	2.95	Wrong 2nd choice
Cut 2/ Element 12-13	2.89	Wrong 3rd choice
Cut 2/ Element 107-108	**2.81**	Correct 4th choice
Cut 1/ Element 4-5	4.18	Wrong 1st choice
Cut 1/ Element 107-108	**2.53**	Correct 2nd choice

*Note: Element 4-5 was adjacent to a pylon in the same span as the shaker. Elements 10-11 and 12-13 were on the opposite end of the bridge from the shaker where static responses were low. Elements 1-2 through 12-13 were on the south side (shaker side) of the bridge moving from east to west. Elements 101-102 through 112-113 were on the damaged north side of the bridge moving from east to west.

OTHER RESULTS

Although the results shown above are encouraging, in a practical sense, a minimum denominator value higher than 1 percent would probably be desirable for this set of data to reduce the potential of contamination of the static flexibility calculations from measurement and data analysis uncertainties. With the experience gained from past work with the STRECH algorithm, the minimum denominator value should probably be on the order of 5 to 10 percent. Using a more conservative level of 10 percent and applying it to this data, the damaged element is eliminated from the STRECH ratio calculations because the baseline rotation differences for the damaged portion of the bridge fall below this criterion. On the shaker side of the bridge, only measurements in the shaker span and the middle span had rotation differences large enough to qualify for calculation. On the damaged side of the bridge, only elements in the shaker span qualified for calculation. All others fell below the 10 percent minimum denominator requirement. However, in every damage case, for this minimum denominator value, the damaged element selected was element 7-8 which is directly across the bridge from the damaged element.

LESSONS LEARNED, PROPOSED IMPROVEMENTS AND ISSUES FOR FURTHER STUDY

In this experience, the STRECH algorithm performed much better on static flexibility data than on individual mode shapes. There are two possible causes for this. The most probable is that this bridge has eight constraint locations, whereas all structures to which this algorithm has been applied heretofore have had only a single constraint location (cantilevered). Although the static approach of the STRECH algorithm is certainly justified in its application to static flexibility shapes, it may not be applicable to *individual* mode shapes for structures as constrained as bridges. It is known that the STRECH algorithm is not applicable for high order mode shapes for any structure. A second possible cause might be that the rotation estimates are not accurate enough near the constrained points. However, the application of STRECH to

static flexibility shapes did not seem to suffer from this problem. A better algorithm for estimating the rotations might exist, or more measurements could be made. In addition to increasing the accuracy of the rotations, additional measurements also increase the sensitivity of these algorithms, since the effect of damage would not be smeared across such a long length of undamaged structure. The drawbacks to more sensors is increased test cost and increased possibility of faulty instrumentation.

Static flexibilities are more sensitive to damage in highly exercised parts of the structure. A future damage detection test series should have multiple excitation locations to exercise all parts of the bridge more fully. If only one location is possible, it should be in a place where as much of the structure is well exercised as possible. For this case, a location in the center span would have provided a better exercising of all parts of the two main girders. The shaker location was chosen to excite the first six modes well for finite element model reconciliation, not for damage detection. There is some technical advantage to placing the exciter *away* from the center of a span as well. If sensitivity to damage near the pylons is of interest, these areas are exercised only in higher modes of the structure (and some of these modes would need to be included in the static flexibility calculation). An exciter location away from the center of the span might be required to excite some of these higher modes better.

Noise on the measurements and uncertainty in the modal extraction process affect the calculations. Getting as much input force as possible for these large structures would be advantageous. If significant energy can be input at low frequencies, a fitting process might be developed to estimate the low frequency displacement/force FRF asymptote to achieve an extremely accurate static flexibility. This might remove the uncertainty of the modal extraction process as well as the errors in static flexibility due to modal truncation. The advantage to using accelerometers as sensors is that they can be placed directly on the bridge. They do not need a quiescent reference mounting location apart from the bridge as displacement or velocity devices require. The disadvantage is the long cabling required to bring the signals to the data acquisition system.

The setting of the minimum denominator for SR calculations is important for filtering out false indications of damage location. If this setting is too low there will be false indications due to noise. If the setting is too high, many possible locations for damage are eliminated from consideration. This value is probably dependent on data quality, modal extraction quality and relative displacement levels in the static flexibility shape. Engineering judgment is still required. A reasonable value for this test setup is around 5 to 10 percent of the largest rotation difference in the author's opinion.

The damage indicator provides some indication of the onset of damage. The big question is what is the threshold. Performing several different modal extractions on the undamaged data may be a reasonable way of establishing some threshold. A statistical analysis using the ordinary coherence function for the data carried through the extraction process would be more quantitative. The value of the damage indicator is possibly dependent on the number and spread of sensors as well. The damage indicator will not be sensitive to damage at a particular location if the static flexibility is not sensitive to that damage.

CONCLUSIONS

This work adds strong supporting evidence to other referenced work that the static flexibility can be sensitive to damage. In addition, it provides some indication that a truncated set of modes in the static flexibility calculation may be acceptable for indicating damage. The value of a displacement gradient type quantity for use in assessing the onset of damage and the damage location has been strengthened. Algorithms for damage indication and damage location have been demonstrated using experimental data from a full scale bridge damage test series. Lessons have been learned to aid in the planning of future bridge damage detection testing.

REFERENCES

[1] Mayes, Randy, *Error Localization Using Mode Shapes - An Application to a Two Link Robot Arm*, Proceedings of the 10th International Modal Analysis Conference, San Diego, CA, 1992.

[2] Woodward, Clinton, Minor, John, White Kenneth, Idriss, Rolla, *Overview of the Nondestructive Evaluation of the I-40 Rio Grande Bridges*, Proceedings of the 13th International Modal Analysis Conference, Nashville, TN, February 1995.

[3] Farrar, Charles, Kone, Kerry, *Vibration Testing of the I-40 Bridge Before and After the Introduction of Damage*, Proceedings of the 13th International Modal Analysis Conference, Nashville, TN, February 1995.

[4] Mayes, Randall L., *A Multi-Degree-of-Freedom Mode Shape Estimation Algorithm Using Quadrature Response*, Proceedings of the 11th International Modal Analysis Conference, pp. 1026-1034, Kissimmee, FL, 1993.

[5] Aktan, A.E., Lee, K.L., Chuntavan, C., and Aksel, T., *Modal Testing for Structural Identification and Condition Assessment of Constructed Facilities,* Proceedings of the 12th International Modal Analysis Conference, pp. 462-468, Honolulu, HA, 1994.

[6] Farrar, C.R., Baker, W.E., Bell, T.M., Cone, K.M., Darling, T.W., Duffey, T.A., Eklund, A., Migliori, A., *Dynamic Characterization and Damage Detection in the I-40 Bridge Over the Rio Grande,* Los Alamos National Laboratory Report No. LA-12767-MS UC-906, pp87, June 1994.

Intentionally Left Blank

APPENDIX F

NOTES ON THE TESTING OF A SIMULATED GUY ANCHOR UNDERGOING CORROSION

Tom Rice

Personal Notes from a Sandia National Laboratories Internally Funded Project
Albuquerque, NM

February, 1995

Intentionally Left Blank

Simulated Guy Anchor

Sandia National Laboratories

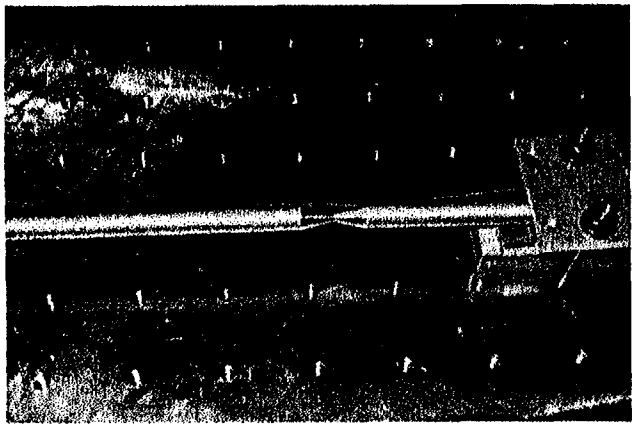

Necked Bar

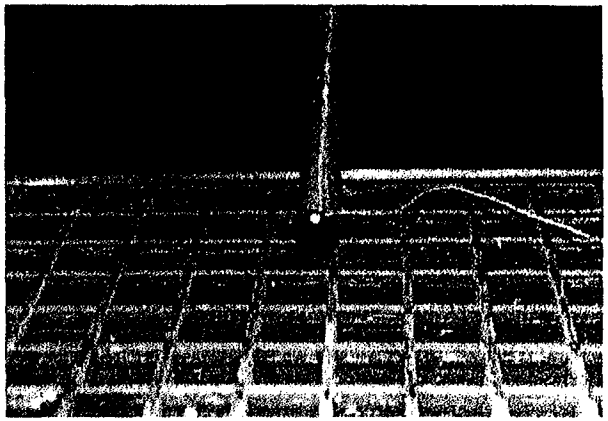

Accelerometer Placement

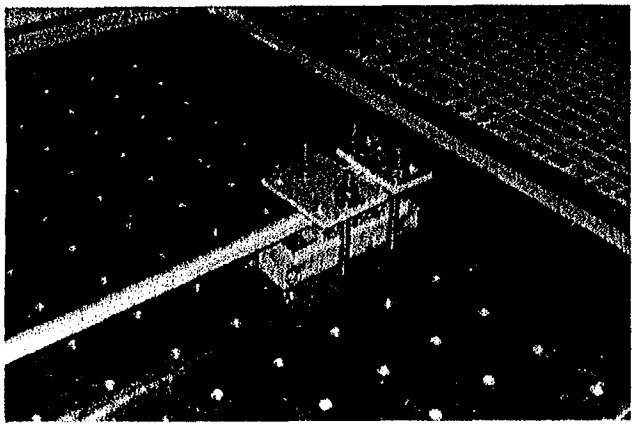

Solid Bar

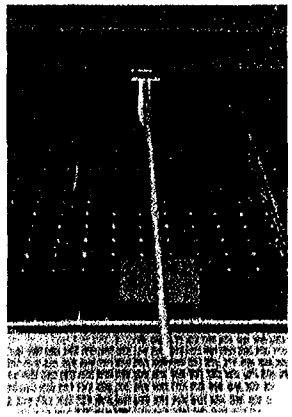

Test Set Up

FLAW DETECTION TEST SET UP (NECKED SECTION SHOWN)

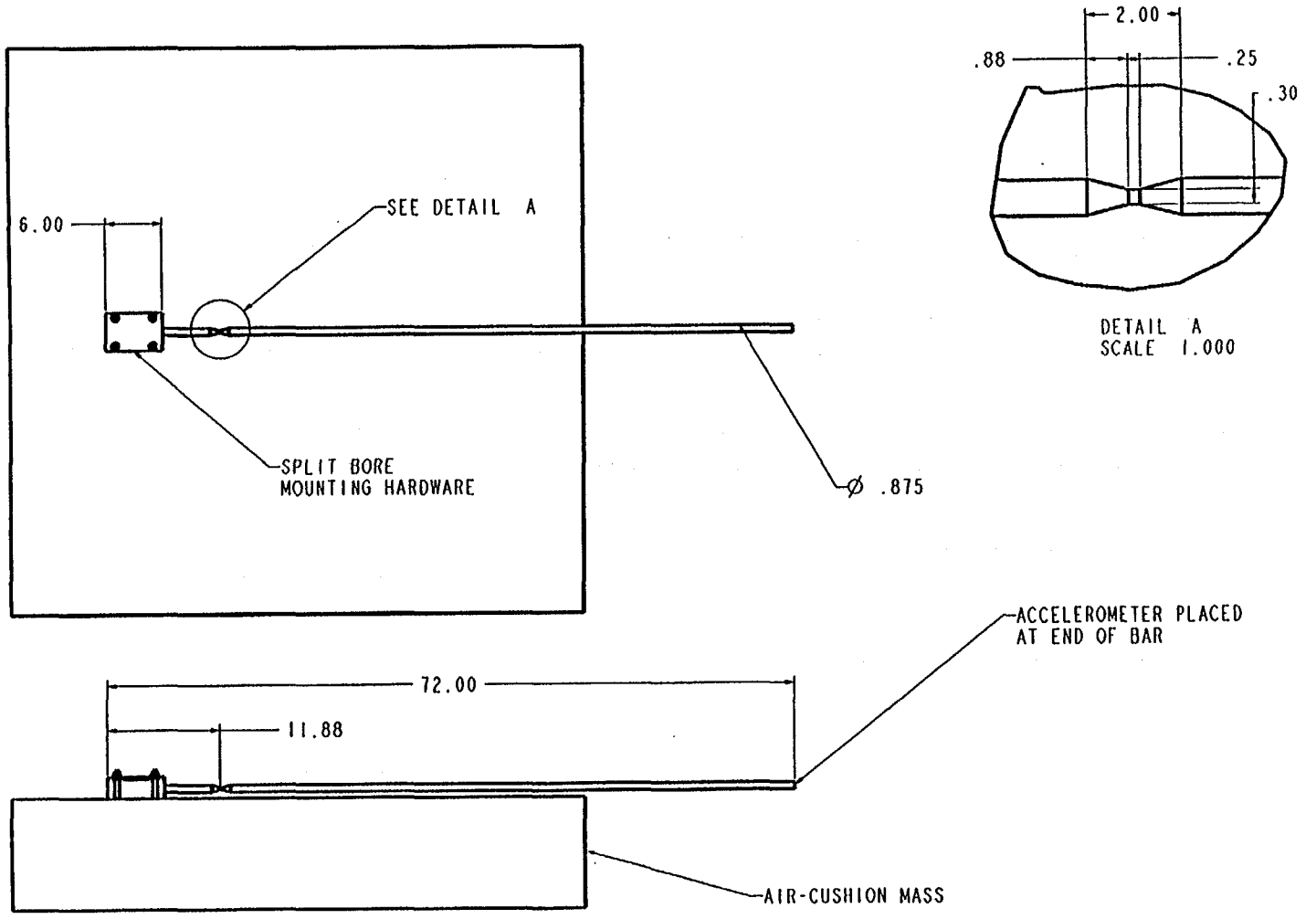

BAR (SOLID), NECKED BAR (DASHED)

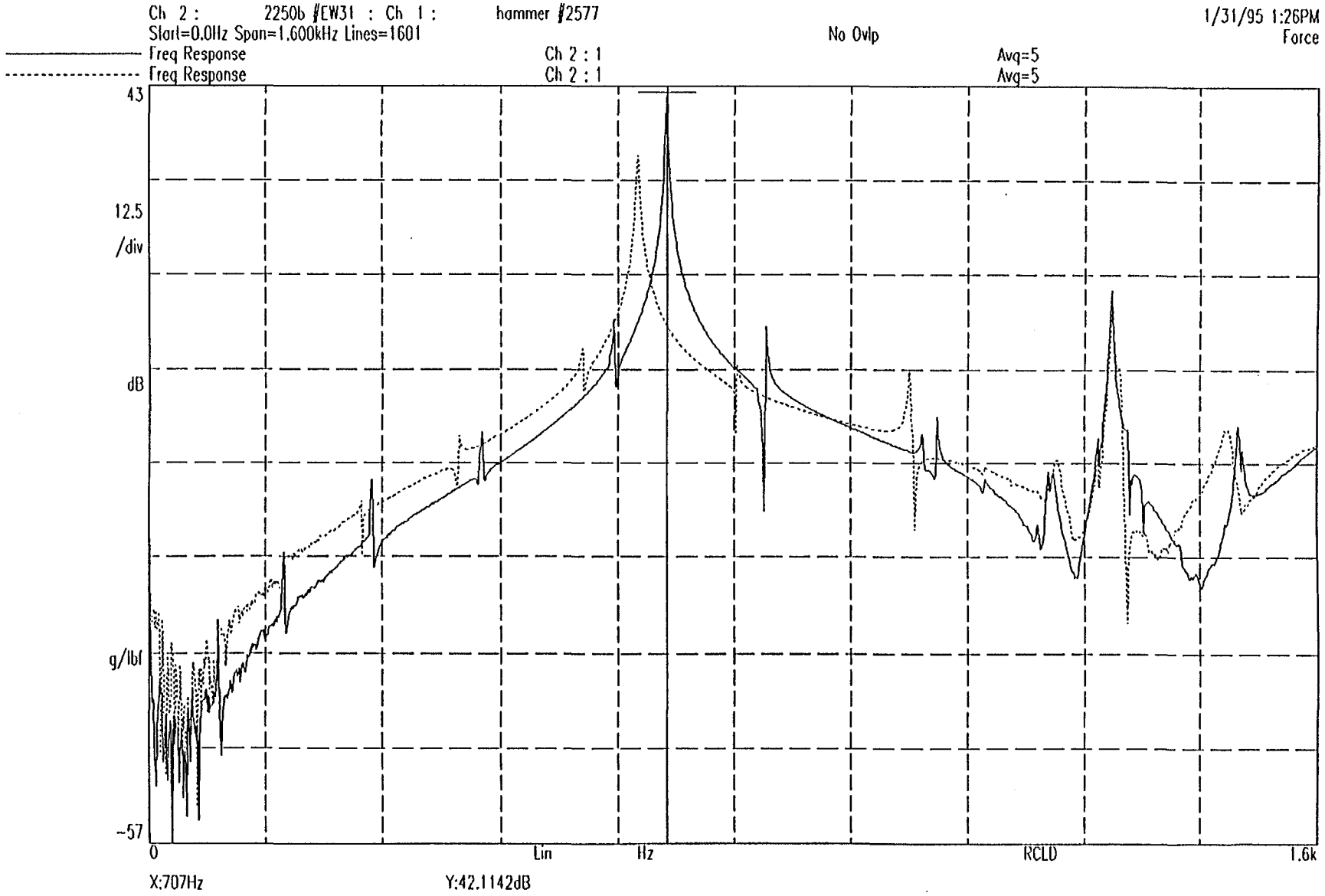

BAR (SOLID), NECKED BAR (DASHED)

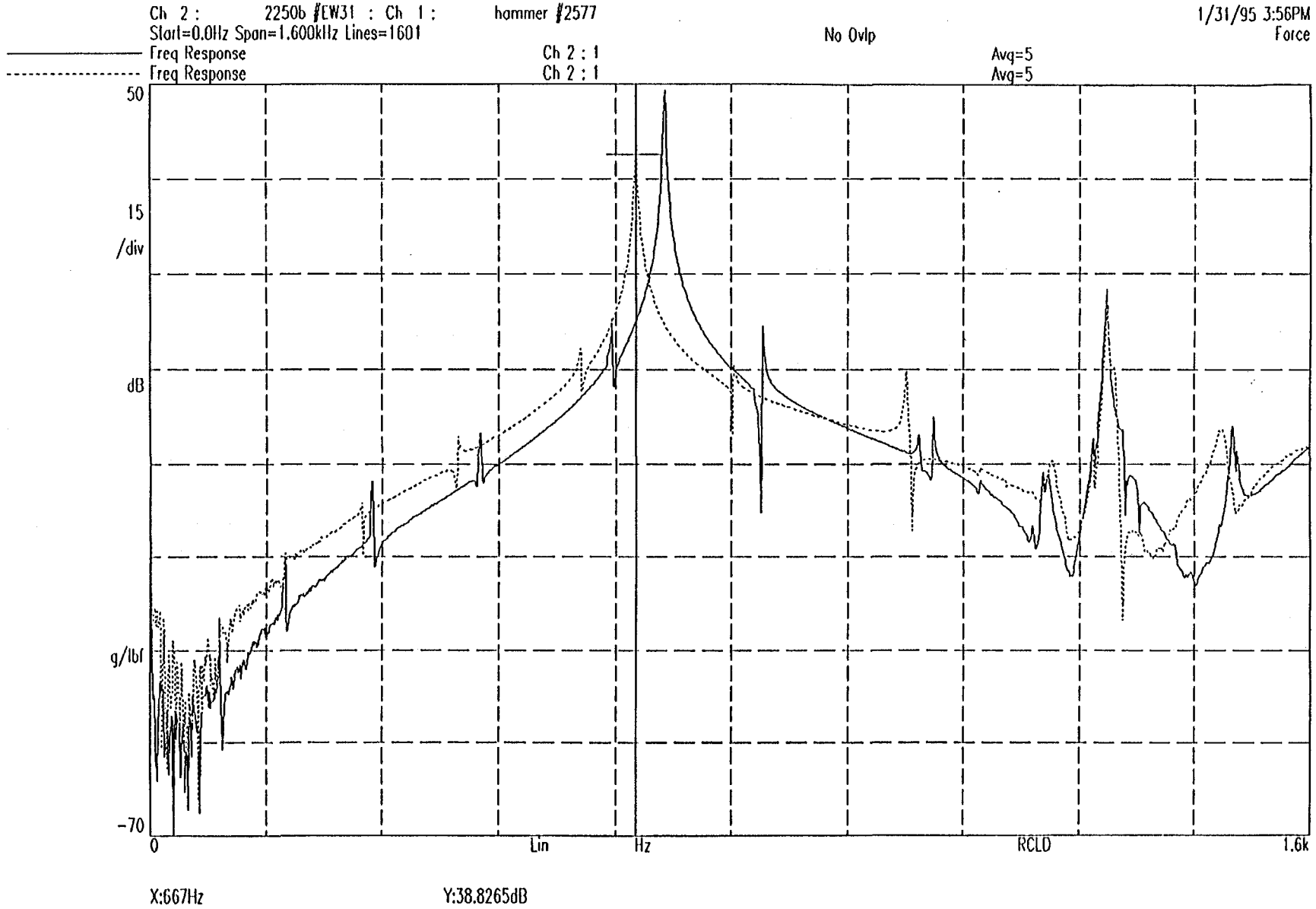

TIME HISTORY OF NECKED ALUMINUM BAR. DATA TAKEN AT 102kHz.

PEAK TO PEAK (709uS-34uS=675uS) FOR RETURN WAVE.

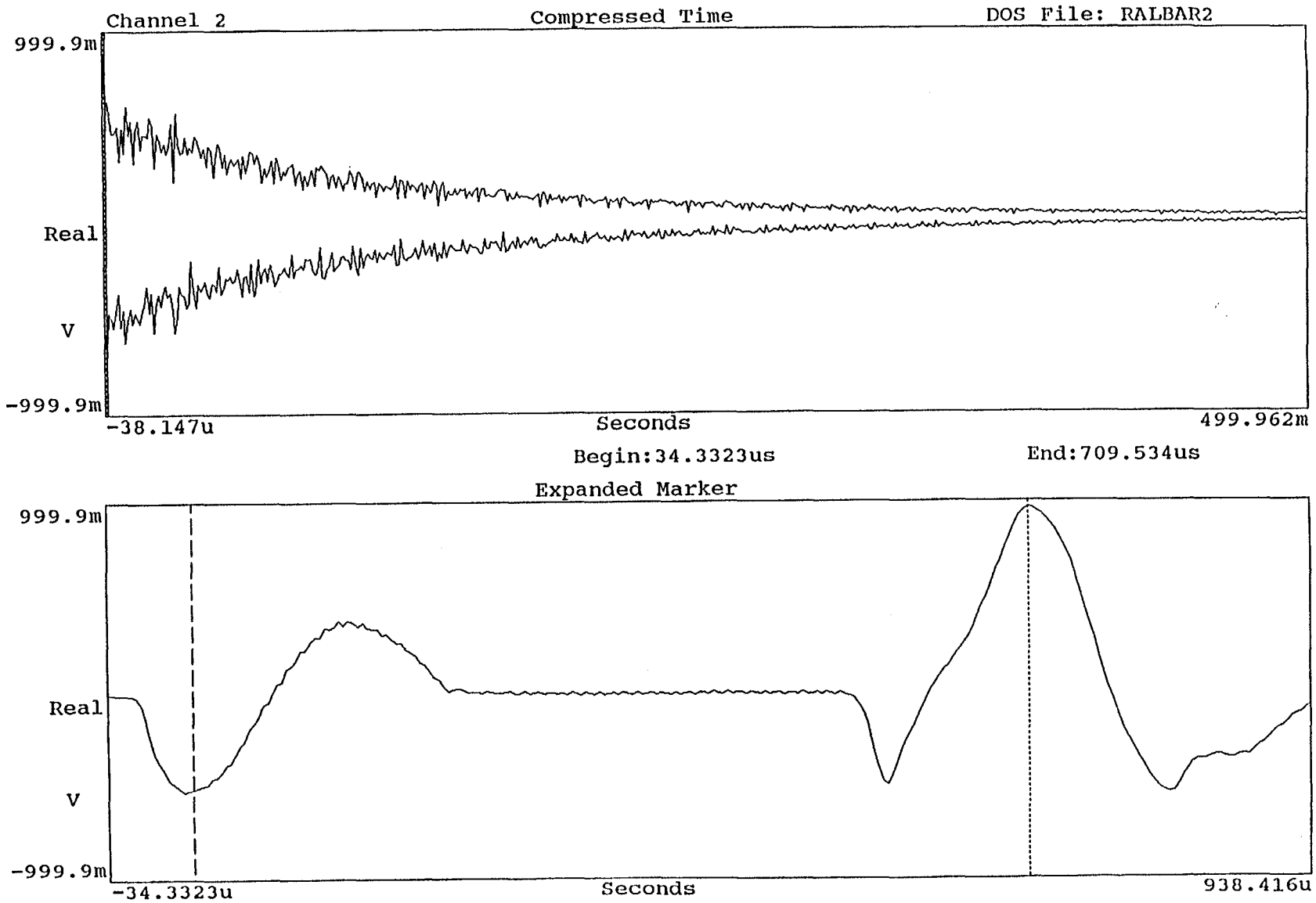

TIME HISTORY OF ALUMINUM BAR. DATA TAKEN AT 102kHz.

PEAK TO PEAK (709uS-34uS=675uS) FOR RETURN WAVE.

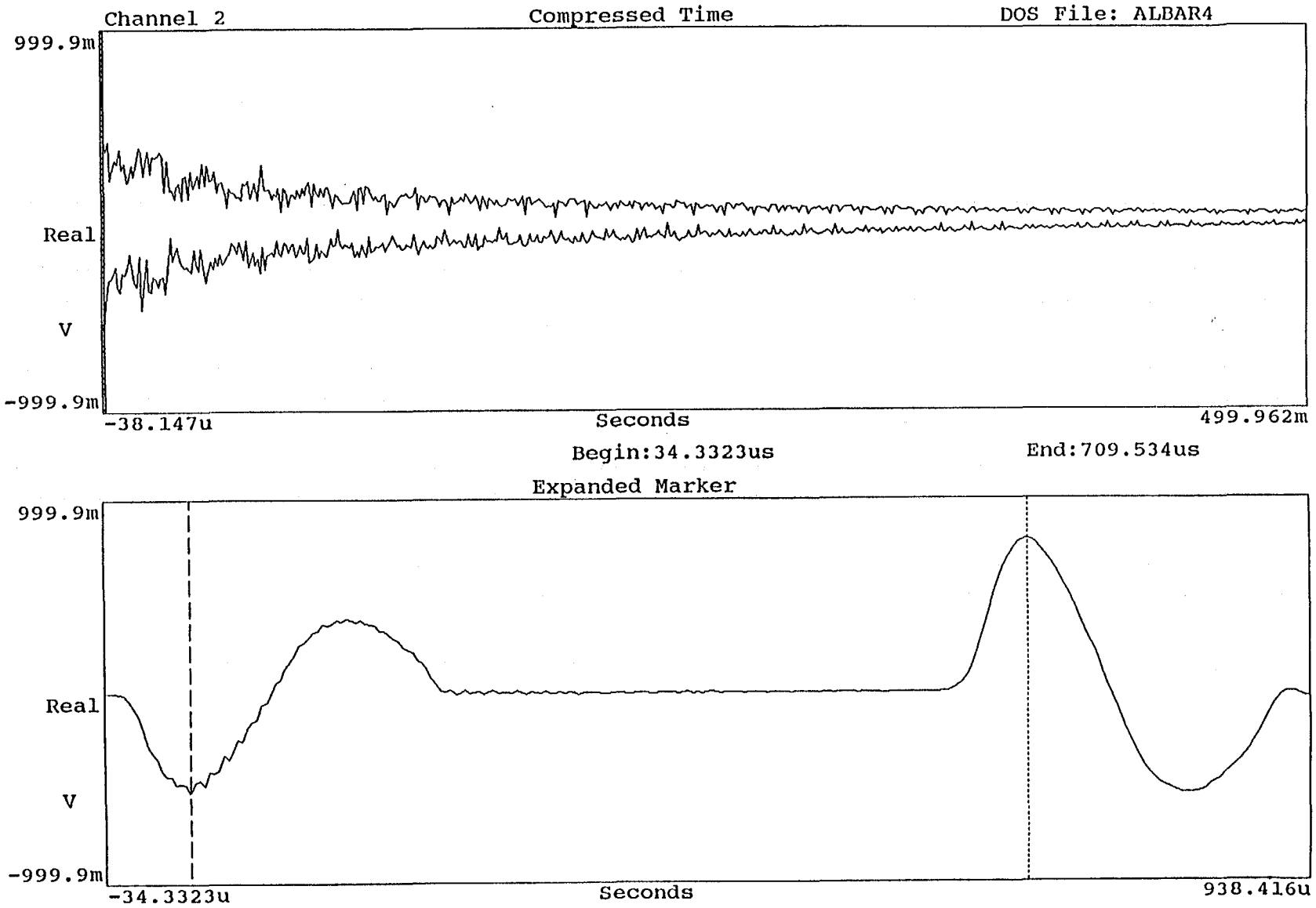

Anchor II, Left Side

Sandia National Laboratories

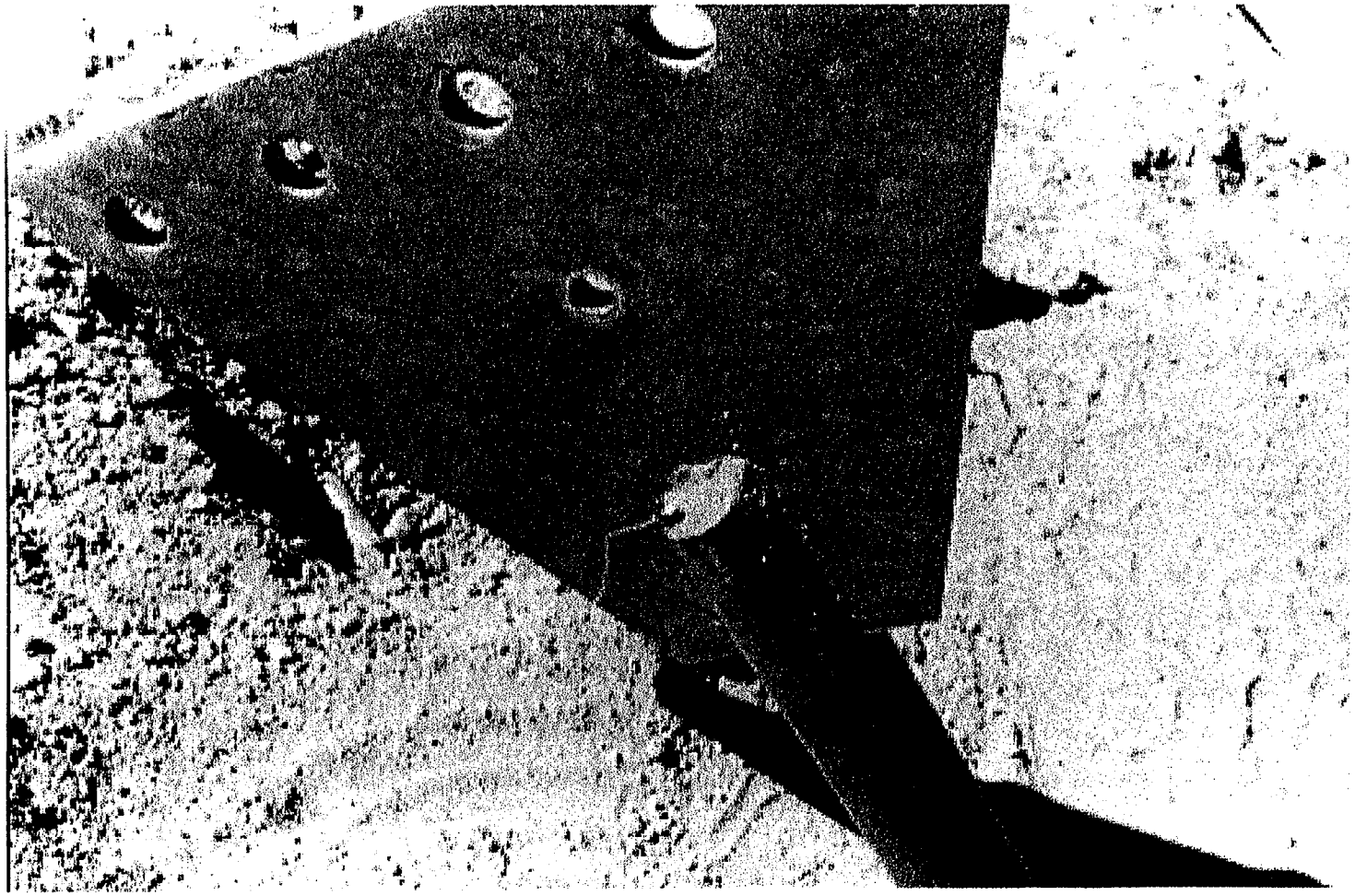

Anchor II, Right Side

Sandia National Laboratories

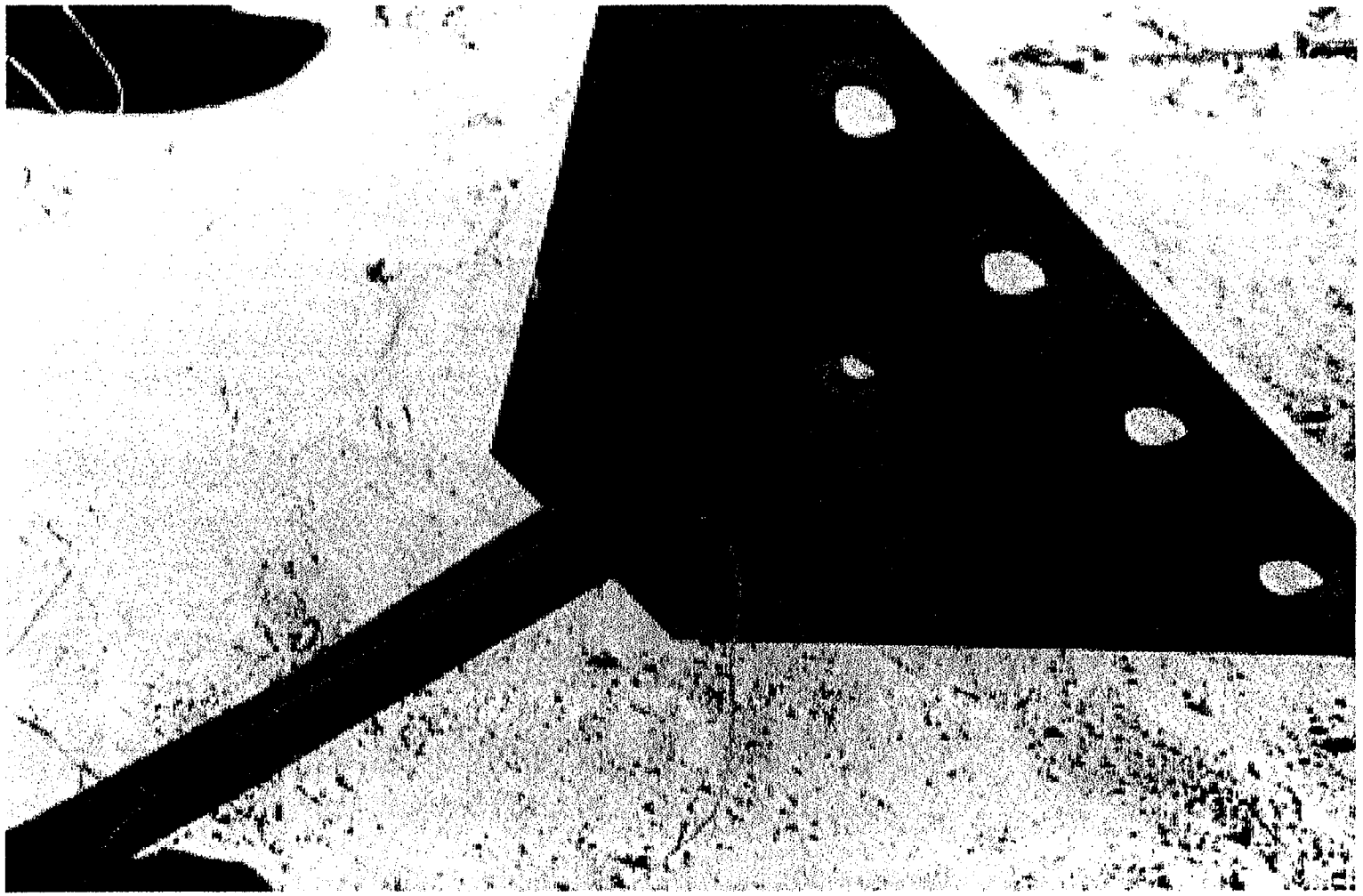

Anchor II, Unearthed After Testing

Sandia National Laboratories

Anchor II, Unearthed

Sandia National Laboratories

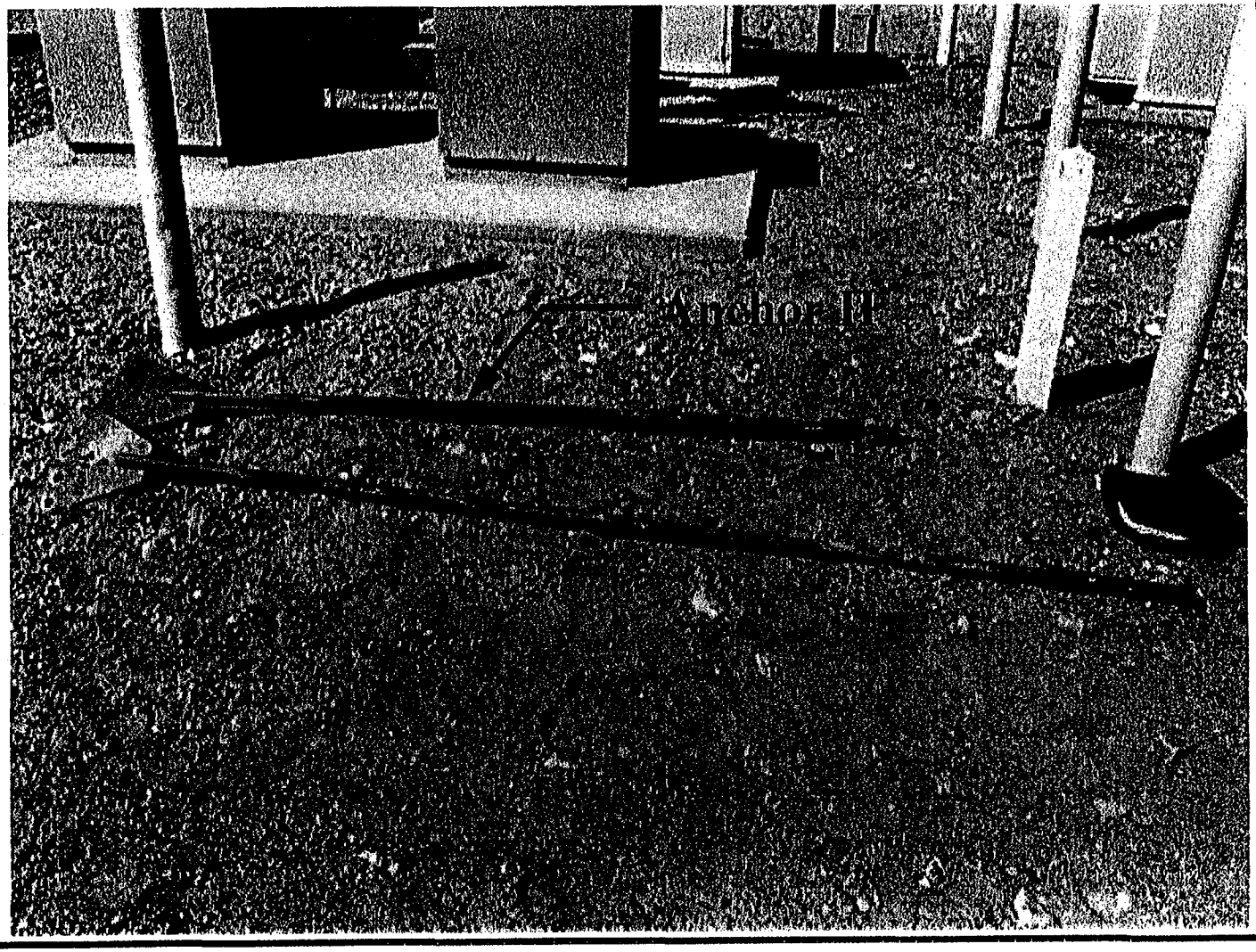

Anchor II, Necking Due to Corrosion

Sandia National Laboratories

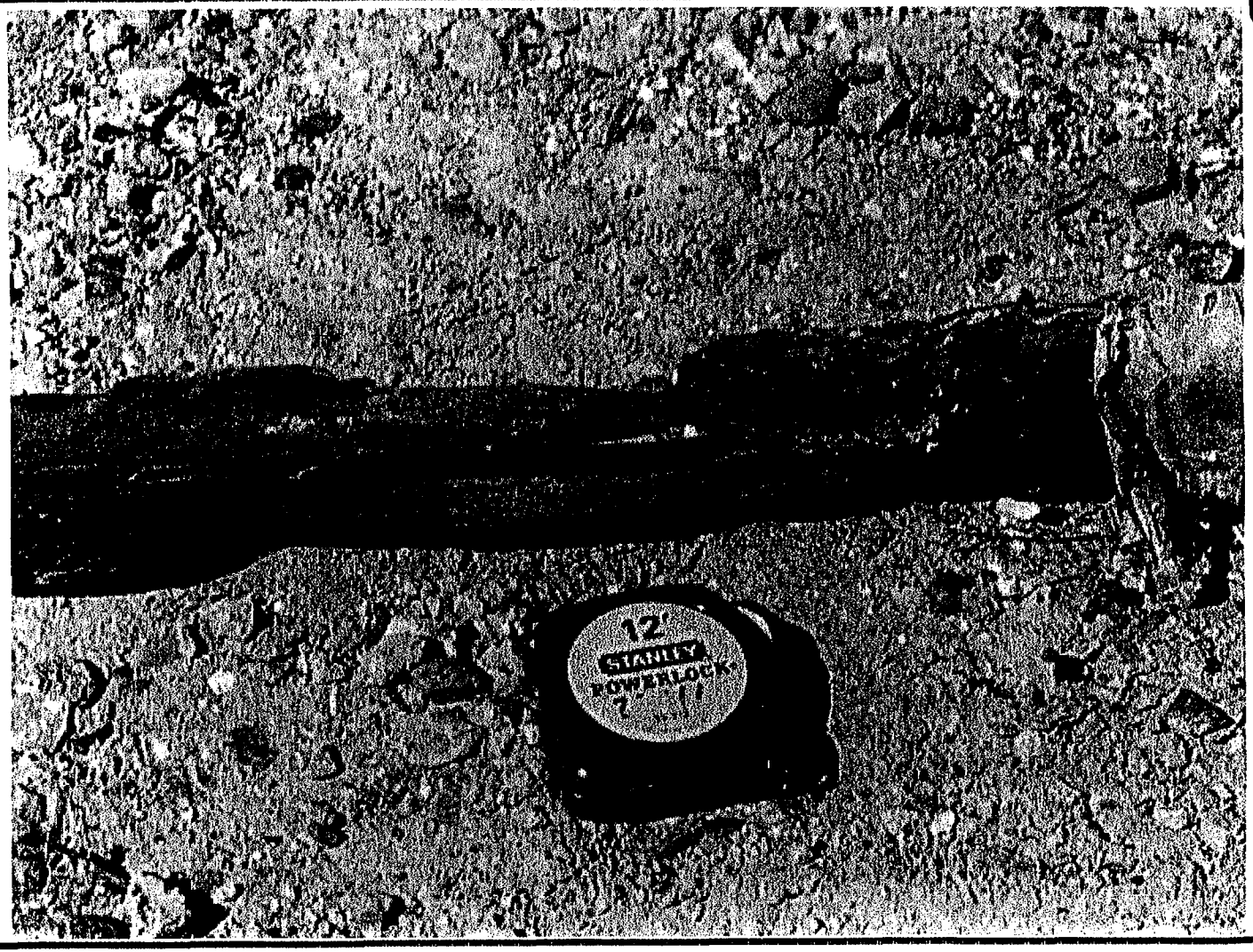

Anchor II, Welded Connection

Sandia National Laboratories

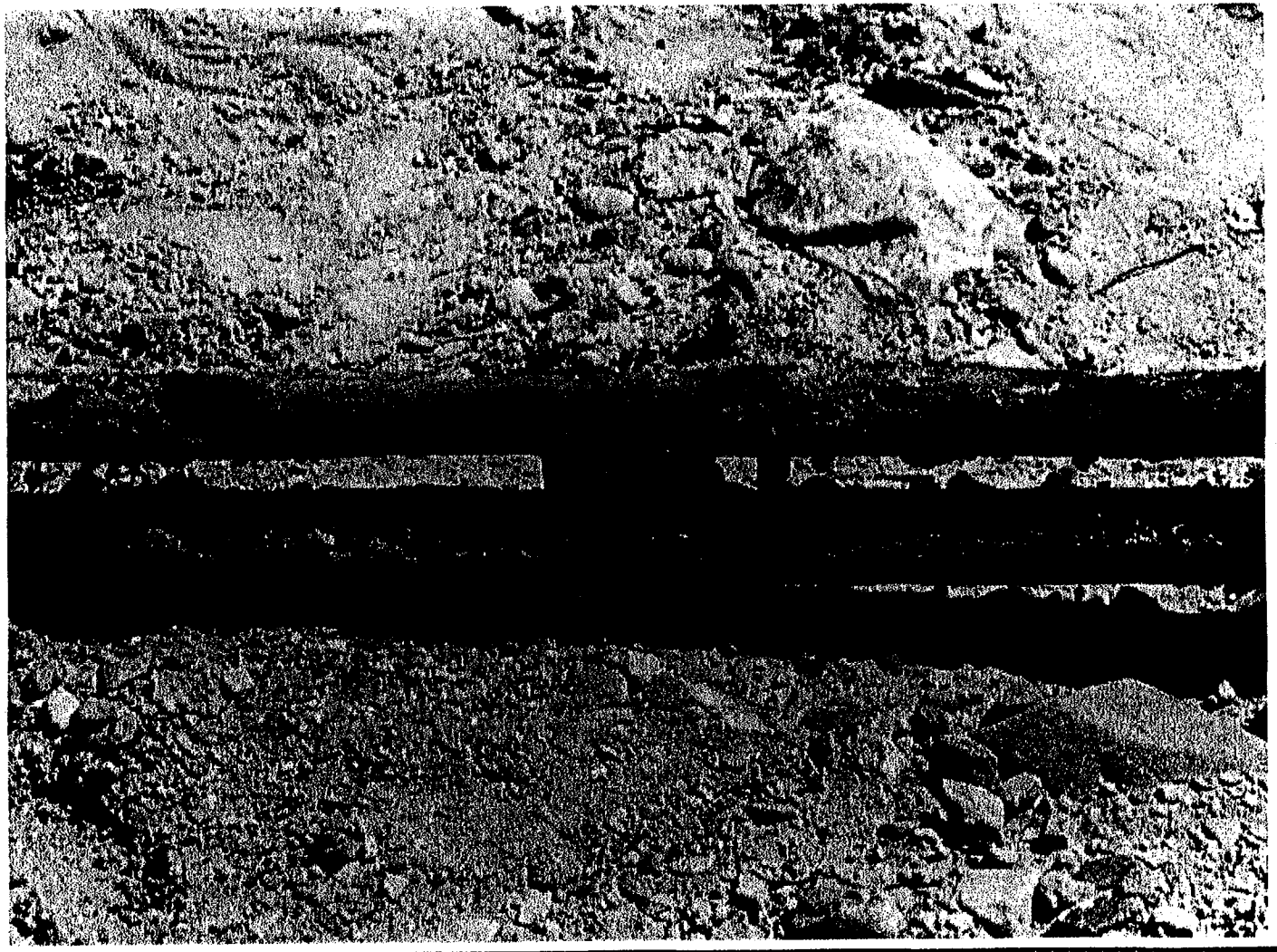

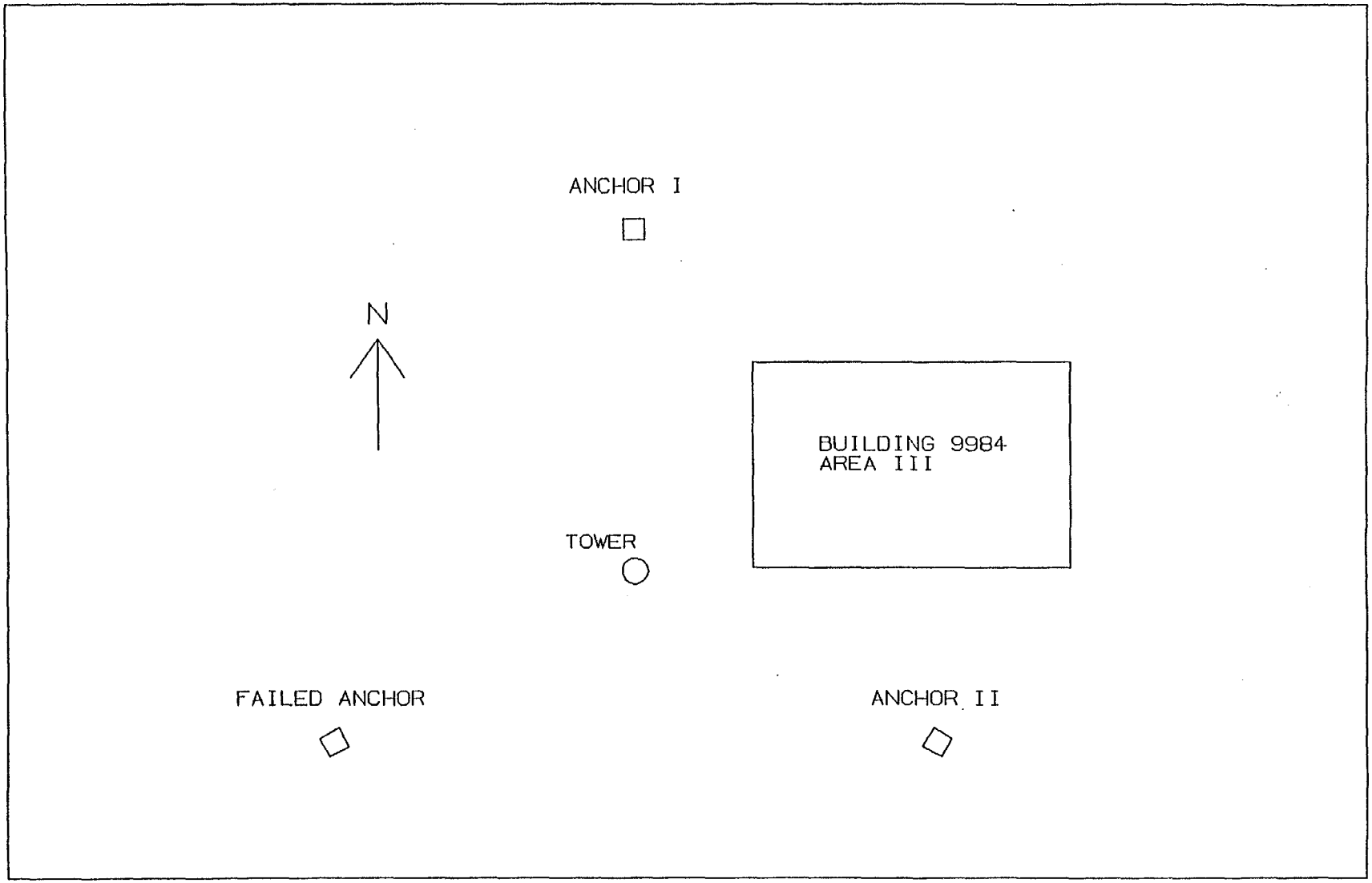
ANCHOR I
N
BUILDING 9984
AREA III
TOWER
FAILED ANCHOR
ANCHOR II

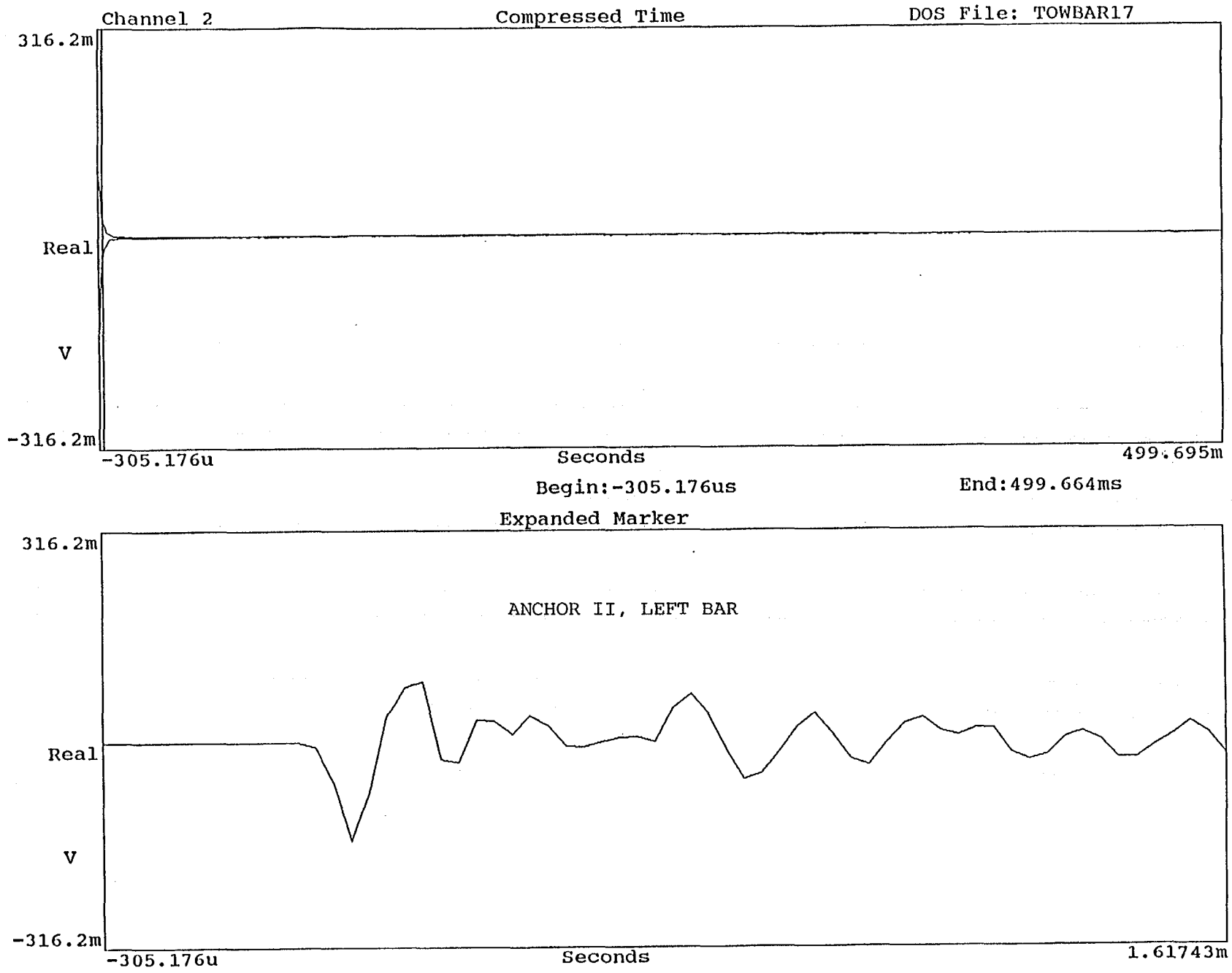
Channel 2
Compressed Time
DOS File: TOWBAR17
316.2m
Real
V
-316.2m
-305.176u
Seconds
499.695m
Begin:-305.176us
End:499.664ms
Expanded Marker
316.2m
ANCHOR II, LEFT BAR
Real
V
-316.2m
-305.176u
Seconds
1.61743m

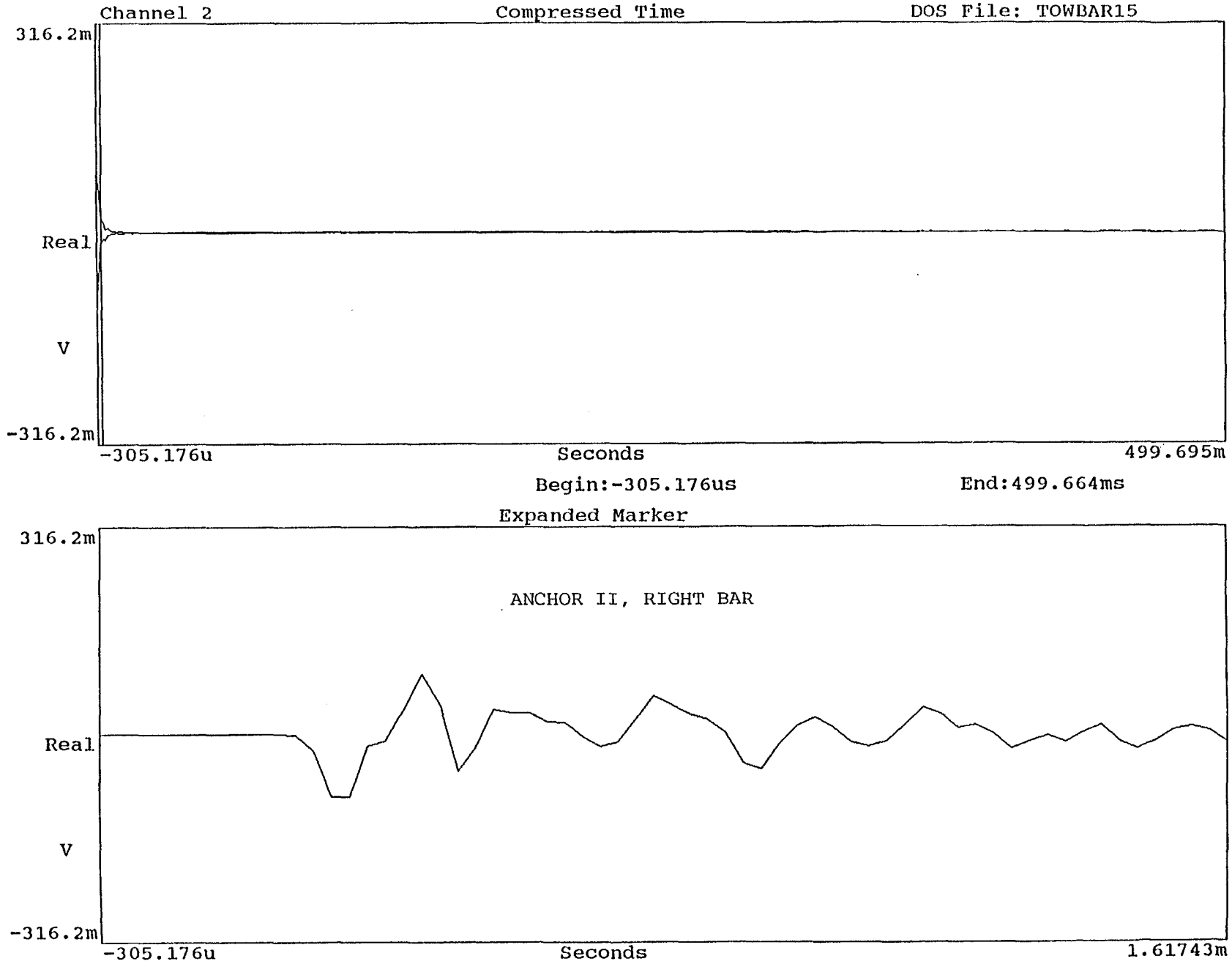
Channel 2
Compressed Time
DOS File: TOWBAR15
316.2m
Real
V
-316.2m
-305.176u
Seconds
499.695m
Begin:-305.176us
End:499.664ms
Expanded Marker
316.2m
ANCHOR II, RIGHT BAR
Real
V
-316.2m
-305.176u
Seconds
1.61743m

INSTR. STATE HAMMER4, PLASTIC TIP, LEFT BAR, ANCHOR 2

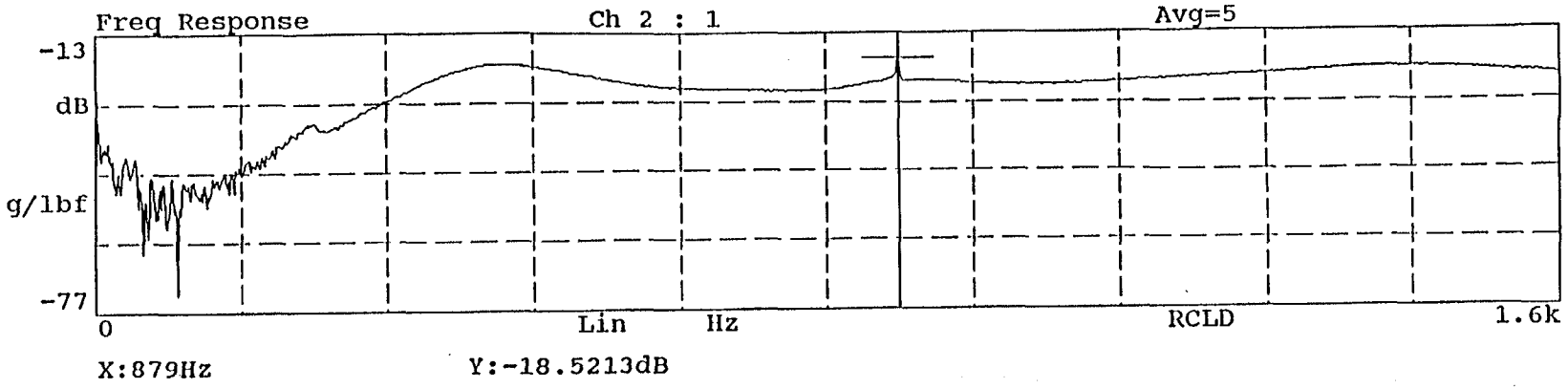

X:879Hz Y:-18.5213dB

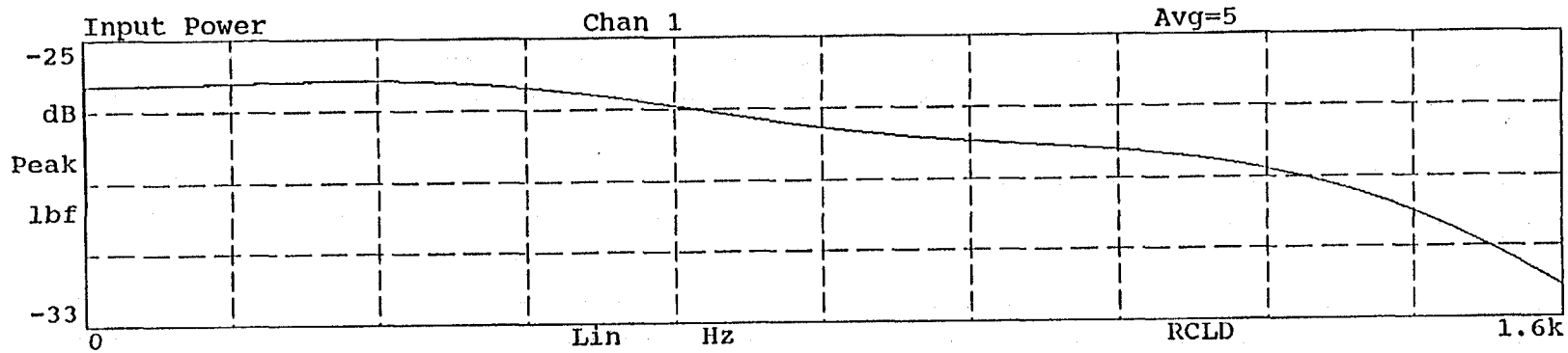

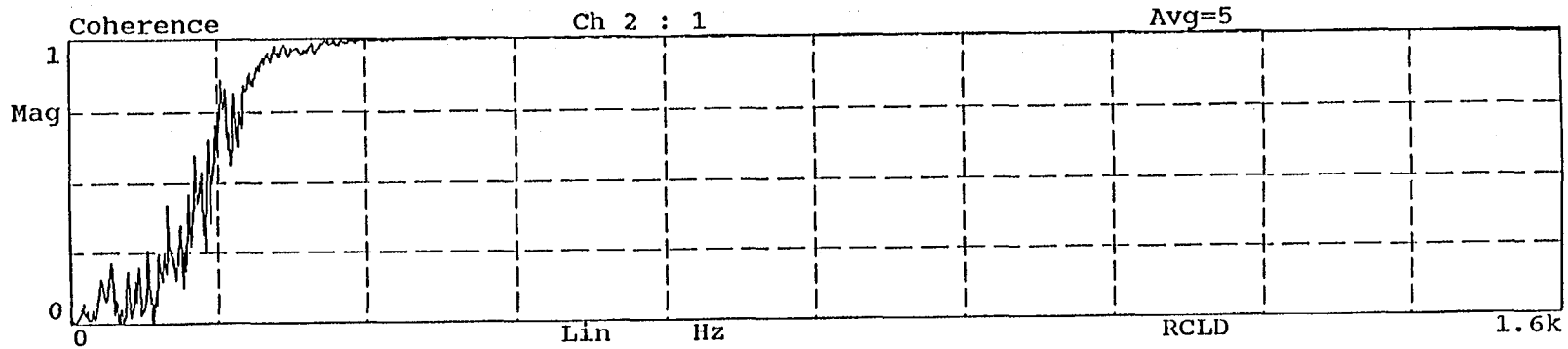

INSTR. STATE HAMMER4, PLASTIC TIP, RIGHT BAR, ANCHOR 2

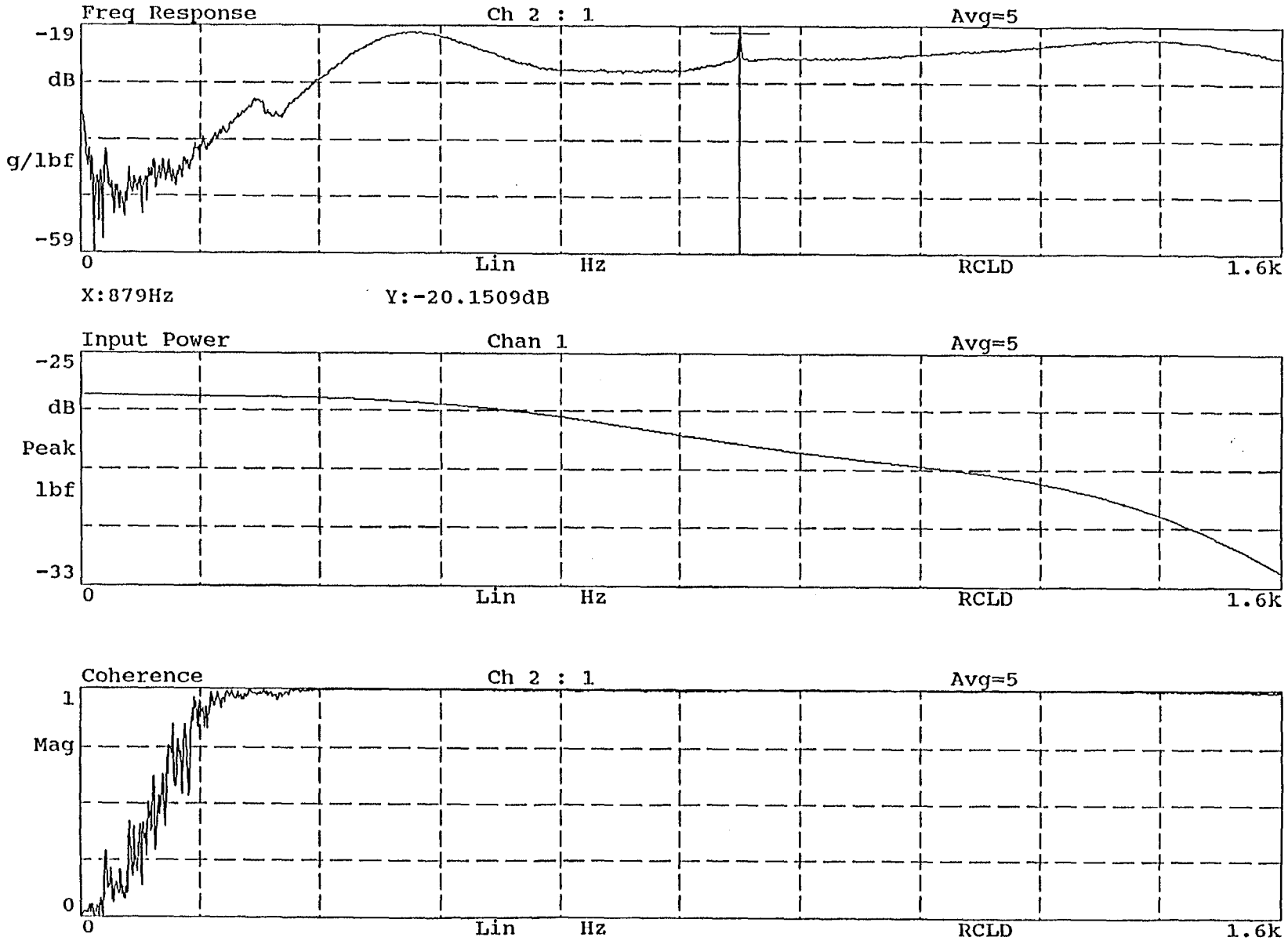

INSTR. STATE HAMMER4, PLASTIC TIP, LEFT-RIGHT BAR, ANCHOR 2

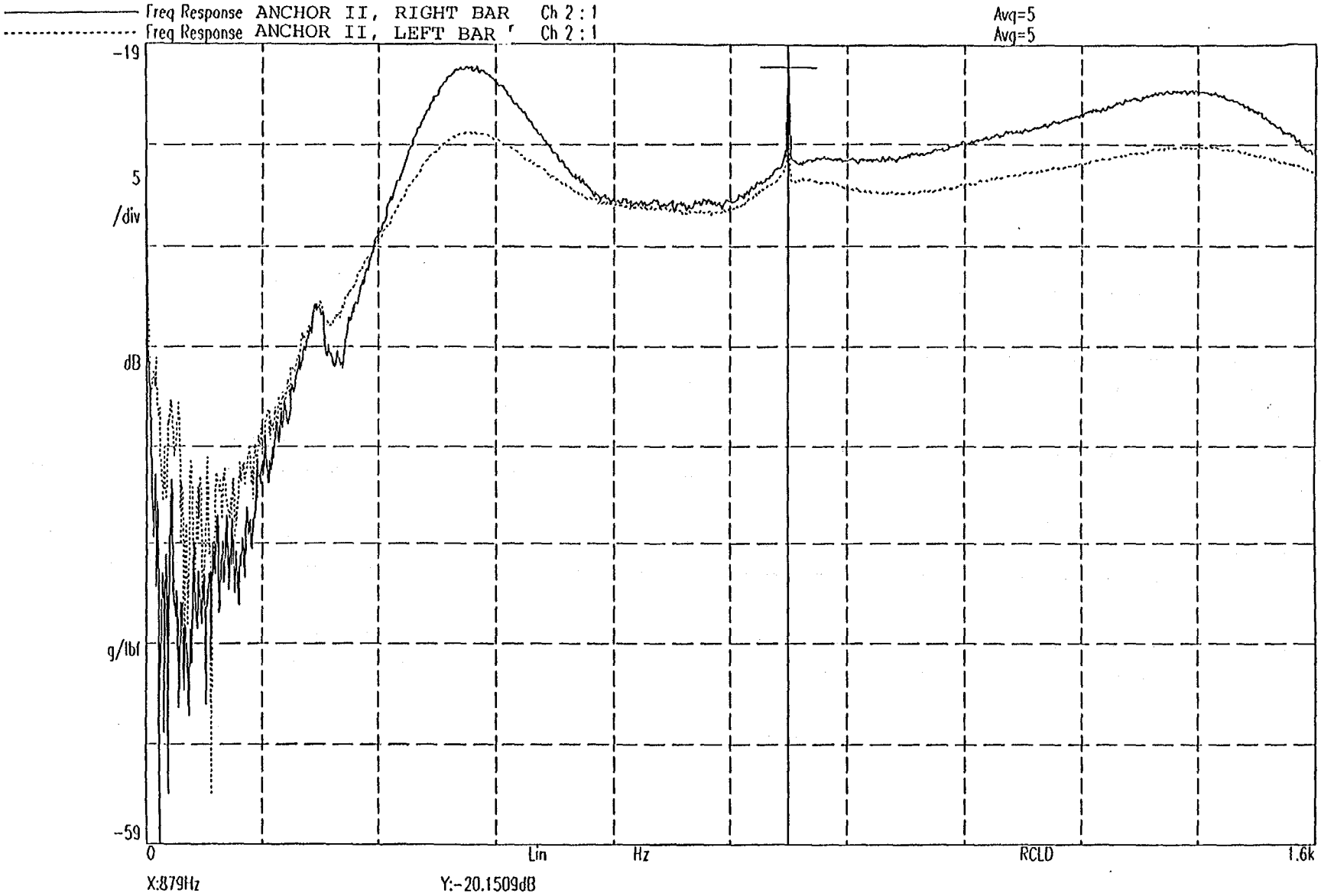

INSTR. STATE HAMMER4, PLASTIC TIP, LEFT-RIGHT ROD, ANCHOR 1

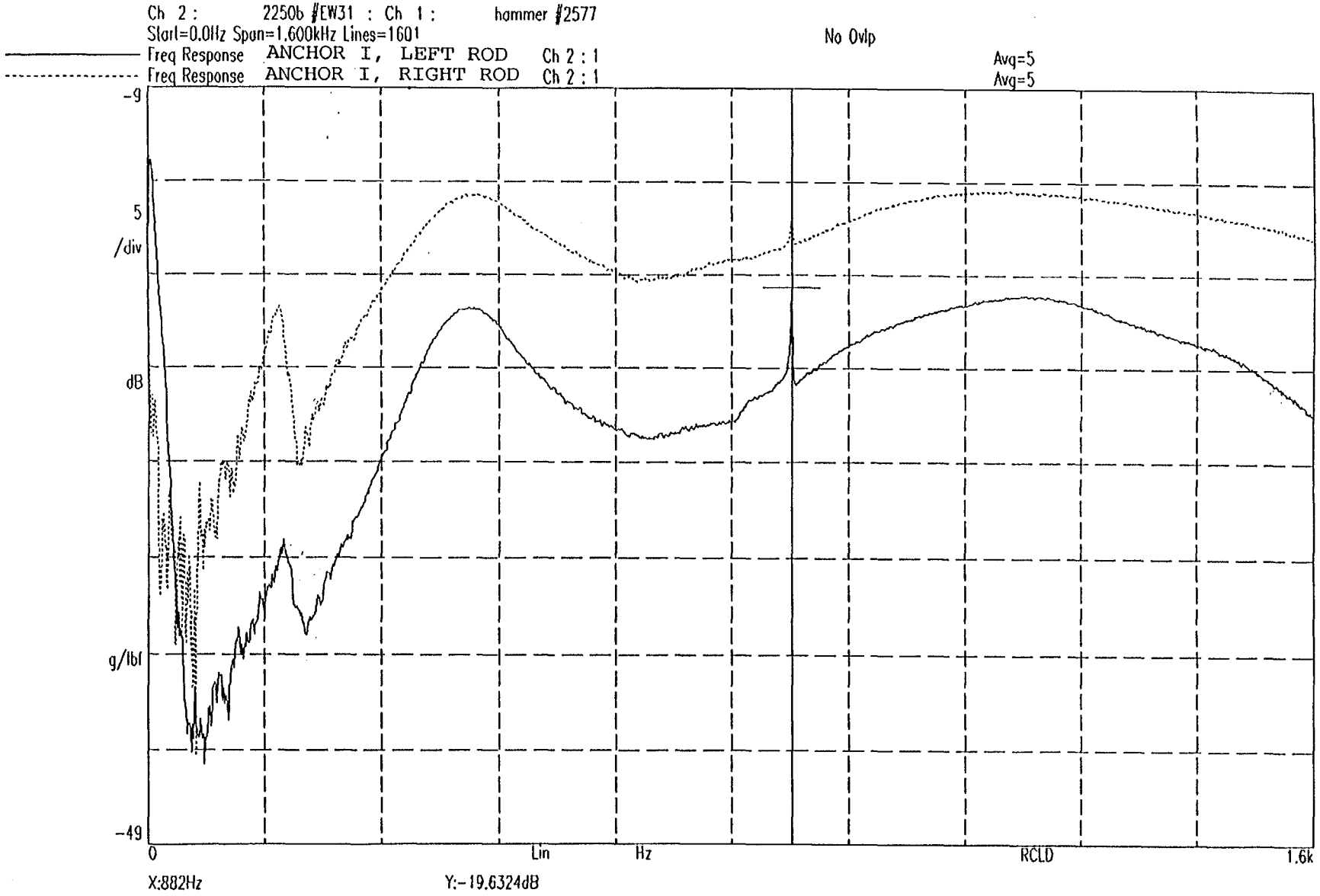

Intentionally Left Blank

APPENDIX G

THE EFFECTS OF FINITE ELEMENT GRID DENSITY ON MODEL CORRELATION AND DAMAGE DETECTION OF A BRIDGE

Todd Simmermacher, David Zimmerman, Randy Mayes, Garth Reese, and George James

Proceedings of the 1995 AIAA Adaptive Structures Forum
In Conjunction with the 1995 Structures, Structural Dynamics, and Materials Conference
New Orleans, LA

April 10-13, 1995

Intentionally Left Blank

The Effects of Finite Element Grid Density on Model Correlation and Damage Detection of a Bridge

Todd Simmermacher
University of Houston
Houston, Tx 77204–4792

Abstract

Variation of model size as determined by grid density is studied for both model refinement and damage detection. In model refinement, it is found that a large model with a fine grid is preferable in order to achieve a reasonable correlation between the experimental response and the finite element (FE) model. A smaller model falls victim to the inaccuracies of the finite element method. As the grid becomes increasing finer, the FE method approaches an accurate representation. In damage detection the FE method is only a starting point. The model is refined with a matrix method which doesn't retain the FE approximation, therefore a smaller model that captures most of the dynamics of the structure can be used and is preferable.

Introduction

Large finite element models are typically used to represent modern structures. The size of the model results from either the representation of the many different parts of the structure or a fine level of discretization. As grid density increases, the model ideally converges to an accurate representation of the behavior of the actual structure or at least more accurately represents the dynamics of the structure. However, as the grid density increases, the model size also increases, demanding more computing power to evaluate the model. Also, although using a very fine mesh increases model accuracy, some form of model correlation will still have to be performed to correct for inaccurate parameters such as modulus or density, or uncertain parameters such as springs at an interface.

Model correlation and model based damage detection, while related, have very different objectives. Model correlation is performed to adjust an FE model's response to approach the experimental response of the structure. The correlated model is then used as an analytical tool for stress/strain analysis, control law development, response to untested conditions, etc. For damage detection, the model must very accurately represent an experimental data set. This accurate representation of the structure will be used as a baseline to determine changes in the mechanical characteristics of the actual structure that result from fatigue, corrosion, unplanned impact, etc.

All of the techniques found in the literature can be used for both damage detection and model refinement. In practice, however, model correlation is usually performed with an algorithm that adjusts the physical parameters such as density in order for the correlated model to remain finite element consistent. In contrast, model based damage detection is typically performed with a matrix update method which does not maintain FE consistency. Survey papers providing an overview of methods of both damage detection and model correlation are provided by Ibrahim [1], and Heylen [2].

A popular method of model correlation is the use of Design Sensitivities (DS) to drive the variation of a given set of parameters. Through a wise choice of parameters and a FE model that represents all relevant behavior of the system, the model can be adjusted to accurately represent the actual structure. The use of DS involves some sort of optimization. Least Squares methods [3] and, more recently, Genetic algorithms [4] have been used successfully to correlate models.

Currently, damage detection for bridges is done largely by a visual inspection. This form of damage detection requires a large time commitment on the part of the inspection team. In a visual inspection, there is a chance that some damage to the structure may go unnoticed because (i) the damage is at a location that may be hard or impossible to inspect visually, (ii) the damage is internal to the structure, or (iii) may be missed by the inspector. A detailed survey of work done on bridge damage detection was performed by Farrar et. al. [5].

In this work, Minimum Rank Perturbation Theory (MRPT) is used for damage detection which has been developed as a computationally efficient method of determining the extent and location of damage in a structure. By constraining the rank of the perturbation matrix, an accurate assessment of the extent of damage can be made. The rank constraint has been found to be consistent with many forms of damage that occur in practice [6], [7].

A tradeoff exists between the level of discretization used in a FE model and the size of the resulting model. The question that arises is "When is the grid fine enough?". This question was addressed for model correlation by Imregun and Ewins [8]. They found that although a finely meshed model produces the best corre-

lated model, a coarsely meshed model wasn't to be discarded.

Model correlation and damage detection have different objectives, therefore it is reasonable to believe that a different mesh resolution would be necessary for each. In this paper, the question of discretization is addressed in both the model correlation and the damage detection problem. The structure used is a portion of the I–40 bridge over the Rio Grande which was extensively tested by Farrar et. al. [5]. The models range from a simple 26 node beam and plate model to a 2682 degree of freedom (DOF) model. The same models are used for both the model correlation and the damage detection for comparison.

Model Correlation Theory

The model correlation was performed using PEGA [4],[9] which utilizes the DS approach coupled to a genetic algorithm optimizer. The genetic algorithm is used because of the possibility of local minima in the solution space. Here, the DS approach uses the sensitivities of the eigenvalues with respect to the chosen parameters to determine corrections to the parameters based upon the linear approximation

$$\underline{\phi_{new}} = \underline{\phi_0} + \frac{\delta\phi}{\delta p}\underline{\Delta p} \tag{1}$$

where ϕ_{new} are the experimental frequencies, ϕ_0 are the frequencies of the FE model and p is a vector of parameters chosen to vary. The rectangular matrix ($\delta\phi/dp$) is known as the design sensitivity matrix and can be determined by MSC/NASTRAN [10], for example.

PEGA uses Eq. (1) to approximate the new ϕ_0 for the evaluation of the Fitness Index (FI) which is defined as

$$FI = \left\{ \sum_{i=1}^{m} \left(w_i^f \left| \frac{\phi_0^i - \phi_{new}^i}{\phi_{new}^i} \right| \right) \right\} \tag{2}$$

where the w^f's are used to weight the individual frequencies.

Figure 1 shows a flow chart that describes the correlation procedure. The models are correlated by a combination of running PEGA which produces changes in the chosen parameters and running MSC/NASTRAN to update the model to the new parameters. A one to one correspondence between the analytical and experimental frequencies is obtained by calculating the Modal Assurance Criterion (MAC) using the analytical and experimental mode shapes. Although PEGA produces an estimate of the updated natural frequencies of the model, these estimates are typically in error and a full run of MSC/NASTRAN is necessary for an evaluation of the correlation. This cycle is repeated until the model has converged. As indicated in [4], when the model form has been properly defined, convergence requires less than ten iterations.

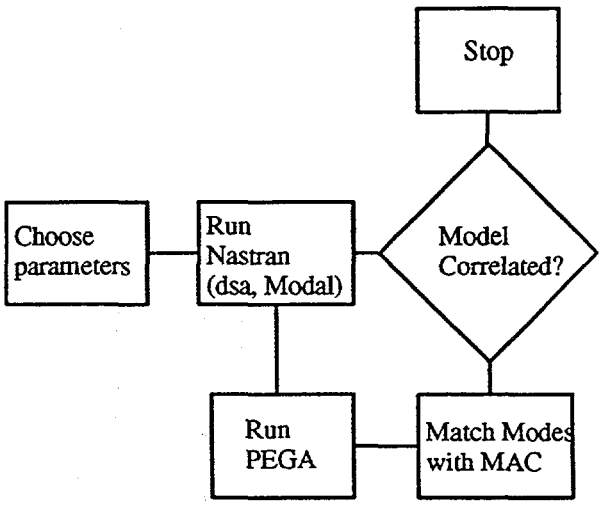

Figure 1 PEGA Correlation Flow Chart

Damage Detection Theory

The goal for the I–40 bridge was to determine if damage was present and, if so, locate the damage, not estimate the extent. The objective was to reduce the work load of an inspection team. If the damage can be determined to lie within a certain area, the inspection team can concentrate its efforts to that area. For this work, MRPT was used for the damage detection which uses modal characteristics of the assumed damaged structure and compares them with a baseline model which has been correlated with the bridge in some assumed healthy state. MRPT was used originally to correlate the model for the damage detection portion of this work. The model was assumed linear although the damage was typically non–linear.

The model correlation portion of damage detection is different from the definition given in the previous section. Here the updated model must match the "healthy" experimental data exactly so that errors in the model are not wrongly interpreted as changes in the structure's health. A parameter based update, while powerful, will rarely allow the FE model's response to exactly match the test data. Matrix methods, specifically MRPT, can exactly place the measured modes in the model. The form of the model must be at least approximately correct for successful damage detection.

The damage detection correlation involves correlating both the mass and stiffness matrix to the experimental data. A brief discussion of the procedure will be pro-

vided here with the details being found in Zimmerman and Kaouk [6].

The measured test data is assumed to satisfy

$$(M_a - \Delta M)\underline{V_{test}}\omega^2_{test} + (K_a - \Delta K)V_{test} = \underline{0} \qquad (3)$$

where M_a and K_a are the original mass and stiffness matrices, ΔM and ΔK are the perturbation matrices sought that correct the analytic model to match the experimental response, V_{test} is the matrix of mass normalized measured mode shapes and ω^2_{test} is a diagonal matrix of the measured frequencies squared. If the known information is grouped on one side of the equal sign and the unknowns on the other, two matrices B_m and B_k can be defined

$$\begin{aligned} B &= M_a V_{test}\omega^2_{test} + K_a V_{test} \\ &= \Delta M V_{test}\omega^2_{test} + \Delta K V_{test} \end{aligned} \qquad (4)$$

If B can be decomposed into B_m and B_k as follows

$$\begin{aligned} B &= B_m\omega^2_{test} + B_k \\ \Delta M V_{test} &= B_m \\ \Delta K V_{test} &= B_k \end{aligned} \qquad (5)$$

then ΔM and ΔK can be calculated using MRPT as

$$\begin{aligned} \Delta M &= B_m\left(B_m^T V_{test}\right)^{-1} B_m^T \\ \Delta K &= B_k\left(B_k^T V_{test}\right)^{-1} B_k^T \end{aligned} \qquad (6)$$

The inversion is possible if B_m and B_k are of full column rank.

The ΔM and ΔK as calculated in Eq. (6) have a few properties that make them attractive for damage detection. One property is that the correction to M_a and K_a, Eq. (6), will exactly place the experimental modes into the analytical model because they will satisfy Eq. (3). Another property is that the corrected mass and stiffness matrices (M_a–ΔM) and (K_a–ΔK) will be symmetric as shown in [6].

A very significant property is that the zero/non–zero pattern of B is reflected in ΔM and ΔK. Determining the location of damage requires the inspection of the zero/non–zero pattern of the dynamic residual, B. If a degree of freedom is affected by damage, a non–zero value will be present at that DOF in B, If that DOF is not affected by damage, a zero will be at that location. Typically noise and model errors will be present making each entry in B be non–zero, therefore "large" values are taken as damaged DOFs.

A final property is that the rank of ΔM and ΔK will be equal to the number of modes used for the calculation of B. This rank constraint allows the adjustment of the rank of ΔM and ΔK by a choice of the number of modes to use. The rank constraint has been found to be consistent with many forms of damage that are typically encountered.

Clearly there is an infinite set of B_m's and B_k's that satisfy

$$B = B_m\omega^2_{test} + B_k \qquad (7)$$

To arrive at a unique solution, physically meaningful constraints must be enforced. Two constraints come from the orthogonality conditions. The mass normal measured modal data must satisfy

$$\begin{aligned} V^T_{test}(M_a - \Delta M)V_{test} &= I \\ V^T_{test}(K_a - \Delta K)V_{test} &= \omega^2_{test} \end{aligned} \qquad (8)$$

By rearranging the orthogonality equations as before, separating the known quantities and the unknown quantities and comparing the result with Eq. (5), Eq. (8) becomes

$$\begin{aligned} V^T_{test}\Delta M V_{test} &= V^T_{test}M_a V_{test} - I = V^T_{test}B_m \\ V^T_{test}\Delta K V_{test} &= V^T_{test}K_a V_{test} - \omega^2_{test} = V^T_{test}B_k \end{aligned} \qquad (9)$$

The pseudo inverse could be used at this point to solve for B_m and B_k, however, that would destroy the important zero/non zero pattern of the resulting B_m and B_k. To preserve the zero/non zero pattern, a formulation similar to the one used to derive Eq. (6) is used. A matrix P is to be found which satisfies

$$P\left(V^T_{test}B\right) = B \qquad (10)$$

which can be found by

$$P = B\left(V^T_{test}B\right)^{-1} \qquad (11)$$

so the decomposition of B can be performed as

$$\begin{aligned} B_m &= P\left(V^T_{test}M_a V_{test} - I\right) \\ B_k &= P\left(V^T_{test}K_a V_{test} - \omega^2_{test}\right) \end{aligned} \qquad (12)$$

The calculation of ΔM requires that the modes be mass normal. Measured modes can be mass normalized if the driving point of the structure in question is measured.

The damage inflicted on the I–40 bridge consisted of making increasingly larger cuts in one of the two plated girders supporting the road bed (Fig. (1)). The first cut

was a 2 ft vertical cut in the center of the web. The second cut extended down to the top of the lower flange. The third cut was made through half of the lower flange. The final cut severed the lower flange. The cuts did not remove any significant mass and therefore can be modeled as only a decrease in stiffness.

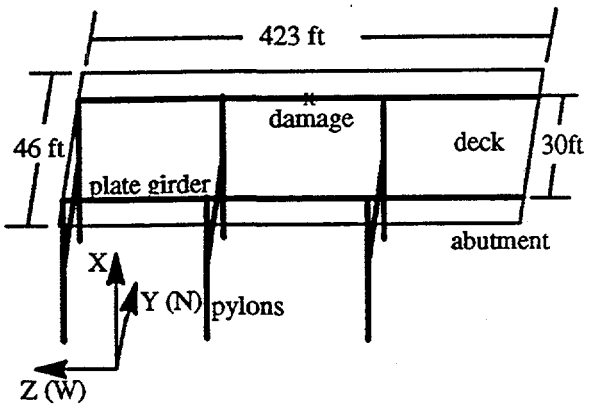

Figure 1. Bridge Model Schematic

Two definitions of the dynamic residual, which are used to locate damage, are used in this work. The first definition of the dynamic residual uses the assumption that the damage only affects the stiffness matrix and is defined as

$$M_h V_d \omega_d^2 + K_h V_d = \Delta K V_d = B \qquad (13)$$

where the subscript h refers to the model correlated to the healthy data as described in Eq. (6) and the subscript d refers to the modal data of the damaged structure. The second definition assumes that both the mass and the stiffness matrices change and uses Eq. (12) to define B_m and B_k, with B_k being used for locating damage. The thought here is that by separating mass and stiffness effects the noise in B_k will be reduced.

Areas that are very stiff relative to the rest of the structure also cause problems in locating damage. Noise in the measurements is magnified by the large value associated with stiff elements which can swamp out the actual damage. For example, a structure with a global stiffness on the order of 10^6 may have a localized stiffness on the order of 10^9. Assume a noise level of 2% and a damage level in the less stiff region of 20%. The 2% noise in the stiff region gives a stiffness variation of $2x10^7$ while the damage in the less stiff region only has a variation of $2x10^5$. The damage would not be apparent unless some form of scaling is present. In this work the scaling used for Eq. (12) is defined as

$$\hat{B}_i = W_i B_i H \qquad \text{(T1a) (14)}$$

and for Eq. (13)

$$\hat{B}_{ik} = W_i B_{ik} \qquad \text{(T2) (15)}$$

where

$$W_i = diag\left(\frac{1}{\|z_i^1\|}, \frac{1}{\|z_i^2\|}, \frac{1}{\|z_i^3\|}, \cdots, \frac{1}{\|z_i^n\|}\right)$$

$$H = diag\left(\frac{1}{\|V_1\|}, \frac{1}{\|V_2\|}, \frac{1}{\|V_3\|}, \cdots, \frac{1}{\|V_n\|}\right) \qquad (16)$$

and

$$Z_i = \begin{bmatrix} z_i^1 \\ z_i^2 \\ z_i^3 \\ \vdots \\ z_i^n \end{bmatrix} = (M_h \omega_i^2 + K_d) \qquad (17)$$

Equation (14) can be alteratively viewed as

$$\tilde{b}_i^j = z_i^j V_i = \|z_i^j\| \, \|V_i\| \cos(\theta_i^j)$$
$$\tilde{b}_i^j = \cos(\theta_i^j) \qquad (18)$$

where $\tilde{b}_{ik}^{j}$ to the component of $\hat{B}$ in the j^{th} row and i^{th} column. The angle θ is a measure of orthogonality of a modeshape to a row of the matrix Z_i. A angle of 90° indicates an undamaged DOF and any deviation from 90° indicates damage. To make both measures of damage consistent, the angle θ is subtracted from 90° as

$$A = 90 - \frac{\pi \cos^{-1}(\tilde{B})}{180} \qquad \text{(T1) (19)}$$

Noise and modeling errors in the measurements can mask damage in any one of the columns of either T1 or T2. In order to extract damage information from all of the modes and filter some of the noise a singular value decomposition can be performed on either T1 or T2 and the location of damage can be determined by inspecting the zero/non–zero pattern of the first left singular vector.

In the bridge model, the pylons are areas of large stiffness when compared to the stiffness of the two plate girders. Without this weighting damage is always located at the pylons.

Description of Models

Two different models were used for this study. The only difference between the models used for correlation and the models used for damage detection was that the

damage detection models have the Y and Z translations and the X rotations grounded to prevent out of plane motion, whereas the model correlation models have the full 6 DOF/node. The measurements were only in the X direction and the modes of interest have very small components in the Y and Z translations and the X rotation. Sensors used for the collection of the experimental data consisted of 13 X direction accelerometers equally spaced between the pylons along each of the main plate girders for a total of 26 measurements. Only the first six modes were measured. The number of DOF's for each model given below refer to the model correlation model.

The large model (2844 DOFs) consisted of the roadbed as modeled with CQUAD4 elements, each of the two main plate girders divided into 48 CBAR elements, and each of the three pylon assemblies are divided up into 3 CBAR elements. Springs connect the pylons to the two plate girders and connect the roadbed to the ground in the X and Y directions at the abutment.

The small model (138 DOFs) consisted of one CBAR element between each of the sensor locations for the two plate girders, a roadbed made up of 12 CQUAD4 elements, crossbars between the two main plate girders at the sensor locations, and springs to ground to represent the pylons and the connection of the roadbed to the ground at the abutment.

Model Correlation Results

The first six modes were correlated with PEGA. The parameters chosen to vary in the optimization are the modulus of elasticity and the thickness of the roadbed, all the spring constants, the two principal area moments of inertia of the two main plate girders, the two principal area moments of inertia and cross sectional area of each of the pylons, the two principal area moments of inertia and the cross sectional area for the beams connecting the pylons, and an added mass term to account for crash barriers that were present on the roadbed for a total of 27 design variables. All correlations are done using the data from the first damage case.

The results for the large model are shown in Table 1. Four iterations were required to get convergence of the frequencies. Most of the frequencies show good correlation. The exceptions are modes four and five which are close in frequency. These two modes are closely spaced and tended to switch during the correlation procedure.

Table 1. Changes in the large model's frequencies (Hz).

Mode	Initial Frequency	Final Frequency	Experimental
1	2.21	2.45	2.51
2	2.71	3.05	2.98
3	3.29	3.66	3.56
4	3.47	4.17	4.12
5	3.60	4.11	4.20
6	4.17	4.67	4.66

The results for the small model are shown in Table 2. Four iterations were also performed on the small model. The second and third modes in the small model were switched from the first iteration and never switched back. A poor frequency correlation resulted for most of the modes, however all the mode shapes were predicted in the model. Since the mesh is so coarse, only the general motion of the bridge could be predicted.

Table 2. Changes in the small model's frequencies (Hz).

Mode	Initial Frequency	Final Frequency	Experimental
1	2.08	2.21	2.51
2	3.42	3.46	2.98
3	3.18	3.37	3.56
4	3.90	4.12	4.12
5	5.00	4.74	4.20
6	6.01	5.87	4.66

Damage Detection Results

The detection of the location of damage was performed using the MRPT detection algorithm presented above. The small model was reduced as depicted in Figure 2 and the large model was reduced as depicted in Figure 3. Once the original model was reduced, the mass and stiffness matrices were updated using the first damage case as was done in the Model Correlation section.

There were some problems identifying the modes from the experimental data. There were 11 other bridge sections of similar construction all within close proximity of the test section. The dominate modes of the bridge were coupled lightly with the similar modes of the adjacent bridge sections, complicating the modal extraction. The test bridge was in series with two other bridges

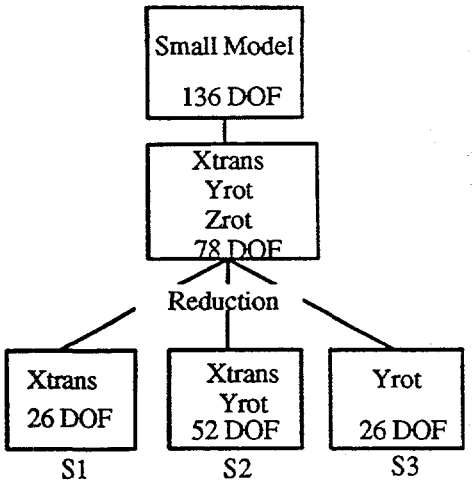

Figure 2. Hierarchy of Small Model

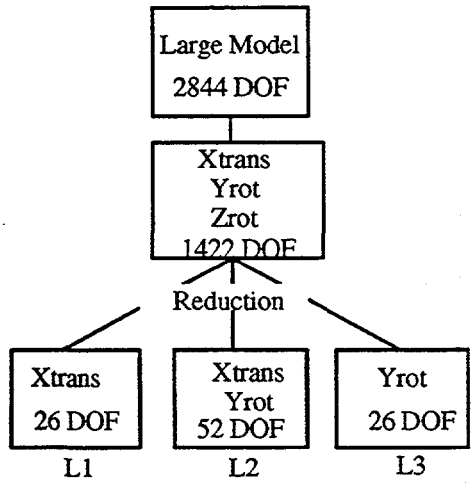

Figure 3. Hierarchy of Large Model

across the Rio Grande. These two were in the process of being demolished while the tests were being performed. This unquantifiable change in the boundary conditions affected the measurements. The frequencies went up about one percent from the pristine test to the first damage case. This is why the first damage case was used as the initial, undamaged data for the correlations.

Four different methods of model reduction were used: two static reduction methods, Guyan [11] and Improved Reduction System (IRS) [12], and two exact reductions, Modal [13] and Hybrid [14] reduction. Guyan reduction produced the best results and all results presented here were produced using Guyan reduction.

Since only 26 X translations were measured, some form of modal expansion had to be performed to calculate the Y rotations for both models. The procedure used was a physically motivated method. A cubic spline was fitted through the measured modal displacements for each mode, one spline for each side of the bridge. The derivative of the spline was taken to calculate the Y translations.

Figures A1–A3 in the appendix summarize the results for the small model. The first left singular vector is shown for both methods T1 and T2. The vector has been scaled such that the maximum component is equal to one. Model S1 correctly locates case 4 using either detection method. Method T2 is able to correctly locate the damage for case 3 and shows indications of damage around DOF 20 for case 2. Case 2 is the hardest state of damage to locate as very little change in stiffness occurred. Recall that case 2 consisted of cutting through 1/2 of the webbing of the plate girder. The webbing provides little stiffness to the plate girder in the direction of loading.

Model S2 in Fig. (A2) correctly locates damage case 4 using method T1. With model S2 entries of the damage vectors corresponding to the translations at the pylons were set equal to zero. This was necessary because the large values at these locations swamped out the actual damage. It is felt that this phenomena is due to errors in the expansion of the eigenvector as it only occurs when the modeshapes are expanded. The damage is only correctly located for damage case 4 using method T1. Method T2 gives an indication of damage for case 3 in the correct location (DOF 40).

The model consisting of Y rotations only (S3) does not correctly locate damage for any of the cases with either T1 or T2. Using method T2 damage is incorrectly located at DOF 13 (south western most pylon (Fig. (1)) for both case 3 and 4. The calculation of the spline used for expansion requires an assumption on the end conditions. The assumption used is the "not a knot" condition which chooses the slopes at the endpoint such that the first two interpolating polynomials are equal and the last two interpolating polynomials are equal [15].

The results for the large model are shown in Fig. (A4–A6). As with the small model the first left singular vector of both T1 and T2 is shown. For model L1 (X translations only) damage case 4 is correctly identified using method T1 (Fig. (A4)). Method T2 shows large changes around the damage, however there are spurious larger changes around DOFs 14–17 which correspond to the northern side of the bridge near the abutment. Large changes are shown correctly around DOF 20 using method T2 for damage cases 3 and 4, however larger changes are indicated at DOFs 23 and 24.

With model L2 damage case 4 is correctly located using method T1. There is no clear indication of damage in any of the other damage vectors. The components in the damage vector corresponding to the translations

at the pylons were once again set equal to zero as before.

Using model L3 damage is incorrectly located at DOF 13 using method T2 for both cases 3 and 4. This error may again be due to the end condition assumed for the spline. Different end conditions were not tried.

Discussion

The model correlation process as used here varies design parameters such as density to adjust a finite element model to approximate an experimental response. The model remains a finite element approximation. Theoretically with finite element models, a finer mesh can result in a better correlation. A finer mesh can make the FE approximation more exact and there can be more design parameters from which to choose.

The larger model of the I–40 bridge, after correlation, did represent the experimental frequencies better than the small model, especially at higher frequencies. For a basic understanding of the characteristics of the bridge a coarse mesh model is sufficient while for any detailed work, the more refined mesh would be more appropriate.

For damage detection, it is the fact that the small model can accurately represent the mode shapes that allows it to be useful. The model is first reduced then corrected using MRPT to place the measured modes in the model exactly. The corrections to the model are mainly to fix the frequencies since the mode shapes are well predicted. The larger models, however, can be corrupted by both the reduction process and the expansion technique used. The model reduction process tends to destroy the load paths present in the full model and thereby decrease the ability to locate damage.

Conclusions

Large and small models are compared from the viewpoint of model correlation and damage detection. For model correlation, large models are necessary to reduce the effects of the discretization error inherent in the finite element method. For damage detection, a small model that captures the approximate nature of the structure, such as mode shapes appears preferable. Using a large model for damage detection is complicated by the significant reduction problem with matrix methods.

References

[1] Ibrahim, S.R. and Saafan, A.A., "Correlation of Analysis and Test in Modeling of Structures, Assessment and Review", Proceedings of the 5th IMAC, pp. 1651–1660, 1987.

[2] Heylen, W. and Sas, P. "Review of Model Optimization Techniques," Proceedings of the 5th International Modal Analysis Conference, pp. 1177–1182, 1987.

[3] Martinez, D., Red–Horse, J., and Allen, J.,"System Identification Methods for Dynamic Structural Models of Electronic Packages," Proceedings of the 32nd SDM Conference, Baltimore, MD, pp 2336–2346, 1991.

[4] Fulcher, C.W., Marek, E.L., and Mayes, R.L.,"Test/Analysis Correlation and Model Updating of the STARS I & II Missile Systems," NAFEMS International Conference on Structural Dynamics Modeling Test, Analysis, and Correlation, Miltion Keynes Conference Centre, UK, July 1993.

[5] Farrar, C.R., Baker, W.E., Bell, T.M., Cone, K.M., Darling, T. W., Duffey, T.A., Eklund, A., Migliori, A.,"Dynamic Characterization and Damage Detection in the I–40 Bridge Over the Rio Grande," Los Alamos National Laboratories Report No. LA–12767–MS, 1994.

[6] Zimmerman, D.C., and Kaouk, M,"Structural Damage Detection Using a Minimum Rank Update Theory," ASME Journal of Vibration and Acoustics????????

[7] Zimmerman, D.C., and Simmermacher, T., "Model Refinement and System Health Monitoring Using Data From Multiple Static Loads and Vibration Tests," accepted, *AIAA Journal.*

[8] Imregun, M. and Ewins, D.J.,"Mesh Density Effects on Finite Element Model Updating," Proceeding of the 10th International Modal Analysis Conference, pp. 1372–1382, 1993.

[9] Reese, G.M.,"PEGA: Parameter Estimation Using the Genetic Algorithm," Users' Guide, Internal Report, Sandia National Laboratories, 1993.

[10] MacNeal–Schwendler Corp., "MSC/NASTRAN Users' Manual," V.66, 1988.

[11] Guyan, R.J."Reduction of Stiffness and Mass Matrices," AIAA Journal, Vol. 3,No. 2, pg. 380, 1965.

[12] O'Callahan, J.,"A Procedure for an Improved Reduced System (IRS) Model," Proceedings of the 7th International Modal Analysis Conference, pp 17–21, January 1989.

[13] Kammer, D.C.,"Test–Analysis Model Development Using an Exact Model Reduction," The International Journal of Analytical and Experimental Modal Analysis, pp. 174–179, October 1987.

[14] Kammer, D.C.,"A Hybrid Approach to Test–Analysis–Model Development for Large Space Structures," Journal of Vibration and Acoustics, pp 325–332, Vol. 113, July 1991.

[15] de Boor, C.,*A Practical Guide to Splines*, Springer–Verlag: New York, 1978.

Appendix

Figures A1–A6 use the following symbols:

(1) S1: Small model with X translations only.

(2) S2: Small model with X translations and Y rotations.

(3) S3: Small model with Y rotations only.

(4) L1: Large model with X translations only.

(5) L2: Large model with X translations and Y rotations.

(6) L3: Large model with Y rotations only.

(7) T1: Damage location determined by Eq. (14).

(8) T2: Damage location determined by Eq. (15).

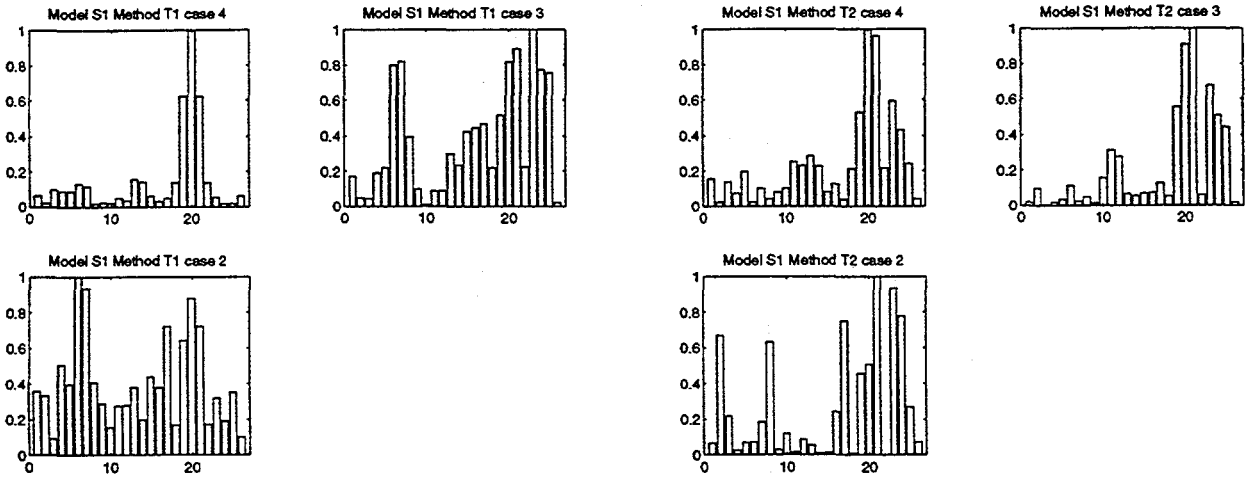

Figure A1. Model S1 Damage Detection Results (damage near DOF 20)

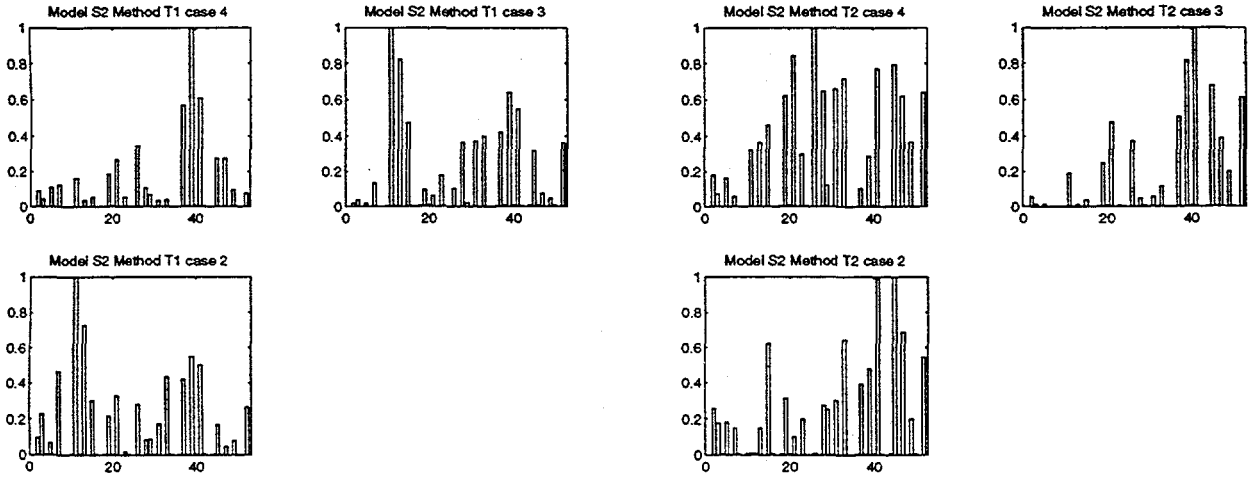

Figure A2. Model S2 Damage Detection Results (damage near DOF 40)

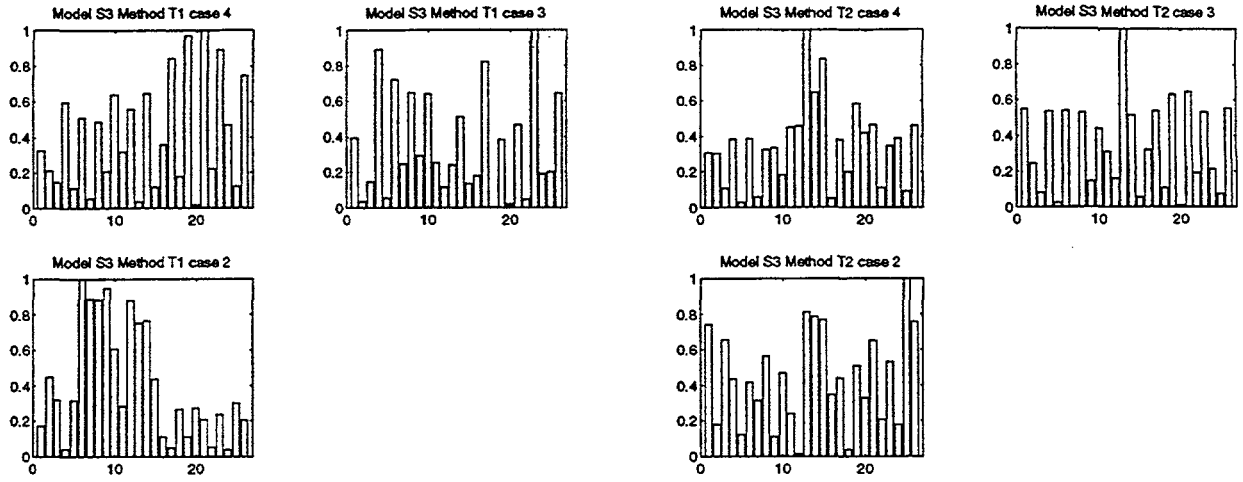

Figure A3. Model S3 Damage Detection Results (damage near DOF 20)

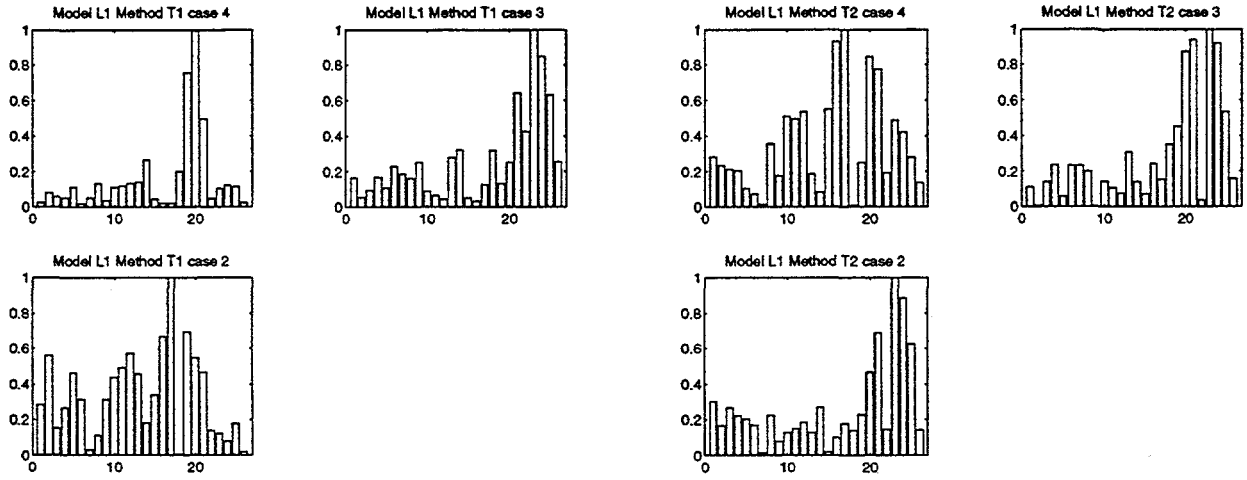

Figure A4. Model L1 Damage Detection Results (damage near DOF 20)

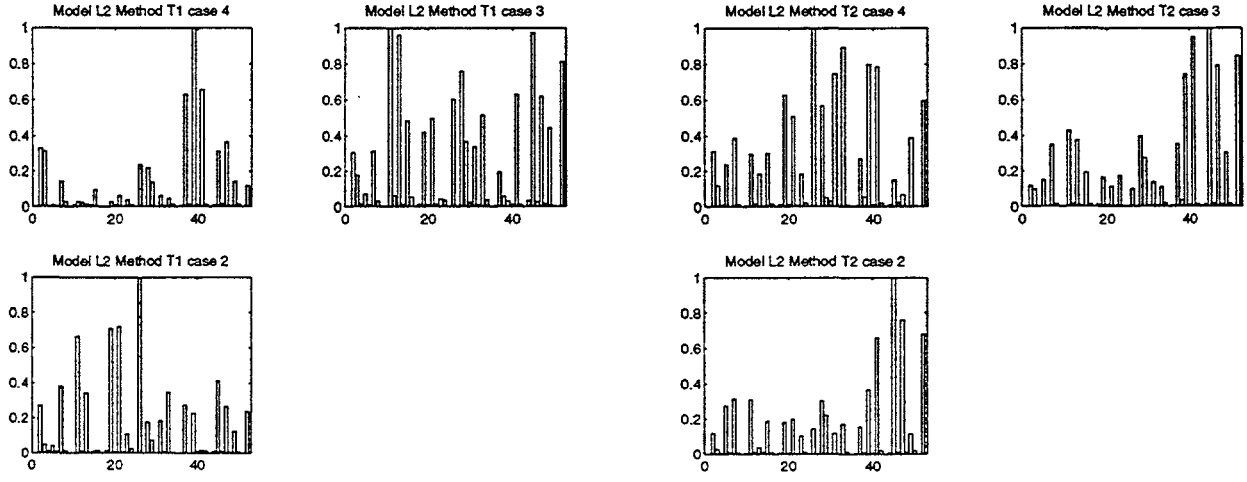

Figure A5. Model L2 Damage Detection Results (damage near DOF 40)

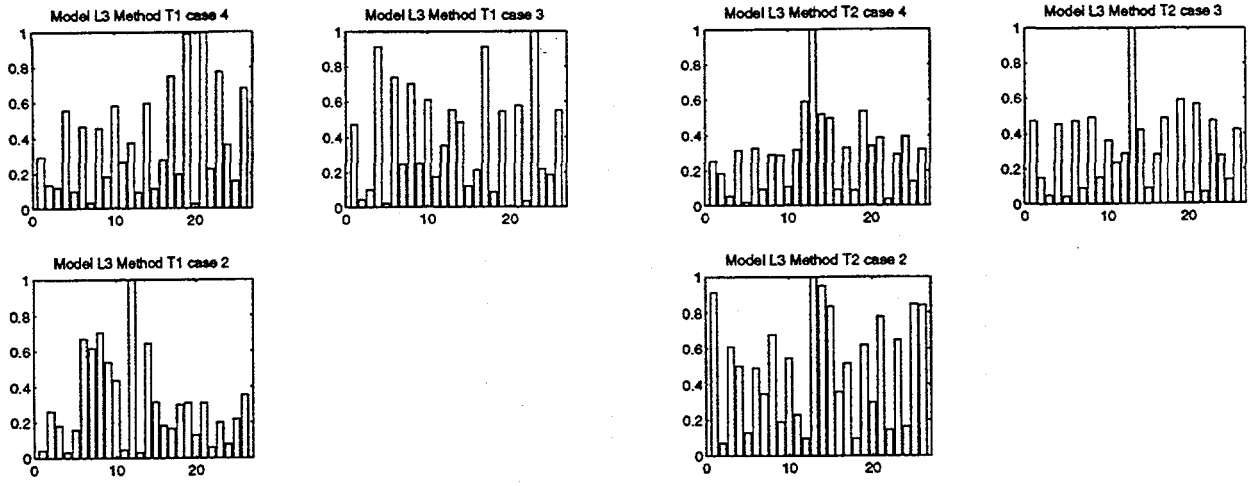

Figure A6. Model L3 Damage Detection Results (damage near DOF 20)

APPENDIX H

IMPROVED CONVERGENCE OF ESTIMATED STIFFNESS PARAMETERS FOR EXPERIMENTS WITH INCOMPLETE RECIPROCITY

Scott Doebling, Ken Alvin, and Lee Peterson

Proceedings of the 1995 AIAA Adaptive Structures Forum
In Conjunction with the 1995 Structures, Structural Dynamics, and Materials Conference
New Orleans, LA

April 10-13, 1995

Intentionally Left Blank

MEASUREMENT OF STATIC FLEXIBILITY MATRICES FOR EXPERIMENTS WITH INCOMPLETE RECIPROCITY

Scott W. Doebling[1], Lee D. Peterson[2]
Center for Aerospace Structures and
Department of Aerospace Engineering Sciences
University of Colorado at Boulder
Boulder, CO 80309-0429
Kenneth F. Alvin[3]
Structural Dynamics Department
Sandia National Laboratories
Albuquerque, NM 87185-0439

ABSTRACT

A technique is presented for estimating the residual flexibility at non-excited structural degrees of freedom from experimental structural vibration data. Using this method, more accurate flexibility matrices can be obtained for experiments with incomplete reciprocity, i.e. when the response and excitation measurement sensors are not fully collocated. By including the effects of residual dynamics in the flexibility matrix, all of the information about structural flexibility contained in the data is used. This information is then augmented by assumptions about structural connectivity and element static displacement shapes. The residual flexibility at the non-excited measurement degrees of freedom is estimated from the residual flexibility at the excited degrees of freedom using assumptions about modal orthogonality. The resulting measured flexibility matrix is then scaled so that it is both statically complete and consistent with the measurements. The fully reciprocal flexibility matrix can be used in applications such as free-interface component mode synthesis, structural parameter identification, location of manufacturing defects and structural health monitoring. Numerical and experimental results are presented which demonstrate the improvement in flexibility shape accuracy achieved by using this method.

NOMENCLATURE

$[G]$	Flexibility matrix
$[G_r]$	Residual flexibility matrix
$[H]$	Frequency response function matrix
$[M_r]$	Residual mass
$R(\omega)$	Residual function
$\{q\}$	Generalized coordinate basis
$[\Phi]$	Mode shape matrix
$[\Lambda]$	Modal eigenvalue matrix (diag$\{\omega^2\}$)
ω	Circular modal frequency

Subscripts (Instrumentation Degrees of Freedom)

m	Instrumented ("measured") degrees of freedom
d	Instrumented degrees of freedom which are driving points (excitation and response)
s	Instrumented degrees of freedom which are not driving points (response only)
o	Non-instrumented ("omitted") degrees of freedom

Subscripts (Component Mode Model Degrees of Freedom)

b	Boundary degrees of freedom in component mode model
i	Internal degrees of freedom in component mode model

Subscripts (Modal Degrees of Freedom)

1. Graduate Research Assistant, Student Member AIAA
doebling@colorado.edu
(303) 492-8551
2. Assistant Professor, Senior Member AIAA, Associate Member ASME
3. Structural Dynamics Research Fellow, Member AIAA

n	Measured modal set
r	Residual modal set

Superscripts (Solution Methods)

o	Orthogonality solution
c	Static completeness solution

INTRODUCTION

The accurate modeling of static and dynamic structural response has been accomplished traditionally using both analytical and experimental methods. One versatile approach involves the use of both experimental modal parameters and measured structural flexibility estimated from vibration data. These parameters can be used to form a statically complete dynamic model of the structure, which can be combined with other analytical or experimental models to predict the dynamic modes of a complex assembly. Such a procedure is termed experimental component mode synthesis (CMS). The flexibility influence coefficients can also be used to directly assess the response of the structure to arbitrary static loading patterns. Finally, the measured flexibility can be utilized to estimate values of stiffness parameters in a set of structural superelements using a method such as structural disassembly [1].

Accurate estimation of the flexibility matrix from vibration data requires not only identification of the observable modes, mode shapes and force participation factors, but also an estimate of the residual flexibility for each measured transfer function. The residual flexibility is a measure of the contribution of the unidentified flexible modes to the measured response within the test bandwidth. These unidentified modes can be modes above the test bandwidth, or modes within the test bandwidth which are poorly excited or unobservable from the measurement degrees of freedom (DOF). Inherent in all of the applications of experimentally determined flexibility matrices is the need to estimate the residual flexibilities between all of the physical DOF to be retained in the flexibility matrix. This requires a value for the residual flexibility between each physical DOF and every other physical DOF. To obtain these parameters using conventional identification techniques, the structure must be excited at each one of the physical DOF of the model. Such an experiment is known variously as "being fully reciprocal", "having complete reciprocity," or having a "collocated" set of measurement and excitation DOF. Such an experiment is usually impractical to implement on most aerospace and civil structures, due to the sometimes large number of measurement DOF. One method to bypass this problem is to use the measured partition of the residual flexibility, while neglecting the remaining entries [2]. However, in order to obtain the diagonal entries in the measured partition (which are the dominant terms), excitations are still required at all of the physical DOF.

In this paper, a method is presented for expanding the measured partition of the residual flexibility matrix, computed using a limited number of experimental excitations, to compute an estimate of the fully reciprocal flexibility matrix. Thus, free-interface component mode synthesis can be applied without measuring residual functions at all boundary DOF, and more accurate flexibility shapes can be obtained for flexibility influence analysis and component stiffness identification. The method uses two primary assumptions about the character of the structure: First, the measured modes and residual modes are assumed to be stiffness-orthogonal to each other. It is shown that this holds in the limit that all system DOF are measured and the inputs span the residual modal space, and that it provides an adequate approximation under testing circumstances. Second, a structural discretization is assumed which uses a set of elemental shape functions. The resulting flexibility matrix is constrained to be statically complete with respect to this shape function set.

Another appealing factor about this method is that in using all identified modal frequencies, mode shapes and all measured partitions of the residual flexibility matrix, it utilizes all available information about the flexibility of the structure. This information is then augmented with assumptions about the structural connectivity and element-level models of each component to obtain the resulting flexibility matrix. Thus, the data is the primary source of information about the structure, and it is augmented with

modeling assumptions to compensate for the information that is missing due to incomplete reciprocity.

The paper is organized in the following manner: An overview of the measured flexibility matrix is presented, along with an example showing its physical meaning. Then, some applications of the measured flexibility are reviewed. The estimation of the residual flexibility from modal test data is presented, including both classical and new techniques. A general solution for the unmeasured partition of the residual flexibility matrix is derived. Then, the solutions for the measured flexibility based on modal orthogonality and static completeness are presented. Finally, numerical examples and experimental applications are shown.

THE MEASURED FLEXIBILITY MATRIX

The response of a structure to a static load can be expressed in terms of the structural flexibility matrix. The flexibility matrix $[G]$ of a second order $(N \times N)$ system is the inverse of the system stiffness matrix $[K]$. The flexibility matrix can be separated into a modal component, $[G_n] = [\Phi_n]\,[\Lambda_n]^{-1}\,[\Phi_n]^T$, and a residual component, $[G_r]$. The response $\{u\}$ to an applied static force vector $\{F\}$ can then be written as

$$\begin{aligned} \{u\} &= [G]\,\{F\} \\ &= \left([\Phi_n]\,[\Lambda_n]^{-1}\,[\Phi_n]^T + [G_r] \right) \{F\} \end{aligned} \tag{1}$$

Where $[\Phi_n]$ is the measured mode shape matrix, $[\Lambda_n]$ is the measured eigenvalue matrix, and $[G_r]$ is the residual flexibility. From the modal test data, $[\Phi_n]$, $[\Lambda_n]$ and a partition of $[G_r]$ corresponding to the driving point locations can all be directly identified. Partitioning $[G_r]$ into the columns corresponding to driving point (d) and non-driving point (s) DOF yields

$$[G_r] = \begin{bmatrix} G_{r_d} & G_{r_s} \end{bmatrix} = \begin{bmatrix} G_{r_{dd}} & G_{r_{sd}}^T \\ G_{r_{sd}} & G_{r_{ss}} \end{bmatrix} \tag{2}$$

In this notation, $[G_{r_d}]$ is the partition of $[G_r]$ estimated from the test measurements. However, since the partition $[G_{r_{ss}}]$ cannot be estimated from the test data, it is difficult to fully characterize the residual flexibility matrix from an experimental data set.

The columns of the flexibility matrix are the displacements associated with the imposition of a unit force on one structural DOF. This can easily be seen by inspection of Eq. (1). Thus, the response of the structure due to a static load at any DOF can be assessed. The flexibility shapes are thus very intuitive and provide a great deal of insight into the static behavior of the structure. To illustrate the physical interpretation of the flexibility shapes, consider the 4DOF cantilevered beam shown in Figure (1). The four static flexibility shapes (columns of $[G]$) of this model are shown in Figure (2). Suppose the test excitation is applied at $\{v_2\}$, so that $\{q_d\} = \{v_2\}$. This DOF is third in the DOF list, so the third column of $[G]$ (flexibility shape 3) is known. Due to reciprocity, the third row of $[G]$ is also known, so that the displacement at the third DOF, $\{v_2\}$, is known for each flexibility shape. In the static completeness method described in this paper, this information is exploited to scale the unmeasured flexibility shapes to be consistent with the measured partition of the flexibility matrix.

The source of residual flexibility can be seen by writing the structural frequency response function (FRF) and separating it into the components below and above the bandwidth of measurement. Suppose that there are n_1 modes below the bandwidth (including rigid-body modes) and n_2 modes in the measurement bandwidth. The undamped inertance (acceleration/force) FRF for response at DOF i due to excitation at DOF j can the be written as [3]

$$H_{ij}(\omega) = -\omega^2 \left(\sum_{k=1}^{n_1} \frac{\phi_k^i \phi_k^j}{\omega_k^2 - \omega^2} + \sum_{k=n_1+1}^{n_2} \frac{\phi_k^i \phi_k^j}{\omega_k^2 - \omega^2} + \sum_{k=n_2+1}^{\infty} \frac{\phi_k^i \phi_k^j}{\omega_k^2 - \omega^2} \right) \tag{3}$$

For the first term, representing the modes below the bandwidth, the limit as $\omega \gg \omega_k$ is

$$\lim_{\frac{\omega_k}{\omega} \to 0} \left\{ -\omega^2 \sum_{k=1}^{n_1} \frac{\phi_k^i \phi_k^j}{\omega_k^2 - \omega^2} \right\} = \sum_{k=1}^{n_1} \phi_k^i \phi_k^j \tag{4}$$

Since this is a constant term relating force to acceleration, the effect of these low-frequency modes is analogous to a mass term, thus it is often referred to as 'residual mass' [3]. Writing a MacLaurin series expansion of the third term and taking the limit as $\omega \ll \omega_k$ yields

$$\lim_{\frac{\omega}{\omega_k} \to 0} \left\{ -\omega^2 \sum_{k=n_2+1}^{\infty} \frac{\phi_k^i \phi_k^j}{\omega_k^2 - \omega^2} \right\} = -\omega^2 \left\{ \sum_{k=n_2+1}^{\infty} \frac{\phi_k^i \phi_k^j}{\omega_k^2} \right\} + \omega^4 \left\{ \sum_{k=n_2+1}^{\infty} \frac{\phi_k^i \phi_k^j}{\omega_k^4} \right\} - \ldots \quad (5)$$

The first term of this series approximates an inverse stiffness term, thus it is often referred to as 'residual flexibility'. It should be noted that form of Equation (3) assumes that all modes within the test bandwidth are observable from the measurement dof. When this is not the case, the effects of these modes are absorbed into the residual terms.

APPLICATIONS OF THE MEASURED FLEXIBILITY MATRIX

The most widespread use of measured flexibility is probably in the formulation of free-interface CMS models. Free-interface CMS is popular for building experimental or hybrid analytical-experimental models because all of the necessary quantities can be measured using standard modal test techniques. CMS is also used to model fixed-based dynamic behavior using data from a free-free modal test [2], [5]. As described by Craig [6], the modal set for this method consists of the free-interface normal modes and a set of attachment or inertia-relief modes, which are the columns of the measured flexibility matrix $[G]$. For a restrained structure, the attachment modes are the displacement patterns which result when a unit load is applied at each boundary DOF, while holding all other external applied forces to zero. For an unrestrained structure (i.e. one which has rigid-body modes), the inertia-relief modes are the shapes which result due to d'Alembert forces (inertial reactions) when a unit load is applied at each boundary DOF.

Including the residual flexibility in the component mode model to account for the out-of-bandwidth structural response was first proposed by MacNeal [7]. MacNeal retains one term of the series expansion in Eq. (5), which approximates a flexible response, hence 'residual flexibility.' Rubin [8] also includes the second term in this expansion, which behaves as an inertia relief effect, hence "residual inertia". Craig and Chang [9] derive a special form of Rubin's method based on the MacLaurin expansion of Eq. (5). However, the Rubin method presented by Craig and Chang does not explicitly retain the boundary DOF $\{q_b\}$. Martinez, et. al., [10] show that this method can be written as a Ritz transformation in terms of the boundary and generalized DOF,

$$\begin{Bmatrix} q_i \\ q_b \end{Bmatrix} = \begin{bmatrix} [\Phi_i] - [G_{r_{bi}}]^T [G_{r_{bb}}]^{-1} [\Phi_b] & [G_{r_{bi}}]^T [G_{r_{bb}}]^{-1} \\ 0 & I \end{bmatrix} \begin{Bmatrix} q_n \\ q_b \end{Bmatrix} \quad (6)$$

Since this transformation explicitly retains the boundary DOF $\{q_b\}$, the resulting model has a final form similar to the Craig-Bampton fixed-interface CMS formulation which is widely used in analytical CMS [11]. Thus Eq. (6) is an attractive form for expressing the free-interface CMS transformation. It is demonstrated by Kammer and Baker [12] that Eq. (6) is statically equivalent to the Craig-Bampton transformation. A comprehensive review of component mode synthesis methods is presented by Craig [6].

Another application of measured flexibility is the direct assessment of static structural responses by observation of flexibility shapes. Recently, this technique has been applied to a deployable truss structure to determine the effects of gravity preload on joint stiffness [13]. The flexibility matrix is also used for direct assessment of structural load-carrying capacity, e.g. for damage detection and health monitoring. One specific application the measured flexibility matrix has been used for is condition assessment of highway bridges [14].

Measured flexibility can also be used for the assessment of structural component stiffnesses. This assessment requires the assumption of an underlying structural connectivity and strain energy distribution. Recent work by the authors [1] presents a

method for decomposing the flexibility matrix to determine the component stiffnesses of structural superelements. That method of "Structural Disassembly" is used in this research to obtain the initial estimates of the structural parameters for the computation of the statically complete flexibility matrix.

A method for creating minimal order mass and stiffness matrices presented by Alvin, et. al., [15] also depends upon having an accurate structural flexibility matrix. As shown in that paper, the inverse of the measured flexibility matrix converges to the system stiffness matrix Guyan-reduced to the measured DOF. Thus, the improved convergence of the flexibility matrix introduced by using residual flexibility increases the accuracy of the structural stiffness and mass matrices computed using that method.

ESTIMATION OF RESIDUAL FLEXIBILITY FROM TEST DATA

The computation of residual flexibility is generally done using "Residual Functions", which are computed by subtracting the reconstructed response of the identified modes from the measured FRF. If $[\Phi_{n_m}]$ are the measured mode shapes at the response DOF, $[\Phi_{n_d}]$ are the measured mode shapes at the excitation DOF and $[\Lambda_n]$ is the measured structural eigenvalue matrix, and only the first order terms of the high-frequency modes are retained, Eq. (3) can be rewritten as

$$H(\omega) = -\omega^2 [\Phi_{n_m}] ([\Lambda_n] - \omega^2 [I])^{-1} [\Phi_{n_d}] - \omega^2 [G_{r_d}] + [M_{r_d}] \quad (7)$$

where the residual flexibility term is

$$[G_{r_d}] = \sum_{k=n_2+1}^{\infty} \frac{\{\phi_{k_m}\} \{\phi_{k_d}\}^T}{\omega_k^2} \quad (8)$$

and the residual mass term is

$$[M_{r_d}] = \sum_{k=1}^{n_1} \{\phi_{k_m}\} \{\phi_{k_d}\}^T \quad (9)$$

The residual function is then computed by rewriting Eq. (3) and subtracting the reconstructed FRF from the data. Thus the residual function $R(\omega)$ is

$$R(\omega) = [M_{r_d}] - [G_{r_d}] \omega^2 = H(\omega) + \omega^2 [\Phi_{n_m}] ([\Lambda_n] - \omega^2 [I])^{-1} [\Phi_{n_d}] \quad (10)$$

So substituting in the identified modal set $[\Phi_{n_m}]$ and $[\Lambda_n]$ yields a value for $R(\omega)$. Curve-fitting $R(\omega)$ over the higher frequencies yields an estimate for the residual flexibility, and curve-fitting the low frequency asymptote of $R(\omega)$ yields an estimate for the residual mass.

However, it is demonstrated by Peterson and Alvin [4] that more accurate modal vectors and residuals can be obtained by simultaneously solving for the output mode shapes, the residual mass, and the residual flexibility. This involves a least-squares fit for the parameters, which can be formulated by rewriting Eq. (7) as

$$H(\omega) = \quad (11)$$

$$\left[[\Phi_{n_m}] \; [G_{r_d}] \; [M_{r_d}] \right] \begin{bmatrix} -\omega^2 ([\Lambda] - \omega^2)^{-1} [\Phi_{n_d}] \\ -\omega^2 [I] \\ [I] \end{bmatrix}$$

Thus, from Eq. (11), the quantities $[\Phi_{n_m}]$, $[G_{r_d}]$ and $[M_{r_d}]$ can be estimated to fit the data in the frequency domain. This can yield more accurate results for both modes and residuals than using residual functions, since the effects of residual mass $[M_{r_d}]$, and residual flexibility $[G_{r_d}]$, are both identified concurrently with the output mode shapes. It should be noted that while the residual mass does not contribute to the identified flexibility shapes, its effect is still in the FRF data, and thus it should be estimated to avoid biasing the mode shape and residual flexibility estimates. As previously noted, the effects of modes which are in the bandwidth but are unobservable are also absorbed into the residual mass and flexibility terms.

GENERAL SOLUTION FOR RESIDUAL FLEXIBILITY AT NON-EXCITED DOF

A problem with the estimated residual flexibility matrix $[G_r]$ is that it is only known with respect to the excited DOF set $\{q_d\}$, i.e. $[G_{r_d}]$ has dimensions $(m \times d)$. Therefore, a driving point response must be obtained at every DOF at which a column of the residual flexibility matrix is desired. For an experimentally derived free-interface CMS model, this means exciting at every DOF in $\{q_b\}$, such that $\{q_d\} = \{q_b\}$. For the minimal-order experimental stiffness matrix, this means exciting at every DOF in $\{q_m\}$, such that $\{q_d\} = \{q_m\}$. These constraints generally add time and cost to the experimental implementation of these methods, due to the sometimes large number of excitations required.

The need to use residual flexibility to obtain accurate local flexibility at the CMS interface DOF is explicitly noted by Rubin [8], but the need to excite all interface DOF has placed major test design constraints on measuring the residual flexibility. The conventional constraint requires the boundary DOF to be a subset of the excited DOF,

$$\{q_b\} \subset \{q_d\} \tag{12}$$

With the new method, however, the boundary DOF are only required to be a subset of the instrumented DOF,

$$\{q_b\} \subset \{q_m\} = \begin{Bmatrix} q_d \\ q_s \end{Bmatrix} \tag{13}$$

The selection of the excitation DOF $\{q_d\}$ will determine, in part, the accuracy of the estimated residual. The effects of input selection on the estimated residuals is discussed by Doebling [19].

To see the form of the residual flexibility and understand its physical relevance, it is important to write a parameterization of the general solution for the unmeasured residual flexibility in terms of the measured quantities. Suppose the full structural mode shape matrix at the response DOF, $[\Phi_m]$, is partitioned into excitation and response DOF, and measured and residual modes. The resulting partitioning looks like

$$[\Phi_m] = \begin{bmatrix} \Phi_{n_d} & \Phi_{r_d} \\ \Phi_{n_s} & \Phi_{r_s} \end{bmatrix} \tag{14}$$

Likewise, the eigenvalue matrix can be partitioned as

$$[\Lambda] = \begin{bmatrix} \Lambda_n & 0 \\ 0 & \Lambda_r \end{bmatrix} \tag{15}$$

Substituting Eq. (14) and Eq. (15) into the expression for total flexibility at the sensor DOF yields

$$\begin{aligned} [G] &= [\Phi_m]\,[\Lambda]^{-1}\,[\Phi_m]^T \\ &= \begin{bmatrix} \Phi_{n_d} \\ \Phi_{n_s} \end{bmatrix} [\Lambda_n]^{-1} \begin{bmatrix} \Phi_{n_d}^T & \Phi_{n_s}^T \end{bmatrix} + \begin{bmatrix} \Phi_{r_d} \\ \Phi_{r_s} \end{bmatrix} [\Lambda_r]^{-1} \begin{bmatrix} \Phi_{r_d}^T & \Phi_{r_s}^T \end{bmatrix} \\ &= [G_n] + [G_r] \end{aligned} \tag{16}$$

The second term in Eq. (16) is the residual flexibility, and can be written

$$[G_r] = \begin{bmatrix} \Phi_{r_d}\Lambda_r^{-1}\Phi_{r_d}^T & \Phi_{r_d}\Lambda_r^{-1}\Phi_{r_s}^T \\ \Phi_{r_s}\Lambda_r^{-1}\Phi_{r_d}^T & \Phi_{r_s}\Lambda_r^{-1}\Phi_{r_s}^T \end{bmatrix} = \begin{bmatrix} G_{r_{dd}} & G_{r_{sd}}^T \\ G_{r_{sd}} & G_{r_{ss}} \end{bmatrix} = \begin{bmatrix} G_{r_d} & G_{r_s} \end{bmatrix} \tag{17}$$

As shown in the previous section, $[G_{r_{dd}}]$ and $[G_{r_{sd}}]$ can be estimated from the measured FRF matrix $H(\omega)$, but the remaining partition $[G_{r_{ss}}]$ cannot. As shown in Eq. (17), this partition can be parameterized by the residual eigenvalues and the partition of the residual modes corresponding to the non-excited DOF $\{q_s\}$ as

$$[G_{r_{ss}}] = [\Phi_{r_s}]\,[\Lambda_r]^{-1}\,[\Phi_{r_s}]^T \tag{18}$$

Using the expression for $[G_{r_{dd}}]$ from Equation (17), we can state without loss of generality that

$$[\Phi_{r_d}]\,[\Lambda_r]^{-1/2} = \left[[G_{r_{dd}}]^{1/2}\ 0\right][T] \qquad (19)$$

where $[T]$ is some unknown orthonormal transformation ($[T]\,[T]^T = [T]^T[T] = [I]$) and $[G_{r_{dd}}]^{1/2}$ is a symbolic Cholesky factorization of $[G_{r_{dd}}]$. Then, using Equation (19) together with the expression for $[G_{r_{sd}}]$ from Equation (17), we have

$$[\Phi_{r_s}]\,[\Lambda_r]^{-1/2} = \left[[G_{r_{sd}}]\,([G_{r_{dd}}]^{1/2})^{-T}\ [X]\right][T] \qquad (20)$$

where $[X]$ is an unknown matrix of dimension $(s \times r)$. Thus, the general solution for $[G_r]$ is given as

$$[G_r] = \begin{bmatrix} [G_{r_{dd}}]^{1/2} & 0 \\ [G_{r_{sd}}]\,([G_{r_{dd}}]^{1/2})^{-T} & [X] \end{bmatrix} [T]\,[T]^T \qquad (21)$$

$$\begin{bmatrix} ([G_{r_{dd}}^{1/2}])^T\,[G_{r_{dd}}]^{-1/2}\,[G_{r_{sd}}]^T \\ 0 \qquad\qquad [X]^T \end{bmatrix}$$

Finally, equating Equation (21) and Equation (17) yields the expression

$$[G_{r_{ss}}] = [G_{r_{sd}}]\,[G_{r_{dd}}]^{-1}\,[G_{r_{sd}}]^T + [X]\,[X]^T \qquad (22)$$

This general solution for the unmeasured partition of the residual flexibility matrix effectively parameterizes all possible solutions in terms of the unknown symmetric matrix $[X]\,[X]^T$. Taking $[X]\,[X]^T = 0$ leads to a basic rank d solution which satisfies certain key orthogonality conditions, as demonstrated in the following section.

ORTHOGONALITY SOLUTION FOR RESIDUAL FLEXIBILITY AT NON-EXCITED DOF

This section shows how the condition of stiffness orthogonality between measured and residual modes can be exploited to obtain an estimate for $[G_{r_{ss}}]$. First, a statement is made about the orthogonality, followed by a proof of the statement.

Statement:

For $[G_r]$ as written in Eq. (17), a solution for $[G_{r_{ss}}]$ which satisfies modal orthogonality is

$$[G_{r_{ss}}] = [G_{r_{sd}}]\,[G_{r_{dd}}]^{-1}\,[G_{r_{sd}}]^T \qquad (23)$$

provided that the driving point DOF $\{q_d\}$ span the residual space $\{q_r\}$ defined by $[\Phi_r]$. Furthermore, this solution satisfies modal orthogonality through the static reduction of the global stiffness matrix to the instrumented DOF $\{q_m\}$, provided that the measured modal vectors $[\Phi_{n_m}]$ in question are preserved by the static reduction. Eq. (23) is thus termed the 'Orthogonality Solution' for $[G_{r_{ss}}]$.

Proof:

If $[\Phi]$ is the set of eigenmodes for a system stiffness matrix $[K]$, normalized such that

$$[\Phi]^T[K]\,[\Phi] = [\Lambda] \qquad (24)$$

then for $i \neq j$, $\{\Phi_i\}$ and $\{\Phi_j\}$ are stiffness-orthogonal, such that

$$\{\Phi_i\}^T[K]\,\{\Phi_j\} = 0 \qquad (25)$$

If $[\Phi]$ is then partitioned into measured and residual modes, by Eq. (25) these modes must be stiffness-orthogonal. This condition can be written

$$[\Phi_n]^T[K]\,[\Phi_r] = 0 \qquad (26)$$

Pre-multiplying Eq. (26) by $[\Phi_n]\,[\Lambda_n]^{-1}$ and post-multiplying by $[\Lambda_r]^{-1}\,[\Phi_r]^T$ yields the condition

$$[G_n]\,[K]\,[G_r] = 0 \qquad (27)$$

Partitioning $[K]$ into columns corresponding to the driving point DOF, $\{q_d\}$, and non-driving point DOF, $\{q_s\}$, yields

$$[K] = \left[K_d\ K_s\right] \qquad (28)$$

and substituting Eq. (17) and Eq. (28) into Eq. (27) yields

$$[G_n]\begin{bmatrix}K_d & K_s\end{bmatrix}\begin{bmatrix}G_{r_{dd}} & G_{r_{sd}}^T\\ G_{r_{sd}} & G_{r_{ss}}\end{bmatrix} = 0 \qquad (29)$$

The equations in the left and right partitions can be expanded to get

$$[G_n]\,[K_d]\,[G_{r_{dd}}] + [G_n]\,[K_s]\,[G_{r_{sd}}] = 0 \qquad (30)$$

$$[G_n]\,[K_d]\,[G_{r_{sd}}]^T + [G_n]\,[K_s]\,[G_{r_{ss}}] = 0 \qquad (31)$$

Assuming $\{q_d\}$ spans $\{q_r\}$, then $[G_{r_{dd}}]$ is invertible, so Eq. (30) can be solved for $[G_n]\,[K_d]$ to get

$$[G_n]\,[K_d] = -[G_n]\,[K_s]\,[G_{r_{sd}}]\,[G_{r_{dd}}]^{-1} \qquad (32)$$

Substituting Eq. (32) into Eq. (31) yields

$$[G_n]\,[K_s]\,[G_{r_{ss}}] = [G_n]\,[K_s]\,[G_{r_{sd}}]\,[G_{r_{dd}}]^{-1}\,[G_{r_{sd}}]^T \qquad (33)$$

Clearly, a particular solution satisfying Equation (33) is

$$[G_{r_{ss}}] = [G_{r_{sd}}]\,[G_{r_{dd}}]^{-1}\,[G_{r_{sd}}]^T \qquad (34)$$

which is the basic term of the general solution for $[G_{r_{ss}}]$ developed in the preceding section. This result also implies that the unknown contribution $[X]\,[X]^T$ to the general solution Equation (22) must lie in the right null space of $[G_n]\,[K_s]$. Unfortunately, since $[G_n]\,[K_s]$ is itself unknown, we cannot directly use this condition to construct $[X]\,[X]^T$.

Now consider the reduction of the system stiffness matrix $[K]$ to the measurement DOF set $\{q_m\}$. The modal matrix is first partitioned into instrumented DOF $\{q_m\}$ and omitted DOF $\{q_o\}$, as well as measured modes $\{q_n\}$ and residual modes $\{q_r\}$. The resulting partitions are

$$[\Phi] = \begin{bmatrix}\Phi_n & \Phi_r\end{bmatrix} = \begin{bmatrix}\Phi_m\\ \Phi_o\end{bmatrix} = \begin{bmatrix}\Phi_{n_m} & \Phi_{r_m}\\ \Phi_{n_o} & \Phi_{r_o}\end{bmatrix} \qquad (35)$$

In this representation, the upper partition $[\Phi_m]$ is the same as in Eq. (14). The upper-left partition, $[\Phi_{n_m}]$ is the matrix of measured mode shapes identified from the test data.

Likewise, the system stiffness matrix $[K]$ can be partitioned into measured and omitted DOF to get

$$[K] = \begin{bmatrix}K_{mm} & K_{mo}\\ K_{mo}^T & K_{oo}\end{bmatrix} \qquad (36)$$

Substituting Eq. (35) and Eq. (36) into Eq. (26) yields an orthogonality condition for the partitioned matrices:

$$\begin{bmatrix}\Phi_{n_m}\\ \Phi_{n_o}\end{bmatrix}^T\begin{bmatrix}K_{mm} & K_{mo}\\ K_{mo}^T & K_{oo}\end{bmatrix}\begin{bmatrix}\Phi_{r_m}\\ \Phi_{r_o}\end{bmatrix} = 0 \qquad (37)$$

Multiplying this equation out yields

$$[\Phi_{n_m}]^T[K_{mm}]\,[\Phi_{r_m}] + [\Phi_{n_m}]^T[K_{mo}]\,[\Phi_{r_o}] + [\Phi_{n_o}]^T[K_{mo}]^T[\Phi_{r_m}] + [\Phi_n^i]^T[K_{oo}]\,[\Phi_{r_o}] = 0 \qquad (38)$$

Now, assume that the measured modes are preserved by static condensation [16], such that

$$[\Phi_{n_o}] = -[K_{oo}]^{-1}[K_{mo}]^T[\Phi_{n_m}] \qquad (39)$$

Substitute Eq. (39) into Eq. (38), and the result is

$$[\Phi_{n_m}]^T[K_{mm} - K_{mo}K_{oo}^{-1}K_{mo}^T]\,[\Phi_{r_m}] = 0 \qquad (40)$$

Pre-multiplying and post-multiplying Eq. (40) by the appropriate factors gives the 'reduced' orthogonality relation

$$[G_{n_m}]^T[\bar{K}]\,[G_{r_m}] = 0 \qquad (41)$$

This form of the orthogonality constraint is important, because it corresponds to the measured partitions of the modal and residual flexibility. Thus Eq. (41) is the form of the orthogonality constraint which is applicable to the experimentally measured quantities.

As shown by Alvin, et. al. [15], the inverse of the measured flexibility is equivalent to the Guyan-reduced system stiffness matrix

$$[\bar{K}] = [K_{mm} - K_{mo}K_{oo}^{-1}K_{mo}^{T}] = [G_m]^{-1} \quad (42)$$

and thus each term in Eq. (41) can be identified (ideally) from the experimental data. Because of the assumption of static condensation, however, Eq. (41) is only satisfied to the extent that Eq. (39) is, i.e. $[G_{n_m}]$ must consist of modes which are well - preserved by static condensation. This condition can sometimes be satisfied when the modes have low frequency, and when all DOF of significant mass excited by that mode are instrumented. Since the flexibility and stiffness matrices in Eq. (41) are measurable, this reduced orthogonality condition can form the basis of an iterative approach to determining other particular solutions for $[X]\,[X]^T$ in $[G_{r_{ss}}]$.

End of Proof

STATIC COMPLETENESS CONSTRAINT FOR MEASURED FLEXIBILITY

In order to ensure that the flexibility model stores energy in a manner consistent with the assumed underlying connectivity and shape functions, it must demonstrate static completeness. Static completeness is satisfied when the deformations of the structure can be discretized as a superposition of a number of shape functions. The stiffness matrix of the structure, which is the inverse of the flexibility matrix, can then be formed from the shape functions such that the strain energy of the structure can be expressed as

$$U = \frac{1}{2}\{u\}^T[K]\{u\} \quad (43)$$

In the formulation of the method of structural disassembly [1], it is shown that the stiffness matrix can be parameterized as a decomposition into a matrix of singular values, $[P]$, which are functions of the stiffness parameters of the structure, and singular vectors $[A]$, which are functions of the assumed element shape functions and the structural connectivity. The stiffness matrix can then be written

$$[K] = [A]\,[P]\,[A]^T \quad (44)$$

Using a parameterization in terms of complementary strain energy, it is shown that an equivalent condition applied to the flexibility matrix can be written as

$$[A]\,[G]\,([A]\,[P]\,[A]^T)\,[G]\,[A]^T = [A]\,[G]\,[A]^T \quad (45)$$

A method of solving Eq. (44) and Eq. (45) for the structural parameters $[P]$, known as "structural disassembly," is presented and discussed in detail by Peterson, et. al., [1].

It is possible to parameterize the flexibility matrix in a similar way so that a statically complete coordinate basis for the flexibility matrix is known. For a statically complete flexibility matrix, this parameterization can be written as the singular value decomposition

$$[G] = \begin{bmatrix} G_d & G_s \end{bmatrix} = \begin{bmatrix} G_{dd} & G_{sd}^T \\ G_{sd} & G_{ss} \end{bmatrix} = [V]\,[\Sigma]\,[V]^T \quad (46)$$

Where diag ($[\Sigma]$) are the singular values and $[V]$ are the singular vectors. Thus, $[V]$ determines the coordinate basis for the flexibility matrix and $[\Sigma]$ determines the scaling. Since the partition of the flexibility matrix corresponding to the driving point DOF, $[G_d]$, is known, this parameterization can be exploited to scale the unknown partition of the measured flexibility matrix such that the known partition is consistent with the measurements.

The procedure for obtaining the statically complete flexibility has the following steps: First, expand the measured partition of the residual flexibility using the orthogonality solution, Equation (23), to get the orthogonality-based estimate of the flexibility matrix, $[G^o]$. This estimate serves as an 'initial value' for the flexibility matrix. Next, substitute $[G^o]$ into Equation (45) and solve for the parameter vector $\{\hat{P}\}$ using structural disassembly. Then, reconstruct a statically complete $[\hat{K}]$ by substituting $[A]$ and $\{\hat{P}\}$ into Equation (44). Then the corre-

sponding statically complete flexibility can be computed using

$$[\hat{G}] = [\hat{K}]^{+} \tag{47}$$

(The use of pseudo-inverse rather than inverse in Equation (47) will work in the general case that the structure contains rigid body modes.) Assuming that $[G^o]$ is not statically complete, then $[\hat{G}] \neq [G^o]$. Now the singular value decomposition of $[\hat{G}]$ can be written as in Equation (46) to get

$$[\hat{G}] = [\hat{V}]\,[\hat{\Sigma}]\,[\hat{V}]^T \tag{48}$$

The decomposition of Equation (48) provides the coordinate basis $[\hat{V}]$ for the statically complete flexibility matrix. It should be noted that since the flexibility matrix $[\hat{G}]$ has dimension $(m \times m)$, solving for the SVD in Eq. (48) is not computationally burdensome.

The known partition of the measured flexibility matrix, $[G_d]$, can be written as a decomposition, using the coordinate basis generated in Equation (48). This decomposition is written as

$$[G_d] = [\hat{V}]\,[\Sigma]\,[\hat{V}_d]^T \tag{49}$$

where $[\hat{V}_d]$ are the columns of $[V]$ corresponding to the driving point dof $\{q_d\}$, and the singular value matrix $[\Sigma]$ is unknown. Rewriting Equation (49) using an element by element tensor notation yields an over-determined system of equations for the singular values:

$$[G_d]_{ij} = \sum_{\beta} (\hat{V}_{i\beta})\,(\hat{V}_{j\beta})\,(\Sigma_{\beta}) \tag{50}$$

which can be solved using a standard least-squares technique. Then the static completeness solution to the unknown partition of the flexibility matrix can be computed as

$$[G^c_{ss}] = [\hat{V}_s]\,[\Sigma]\,[\hat{V}_s] \tag{51}$$

so that the static completeness solution for $[G]$ is

$$[G^c] = \begin{bmatrix} G_{dd} & G_{sd}^T \\ G_{sd} & G^c_{ss} \end{bmatrix} \tag{52}$$

As shown in the experimental example, the static completeness expansion is limited by the accuracy of the measured partition of the flexibility matrix, $[G_d]$. Thus the completeness solution $[G^c]$ should be considered to contain at least the same level of error as $[G_d]$.

NUMERICAL EXAMPLES

The application of this flexibility estimation technique is demonstrated for the cantilevered beam models and properties shown in Figure (1). The modes for these examples were generated using the continuous solution to the fourth-order boundary value problem for a Bernoulli-Euler beam [17].

Example 1: 2 DOF Cantilevered Beam

Consider the 2-DOF model with an input at the vertical tip DOF, so that the dof sets are defined as

$$\{q_m\} = \begin{Bmatrix} v_1 \\ \theta_1 \end{Bmatrix} \quad \{q_d\} = \{v_1\} \quad \{q_s\} = \{\theta_1\} \tag{53}$$

For 1 measured bending mode, the modal flexibility and the measured partition of the residual flexibility are

$$[G_n] = \begin{bmatrix} 1.80 & -1.65 \\ -1.65 & 1.51 \end{bmatrix} \times 10^{-3}$$
$$[G_{r_d}] = \begin{bmatrix} 5.45 \\ -20.2 \end{bmatrix} \times 10^{-5} \tag{54}$$

Then the orthogonality solution $[G^o]$, the completeness solution $[G^c]$, and the exact solution $[G]$ are

$$[G^o] = \begin{bmatrix} 1.85 & -1.85 \\ -1.85 & 2.27 \end{bmatrix} \times 10^{-3}$$

$$[G^c] = \begin{bmatrix} 1.85 & -1.85 \\ -1.85 & 2.47 \end{bmatrix} \times 10^{-3} \qquad (55)$$

$$[G] = \begin{bmatrix} 1.85 & -1.85 \\ -1.85 & 2.47 \end{bmatrix} \times 10^{-3}$$

So the error in $[G_{ss}]$ is 39% for modal flexibility, 8% for the orthogonality solution and zero for the completeness solution. Thus, for the one element cantilevered beam, the full flexibility can be found exactly using one mode and one input DOF.

Example 2: 4 DOF Cantilevered Beam

Consider the 2-element, 4-DOF model shown in Figure (1). Assume that there is one test excitation at the vertical DOF of node 2. Thus, the DOF sets are

$$\{q_m\} = \begin{Bmatrix} v_1 \\ \theta_1 \\ v_2 \\ \theta_2 \end{Bmatrix} \qquad \{q_d\} = \{ v_2 \}$$

$$\{q_s\} = \begin{Bmatrix} v_1 \\ \theta_1 \\ \theta_2 \end{Bmatrix} \qquad (56)$$

The modal flexibility $[G_n]$, the orthogonality solution $[G^o]$ and the completeness solution $[G^c]$ are then computed for an increasing number of measured modes. For this example, $[G_{ss}]$ is not a scalar, so the error in $[G_{ss}]$ is expressed in terms of the percent error in the 2-Norm, $\|\Delta G_{ss}\| / \|G_{ss}\|$. The convergence of this error as the number of measured modes increases is shown in Figure (3), which also includes an additional constraint to keep the parameters of each beam element equal. This measure of error indicates that the orthogonality solution $[G^o]$ is always better than the modal flexibility, and that the completeness solution $[G^c]$ has the minimum error for any number of measured modes. The physical meaning of this error criterion is difficult to interpret, however.

For a more physically meaningful error indicator, consider the beam stiffness parameter EI, which is computed from the measured flexibility using structural disassembly. The convergence of EI as the number of measured modes increases is shown in Figure (4). Using this error indicator, the statically complete solution $[G^c]$ is once again clearly the best. It is interesting to note the value obtained using the orthogonality solution $[G^o]$ is not always better than that obtained from the modal flexibility $[G^n]$. This is because the beam parameter EI depends on off-diagonal terms in $[G]$ as well as on-diagonal terms, and the off-diagonal terms do not converge monotonically as the number of measured modes increases.

EXPERIMENTAL APPLICATION

In this section, the computation of flexibility shapes is shown for an experiment on a simple structure with a non-reciprocal instrumentation configuration. Consider the cantilevered beam test shown in Figure (5). The beam was tested using a modal impact hammer applied vertically near the tip. Due to the low fundamental frequency of this beam (4 Hz), the sample window was set at 32 seconds. The data were sampled at 500 Hz so that the first 4 bending modes could be identified. The driving point FRF is shown in Figure (6), overlaid with the 4-mode reconstruction (including residual flexibility). The reconstruction is so close to the data that the only difference can be seen above 200 Hz, which is where the test bandwidth cutoff is set. A modal model consisting of mode shapes, modal frequencies, residual mass and residual flexibility was identified from the data using an efficient variant of the Eigensystem Realization Algorithm (ERA) [18] and the previously described frequency domain modal/residual estimation technique [4].

The flexibility shape obtained using the first four measured modes plus residual flexibility is shown for the reciprocal input degree of freedom in Figure (7) and Figure (8). The flexibility shape in Figure (7) corresponds to the translational displacements for an applied vertical force at the tip of the cantilevered beam. Since this is the actual input location, the measured partition of the modes and residual flexibility are sufficient to determine the complete flexibility shape. The orthogonality solution, therefore, uses just the partition of the residual flexibility $[G_{r_d}]$ directly estimated from the measured response functions. The completeness solution, on the other hand,

is slightly different as it reconstructs both the measured and unmeasured partitions of the flexibility matrix using assumed static shapes with a scaling determined from the directly estimated flexibility. Both flexibility shapes which use the residual flexibility show only minor differences as compared to the modal flexibility $[G_n]$ of the measured modes, reflecting the fact that the residual flexibility has a small magnitude.

As shown, the modal test-estimated flexibility does a poor job of fitting the analytical prediction. This error between the "exact" solution and that estimated from testing can be due to differences between the assumed and actual material and cross-sectional behavior (i.e. modeling errors). It should be noted, however, that the flexibility shape obtained from the test data is also an estimate because it is reconstructed from parameters estimated using acceleration measurements at offset sensor locations. Thus, errors in the identified frequencies and errors in the scaling of the estimated modal shapes and residual flexibilities (i.e. modal parameter estimation errors) may also contribute to the total error seen in Figure (7).

The flexibility shape at the rotational DOF for the same vertical force input is shown in Figure (8). These DOF are actually estimated by a finite difference approximation of the variation of longitudinal acceleration across the vertical dimension of the beam cross-section, a process which may engender additional measurement errors. These DOF exhibit more significant error with respect to the assumed "exact" solution. Again, the orthogonality solution for residual flexibility contributes little to the total flexibility. Significant improvement is seen, however, with using the static completeness solution. This may indicate that systematic errors in the estimation of the beam rotations from translational DOF can be mitigated somewhat by the assumed static mode shapes provided in the static completeness solution.

The remaining error in the static completeness solution of both the displacement and the rotation DOF is at least partially attributable to the fact that the measured flexibility partition $[G_{r_d}]$ is itself not consistent with the static shapes assumed through disassembly. Since this partition is not statically consistent, the estimate of the full statically complete flexibility matrix is also erroneous. Thus, static completeness is insufficient to get accurate flexibility estimates when the measured partition is not consistent with the assumed structural connectivity. This problem underscores the need for highly precise experimental results. Further experimental studies are in progress to improve the results for the measured flexibility, so that a fair validation of the present procedure for estimating unmeasured flexibility partitions can be completed.

CONCLUSION

A method for expanding the residual flexibility to account for incomplete measurement reciprocity has been presented. It incorporates a modal orthogonality condition to estimate the unmeasured partition of the residual flexibility matrix. The resulting flexibility matrix is adjusted using a static completeness constraint to ensure that the resulting flexibility shapes are consistent with the measured flexibility. It is shown that the method works well on numerical data, and to a limited extent on experimental data. Further studies are underway to improve the experimental application of the method, and to derive criteria for determining the best set of test input locations [19].

ACKNOWLEDGMENTS

This paper reports work supported by Sandia National Laboratories under Contract No. AJ-4223 with Dr. George H. James III and Dr. John R. Red-Horse as technical monitors. The authors would like to thank Prof. K.C. Park and Prof. Carlos Felippa for their encouragement and valuable technical insights. Also, the authors wish to recognize University of Colorado undergraduate students Ms. Nikki Robinson and Ms. Trudy Schwartz for their invaluable contributions to the experimental portion of this research.

REFERENCES

[1] Peterson, L.D., Doebling, S.W., and Alvin, K.F., "Experimental Determination of Local Structural Stiffness by Disassembly of Measured

Stiffness Matrices," *Proc. of 36th AIAA/ASME Structures, Structural Dynamics and Materials Conference*, April 1995, AIAA Paper No. 95-1090.

[2] Admire, J.R., Tinker, M.L. and Ivey, E.W., "Residual Flexibility Test Method for Verification of Constrained Structural Models," *AIAA Journal*, Vol. 32, No. 1, January 1994, pp. 170-175.

[3] Ewins, D.J., *Modal Testing: Theory and Practice*, John Wiley and Sons, New York, 1984.

[4] Peterson, L.D. and Alvin, K.F., "A Time and Frequency Domain Procedure for Identification of Structural Dynamic Models," *Proc. of 35th AIAA/ASME Structures, Structural Dynamics, and Materials Conference,* 1994, AIAA Paper No. 94-1731. Submitted to *Journal of Sound and Vibration*.

[5] Smith, K.S. and Peng, C.-Y., "SIR-C Modal Survey: A Case Study in Free-Free Testing," *Proc. of 12th International Modal Analysis Conference*, January 1994, pp. 176-183.

[6] Craig, R.R., Jr., "A Review of Time-Domain and Frequency-Domain Component Mode Synthesis Methods," *Journal of Modal Analysis*, April 1987, pp. 59-72.

[7] MacNeal, R.H., "A Hybrid Method of Component Mode Synthesis," *Computers and Structures*, Vol. 1, pp. 581-601, 1971.

[8] Rubin, S., "Improved Component-Mode Representation for Structural Dynamic Analysis," *AIAA Journal*, Vol. 13, No. 8, August 1975, pp. 995-1006.

[9] Craig, R.R., Jr. and Chang, C.-J., "On the Use of Attachment Modes in Substructure Coupling for Dynamic Analysis," *Proc. of 18th AIAA/ASME Structures, Structural Dynamics, and Materials Conference*, 1977, AIAA Paper No. 77-405.

[10] Martinez, D.R., Carne, T.G., Gregory, D.L. and Miller, A.K., "Combined Experimental/Analytical Modeling using Component Mode Synthesis," *Proc. of 25th AIAA/ASME Structures, Structural Dynamics, and Materials Conference*, 1984, AIAA Paper No. 84-0941.

[11] Craig, R.R., Jr. and Bampton, M.C.C., "Coupling of Substructures for Dynamic Analyses," *AIAA Journal*, Vol. 6, No. 7, July 1968, pp. 1313-1319.

[12] Kammer, D.C. and Baker, M., "A Comparison of the Craig-Bampton and Residual Flexibility Methods for Component Substructure Representation," *Proc. of 26th AIAA/ASME Structures, Structural Dynamics, and Materials Conference*, 1985, AIAA Paper No. 85-0817.

[13] Hinkle, J.D. and Peterson, L.D., "Examining the Effects of Gravity Off-load on a Precision Deployable Structure," *Proc. of 36th AIAA/ASME Structures, Structural Dynamics and Materials Conference*, April 1995, AIAA Paper No. 95-1440.

[14] Aktan, A.E., Lee, K.L., Chuntavan, C. and Aksel, T., "Modal Testing for Structural Identification and Condition Assessment of Constructed Facilities," *Proc. of 12th International Modal Analysis Conference*, January 1994, pp. 462-468.

[15] Alvin, K.F., Peterson, L.D., and Park, K.C., "Method for Determining Minimum-Order Mass and Stiffness Matrices from Modal Test Data," *AIAA Journal*, Vol. 33, No. 1, pp. 128-135, 1994.

[16] Guyan, R.J., "Reduction of Stiffness and Mass Matrices," *AIAA Journal*, Vol. 3, No. 2, p. 380, 1965.

[17] Blevins, R.D., *Formulas for Natural Frequency and Mode Shape*, Krieger Publishing, Malabar, FL, 1993.

[18] Peterson, L.D., "Efficient Computation of the Eigensystem Realization Algorithm," *Proc. of the 10th International Modal Analysis Conference*, Feb. 1992, to appear in *Journal of Guidance, Control and Dynamics*.

[19] Doebling, S.W., *Measurement of Structural Flexibility Matrices for Experiments with Incomplete Reciprocity*, Ph. D. Dissertation, University of Colorado, Boulder, CO, April 1995.

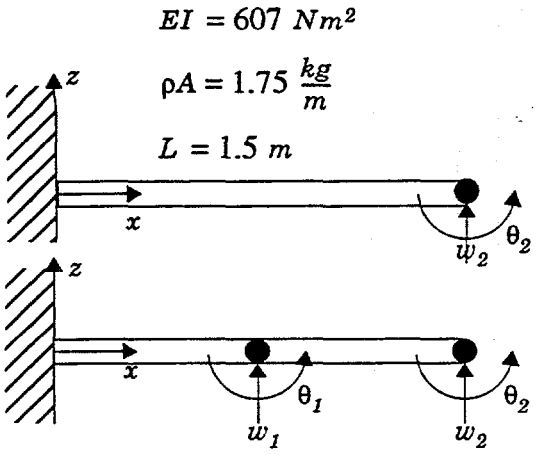

Figure 1. : 2-DOF and 4-DOF Models of Cantilevered Beam

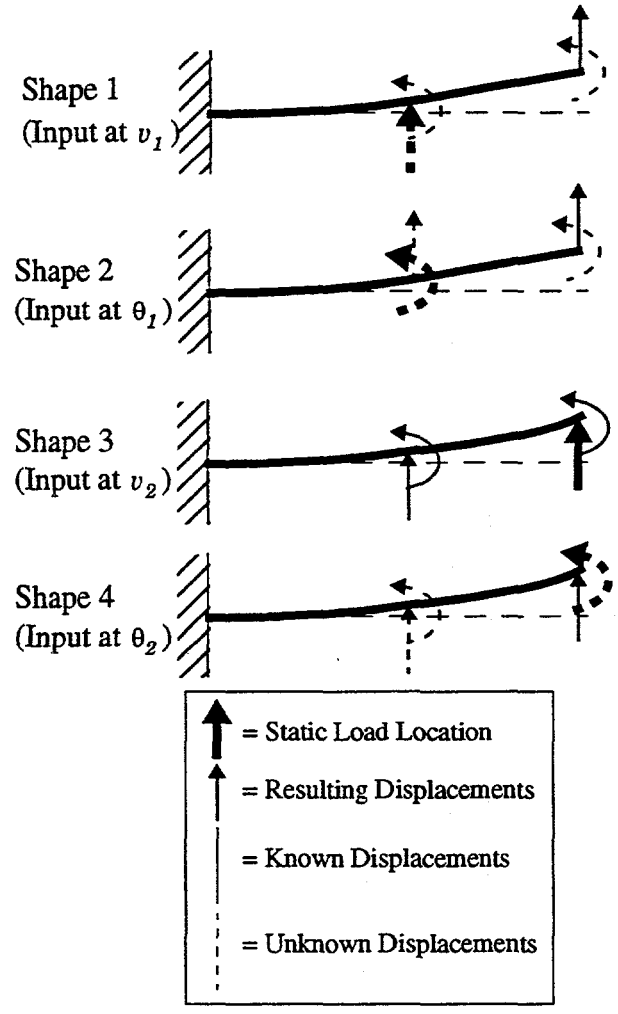

Figure 2. The Flexibility Shapes of a 2D Beam with 4 DOF - Load Applied Vertically at Tip

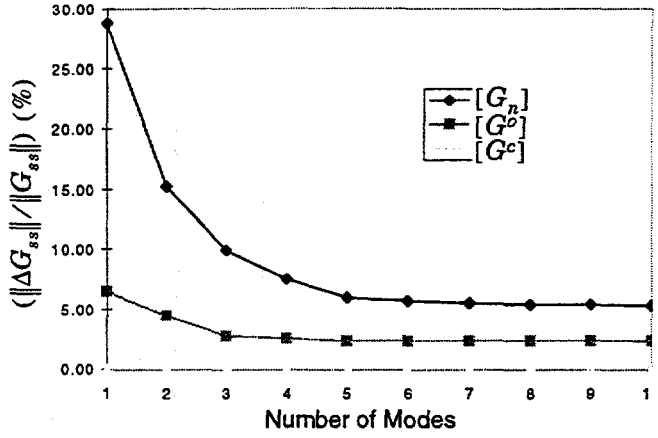

Figure 3. Convergence of Error in $\|G_{ss}\|$ for 4DOF Cantilevered Beam Model

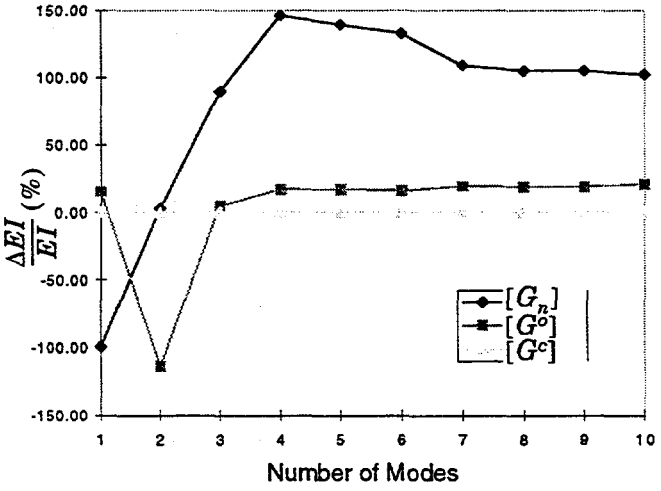

Figure 4. Convergence of Error in EI for Element 1 of 4DOF Cantilevered Beam Model

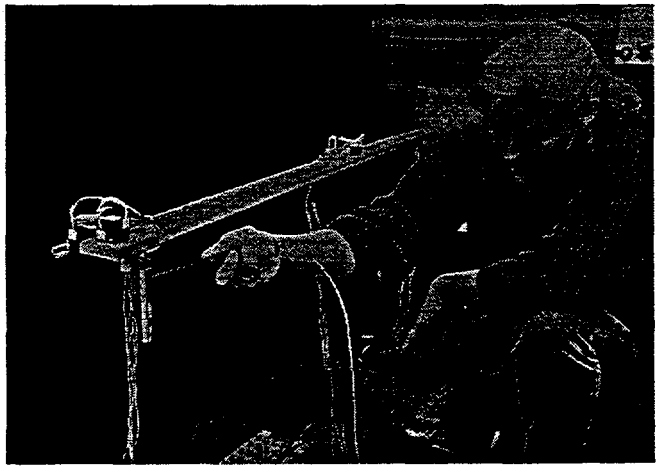

Figure 5. Test Configuration for Cantilevered Beam

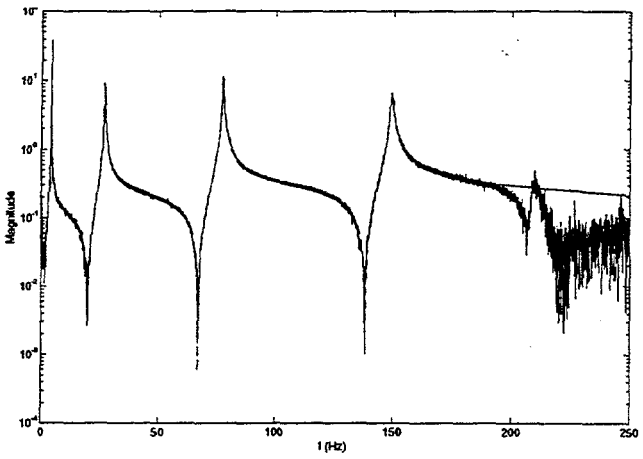

Figure 6. Driving Point Frequency Response Function Magnitude for Cantilevered Beam

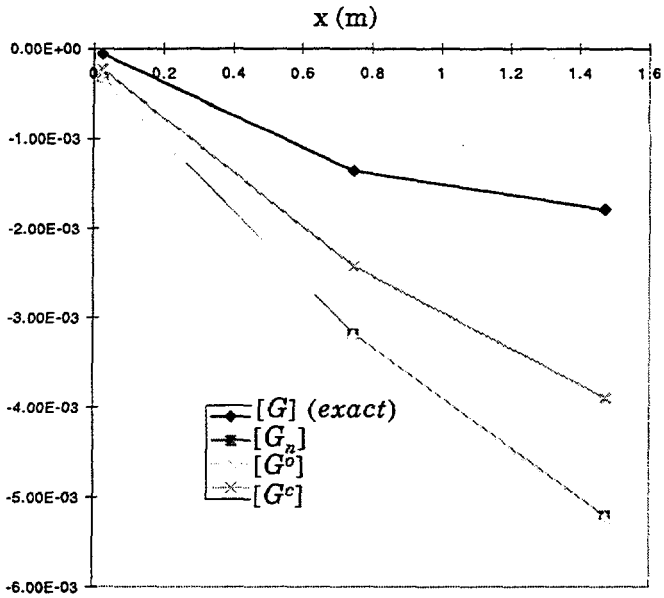

Figure 8. Rotation Flexibility Shape for Vertical Tip Input for Cantilevered Beam (4 modes)

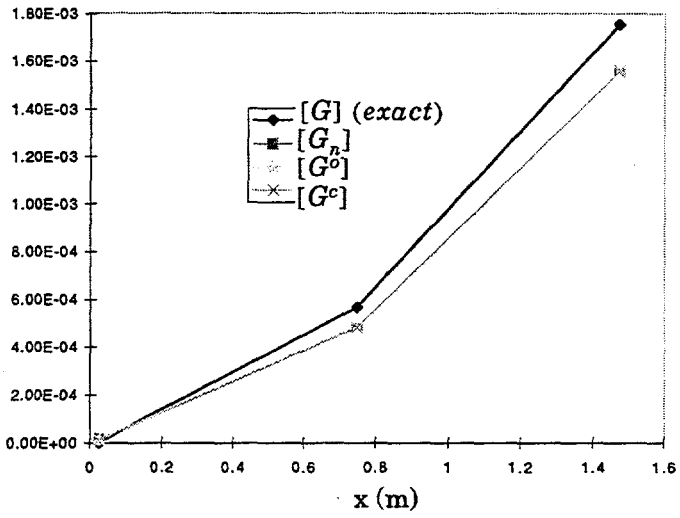

Figure 7. Displacement Flexibility Shape for Vertical Tip Input for Cantilevered Beam (4 modes)

Intentionally Left Blank

APPENDIX I

EXPERIMENTAL DETERMINATION OF LOCAL STRUCTURAL STIFFNESS BY DISASSEMBLY OF MEASURED STIFFNESS MATRICES

Lee Peterson, Ken Alvin, and Scott Doebling

Proceedings of the 1995 AIAA Adaptive Structures Forum
In Conjunction with the 1995 Structures, Structural Dynamics, and Materials Conference
New Orleans, LA

April 10-13, 1995

Intentionally Left Blank

EXPERIMENTAL DETERMINATION OF LOCAL STRUCTURAL STIFFNESS BY DISASSEMBLY OF MEASURED FLEXIBILITY MATRICES

Lee D. Peterson,[1] Scott W. Doebling[2]
University of Colorado
Center for Aerospace Structures and
Department of Aerospace Engineering Sciences
Boulder, Colorado 80309-0429
Kenneth F. Alvin[3]
Structural Dynamics Department
Sandia National Laboratories
Albuquerque, NM 87185-0439

ABSTRACT

A new method is presented for identifying the local stiffness of a structure from vibration test data. The method is based on a projection of the experimentally measured flexibility matrix onto the strain energy distribution in local elements or regional superelements. Using both a presumed connectivity and a presumed strain energy distribution pattern, the method forms a well-determined linear least squares problem for local stiffness eigenvalues. These eigenvalues are directly proportional to the stiffnesses of individual elements or superelements, including the bending stiffnesses of beams, plates, and shells, for example. An important part of the methodology is the formulation of nodal degrees of freedom as functions of the measured sensor degrees of freedom to account for the location offsets which are present in physical sensor measurements. Numerical results are presented which show the application of the approach to example problems.

INTRODUCTION

An important facet of state-of-the-art structural technology is the ability to determine and monitor the mechanical condition of an aerospace structure during both manufacture and operation. Such a capability would lower fabrication costs and ensure that both performance and safety are maintained during the structural lifetime. Such technology enables the measurement and identification of the localized stiffness of manufactured components, as well as the detection of errors, flaws, and damage due to fabrication. This technology also enables the development of high fidelity finite element models early in the design cycle by allowing validation of local structural stiffness values at the junctions and interfaces within prototype structural hardware.

The diagnosis of the mechanical condition of a structure is primarily a problem of determining the mass and stiffness distribution within the structure, using a few discrete measurements of the vibration response. This issue remains largely unsolved primarily because it is an inverse modeling problem. Ordinarily, structural analysis begins with the mechanical properties, from which the dynamic response is simulated. In the current problem, however, the known quantity is the dynamic response, from which the mechanical properties must be extracted.

A significant amount of research in this area has focused on the use of a detailed dynamic finite element model to determine the local mechanical properties. In these methods, the error between modal test data and predicted finite element modal behavior is minimized by adjusting the parameters which determine the finite element model stiffness and mass distribution. While these methods are generally successful at updating the dynamic model, they ordinarily involve the minimization of a nonlinear error norm, and, consequently, are not suitable for on-line, real-time data analysis.

A set of algorithms more suitable for on-line monitoring can be found in References [1], [2], [3]. In these methods, the deviation of the stiffness and mass from a preexisting finite element model is indicated by residual modal force errors at nodes in the model. These methods indicate the degrees of freedom (DOF) associated with error or damage, and, using appropriate elemental projections, can determine the magnitude of stiffness errors within the structure. They still, however, rely exclusively on a subset of measured modal parameters. This shortcoming has discouraged the widespread use of these other-

1. Assistant Professor, Senior Member AIAA, Associate Member ASME
ldpeter@Colorado.EDU
(303) 492-1743
2. Graduate Research Assistant, Student Member AIAA
3. Structural Dynamics Research Fellow, Member AIAA

wise attractive methods. Because the modes themselves may change significantly when the stiffness changes, the comparison will be biased by the selection of modes to include in the comparison set. There is little physical intuition available for the selection of these modes. Also, these methods find the magnitude of *nodally concentrated* errors and stiffness changes, so it is difficult to use them to localize the elemental stiffness errors and changes when the structure has load-path redundancy.

Recently, the authors have developed a wholly different approach that measures structural stiffness from test data without the use of an intervening finite element model [4],[5]. The basis of this approach is the determination of a stiffness matrix for the structure in which the model DOF are the DOF of the response sensor set. As shown in [5], the measured flexibility matrix is formed from the measured modal vectors, modal eigenvalues, and residual flexibilities as:

$$[G] = [\Phi_n] [\Lambda_n]^{-1} [\Phi_n]^T + [G_r] \quad (1)$$

The resulting flexibility matrix is the inverse (or pseudo inverse) of the structural stiffness matrix statically reduced to the sensor DOF:

$$[K] = [G]^+ \quad (2)$$

Efficient, reliable methods for measuring perhaps 60 to 100 modes of a structure has made it possible to determine structural stiffness matrices using Equation (1) and Equation (2) reliably, although the success is largely dependent on the quality of the experimental configuration and the system identification algorithm used in the data analysis [6]. Reference [5] presents methods for estimating the stiffness matrix using a reduced set of modes augmented by the residual flexibility, a procedure which improves convergence even for measurement sets with incomplete reciprocity, i.e. when the excitations and responses are not fully collocated. It is those results that provide a basis for accurate measurement of flexibility matrices.

The ability to measure $[G]$ from vibration data motivates the possibility of extracting information about the local stiffness properties of the structure. However, the elements of $[G]$ or $[K]$ themselves do not directly indicate the local stiffness. They indicate the stiffness associated with individual DOF, not individual elements. Reference [7] attempted to use a static condensation of the global stiffness matrix onto the DOF bounding a particular element. While this works perfectly in statically determinate structures, in a redundant structure multiple load paths prevent the element stiffnesses from being determined uniquely. A more complete theory, using all the load paths of the structure, is required to obtain local stiffness measurements from the flexibility matrix.

It is important to note that the flexibility matrix $[G]$ is directly computed from the identified model, and then inverted to get $[K]$. This is an important consideration because the error in $[G]$ tends to be concentrated in specific partitions, particularly those associated with non-excited DOF. The isolation of the error allows the results to be interpreted appropriately. The inversion process tends to spread the error throughout all the stiffness matrix entries, so that it is difficult to isolate the specific elements which have a high error content.

This paper presents such a generalized method, based on the decomposition of the measured flexibility matrix into the stiffness of an assumed set of superelements within the structure. The presumption is that the load paths of the structure are known within superelements whose boundaries are defined by the measurement sensors. Using the presumed connectivity and strain energy distribution pattern, a solution of the "flexibility matrix disassembly problem" is presented for which it is possible to always find a unique solution for the stiffness parameters of the superelements.

The key to this procedure is the fact that any structural superelement can be presumed to be a combination of elemental stiffness eigenvectors (not to be confused with the structural $[M]$ and $[K]$ eigenvectors). A well-determined linear problem is then defined, which can be solved for the stiffness parameters (eigenvalues) of the presumed superelements. One choice of superelements are the finite element stiffness matrices. For example, for 2DOF bar elements, the stiffness parameters are the longitudinal spring stiffness; for beams they are the extensional stiffness, the torsional stiffness, and the two bending stiffnesses; and for plates they are the corresponding bending and extensional stiffnesses. More general elements, including those for orthotropic materials and shells, are also included within this framework. It should be noted that any superelement can be included provided there is an underlying set of shape functions or other parameters which define the elemental strain energy distribution.

The practical implementation of the flexibility disassembly method requires the consideration of how measurement degrees of freedom at the sensors correspond to the nodal degrees of freedom used in

the corresponding superelement discretization. This consideration compensates for the fact that the global DOF measurements are generally inferred from translational sensor measurements made at several locations which are physically offset from the node. Two cases are considered. In the first, the measurement sensors are presumed to fully determine or overdetermine the nodal degrees of freedom at a point by rigid body connections. This case results in a well-formulated linear algebra problem for the stiffness parameters. In the other case, the sensor DOF underdetermine the nodal DOF at a point, and several interpolation methods are described, including a Guyan reduction onto the measured DOF. This latter problem results in a (slightly) nonlinear problem for the stiffness parameters, the solution of which is not investigated in the current research.

The paper is organized as follows: The first section presents the theory whereby the flexibility matrix is disassembled into the stiffnesses of local superelements by projection onto the stiffness energy shape vectors. An equivalence of complementary and ordinary strain energy is used to formulate a square, invertible linear algebra problem for the local stiffness parameters. Next, a projection of the nodal DOF onto the measurement DOF is considered, both in the well-determined and the underdetermined cases. The paper concludes with numerical application of the technique to a cantilevered beam.

THEORETICAL BASIS OF DISASSEMBLY

This section presents the formulation of the quantities necessary for the disassembly of the measured stiffness and flexibility matrices. Begin by presuming that the global stiffness of the structure can be modeled using an assemblage of n_e finite elements or superelements, connecting n_q global DOF, $\{q^G\}$. Each of the n_e elements itself connects n_α elemental DOF, $\{q^E\}$, $\alpha = 1 \ldots n_e$. The corresponding $n_\alpha \times n_\alpha$ elemental stiffness matrix in this coordinate basis is $[K^E]_\alpha$. If the elemental DOF are related by a rectangular transformation to the global DOF according to:

$$\{q^E\}_\alpha = [T]_\alpha \{q^G\} \tag{3}$$

then the global stiffness matrix can be formed by assembling all the elemental matrices according to:

$$[K^G] = \sum_{\alpha=1}^{m} [T]_\alpha^T [K^E]_\alpha [T]_\alpha \tag{4}$$

The elemental-to-global DOF transformation matrices $[T]_\alpha$ include coordinate rotations from the elemental frames to the global frame, the table lookup for the correspondence between elemental and global DOF, and the effect of constraints such as pinned or fixed connections.

It is important to note that Equation (4) is not a minimum rank definition of the disassembly problem. This means that the unknowns in all the elemental matrices $[K^E]_\alpha$ are not independent. Besides being symmetric, each elemental stiffness matrix is always rank deficient. Because $[K^E]_\alpha$ is symmetric, it has $(n_\alpha(n_\alpha+1))/2$ unknown elements, but because of its rank, only a few of these are actually independent unknowns. Consider as an example a simple spring element connecting two nodes, each of which includes three *(x,y,z)* displacements as DOF. Because this elemental stiffness matrix is 6x6, it potentially has 21 unknown elements. However, the rank of the elemental stiffness matrix is only 1 because of the stiffness connectivity, and therefore the stiffness of the element is completely specified by the value of 1 unknown parameter, which, in this case, is the longitudinal stiffness of the spring.

In general, then, it is necessary to decompose the rank r_α elemental stiffness matrix $[K^E]_\alpha$ into its static eigenvalues and eigenvectors so that:

$$[K^E]_\alpha = [\kappa]_\alpha [p]_\alpha [\kappa]_\alpha^T \tag{5}$$

in which $[\kappa]_\alpha$ is the $n_\alpha \times r_\alpha$ matrix of static eigenvectors for the α-th element, and $[p]_\alpha$ is a diagonal matrix of the nonzero static eigenvalues $\{p\}_\alpha$ for the α-th element. Physically, the columns of $[\kappa]_\alpha$ are the distinct, statically-equilabrated deformational shapes of the element which have nonzero strain energy. They are normalized to have unit magnitude, so that:

$$[\kappa]_\alpha^T [\kappa]_\alpha = [I_{r_\alpha}] \tag{6}$$

This static decomposition can be substituted into Equation (4) to get:

$$[K^G] = \sum_{\alpha=1}^{m} [T]_\alpha^T [\kappa]_\alpha [p]_\alpha [\kappa]_\alpha^T [T]_\alpha \tag{7}$$

This expression can be further simplified to:

$$[K^G] = [A][P][A]^T \tag{8}$$

where the "connectivity matrix" $[A]$ is a sparse matrix defined by:

$$[A] = \left[([T]_1^T [\kappa]_1) \ ([T]_2^T [\kappa]_2) \ \ldots \ ([T]_{n_e}^T [\kappa]_m) \right] \tag{9}$$

and $[P]$ is a diagonal matrix of the elemental stiffness eigenvalues $\{P\}$ where:

$$\{P\} = \begin{bmatrix} \{p\}_1 \\ \{p\}_2 \\ \ldots \\ \{p\}_{n_e} \end{bmatrix} = \begin{bmatrix} P_1 \\ P_2 \\ \ldots \\ P_{n_p} \end{bmatrix} \qquad n_p = \sum_{\alpha=1}^{m} r_\alpha \tag{10}$$

The columns of $[A]$ mathematically embody the connectivity of the structure by defining how a particular superelement stiffness parameter P_i influences the stiffness at the structural DOF. It is important to note that Equation (8) does not imply that the $\{P\}$ are the eigenvalues of $[K^G]$. This is because, in general and in practice, the columns of $[A]$ do not form an orthogonal basis.

Elemental Stiffness Decomposition for Representative Elements

Most generally, the $[\kappa_\alpha]$ can be considered to be the eigenvectors of the static condensation of a superelement's stiffness matrix onto its boundary DOF. In this sense, they can be derived from a solution of a partial differential equation or a large order finite element model. The only constraint is that the resulting stiffness parameters $\{p_\alpha\}$ must have a physical interpretation in terms of the stiffness of the superelement. This is most directly done by using an ordinary finite element interpolation function for the element. However, it should be noted that any number of alternative shape functions can be used.

Consider as a first example a bar element with stiffness k connecting two nodes, as shown in Figure (1). For this element, the stiffness matrix is

$$[K^E] = \begin{bmatrix} k & -k \\ -k & k \end{bmatrix} \qquad \{q^E\} = \begin{Bmatrix} q_1 \\ q_2 \end{Bmatrix} \tag{11}$$

Performing a singular value decomposition on $[K^E]$ yields the corresponding stiffness eigenvectors and parameters are:

$$[\kappa] = \begin{bmatrix} \frac{1}{\sqrt{2}} \\ \frac{1}{\sqrt{2}} \end{bmatrix} \qquad \{p\} = 2k \tag{12}$$

As a second example, consider a beam element connecting two 6 DOF nodes, as shown in Figure (2). For this element, the elemental DOF are:

$$\{q^E\} = \left\lfloor u_1 v_1 w_1 \theta_{x_1} \theta_{y_1} \theta_{z_1} u_2 v_2 w_2 \theta_{x_2} \theta_{y_2} \theta_{z_2} \right\rfloor^T \tag{13}$$

and the corresponding stiffness eigenvectors and parameters are listed in Appendix A.

It should be noted that the unusual mixed units of length and radians in the beam element eigenvectors is a consequence of the orthonormality of $[\kappa]$, and it does not affect the units of the resulting stiffness matrix. Notice also that for each beam bending stiffness, there are two corresponding parameters. In any calculation for the parameters, each pair of bending eigenvalues are constrained through their linear dependence on the corresponding EI.

DISASSEMBLY IN GLOBAL COORDINATES

In this section, the implementation of the disassembly procedure is outlined. First the disassembly of the global stiffness matrix is presented, and then the disassembly of the flexibility matrix.

Disassembly of the Global Stiffness Matrix

Now consider the situation where the global stiffness matrix $[K^G]$ and a connectivity matrix $[A]$ are known, and the stiffness parameters $\{P\}$ are to be determined. The corresponding problem statement contained in Equation (8) includes as unknowns the n_p elements of $\{P\}$. The number of equations is equal to the number of unique elements in $[K^G]$. Because of symmetry, there are therefore $(n(n+1))/2$ equations and n_p unknowns. Except for the pathological case in which the assumed connectivity has precisely redundant load paths in its element definitions, there can never be more unknowns than equations. An example of such a case is a pair of springs in parallel between the same DOF. In this case, there is insufficient independent data

about the elements, so two columns of $[A]$ are identical. Even for a completely redundant structure the solution is overdetermined, because in a completely connected structure there is a virtual spring from each DOF to each other DOF and from each DOF to ground for a total of $(n(n+1))/2$ unknown elements of $\{P\}$. Thus, it will be true that for any structure with a non-pathological presumed connectivity that:

$$n_p \leq \frac{n(n+1)}{2} \tag{14}$$

Consequently, the above disassembly problem always has fewer unknowns than equations, and a unique least-squares solution always exists.

To mathematically compute the solution to this problem, however, it is necessary to recast the above matrix formulation in a form amenable to linear equation solvers by writing down each element in Equation (8). This is accomplished using a summation (tensor) notation, in which repeated indices indicate a sum over the values of that index. Define K^G_{ij} to be the tensor equivalent of $[K^G]$, define $A_{i\beta}$ to be the tensor equivalent of $[A]$, and define P_β to be the tensor equivalent of $\{P\}$. In this notation, $i, j \in \{1 \ldots n\}$ and $\beta \in \{1 \ldots n_p\}$. Then, Equation (8) can be written as:

$$\begin{aligned} K^G_{ij} &= A_{i\beta} P_\beta A_{j\beta} \\ &= (A_{i\beta} A_{j\beta}) P_\beta \end{aligned} \tag{15}$$

This tensor equation is equivalent to the following linear algebra problem:

$$[C]\{P\} = \{B\} \tag{16}$$

in which $\{B\}$ is formed from the $\frac{n(n+1)}{2}$ unique elements of K^G_{ij} by cycling i from 1 to n and j from i to n. The corresponding (i, j) row of $[C]$ is given by:

$$\lfloor C_{ij} \rfloor = \left[(A_{i1}A_{j1}) \;\; (A_{i2}A_{j2}) \;\; \ldots \;\; (A_{in_p}A_{jn_p}) \right] \tag{17}$$

Note that the matrix $[C]$ is a tall, rectangular matrix, so Equation (17) can be solved uniquely. As a practical matter, $[C]$ is a sparse matrix, and so Equation (17) is solved using sparse linear algebra subroutines (such as those available in MATLAB [8]) instead of forming its pseudo-inverse.

Disassembly of the Global Flexibility Matrix

In many cases the above formulation of the disassembly problem is impractical, since it requires the numerical inversion of $[G]$ to get $[K]$, as shown in Equation (2). For many data sets, this is problematic because there are usually fewer modes than DOF, so $[G]$ is singular. This is true even using the reciprocity completion algorithms presented in Ref. [5]. The following alternative algorithm avoids this problem, and has other advantages described below.

First note that for a given deformation of the structure with DOF values $\{q\}$, the total strain energy is:

$$U = \frac{1}{2}\{q\}^T [K]\{q\} \tag{18}$$

and the complementary strain energy for the corresponding nodal force vector $\{Q\}$ is

$$U_c = \frac{1}{2}\{Q\}^T [G]\{Q\} \tag{19}$$

For a linear structure, the nodal forces and displacements are related as

$$\{q\} = [G]\{Q\} \tag{20}$$

Due to energy conservation in a linear structure, $U = U_c$, so the following must always hold:

$$\{Q\}^T [G][K][G]\{Q\} = \{Q\}^T [G]\{Q\} \tag{21}$$

Denoting the columns of $[A]$ by $\{A_\beta\}$, Equation (8) can be written as

$$[K] = \sum_{\beta=1}^{n_p} p_\beta \{A_\beta\}\{A_\beta\}^T \tag{22}$$

This implies via Equation (22):

$$\begin{aligned} &\sum_{\beta=1}^{n_p} p_\beta (\{Q\}^T [G]\{A_\beta\}\{A_\beta\}^T [G]\{Q\}) \\ &\qquad = \{Q\}^T [G]\{Q\} \end{aligned} \tag{23}$$

Since this must apply for any force pattern $\{Q\}$, a well-posed problem can be formed for $[P]$ by choosing n_p different force vectors which span the possible complementary strain energy states of the structure. The columns of $[A]$ satisfy this requirement because they include as a coordinate basis the elemen-

tal eigenvectors $[\kappa]$. Applying this force vector to Equation (24) yields

$$\sum_{\beta=1}^{n_p} p_\beta (\{A_\alpha\}^T [G] \{A_\beta\} \{A_\beta\}^T [G] \{A_\alpha\}) = \{A_\alpha\}^T [G] \{A_\alpha\} \quad \alpha = 1 \ldots n_p \tag{24}$$

So, as with stiffness disassembly, the problem is of the form

$$[C] \{P\} = [B] \tag{25}$$

where now the (α, β) row and column element of $[C]$ is

$$C_{\alpha\beta} = \{A_\alpha\}^T [G] \{A_\beta\} \{A_\beta\}^T [G] \{A_\alpha\} \tag{26}$$

and the rows of $\{B\}$ are

$$B_\alpha = \{A_\alpha\}^T [G] \{A_\alpha\} \tag{27}$$

This formulation in terms of the flexibility matrix has several advantages over the stiffness disassembly formulation in Equation (17). First, it avoids the formation of $[K]$ by inverting the possibly reduced rank $[G]$. Second, the matrix $[C]$ can be shown to be positive definite. This means that the stiffness parameters $\{P\}$ are positive so long as the elements of $\{B\}$ are positive. Physically, each row of $\{B\}$ is the complementary strain energy associated with the applied force vector $\{A_\alpha\}$, which must be positive by definition. Finally, this set of equations is square and generally invertible, unless the connectivity matrix $[A]$ is improperly formed to allow internal rigid body modes in the structure.

Application to a Simple Spring System

To illustrate and clarify the above notation, first consider the simple 2 DOF spring system shown in Figure (3). The global DOF are defined to be

$$\{q^G\} = \begin{Bmatrix} q_1 \\ q_2 \end{Bmatrix} \tag{28}$$

For each of the three elements, the corresponding stiffness eigenvalue is the value of spring stiffness. Therefore, for Element 1:

$$\{q^E\}_1 = q_1 \qquad [T]_1 = [1\ 0] \qquad [K^E]_1 = k_1 \qquad [\kappa]_1 = \frac{1}{\sqrt{2}} \qquad P_1 = 2k_1 \tag{29}$$

and for Element 2:

$$\{q^E\}_2 = \begin{Bmatrix} q_1 \\ q_2 \end{Bmatrix} \qquad [T]_2 = \begin{bmatrix} 1 & 0 \\ 0 & 1 \end{bmatrix} \qquad [K^E]_2 = \begin{bmatrix} k_2 & -k_2 \\ -k_2 & k_2 \end{bmatrix} \qquad [\kappa]_2 = \begin{Bmatrix} \frac{1}{\sqrt{2}} \\ -\frac{1}{\sqrt{2}} \end{Bmatrix} \qquad P_2 = 2k_2 \tag{30}$$

and for Element 3:

$$\{q^E\}_3 = -q_2 \qquad [T]_3 = [0\ -1] \qquad [K^E]_3 = k_3 \qquad [\kappa]_3 = \frac{1}{\sqrt{2}} \qquad P_3 = 2k_3 \tag{31}$$

So the resulting connectivity matrix is:

$$[A] = \frac{1}{\sqrt{2}} \begin{bmatrix} 1 & 1 & 0 \\ 0 & -1 & -1 \end{bmatrix} \tag{32}$$

and the global stiffness matrix is given by:

$$[K^G] = \frac{1}{\sqrt{2}} \begin{bmatrix} 1 & 1 & 0 \\ 0 & -1 & -1 \end{bmatrix} \begin{bmatrix} 2k_1 & 0 & 0 \\ 0 & 2k_2 & 0 \\ 0 & 0 & 2k_3 \end{bmatrix} \frac{1}{\sqrt{2}} \begin{bmatrix} 1 & 0 \\ 1 & -1 \\ 0 & -1 \end{bmatrix}$$

$$= \frac{1}{2} \begin{bmatrix} 1 & 1 & 0 \\ 0 & -1 & -1 \end{bmatrix} \begin{bmatrix} 2k_1 & 0 \\ 2k_2 & -2k_2 \\ 0 & -2k_3 \end{bmatrix} \tag{33}$$

$$= \begin{bmatrix} k_1 + k_2 & -k_2 \\ -k_2 & k_2 + k_3 \end{bmatrix}$$

This means that the unknown springs can be solved from the elements of $[K^G]$ using Equation (17) as follows:

$$\begin{Bmatrix} K_{11}^G \\ K_{12}^G \\ K_{22}^G \end{Bmatrix} = \begin{bmatrix} 1 & 1 & 0 \\ 0 & -1 & 0 \\ 0 & 1 & 1 \end{bmatrix} \begin{Bmatrix} k_1 \\ k_2 \\ k_3 \end{Bmatrix} \tag{34}$$

Note that the resulting $[C]$ matrix is full rank and invertible; therefore, this problem can be solved exactly.

DISASSEMBLY IN SENSOR COORDINATES

Although the above formulation is sufficient to solve the disassembly problem when the connectivity is exact, it is insufficient for most practical problems. The reason for this is that the measurements used to form the stiffness matrix are not typically located conveniently with respect to the nodes of the discrete model. A common case in which this occurs is shown in Figure (4). Although a beam element has 6 DOF at each node, these are never directly measured, so it is necessary to consider the effect of correlating measurement and model DOF in the formulation of the flexibility disassembly.

As a consequence, it is necessary to modify the above theory to make a distinction between the measured and nodal models. The underlying global elemental model's stiffness matrix will continue to be referred to as $[K^G]$, and a measured set of DOF $\{q^M\}$ is introduced which can be related to the global DOF by:

$$\{q^G\} = [L]\{q^M\} \tag{35}$$

In Eq. (36), $[L]$ is an $n \times n_M$ transformation matrix with $n_M \geq n$. The selection of $[L]$ is critical and problem dependent, and is discussed in the sections below. Also required is an inverse transformation that relates the global DOF to the measured DOF:

$$\{q^M\} = [H]\{q^G\} \tag{36}$$

in which $[L]$ can be computed from $[H]$ using:

$$[L] = [H]^+ \tag{37}$$

which is a unique pseudo-inverse since $n_M \geq n$.

Using Equation (36), the measured stiffness matrix can be related to the global stiffness matrix by:

$$[K^M] = [L]^T [K^G][L] \tag{38}$$

This means that the disassembly problem of Equation (8) becomes:

$$[K^M] = [L]^T [A][P][A]^T [L] \tag{39}$$

Note that the product $[L]^T[A]$ has the role of a modified connectivity matrix which generally is fully populated, depending on the transformation $[L]$. A similar transformation exists for flexibility disassembly.

Disassembly Using Fewer Measurements than DOF

One method to solve for the global displacements and rotations given an underdetermined sensor configuration is by the using of statically condensed mode shapes. The static condensation approach is motivated by the fact that it results in a matrix reduction which exactly solves the static load problem for forces applied at the measurement DOF. The global DOF are divided into a set of measurement DOF $\{q^m\}$ and a set of unmeasured ("omitted") DOF $\{q^o\}$, so that the global stiffness matrix can be partitioned as:

$$[K^G] = \begin{bmatrix} K_{mm}^G & K_{mo}^G \\ K_{om}^G & K_{oo}^G \end{bmatrix} \tag{40}$$

A static reduction of this matrix implies that

$$\{q^o\} = -[K_{oo}^G]^{-1}[K_{om}^G]\{q^m\} \tag{41}$$

Under the assumption of Equation (42), the transformation $[L]$ can be written as

$$[L] = \begin{bmatrix} I \\ -[K_{oo}^G]^{-1}[K_{om}^G] \end{bmatrix} \tag{42}$$

Although this formulation is theoretically attractive, it is limited by the fact that the global stiffness matrix $[K^G]$ is unknown until the disassembly problem is solved. For this reason, the resulting disassembly equation is a nonlinear least-squares problem.

An alternative to static condensation onto the measured DOF is to develop global interpolation functions for the entries of $[L]$. If 3 dimensional interpolation functions are used which are C^1 continuous, then the measurement set can be expanded to include all 6 displacement and rotation DOF at each measurement node. The result is equivalent to expanding the modal vectors before performing the stiffness matrix synthesis.

NUMERICAL EXAMPLES

In this section, the disassembly of measured flexibility is demonstrated for a 2-element, 4DOF cantilevered beam. All intermediate quantities are shown and some pertinent issues are discussed. To illustrate disassembly in this case, consider the measurement of the bending stiffness of the beam shown in Figure (5). The global and measured DOF are related by:

$$\begin{Bmatrix} v_1^G \\ \theta_{z1}^G \\ v_2^G \\ \theta_{z2}^G \end{Bmatrix} = \begin{bmatrix} 0 & 1 & 0 & 0 \\ -\frac{1}{d} & 0 & 0 & 0 \\ 0 & 0 & 0 & 1 \\ 0 & 0 & -\frac{1}{d} & 0 \end{bmatrix} \begin{Bmatrix} u_1^M \\ v_1^M \\ u_2^M \\ v_2^M \end{Bmatrix} \tag{43}$$

This implies that the $[L]$ and $[H]$ matrices are:

$$[L] = \begin{bmatrix} 0 & 1 & 0 & 0 \\ -\frac{1}{d} & 0 & 0 & 0 \\ 0 & 0 & 0 & 1 \\ 0 & 0 & -\frac{1}{d} & 0 \end{bmatrix} \qquad [H] = \begin{bmatrix} 0 & -d & 0 & 0 \\ 1 & 0 & 0 & 0 \\ 0 & 0 & 0 & -d \\ 0 & 0 & 1 & 0 \end{bmatrix} \tag{44}$$

Using the element $[\kappa]$ and $\{p\}$ for a beam from Equation (14), and removing the parameters and corresponding columns of $\{\kappa\}$ that do not include EI_{zz} (since that is the only parameter of interest) yields

$$[\kappa] = \begin{bmatrix} 0 & \frac{\sqrt{2}}{\sqrt{L^2+4}} \\ -\frac{1}{\sqrt{2}} & \frac{L}{\sqrt{2}\sqrt{L^2+4}} \\ 0 & \frac{-\sqrt{2}}{\sqrt{L^2+4}} \\ \frac{1}{\sqrt{2}} & \frac{L}{\sqrt{2}\sqrt{L^2+4}} \end{bmatrix} \{p\} = \begin{Bmatrix} \frac{2EI_{zz}}{L} \\ \frac{6EI_{zz}(L^2+4)}{L} \end{Bmatrix} \tag{45}$$

Suppose that the geometric and material properties are

$$\begin{aligned} EI &= 607 Nm^2 \\ \rho A &= 1.75 kg/m \\ L &= 0.75m \\ d &= 0.02m \end{aligned} \tag{46}$$

Then the expressions of Equation (46) can be evaluated to get

$$[\kappa] = \begin{bmatrix} 0 & 0.6621 \\ -0.7071 & 0.2483 \\ 0 & -0.6621 \\ 0.7071 & 0.2483 \end{bmatrix} \{p\} = \begin{Bmatrix} 1.62\times10^3 \\ 3.94\times10^4 \end{Bmatrix} \tag{47}$$

The transformation of T for each element is then

$$[T_1] = \begin{bmatrix} 0 & 0 & 1 & 0 \\ 0 & 0 & 0 & 1 \\ 0 & 0 & 0 & 0 \\ 0 & 0 & 0 & 0 \end{bmatrix} \qquad [T_2] = \begin{bmatrix} 1 & 0 & 0 & 0 \\ 0 & 1 & 0 & 0 \\ 0 & 0 & 1 & 0 \\ 0 & 0 & 0 & 1 \end{bmatrix} \tag{48}$$

so $[A]$ is formed using Equation (9) to get

$$[A] = \begin{bmatrix} 0 & 0.6621 & 0 & -0.6621 \\ -0.7071 & -0.2483 & 0.7071 & -0.2483 \\ 0 & 0 & 0 & 0.6621 \\ 0 & 0 & -0.7071 & -0.2483 \end{bmatrix} \tag{49}$$

and $\{P\}$ is formed using Equation (10) to get

$$\{P\} = \begin{Bmatrix} 1.62\times10^3 \\ 3.94\times10^4 \\ 1.62\times10^3 \\ 3.94\times10^4 \end{Bmatrix} \tag{50}$$

Now the measured flexibility matrix will be simulated and disassembled to show that the extracted parameters are the same as in Equation (51). Using the continuous solution for a Bernoulli-Euler beam [9], the first modal eigenvalue and mode shape at the measurement DOF are

$$[\Phi^M] = \begin{bmatrix} -1.92\times10^{-2} \\ 4.19\times10^{-1} \\ -2.27\times10^{-2} \\ 1.23 \end{bmatrix} \qquad [\Lambda] = 847.8 \qquad (51)$$

The mode shape is converted to the global coordinate system using Equation (36) to get

$$[\Phi^G] = \begin{bmatrix} 4.19\times10^{-1} \\ 9.58\times10^{-1} \\ 1.23 \\ 1.13 \end{bmatrix} \qquad (52)$$

So the modal flexibility is

$$[G_n] = [\Phi^G]\,[\Lambda]^{-1}\,[\Phi^G]^T = \qquad (53)$$

$$\begin{bmatrix} 2.07\times10^{-4} & 4.74\times10^{-4} & 6.11\times10^{-4} & 5.60\times10^{-4} \\ 4.74\times10^{-4} & 1.08\times10^{-3} & 1.39\times10^{-3} & 1.28\times10^{-3} \\ 6.11\times10^{-4} & 1.39\times10^{-3} & 1.80\times10^{-3} & 1.65\times10^{-3} \\ 5.60\times10^{-4} & 1.28\times10^{-3} & 1.65\times10^{-3} & 1.51\times10^{-3} \end{bmatrix}$$

The residual flexibility matrix (which can be simulated by summing a large number of continuous modes or subtracting the modal flexibility from the analytical stiffness matrix) is then

$$[G_r] = \qquad (54)$$

$$\begin{bmatrix} 2.43\times10^{-5} & -1.02\times10^{-5} & -3.15\times10^{-5} & -9.71\times10^{-5} \\ -1.02\times10^{-5} & 1.54\times10^{-4} & -4.77\times10^{-6} & -4.44\times10^{-5} \\ -3.15\times10^{-5} & -4.77\times10^{-6} & 5.45\times10^{-5} & 2.03\times10^{-4} \\ -9.71\times10^{-5} & -4.44\times10^{-5} & 2.03\times10^{-4} & 9.56\times10^{-4} \end{bmatrix}$$

Summing the residual and modal flexibility yields the measured flexibility matrix:

$$[G] = [G_n] + [G_r] = \qquad (55)$$

$$\begin{bmatrix} 2.32\times10^{-4} & 4.63\times10^{-4} & 5.79\times10^{-4} & 4.63\times10^{-4} \\ 4.63\times10^{-4} & 1.24\times10^{-3} & 1.39\times10^{-3} & 1.24\times10^{-3} \\ 5.79\times10^{-4} & 1.39\times10^{-3} & 1.85\times10^{-3} & 1.85\times10^{-3} \\ 4.63\times10^{-4} & 1.24\times10^{-3} & 1.85\times10^{-3} & 2.47\times10^{-3} \end{bmatrix}$$

Substituting Equation (56) and Equation (50) into Equation (25) and solving for $\{P\}$ yields

$$\{P\} = \begin{Bmatrix} 1.62\times10^{3} \\ 3.94\times10^{4} \\ 1.62\times10^{3} \\ 3.94\times10^{4} \end{Bmatrix} \qquad (56)$$

Comparing Equation (57) and Equation (51) demonstrates that the proper parameters are recovered from the simulated flexibility matrix.

CONCLUSIONS

A new theoretical method has been developed which makes it possible to measure local structural stiffness by disassembly of a measured stiffness matrix. The method presumes a connectivity pattern for the structure and solves for the eigenvalues of the elemental stiffness matrices. It was shown that a unique solution of this problem exists for all structures, except when redundant elements are presumed in the connectivity pattern. The method has also been extended to solve the more practical problem of a mismatch between the measured DOF and the nodal DOF of the presumed connectivity pattern. Research is currently underway to apply the technique to experimental results.

ACKNOWLEDGMENTS

This paper reports work supported by Sandia National Laboratories under Contract No. AJ-4223 with Dr. George H. James III and Dr. John R. Red-Horse as technical monitors. The authors would like to

thank Prof. K.C. Park and Prof. Carlos Felippa for their encouragement and valuable technical insights. Also, the authors wish to recognize University of Colorado undergraduate students Ms. Nikki Robinson and Ms. Trudy Schwartz for their invaluable contributions to the experimental portion of this research.

REFERENCES

[1] Kaouk, M. and D.C. Zimmerman, "Structural Damage Assessment Using a Generalized Minimum Rank Perturbation Theory" *AIAA Journal*, Vol. 32, No. 4, April 1994, pp 836-842.

[2] Lim, T.W. and T.A. Kashangaki, "Structural Damage Detection of Space Truss Structures Using Best Achievable Eigenvectors" *AIAA Journal*, Vol. 32, No. 5, May 1994, pp 1049-1057.

[3] Sheinman, I. "Damage Detection in Framed Structures" *AIAA Journal*, Vol. 32, No. 5, May 1994, pp 1103-1105.

[4] Alvin, K.F., L.D. Peterson, and K.C. Park, "A Method for Determining Minimum-Order Mass and Stiffness Matrices from Modal Test Data," To appear in *AIAA Journal*

[5] Doebling, S.W., K.F. Alvin, L.D. Peterson, "Improved Convergence of Estimated Parameters for Experiments with Incomplete Reciprocity" Proceedings of the *36th AIAA Structures, Structural Dynamics and Materials Conference*, April 1995.

[6] Peterson, L.D., "Efficient Computation of the Eigensystem Realization Algorithm," *Proc. of the 10th International Modal Analysis Conference*, Feb. 1992, to appear in *Journal of Guidance, Control and Dynamics.*

[7] Peterson, L.D., K.F. Alvin, S.W. Doebling, K.C. Park, "Damage Detection Using Experimentally Measured Mass and Stiffness Matrices" AIAA-93-1482 *Proc. of the 34th AIAA Structures, Structural Dynamics, and Materials Conference*, April 1993.

[8] MATLAB, *User's Guide*, The Mathworks, Inc., September 1993.

[9] Blevins, R.D., *Formulas for Natural Frequency and Mode Shape*, Krieger Publishing, Malabar, FL, 1993.

[10] Peterson, L.D. and Alvin, K.F., "A Time and Frequency Domain Procedure for Identification of Structural Dynamic Models," *Proc. of 35th AIAA/ASME Structures, Structural Dynamics, and Materials Conference,* 1994, AIAA Paper No. 94-1731. Submitted to *Journal of Sound and Vibration.*

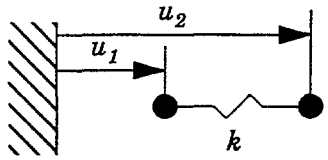

Figure 1. A 2DOF spring element

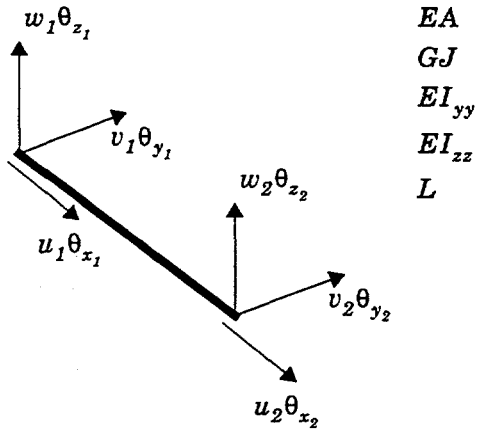

Figure 2. General 12 DOF Beam Element

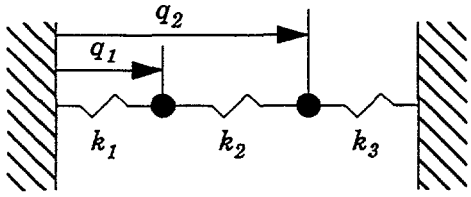

Figure 3. Simple 2DOF spring system used to illustrate the disassembly problem solution.

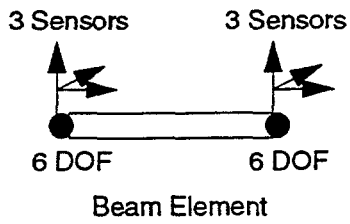

Figure 4. An illustration of measured DOF offset from elemental DOF locations.

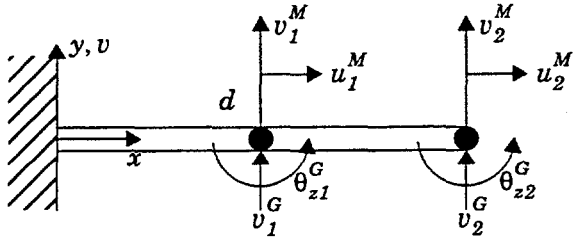

Figure 5. 2 D Cantilevered Beam to Illustrate the Effect of Sensor Offsets

APPENDIX A: ELEMENTAL EIGENSOLUTION FOR BEAM ELEMENT

The parameters $[\kappa]$ and $\{p\}$ for the 4-th order Bernoulli-Euler beam element are:

$$[\kappa] = \begin{bmatrix} \frac{1}{\sqrt{2}} & 0 & 0 & 0 & 0 & 0 \\ 0 & 0 & 0 & \frac{\sqrt{2}}{\sqrt{L^2+4}} & 0 & 0 \\ 0 & 0 & 0 & 0 & 0 & \frac{\sqrt{2}}{\sqrt{L^2+4}} \\ 0 & \frac{1}{\sqrt{2}} & 0 & 0 & 0 & 0 \\ 0 & 0 & 0 & 0 & \frac{1}{\sqrt{2}} & -\frac{L}{\sqrt{2}\sqrt{L^2+4}} \\ 0 & 0 & -\frac{1}{\sqrt{2}} & \frac{L}{\sqrt{2}\sqrt{L^2+4}} & 0 & 0 \\ -\frac{1}{\sqrt{2}} & 0 & 0 & 0 & 0 & 0 \\ 0 & 0 & 0 & -\frac{\sqrt{2}}{\sqrt{L^2+4}} & 0 & 0 \\ 0 & 0 & 0 & 0 & 0 & -\frac{\sqrt{2}}{\sqrt{L^2+4}} \\ 0 & -\frac{1}{\sqrt{2}} & 0 & 0 & 0 & 0 \\ 0 & 0 & 0 & 0 & -\frac{1}{\sqrt{2}} & -\frac{L}{\sqrt{2}\sqrt{L^2+4}} \\ 0 & 0 & \frac{1}{\sqrt{2}} & \frac{L}{\sqrt{2}\sqrt{L^2+4}} & 0 & 0 \end{bmatrix}$$

$$\{p\} = \begin{bmatrix} \frac{2EA}{L} \\ \frac{2GJ}{L} \\ \frac{2EI_{zz}}{L} \\ \frac{6EI_{zz}(L^2+4)}{L^3} \\ \frac{2EI_{yy}}{L} \\ \frac{6EI_{yy}(L^2+4)}{L^3} \end{bmatrix}$$

Intentionally Left Blank

APPENDIX J

HEALTH MONITORING OF OPERATIONAL STRUCTURES - INITIAL RESULTS

George James, Tom Carne, Bruce Hansche, Randy Mayes, Garth Reese, and Todd Simmermacher

Proceedings of the 1995 AIAA Adaptive Structures Forum
In Conjunction with the 1995 Structures, Structural Dynamics, and Materials Conference
New Orleans, LA

April 10-13, 1995

Intentionally Left Blank

HEALTH MONITORING OF OPERATIONAL STRUCTURES - INITIAL RESULTS

George James, Randy Mayes, Thomas Carne
Experimental Structural Dynamics Department
Sandia National Laboratories
Albuquerque, NM 87185-0557

Todd Simmermacher
University of Houston

James Goodding
CSA Engineering, Inc.

ABSTRACT

Two techniques for damage localization (Structural Translational and Rotational Error Checking - STRECH and MAtriX COmpletioN - MAXCON) are described and applied to operational structures. The structures include a Horizontal Axis Wind Turbine (HAWT) blade undergoing a fatigue test and a highway bridge undergoing an induced damage test. STRECH is seen to provide a global damage indicator to assess the global damage state of a structure. STRECH is also seen to provide damage localization for static flexibility shapes or the first mode of simple structures. MAXON is a robust damage localization tool using the higher order dynamics of a structure. Several options are available to allow the procedure to be tailored to a variety of structures.

INTRODUCTION

Today's society depends upon many structures (such as aircraft, bridges, wind turbines, offshore platforms, and buildings) which are nearing the end of their design lifetime. Since many of these structures cannot be economically replaced, techniques for damage detection and health monitoring must be developed and implemented. Modal and structural dynamics measurements hold promise for the global non-destructive inspection of a variety of structures since surface measurements of a vibrating structure can provide information about the health of the internal members without costly (or impossible) dismantling of the structure. Advanced signal processing, non-contacting and embedded sensors, and analysis/test correlation technologies combine to make this a promising approach for the health monitoring of operational structures.

An operational structure is defined to be one which can perform, is performing, or has performed its intended function as opposed to a laboratory test article or a computer model. Operational structures are often geometrically complex and may be too large to test in a laboratory. These structures are rarely truss-like and in fact tend to be more plate-like. Also, the boundary conditions associated with such structures are not known as well as a laboratory test structure or a computer model. And finally, the environment associated with an operational structure (e.g. weather, traffic patterns, or location) is usually changing and has a serious impact on the measured structural response. Therefore, it is desirable to perform health monitoring research and development on structures possessing such characteristics. This work discusses damage detection studies using three different operational structures.

Three bodies of research have been instrumental in the development of a health monitoring capability at Sandia National Laboratories. The work of Zimmerman, Simmermacher, and others at the University of Houston [1-7]; the research team at the University of Colorado at Boulder (Alvin, Doebling, Park, and Peterson) [8-13]; and Mayes, James, Hansche and others at Sandia National Laboratories

[14-18]. The work presented herein draws heavily off these works.

The paper begins by describing the approach used to locate damage. A technique (Structural Translation and Rotation Error CHecking algorithm or STRECH) used for damage localization and calculating a global damage indicator is described [18]. Another new technique (MAtriX COmpletioN or MAXCON) for damage localization which is an extension of Zimmerman's [7] and the UC-Boulder [12] work is then described. These techniques are applied to two data sets including a fatigue test of a wind turbine blade and a bridge undergoing an induced damage test [19].

STRECH

STRECH originated as a static concept to locate soft or stiff areas of a finite element model by comparing the lowest cantilevered mode shapes from a modal test with the Finite Element Model (FEM). A description of the algorithm utilizing static displacements from a two degree of freedom system has been provided in reference [18]. Although this concept is a static one, success has been realized by application to the first cantilevered mode shape when the mode shape looks a great deal like the static displacement shape [14] or to static flexibility shapes as estimated from dynamic mode shapes [18]. STRECH has been utilized for FEM error localization on a cantilevered robot arm, a cantilevered missile payload, and a cantilevered third stage of a missile with payload. In each case significant stiffness differences between a finite element model and a modal test mode shape were identified, enabling the analyst to identify critical parameters to update in the finite element model. STRECH has been extended to perform damage detection using experimental results before and after damage has occurred [18]. In this mode, STRECH has been applied to highway bridge [18], a simulated aircraft panel [20], and to a cantilevered wind turbine blade, as will be reported herein.

The user of STRECH defines a series of load paths which connect the sensor locations of the structure under test in a physically meaningful sense. This usually entails linking a sensor to its nearest neighbors. The STRECH Ratio (SR) between two sensors (denoted by subscripts i and j) is calculated as follows:

$$SR_{ij} = \frac{x_{ij}^{d}}{x_{ij}} \bullet \frac{\sum_{kl} x_{kl}}{\sum_{kl} x_{kl}^{d}}, \qquad (1)$$

where xij are measured relative displacements.

The superscript ^{d} indicates data from the potentially damaged state. Data with no superscript is the baseline data which is considered undamaged. The summations are for all displacement differences defined along the load paths by the engineer. This basically defines the displacement difference x_{ij} as a fraction of the sum of all displacement differences measured for the structure's specific state. This normalization has been applied to handle problems such as global scaling errors which often occur in acquiring and fitting experimental data.

Although the average SR is not always exactly equal to one, it is generally very near one. This makes the interpretation of the data much easier, as a value much greater than one will indicate an area of the structure that has been significantly reduced in stiffness (i.e. damaged). The highest SR should correspond to the part of the structure most likely to be damaged. In practice, x is usually a displacement difference between two points on the structure, each of which has three coordinates. The algorithm calculates the square root of the sum of the squares of the three coordinate displacement differences, so that all x quantities shown in equation 1 are positive values. In many applications, not all accelerations are measured, however the accelerations in unmeasured coordinate directions are considered zero.

From equation 1 it can be seen that if x_{ij} is very small, the SR can become very uncertain. Since all experimental data has noise associated with it, and data fitting algorithms are not perfect either, a false SR that is very large (because of a small denominator corrupted significantly by noise) may be calculated. A small value of x_{ij} in the denominator means that the structure is not being exercised between points i and j in the baseline structure. If this is the case, the true response should be insensitive to damage between those two points. Therefore, the engineer establishes a minimum denominator value for x_{ij} below which the SR is not calculated at all. In the algorithm, the minimum denominator value is set as a percentage of the largest displacement difference for the baseline structure.

Experience has shown that SRs based on differences in rotational coordinates can provide more information than those based on translational coordinates. Field measurements are most often measured accelerations in the translational directions. Estimates of the rotations can be obtained from displacement shape data by passing a parabola through three adjacent displacements on the structure. The slope of the parabola at the middle point can be utilized as the estimate for the rotation of that point.

In some applications, SR calculations are more successful in detecting the location of damage when applied to a static deflection shape. An estimate of the static flexibility (the static deflection shape due to a unit load) can be obtained from the modal parameters by use of the following well known formula for the frequency response function based on real modes:

$$\frac{x(\omega)}{f(\omega)} = \sum_{r=1}^{\infty} \frac{\Psi_i^r \Psi_k^r}{m_r(\omega_r^2 - \omega^2 + 2j\varsigma_r\omega\omega_r)} \qquad (2)$$

where $x(\omega)$ is displacement as a function of frequency, $f(\omega)$ is an applied point force as a function of frequency, Ψ_i^r is the mode shape at the response point for the rth mode, Ψ_k^r is the mode shape at the driving point for the rth mode, m_r is the modal mass, ζ_r is the damping ratio, ω is the frequency in radians/second, ω_r is the rth natural frequency and the summation is for all modes. An estimate of the static flexibility is achieved by evaluating equation 2 at zero frequency. In this case a truncation is made using only n modes:

$$\frac{x(0)}{f(0)} = \sum_{r=1}^{n} \frac{\Psi_i^r \Psi_k^r}{m_r \omega_r^2} \qquad (3)$$

It should be noted that the engineer is free to chose any measured output location as the input location for these calculations. The SR calculated with damage location as the input has the greatest sensitivity to damage. Unfortunately, this location will not be known a priori in real applications.

Displacement differences can be combined to calculate a global damage indicator for the onset of recognizable damage. A threshold value for that quantity needs to be established which is high enough to discount the effects of noise, but low enough to sense significant damage. A quantity which has been developed to perform this function:

$$\text{Damage Indicator (DI)} = \frac{\sum_{ij} \left| x_{ij} - x_{ij}^d \right|}{\sum_{ij} x_{ij}} \qquad (4)$$

where the terminology is the same as in equation (1). A procedure for establishing a noise floor for the damage indicator has been to extract the modal parameters two or more times using different extraction methods. The damage indicator variation calculated from these cases can provide an indication of the noise level to be expected.

The following sections details another damage detection approach which estimates mass and stiffness matrices directly from data and uses that representation to localize changes in the structure from subsequent tests.

MAXCON

Zimmerman's approach to damage detection involves using modal frequencies (ω_r^d) and mass-normalized mode shapes (Ψ_r^d) measured on the damaged structure as well as undamaged mass and stiffness matrices (M and K - typically from a FEM reduced to the test degrees of freedom or some intermediate value) [6,7]. An error vector B_r can be calculated for each mode and subsequently collected in matrix form:

$$B = -M\Psi^d \omega^{d2} + K\Psi^d = \left[B_1 \mid B_2 \mid \cdots \mid B_n \right] \qquad (5)$$

where all of the above quantities are matrix quantities containing information from all of the measured modes. The matrix ω^2 is a diagonal matrix with the squares of the modal frequencies from the damaged test on the diagonal. Note that B would be a matrix of zeros if the undamaged modal properties are used. In theory, the zero/non zero pattern of the dynamic residual, B, will provide the information as to the location of the damage when damaged modal properties are used. In actuality, noise and modeling issues will corrupt this zero/non zero pattern. Also, FEM reduction procedures will tend to mask the true location of the errors [6,7].

Also, areas of the structure which are very stiff will tend magnify noise measurements in the data and provide false indications of damage. Therefore, a scaling can be performed to reduce this effect:

$$\hat{B}_r = W_r B_r / \left\| \Psi_r^d \right\| \tag{6}$$

where

$$W_r = \mathrm{diag}\left(\frac{1}{\|z_1\|}, \frac{1}{\|z_2\|}, \ldots, \frac{1}{\|z_n\|} \right); \text{and}$$

$$Z_r = \begin{bmatrix} z_r^1 \\ \hline z_r^2 \\ \hline \vdots \\ \hline z_r^n \end{bmatrix} = -M\omega_r^{d^2} + K.$$

Analyzing the dynamic residual matrix, B, to determine the damage locations can be difficult. However, the most important information can be extracted by performing a Singular Value Decomposition (SVD) on the matrix and viewing the first left singular vector.

To avoid the problems associated with reducing a FEM to the test degree's of freedom, this work uses mass and stiffness matrices which are calculated from data as Alvin, Peterson, Park, and Doebling have done [11,12]. The inverses of these matrices can be thought of as sums of the measured parameters:

$$\begin{aligned} M^{-1} &= \Psi\Psi^T; \text{and} \\ K^{-1} &= \Psi\omega^{-2}\Psi^T. \end{aligned} \tag{7}$$

If the test data contains as many modes as sensor locations then these matrices could be inverted directly. However, the typical situation in testing is to acquire data from many more sensor locations than the number of extracted modes. Therefore the inverse matrices are rank deficient and not invertable. A pseudo-inverse can be used to calculate rank-deficient mass and stiffness matrices [12]. Another approach is to augment the measured mode shapes with the null space of the rank-deficient M^{-1} matrix similar to the approach used in reference [11]. The null space (U^N) of this matrix can be calculated using the SVD:

$$M^{-1} = \left[U^R \;\vdots\; U^N \right] \begin{bmatrix} \mathrm{diag}(S) & 0 \\ 0 & \mathrm{diag}(0) \end{bmatrix} \begin{bmatrix} U^{R^T} \\ \hline\hline U^{N^T} \end{bmatrix}. \tag{8}$$

The null space will be scaled by replacing diag(0) with a diagonal matrix of non-negative entries, denoted by $\mathrm{diag}(X^{-1})$, chosen to have the final mass matrix M meet some prearranged criteria. The final mass matrix will then have the following form:

$$M = \left[U^R \;\vdots\; U^N \right] \begin{bmatrix} \mathrm{diag}(S^{-1}) & 0 \\ 0 & \mathrm{diag}(X) \end{bmatrix} \begin{bmatrix} U^{R^T} \\ \hline\hline U^{N^T} \end{bmatrix}. \tag{9}$$

This then allows the matrix to be completed (hence the acronym MAXCON) in spite of the rank-deficiency. The criterion used in this work is to attempt to force certain elements of M to be zero to reflect an assumed model of the structure. This requires the user to select load paths similar to that done for the STRECH algorithm. The work reported herein assumes springs are connecting each sensor to its nearest neighbor as well as additional springs to ground. This allows the elements of X to be chosen in a least squares sense to drive the required elements of M toward zero. It should be noted that the problem must be constrained if any elements of X are less than zero. The problem as posed above will not produce any zeros in the mass matrix as there is noise in the measurements and the simple underlying model will not usually capture the dynamics of the full system. Also, no attempt has been made in this work to constrain the selection of the values in X to match any other known quantities such as total mass or total inertia of the system. Adding such constraints should be included in future research.

The stiffness matrix is then calculated from the mass matrix as follows:

$$\begin{aligned} K = {} & M\Psi\omega^2\Psi^T M + \\ & MU^N \mathrm{diag}\left(X^{1/2}\right) \mathrm{diag}(Y) \mathrm{diag}\left(X^{1/2}\right) U^{N^T} M; \end{aligned} \tag{10}$$

where diag(Y) is chosen to reduce the elements of K which are expected to be zero based on the load paths chosen by the engineer. This calculation is complicated by the fact that the elements in Y must be larger that all the elements in ω^2 to avoid the completion procedure placing unrealistic modes in the measured frequency band. Therefore additional inequality constraints are required. As with the mass matrix completion, no attempt has been made in this work to constrain the elements of Y to reproduce the

measured stiffness residual terms [21]. This physical constraint should also be added to the procedure.

Since a mass and stiffness representation of the structure can be provided for each damage case tested, equation (5) can be rewritten as follows:

$$B = -\Delta M \Psi^d \omega^{d2} + \Delta K \Psi^d = B_M \omega^{d2} + B_K \quad (11)$$

where ΔM and ΔK are perturbation matrices formed by differencing the respective matrices before and after damage.
Therefore, if the matrices capture enough of the major dynamics of the system, an indication of whether a mass or a stiffness change occurred may be possible.

Additionally, since a simple underlying model of the structure has been assumed, a "disassembly" may be performed to further understand the source of the changes in the system [22]. Therefore, the mass and stiffness matrices may be written in the following expanded form:

$$M = C^T M_e C = C_1^T M_{e1} C_1 + C_2^T M_{e1} C_2; \text{ and}$$
$$K = C^T K_e C = C_1^T K_{e1} C_1 + C_2^T K_{e1} C_2 \quad (12)$$

where C is a connectivity matrix of 1's and 0's, M_e and K_e are block diagonal matrices of the local mass and stiffness elements, M_{e1} and K_{e1} are matrices containing only the elements associated with the assumed simple model of the structure, M_{e2} and K_{e2} are matrices containing only the additional elements modeling the load paths that are not contained in the simple model, and C_1 and C_2 are the connectivity matrices for the corresponding submatrices.

With this separation, the B matrix can be written as the sum of a part that is due to changes in the simple model of desired load paths and a part due to changes in the extra load paths. This can be very useful, especially when the model errors are pronounced. It should be noted that no attempt has been made to assure that all of the resulting spring elements represented in M_e and K_e have a physically realizable spring constant, although the bulk of the elements are signed correctly. This is an additional constraint which could be applied to the problem.

The following section applies STRECH and MAXCON to a fatigue test of a Horizontal Axis Wind Turbine (HAWT) Blade.

HAWT BLADE FATIGUE TEST

A fatigue test to failure of a composite wind turbine blade was performed at the National Renewable Energy Laboratory. Periodic modal tests were performed during this test as well as acoustic emissions tests. This data will be utilized to further study the application of health monitoring techniques. When coupled with a non-contact transducer such as a scanning laser vibrometer, this technology could be applied in the field to periodically monitor a field of wind turbines and estimate remaining life in the blades.

Description of Test

The blade was constructed of fiberglass and included a tapered fiberglass airfoil on a tapered fiberglass spar. The blade was bonded to short steel rod used to cantilever the blade to a stifback. The final visible failure was a bond failure between the fiberglass blade and the steel connecting rod. A hydraulic actuator was used to fatigue the specimen at 1 Hz.

The fatigue test of the blade was periodically stopped to allow modal testing to be performed. The hydraulic actuator was removed and impact excitation with a three pound instrumented mallet was used for the modal tests. Accelerometers were placed at 30 locations on the 32 foot long blade and data was acquired to 64 Hz. Approximately eleven modal frequencies are consistently present in this band. National Renewable Energy Laboratory personnel performed the modal tests using Sandia Lab equipment and consulting. There were 51 days of testing and 32 modal tests spread over a four month period.

The test data included some unexpected phenomena. Following an initial drastic drop in all modal frequencies, most of the modal frequencies stayed constant until failure. At failure, most of the frequencies increased. The static stiffness also seemed to increase. One would expect the stiffness and therefore the frequencies to decrease with damage. An explanation for these phenomena has not been found at this writing. However, the test fixture was reoriented and hydraulic actuators changed at least three times during the test. Also during the four months of testing, a broad range of environmental changes were seen. These changes may have contributed to the unexplained phenomena seen in the data.

STRECH

The STRECH approach was applied to this data to determine the global extent of damage and to localize

the data. The data set included a series of thirteen accelerometer locations along the center line of the test item. All sensors measured motion in the most flexible direction. Additional sensors were placed at the root to monitor that most critical area. The chosen load path treated the blade as a simple cantilever beam. Therefore only sensors along the centerline were used and each was assumed connected to its nearest neighbor. Along the blade, rotations were estimated by the parabolic fit approach. At the root, sensors were provided above and below the shaft in the axial direction. This allowed rotations at the root to be estimated by differencing two sensors. The eleven modes were used to calculate the static flexibility shape, which was used in analyzing this data set.

Figure 1 provides the global damage indicator calculated using SRs estimated from translation sensors only. The reader should realize that only 13 tests (1, 3, 4, 5, 6, 10, 15, 20, 25, 29, 30, 31, and 32) have been analyzed to date. It can be seen that a sharp drop occurs between test 10 and test 15. Work is underway to attempt to correlate the large variations in this factor to changes in the test set-up.

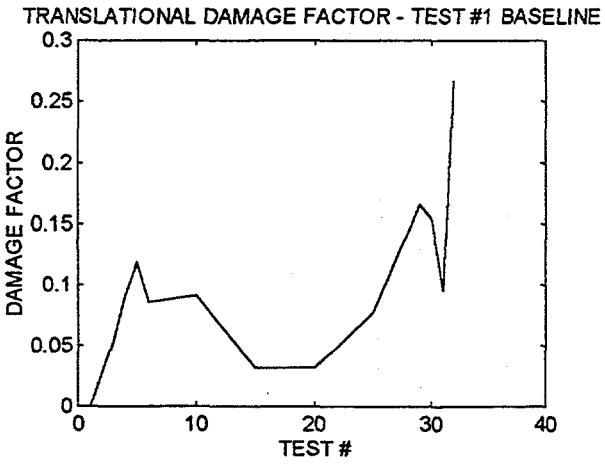

Figure 1. Damage Factor Using Actual Input Location

Figure 2 provides the same translational damage factor, however the static shape calculations use a sensor location near the root of the blade (and near the failure point) as the simulated input. The data is much more consistent, due to the lack of extreme local variations, than that shown in the previous plot. In fact, after test 15 the trend is as would be expected which is constantly increasing until final failure. However, the initial rise and steep drop after test 10 is still present in the data. The sharp rise between test 1 and test 3 is a result of the initial changes that caused the frequencies to drop. As with the previous data, further study is needed to attempt to explain the characteristics of the data in terms of identifiable changes in the test set-up. Also since the input location was moved to the known damage location, this analysis would require a certain amount of engineering insight to use in a field application.

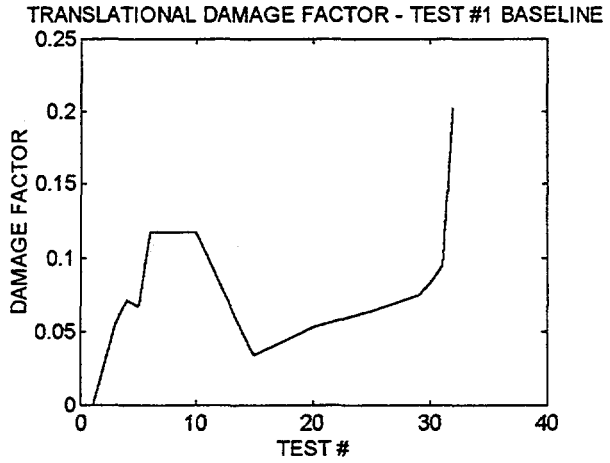

Figure 2. Damage Factor Using Simulated Root Input

MAXCON

The MAXCON analysis utilized the same beam-like load path as used in STRECH. Translations and rotations calculated as with STRECH were also used. Scaling (as described in equation (6)) was found to be unnecessary and in fact detrimental. The mass/stiffness separation as described in equation (11) was found to be necessary to achieve success. Disassembly, as described in equation (12), has not been attempted to date. All eleven modes were used in the analyses presented herein.

Figure 3 provides the absolute values of the first singular vector for both the mass and the stiffness parts of the dynamic residual using test 1 as the undamaged case and test 3 as the damaged case. Therefore, these plots reflect the changes which caused the initial drop in modal frequencies. It should be noted that there are thirteen sensor locations used in this analysis. Each location has a measured translational and a calculated rotational Degree Of Freedom (DOF). In Figure 3, the odd-numbered DOF's are translations. The rotational DOF's are even-numbered in Figure 3. The cantilever is at DOF's 25 and 26. The final visible damage is between DOF's 19 and 24 as shown in the stiffness

plot marked BK. Hence, this plot shows an initial stiffness change in the expected failure region and at the cantilever. The plots also show large mass changes at several locations closer to the free end of the beam. Since no significant mass changes are expected, they might be associated with errors in the model due to the matrix completion procedure. Constraining the mass matrix completion to maintain the known mass quantities might alleviate some of these discrepencies.

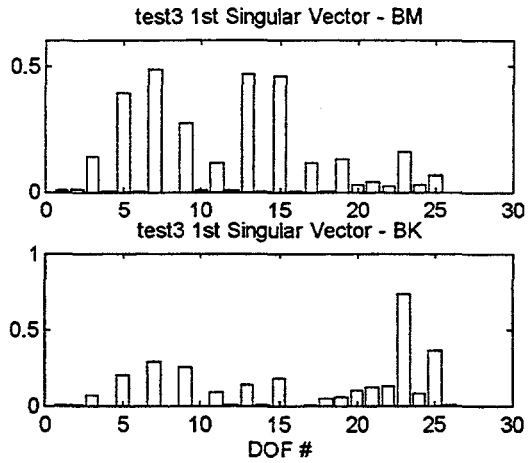

Figure 3. Test 1 To Test 3 Damage Localization

Figure 4 provides the same damage localization analysis as Figure 3. However, the undamaged or baseline test is Test 3 and the damaged or comparison test is Test 32. The stiffness changes are shown to be at DOF's 21 and 23. This is the final failure area. It should be noted that this is the region of highest stiffness in the structure and hence the most sensitivity to stiffness changes and/or noise. However, the mass changes also show large changes at the same locations.

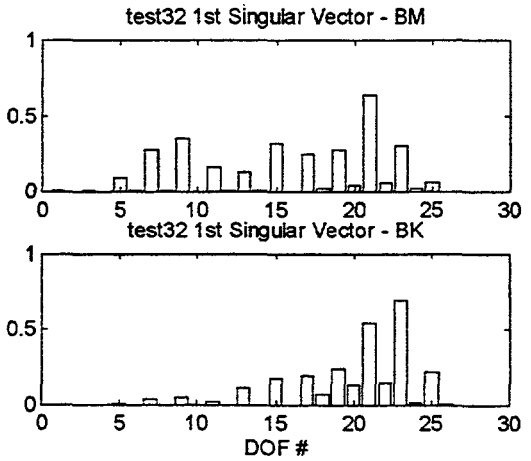

Figure 4. Test 3 To Test 32 Damage Localization

Complete analysis of this test series will require a more complete understanding of the test procedures and any test anomalies which may have occurred during the experiments. However, the results for damage detection from this structure are encouraging. The next section will apply STRECH and MAXCON to an induced damage test of a highway bridge.

I40 Bridge Test

The Interstate 40 bridge over the Rio Grande in Albuquerque, New Mexico was a fracture critical bridge which means it was constructed without structural redundancy. Figure 5 provides a schematic of this structure. The primary structural members were two 10' deep plate girders which ran the length of the bridge. If one of these members failed, the bridge could be expected to collapse. Since many similar bridges are still in operation, the Federal Highway Administration and the National Science Foundation provided funds to New Mexico State University (NMSU) to develop and test new nondestructive inspection techniques. NMSU was supported by both Los Alamos [19] and Sandia National Laboratories [15] as well as Texas A&M University [23]. All three support institutions have performed some form of damage detection on the data [18, 19, 23].

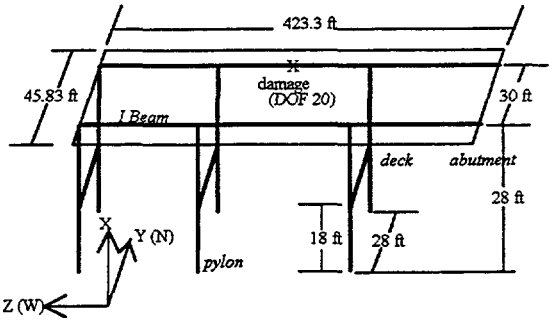

Figure 5. Rio Grande/I40 Bridge Schematic

Description of Test

The Rio Grande/I40 bridge tests were a set of induced damage tests performed on the decommissioned structure. Before demolition of the bridge, a series of progressively more serious cuts were made in one support beam of the bridge [19]. Los Alamos performed a series of modal tests on the bridge as well as extensive modeling. Modal tests were performed in the initial condition and after each cut. Los Alamos personnel also applied the Sandia-developed Natural Excitation Technique (NExT) [24] to the bridge data which allowed extraction of modal

parameters during traffic excitation. A new type of non-contact sensor based on microwave interferometry was also used on the bridge by Los Alamos personnel. Sandia designed and operated the exciter system for the dynamics tests. Sandia personnel also acted as consultants for the application of NExT and provided some logistics support during the modal tests.

A series of four cuts were made in the plate girder after the bridge was closed to all traffic. The fourth cut completely severed the lower half of the plate girder I section. Random excitation was provided from 2-12 Hz with a peak input of 2,000 lbs. Uniaxial sensors at 26 locations were used as the primary instrumentation set. All sensors and the force input were in the vertical direction. Six vertical modes were extracted. Power spectral density data from 10 additional sensor locations for the Texas A&M work were also acquired. Also, stepped sine testing was provided for the Los Alamos microwave sensors.

Table 1 lists the modal frequencies for the first six modes after each cut. Notice the slight increase in frequency after the first cut. This inconsistency is believed to be due to mass being removed from an adjacent bridge which shares the same pylon. However, analysis using MAXCON points to a major change at only one side of the bridge, and has tended to point to a stiffness change. In general the changes in frequency become obvious only after the fourth cut.

Table 1. Modal Frequencies vs. Damage Case

	DAMAGE CASE				
MODE (Hz)	**0**	**1**	**2**	**3**	**4**
1	2.48	2.51	2.52	2.46	2.29
2	2.96	2.99	2.99	2.94	2.84
3	3.54	3.57	3.52	3.48	3.49
4	4.09	4.12	4.10	4.04	3.99
5	4.16	4.21	4.19	4.14	4.15
6	4.64	4.67	4.66	4.58	4.52

STRECH

The most successful STRECH calculations used static flexibility and estimated rotations. The first extraction of undamaged modal parameters was used as the baseline for the STRECH calculations. The results for the global indicator are printed in Table 2. The first two rows are the damage indicators for the undamaged bridge where the same data was used, but different modal extraction techniques were utilized to form the static flexibility. Then the damage indicators are calculated for each cut. Although this is not a statistically conclusive study, it appears that the damage indicator begins to rise significantly enough at cut 2 to indicate the presence of damage.

Table 2 - Damage Indicators

Case	Damage Indicator
Undamaged - Extraction 2	**9%**
Undamaged - Extraction 3	**8%**
Cut 1	**14 %**
Cut 2	**28%**
Cut 3	**40 %**
Cut 4	**33%**

For the damage localization calculations, a minimum denominator value of only one percent (of the maximum rotation difference in the undamaged case) was used to filter the most noisy calculations. The location of damage was correctly identified for the two worst damage cases, cuts 3 and 4. For cut 1 the damaged location was the second choice of the algorithm. For cut 2 the damaged location was the fourth choice. The fidelity of the cut 1 data was higher than for cut 2. This would provide a better signal to noise ratio in the FRFs which could lead to a more accurate static flexibility shape for cut 1 than for cut 2. Even though the signal to noise ratio might not have been as good for cut 4, the damage was so significant that the noise did not matter so much. Note that the SR increases with increasing level of damage in the actual damaged element (number 107-108). Table 2 lists the results.

Table 2 - Predicted Damage Locations for Static Flexibility

Case/Element No.	STRECH Ratio	Comment
Cut 4/ Element 107-108	**13.2**	Correct 1st choice
Cut 3/ Element 107-108	**10.5**	Correct 1st choice
Cut 2/ Element 4-5	7. 07	Wrong 1st choice
Cut 2/ Element 10-11	2.95	Wrong 2nd choice
Cut 2/ Element 12-13	2.89	Wrong 3rd choice
Cut 2/ Element 107-108	**2.81**	Correct 4th choice
Cut 1/ Element 4-5	4.18	Wrong 1st choice
Cut 1/ Element 107-108	**2.53**	Correct 2nd choice

*Note: Element 4-5 was adjacent to a pylon in the same span as the shaker. Elements 10-11 and 12-13 were on the opposite end of the bridge from the shaker where static responses were low. Elements 1-2 through 12-13 were on the south side (shaker side) of the bridge moving from east to

west. Elements 101-102 through 112-113 were on the damaged north side of the bridge moving from east to west.

MAXCON

For the MAXCON analysis both rotations and translations were used. The load paths were defined assuming simple springs connected each sensor to its nearest neighbors. This included the sensors directly and diagonally across the bridge. The rotations and translations were connected as one could expect from beam-type elements. Additional springs to ground were also assumed. It was not useful to separate mass and stiffness properties as seen in equation (11). However, to obtain successful results the model had to be separated to allow changes only in the assumed model form as described in equation (12). Scaling, as described by equation (6) was also required.

Figure 6 provides a bar chart of the entries in the first singular vector of the scaled B matrix which is the dynamic residual associated with the assumed model. This data set was calculated using the undamaged data set as the baseline and cut_1 as the comparison case. Note that there are 26 translation DOF's with 13 on each side of the bridge. These are the odd-numbered DOF's. The 26 rotations are the even-numbered DOF's. The expected damage location is between DOF 39 and DOF 42. This data shows the largest indication of damage at DOF 39 with large changes at DOF 37 and DOF 41. Also another large indication of damage is seen at the end of the bridge at DOF 51. This may be indicative of the changes that caused the modal frequencies to increase after the first cut.

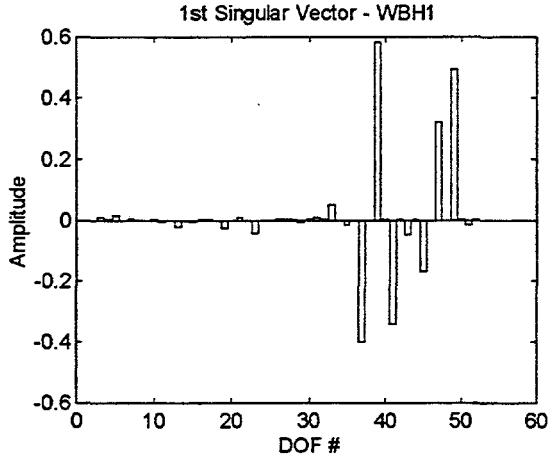

Figure 6. Pristine To Cut 1 Damage Localization

Figure 7 provides the same information for cut 2 with similar results as seen in Figure 6. Figure 8 provides the information for cut 3, again with similar results. And finally, Figure 9 provides the cut 4 data. One can see that the known damage location (DOF 39) is starting to increase relative to the phenomena at the end of the span.

SUMMARY AND CONCLUSIONS

Initial studies on damage detection and health monitoring have been performed using two techniques for damage localization. These techniques have been applied to two operational structures: a HAWT blade undergoing a fatigue test and a bridge undergoing an induced damage test. The STRECH algorithm provides a damage localization as well as a global damage indicator. It works best on static data, which may include static flexibility shapes estimated from dynamic mode shapes or the first mode of simple systems. The global indicator is fairly consistent, however more work needs to be performed to define a noise floor consistently. The MAXCON approach appears to be more robust for damage localization, but does not include a global indicator. Several measurable physical quantities are available to act as further constraints during completion of the matrices. Also, choosing the scaling on the null space to simultaneously zero the expected entries in the mass and stiffness matrices would be a much more desirable approach.

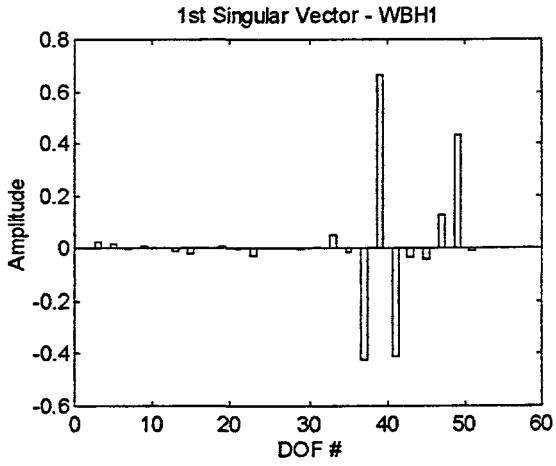

Figure 7. Pristine To Cut 2 Damage Localization

ACKNOWLEDGMENTS

Our appreciation goes out to Chuck Farrar at Los Alamos National Labs and the Civil Engineering Department of New Mexico State University for allowing us to participate in the I40 bridge test.

Engineers at the National Renewable Energy Lab were largely responsible for performing the wind turbine blade modal tests. The authors also wish to thank Lee Peterson, K.C. Park, and Scott Doebling of the University of Colorado at Boulder; David Zimmerman of the University of Houston; and Ken Alvin, Garth Reese, Bruce Hansche, Ron Rodeman, Dennis Roach, and Paul Veers of Sandia National Laboratories for their collaboration and insight. This work was supported by the United States Department of Energy under Contract DE-AC04-94AL85000.

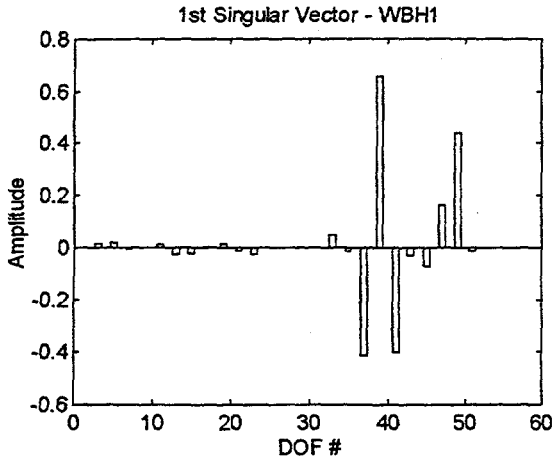

Figure 8. Pristine To Cut 3 Damage Localization

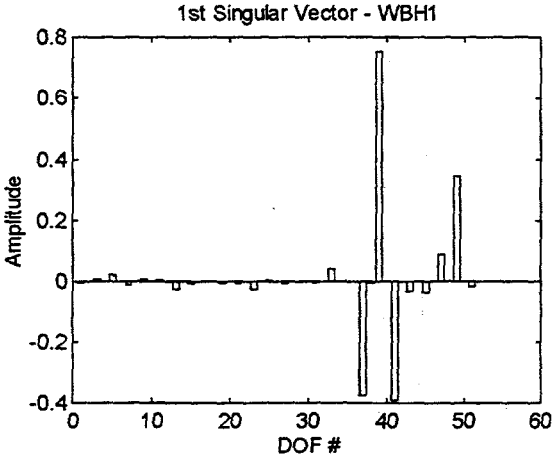

Figure 9. Pristine To Cut 4 Damage Localization

REFERENCES

1. Zimmerman, D. C. and Widengren, M., "Correcting Finite Element Models Using a Symmetric Eigenstructure Assignment Technique", AIAA Journal, Vol. 28, No. 9, September 1990, pp. 1670-1676.

2. Zimmerman, D. C. and Kaouk, "An Eigenstructure Assignment Approach For Structural Damage Detection", AIAA Journal, Vol. 30, No. 7, July 1992, pp. 1848-1857.

3. Kaouk, Mohamed and Zimmerman, David C., "Structural Damage Assessment Using a Generalized Minimum Rank Pertubation Theory", AIAA-93-1483-CP, presented at the 34th Structures, Structural Dynamics, and Materials Conference, La Jolla, CA, April, 1993.

4. Kaouk, Mohamed and Zimmerman, David C., "Structural Damage Detection Using Measured Modal Data and No Original Analytical Model", presented at the 12th International Modal Analysis Conference, Honolulu, Hawaii, January 31 - February 3, 1994.

5. Zimmerman, David C. and Simmermacher, Todd, "Model Refinement and System Health Monitoring Using Data From Multiple Static Loads and Vibration Tests", AIAA-94-1714-CP, presented at the AIAA SDM Dynamics Specialists Conference, Hilton Head, SC, April 21-22, 1994.

6. Zimmerman, D. C., Smith, S. W., Kim, H. M., and Bartkowicz, T. J., "An Experimental Study of Structural Damage Detection Using Incomplete Measurements", AIAA-94-1712-CP, presented at the AIAA SDM Dynamics Specialists Conference, Hilton Head, SC, April 21-22, 1994.

7. Simmermacher, T. W., Zimmerman, D. C., Mayes, R. L., Reese, G. M., and James, G. J., "The Effects of Finite Element Grid Density on Model Correlation and Damage Detection of a Bridge", paper AIAA 95-1072, to be presented at the AIAA Adaptive Structures Forum, New Orleans, LA, April 13-14, 1995.

8. Doebling, S. W.; Hemez, F. M.; Barlow, M. S.; Peterson, L. D.; and Farhat, C., "Damage Detection in a Suspended Scale Model via Model Update", proceedings of the 11th IMAC conference, Kissimmee Florida, February 1-4, 1993.

9. Doebling, S. W.; Hemez, F. M.; Barlow, M. S.; Peterson, L. D.; and Farhat, C., "Selection of Experimental Modal Data Sets for Damage Detection via Model Update", paper AIAA-93-1481-CP, proceedings of the 34th SDM conference, La Jolla, CA, April 1993.

10. Alvin, Kenneth F., "Second-Order Structural Identification Via State Space-Based System Realizations," CU-CSSC-93-09, Center for Space Structures and Controls, University of Colorado, Boulder, Colorado, April 1993.

11. Alvin, K. F.; Peterson, L. D.; and Park, K. C., "A Method for Determining Minimum-Order Mass and Stiffness Matrices from Modal Test Data", AIAA Journal, Vol. 33, No.1, pp. 128-135, 1995.

12. Peterson, L. D.; Alvin, K. F.; Doebling, S. W.; and Park, K. C., "Damage Detection Using Experimentally Measured Mass and Stiffness Matrices", paper AIAA-93-1482-CP, proceedings of the 34th SDM conference, La Jolla, CA, April 1993.

13. Doebling, Scott W., Alvin, Kenneth F., and Peterson, Lee D., "Limitations of State-Space System Identification Algorithms for Structures with High Modal Density", presented at the 12th International Modal Analysis Conference, Honolulu, HI, January 31 - February 3, 1994.

14. Mayes, Randy L., "Error Localization Using Mode Shapes - An Application to a Two Link Robot Arm", presented at the 10th International modal Analysis Conference, San Diego, CA, February 3-7, 1992.

15. Mayes, Randy L. and Nusser, Michael A., "The Interstate-40 Bridge Shaker Project", SAND 94-0228, Sandia National Laboratories, Albuquerque, NM, April 1994.

16. Hansche, B., James, G., Pride, N., Roach, D., Schmidt, T., and Webster, J., "Initial Studies on the Use of Laser Velocimetry, in the Inspection and Health Monitoring of Aircraft", Proceedings of the Quantitative Nondestructive Evaluation Conference", Snowmass, CO, August 2, 1994.

17. James, G., Mayes, R., Carne, T., and Reese, G., "Damage Detection and Health Monitoring of Operational Structures", AD-Vol. 45, MD-Vol. 54, Adaptive Structures and Composite Materials: Analysis and Application, Edited by E. Garcia, H. Cudney, and A. Dasgupta, ASME, presented at the 1994 ASME Winter Annual Meeting, Chicago, IL, November 6-11, 1994.

18. Mayes, Randall L., "An Experimental Algorithm for Detecting Damage Applied to the I-40 Bridge Over the Rio Grande", presented at the 13th International Modal Analysis Conference, Nashville, TN, February 13-16, 1995.

19. Farrar, C. R., Baker, W. E., Bell, T. M., Cone, K. M., Darling, T. W., Duffey, T. A., Eklund, A., and Migliori, A., "Dynamic Characterization and Damage Detection in the I-40 Bridge over the Rio Grande", LA-12767-MS, Los Alamos National Labs, Los Alamos, NM, June 1994.

20. Doebling, Scott, "Report on Development of a Laser Doppler Velocimeter System", final report for Outstanding Student Summer Program at Sandia National Laboratories, Experimental Structural Dynamics Department, August 1993.

21. Doebling, S., Alvin, K., and Peterson, L., "Improved Convergence of Estimated Stiffness Parameters for Experiments with Incomplete Reciprocity", to be presented at the 1995 Structures, Structural Dynamics, and Materials Conference, New Orleans, LA, April, 1995.

22. Peterson, L., Alvin, K., and Doebling, S., "Experimental Determination of Local Structural Stiffness by Disassembly of Measured Stiffness Matrices", to be presented at the 1995 Structures, Structural Dynamics, and Materials Conference, New Orleans, LA, April, 1995.

23. Stubbs, Norris, Kim, Jeont-Tae, and Farrar, Charles, "Field Verification of a Nondestructive Damage Localization and Severity Estimation Algorithm", presented at the 13th International Modal Analysis Conference, Nashville, TN, February 13-16,1995.

24. James, George H., Carne, Thomas G., and Lauffer, James P., "The Natural Excitation Technique (NExT) for Modal Parameter Extraction from Operating Wind Turbines", SAND92-1666, Sandia National Laboratories, Albuquerque, NM, 1993.

Intentionally Left Blank

APPENDIX K

REPORT ON A SANDIA NATIONAL LABORATORY - OFFSHORE OIL INDUSTRY INFORMATION MEETING

Ward Turner - Exxon Production Research Company

A Memo to API Task Group 92-5 on Assessment of Existing Platforms to Demonstrate Fitness for Purpose

August 28, 1995

Intentionally Left Blank

EXXON PRODUCTION RESEARCH COMPANY
POST OFFICE BOX 2189 • HOUSTON, TEXAS 77252-2189

August 28, 1995

API BUSINESS

To: API Task Group 92-5 on Assessment of Existing Platforms to Demonstrate Fitness for Purpose

Sandia National Laboratory - Offshore Oil Industry Information Meeting

Summary

At the March 2, 1995 meeting of API Task Group 92-5, a presentation was made by representatives of Sandia and Los Alamos National Laboratories related to technology that might be applicable to health and condition monitoring of aging offshore structures. As a result of this meeting, an invitation was extended to visit Sandia to discuss these issues in further detail and to see demonstrations of relevant technology. In response to this invitation, Brad Campbell (Exxon), Denby Morrison (Shell), and Ward Turner (Exxon) visited the Sandia National Laboratory on July 11-12, 1995.

As a result of these meetings, several areas were identified where Sandia and Los Alamos National Laboratories are performing work with potential application in the oil industry. The Laboratorys' next step will be to identify potential internal funding sources and to propose a few focused topics to pursue in pilot studies on a joint-industry basis. Such studies would likely be highly leveraged through the internal funds that have been made available to the National Laboratories.

Overview

On July 11 and 12, 1995, a series of meetings and demonstrations was held at Sandia National Laboratory (Albuquerque, NM) related to technologies that could possibly be applied to inspection and assessment of aging offshore platforms. In addition to Sandia personnel, presentations were also made by representatives of the Los Alamos National Laboratory and two professors, one from the University of Houston and one from the University of Colorado.

The National Laboratories are faced with changing policies and strategic directions. Until recently, they have focused their efforts principally on national defense and in providing technical support to other governmental agencies. Recently, however, they have been charged with making relevant technologies available to U. S. Industry. As a result of these changes, Dr. George James of Sandia contacted Kris Digre of Shell, who is leader of the API task group on the assessment of existing platforms. During a regular API task group meeting held in New Orleans on March 2, 1995, a special time was set aside for a presentation by Sandia and Los Alamos. The technologies that they discussed included:

- Non-contact vibration monitoring
- Aging aircraft inspections
- Calibration of dynamic analytical modeling with experimental data
- Acoustic monitoring technologies
- Special time-domain analysis methods

Based on the technology that was presented at the New Orleans meeting, it was suggested that a more detailed follow-up meeting be held at Sandia where a full range of related topics could be discussed in greater detail. This would also allow for demonstrations and tours of the Laboratory facilities. Such a meeting was then held on July 11-12, 1995 and is the subject of this documentation.

National Laboratory Initiatives

Historically, the Los Alamos and Sandia National Laboratories have principally focused on the development of nuclear weapons, with Los Alamos performing scientific development and Sandia performing engineering development. During the past decade, both laboratories have been expanding their focus to include work for other governmental agencies, and more recently, to perform work on behalf of civilian enterprises. The principal strengths that the National Laboratories bring to such work is a very diverse group of engineers and scientists backed by laboratory testing facilities that are among the best available in the world.

Over the last several years, the U. S. Defense industry has been shrinking and questions have been raised at the national level regarding the function and purpose of these laboratories. One response has been the allocation of tax funding to the National Laboratories to initiate joint programs with industry. In general, these programs are heavily funded by tax dollars, but are mixed with industry participation through joint industry funding, payments in kind, etc. In particular, Sandia and the oil industry have participated together via the "Advanced Computational Technology Initiative", also known as ACTI funding. At this time, however, it is not known whether there will be a continuation of the ACTI program.

Another funding avenue for such joint projects is the "Oil & Gas Partnership" with funding via the U. S. Department of Energy (DOE). At the meeting, we were told that this program is likely to be changed to include an offshore component; although at this time, the specifics of the new program are uncertain.

Finally, there is often an academic component pursued in National Laboratory / Industry projects. This is often through collaborative research at U. S. Universities, which may be supported by the National laboratories and from other university funding sources.

Meeting Objectives

The objectives of Sandia and Los Alamos for having the meeting were primarily to discuss issues with oil company representatives that could become common ground for research initiatives with the oil industry. Although several other oil industry organizations (petroleum companies and contractors) had expressed various degrees of interest, only Exxon and Shell were represented at the meetings. A fundamental assumption by the representatives of both companies going into the meetings was that any future work would likely be in the form of joint industry projects (JIPs) rather than individual corporate contracts.

At the initial meeting presentation, Sandia Laboratories expressed their objectives for the meetings as follows:

1. To give us a broader view of the National Laboratories.

2. For them to learn more about our technical issues.

3. To determine a "next step" that could lead to future work initiatives.

Presentations by Sandia

The agenda for the meetings is given in attachment I. The morning of the first day (July 11) focused on overview presentations. This was followed by laboratory visits in the afternoon. The morning of the second day (July 12) focused on presentations of technical procedures that are relevant to the analysis of aging structures. The meetings were then concluded with a discussion led by the industry representatives on the technical challenges being faced. This then led to the identification of potential studies that could be proposed within this framework.

A summary of the detailed presentations and laboratory demonstrations is given in Attachment II.

Key Technical Issues

Part of the motivation for attending the meeting was the hope that significant technical advances had been made in other structural engineering fields that might have direct application to aging offshore platform integrity issues. In particular, our interests included methods that might be used to detect structural damage via inspections or through the analytical interpretation of structural vibration data.

Early on in the presentations, it became apparent that strides have been made in the analysis and interpretation of data. However, with reference to the underwater data that would be required to assess an offshore platform, the fundamental problem of how to cost

effectively obtain the data remains the significant issue. In particular for offshore platforms, the placement of an adequate number of accelerometers, the cost of running electrical conduits, and the required robustness needed to assure the long term integrity of the system still remain the major hurdles to the instrumentation of platforms.

Although many technology components were identified that would help reduce the costs of such data collection systems on platforms, there did not appear to be any breakthroughs that could immediately lead to substantial changes in current technology or costs.

Identification of "Next Steps"

In the wrap-up meetings, the participants attempted to develop a strategy that would best allow for the transfer of National Laboratory technology to the offshore oil industry. The guiding principles of this strategy are as follows:

1. Focus on Breakthroughs Any participation with the National Laboratories should be focused on non-routine, breakthrough technology. Such work would typically be characterized as having a high benefit to industry, but may have only a low probability of success. This concept is also in line with the National Laboratory guidelines that they should not be competing with industry, which in this case would be the many vendors and contractors who supply technology to the petroleum companies.

2. Identify Relatively Small Pilot Type Studies Initial projects should have relatively well defined goals and a narrow focus. If such initial projects are successful, then more general topical issues could follow.

3. Work Through Multi-Participant Agreements All work should be done through industry groups, such as through joint industry projects (JIPs) or the American Petroleum Institute (API). This is consistent with the National Laboratory funding guidelines which typically require the showing of "broad" industrial support. The industrial sponsors must also be prepared to provide some support via funding or payments in kind, such as through manpower devoted to the project, providing data, or providing access to offshore facilities for trials, etc.

4. Include Academic Research Input Where appropriate, academic support through parallel research programs should be supported and/or funded via the projects.

5. Seek Funding Through National Laboratory Sources As part of the changing focus of work at the National Laboratories, funding sources are being allocated to support projects as envisioned. Likely sources include the ACTI funds or the Oil & Gas Partnership. As a result of these funding sources being added to the participant contributions, the leverage factors per industrial participant would be very high.

Identification of Potential Projects

Several projects were identified during the meeting as being possible technology areas to pursue with Sandia and Los Alamos National Laboratories. These projects meet the objectives outlined for small pilot type studies mentioned in item No. 2 above, but are not necessarily all related to the aging offshore structure topic that was the original focus of the meeting. They are listed as follows:

1. TLP Tendon Inspection Methods The industry TLP project teams have recognized that inspection techniques for TLP tendons are not presently cost effective. From a data interpretation perspective, this item was identified as having a higher likelihood of success since each tendon is structurally non-redundant. One potential avenue of study that could be applied includes acoustic emissions.

2. Pile Penetration Detector A key parameter for the assessment of any old offshore platform is knowing the pile penetrations. Unfortunately, due to poor record keeping, the pile penetrations are unknown for many old platforms. The goal of this study would be to develop a device that would use reflected sound pulses to travel along the length of piles to determine their driven penetration. Known technical difficulties include the effects of grouting, binding shims, variable soil conditions, etc.

3. Floater Inspections Floating structures typically have a very large number of web stiffeners, which complicate inspection procedures. The goal of this study would be to develop sensor technology that continuously monitors a structure for the development of fatigue cracks. Additionally, the data transmission difficulties associated with transmitting data through bulkheads would be addressed.

4. Corrosion Mapping One of the more costly inspection problems is mapping areas of known corrosion in both platform braces and in pipelines. The focus of this study would be to develop methods that would simplify how this data is currently obtained.

5. Mapping of Ice Features With the many special non-contact sensing devices that were shown, it is possible that there may be better methods than currently used for the mapping of ice features.

6. Inspection of Concrete Structures It is well known within the industry that concrete platform inspection techniques are not very well developed. The focus of this study would be to improve the technology associated with this problem.

7. Detection of Hydrates and Wax Deposits Methods associated with the detection of hydrates and waxes in subsea connections to host platforms are a problem that could be worthy of study.

Work Plan

With the completion of this initial survey of National Laboratory technology related to aging offshore structures, the next step will be for Sandia and Los Alamos to determine their likely internal funding sources. We were told by George James of Sandia that they will have a better understanding of likely direction by this fall. At that time, they will return to the oil industry to see if any viable projects could be proposed.

Closure

Assistance in the preparation of this document was provided by Brad Campbell, George James, and Denby Morrison. If you have any questions, please call Ward Turner at 713-965-7314.

J. Ward Turner

File: 3683

- API TG ASSESSMENT OF EXISTING PLATFORMS TO DEMONSTRATE FITNESS FOR PURPOSE

Mr. Kris A. Digre (Chairman)
c/o Shell Offshore Inc.
P. O. Box 576
Houston, TX 77252-0576
(713) 544-4104
(713) 544-4817 (Fax)

Mr. Steve Guynes PRC-J1424
c/o Arco Exploration Prod. Tech.
2300 W. Plano Parkway
Plano, TX 75075
(214) 509-3077
(214) 509-3920 (Fax)

Mr. ~~Flex~~ Felix Dyhrkopp
c/o Minerals Management Service
1201 Elmwood Park Boulevard
New Orleans, LA 70123-2394
(504) 736-2893
(504) 736-2610 (Fax)

Mr. C. Petrauskas
c/o Chevron Petroleum Tech. Co.
1300 Beach Boulevard (90631)
P. O. Box 446
La Habra, CA 90633
(310) 694-7556
(310) 694-9283 (Fax)

Mr. Jack T. Irick
c/o Casbarian & Barnett, Inc.
9225 Katy Freeway, Suite 307
Houston, TX 77024-1596
(713) 467-6713
(713) 468-0613 (Fax)

Mr. J. Ward Turner
c/o EPRCO
3616 Richmond (77046)
P. O. Box 2189
Houston, TX 77252-2189
(713) 965-7314
(713) 965-7775 (Sec'y)
(713) 966-6304 (Fax)

Mr. Bill Krieger
c/o Chevron Petroleum Tech.
2400 Camino Ramon
BR6, K1082
San Ramon, CA 94583
(510) 842-8135
(510) 842-8626 (Fax)

Mr. Robert G. Bea
c/o Univ. of Calif.
Department of Civil Engrg.
212 McLaughlin Hall
Berkeley, CA 94720
(510) 642-0967
(510) 642-0967 (Fax)

Mr. Griff C. Lee
c/o McDermott Inc.
P. O. Box 60035
New Orleans, LA 70160
(504) 539-7070
(504) 539-7203 (Fax)

Mr. Jorge Calvo
Mobil Res. & Dev. Co.
13777 Midway Road
Dallas TX 75244-4390
(214) 851-8428
(214) 851-8349 (Fax)

- API TG ASSESSMENT OF EXISTING PLATFORMS TO DEMONSTRATE FITNESS FOR PURPOSE

Mr. Joe Kallaby
c/o Offshore Structures Inc.
8950 Westpark, Suite 122
Houston, TX 77063
(713) 974-2760
(713) 932-9901 (Fax)

Mr. Dave Wisch
% Texaco
4800 Fournace Pl. #W.946 (77401)
P. O. Box 430
Bellaire, TX 774020430
(713) 432-3498
(713) 432-3085 (secretary)
(713) 432-3290 (Fax)

Mr. Pat O'Conner
c/o Amoco Prod. Co.
Westlake II, Mail Code 366
P. O. Box 3092 Hou,TX 77253-3092
(713) 366-4007
(713) 366-7555 (Fax)

Mr. J. H. Chen
c/o Chevron Petroleum Tech. Co.
P. O. Box 446
La Habra, CA 90633-0446
1300 Beach Boulevard
La Habra, CA 90631
(310) 694-7391
(310) 694-9283 (Fax)

Mr. Denby Morrison
c/o Shell E&P Technology Co.
PO Box 481
Houston,
TX 77001
(713) 245-7409
(713) 245-7233 (Fax)

Dr. George James
c/o Sandia National Laboratory
Albuquerque, N.M.
87185-0557

505-844-4535
505-844-0078 (Fax)

Dr Charles Farrar
c/o Los Alamos National Laboratory
Los Alamos,
N.M. 87545
505-667-4551
505-665-2137 (Fax)

CORRESPONDING MEMBERS

Mr. Fred Moses
Chair Dept. of Civil Engrg.
University of Pittsburg
949 Benedum Hall
Pittsburg, PA 15261-2294
(412) 624-9870
(412) 624-0135 (Fax)

Mr. Roger L. Thomas
Phillips Petroleum Co.
7th Floor, Phillips Building
420 Keeler Street
Bartlesville, OK 74004
(918) 661-4903
(918) 662-2242 (Fax)

Mr. Martin L. Eskijian
State of California
State Lands Commission
245 W. Broadway, Suite 425
Long Beach, CA 90802-4471
(310) 590-5198
(310) 590-5295 (Fax)

Mr. R. C. Visser
Belmar Engrg. & Mgmt. Svcs. Co.
1650 S. Pacific Coast Hwy.,Ste.301
Redondo Beach, CA 90277-5613
(310) 316-5934
(310) 316-5974 (Fax)

Mr. Frank J. Puscar
c/o PMB Engineering Inc.
3000 Post Oak Blvd.
19th Floor
Houston, TX 77056
(713) 235-2770
(713) 235-2597 (Fax)

Mr. Paul E. Versowsky
Offshore Oprs. Committee, Rep.
c/o Chevron Petrol. Tech. Company
935 Gravier Street, Room 1304
New Orleans, LA 70112
(504) 592-6245
(504) 592-7073 (Fax)

Dr. J. M. Ricles
Lehigh University
117 Atlas Drive, H. Bldg.
Bethlehem, PA 18015-4729
610 (215) 758-3535
610 (215) 758-5553 (Fax)

Leslie Monahan
Minerals Management Service
770 Paseo Camarillo
Camarillo, CA 93010
(805) 389-7568
(805) 389-7592 (Fax)

Dr. Terry L. Kohutek
Texas A&M University
Dept. of Civil Engineering
College Station, TX 77843-3136
(409) 845-7435
(409) 845-6554 (Fax)

Mr. James M. Light
AMOCO Production
4502 East 41st Street
P. O. Box 3385
Tulsa, OK 74102
(918) 660-3212
(918) 660-3274 (Fax)

CORRESPONDING MEMBERS

Mr. Dan Dolan
c/o PMB Engineering Inc.
500 Sansome Street
San Francisco, CA 94111
(415) 986-4166
(415) 986-2699 (Fax)

Mr. Dave M. Hopper
c/o Hopper & Associates Engineers
300 Vista Del Mar
Redondo Beach, CA 90277
(310) 373-5573
(310) 791-7308 (Fax)

Mr. Michael Craig
c/o Union Oil Co. of Calif.
4021 Ambassador Caffery Pky (70503)
P. O. Box 39200
Lafayette, LA 70593-9200
(318) 295-6551
(318 295-6393 (Fax)

Mr. Rick Birdwell
c/o Exxon Company USA
P. O. Box 2180, Rm. 2005A
Houston, TX 77252
(713) 656-0155
(713) 656-1512 (Fax)

Mr. Neal M. Hennegan
c/o Shell Offshore Inc.
P. O. Box 60159
New Orleans, LA 70160
(504) 588-7148
(504) 588-0825 (Fax)

Mr. Dirceu Botelho
c/o Chevron Petroleum Tech. Co.
1300 Beach Blvd. (90631)
P. O. Box 446
La Habra, CA 90633
(310) 694-7677
(310) 694-9283 (Fax)

Mr. Gary R. Imm
c/o Amoco Production Co.
P. O. Box 3385
Tulsa, OK 74102-3385
(918) 660-4329
(918) 660-3274 (Fax)

Mr. James E. Boarman
c/o Enercon Engineering, Inc.
16010 Barker's Point Lane, Ste. 400
Houston, TX 77079
(713) 496-9300
(713) 496-9222 (Fax)

Mr. Charles E. Smith
c/o Minerals Management Service
381 Elden Street MS647
Herndon, VA 22070-4817
(703) 787-1559
(703) 787-1010 (Fax)

Mr. D. P. Chancellor
c/o Chevron Research & Tech. Co
935 Gravier Street
New Orleans, LA 70112
(504) 592-6622
(504) 592-7073 (Fax)

Dr. Allan M. Reece
c/o Shell Development Company
3737 Bellaire Boulevard
Houston, TX 77025
(713) 245-7437
(713) 245-7233 (Fax)

Dr. Rabi S. De
c/o Shell Development Company
3737 Bellaire Boulevard
Houston, TX 77025
(713) 245-7438
(713) 245-7233 (Fax)

Attachment I

Sandia National Laboratories

Albuquerque, New Mexico 87185

date: July 7, 1995

to: Distribution

George James III

from: G. H. James, 2741 MS0557

subject: Updated Agenda and Directions for Offshore Oil Industry Information Meeting

This memo provides an updated schedule for the meetings scheduled on July 11 and 12:

July 11 - Bldg. 860, Room 212

9:30 - 10:00 Meet at Badge Office - Bldg. 800
10:00 - 10:30 Introductions and Opening Discussion - James, Red-Horse, & Farrar
10:30 - 11:00 Summary of Presentations to API TG 92-5 - Farrar, James, & Red-Horse
11:00 - 11:30 Oil & Gas Programs at Sandia - Dave Northrop & Elaine Gorham (SNL)
11:30 - 12:00 Aging Aircraft NDI Validation Center - Shurtleff (SNL)
12:00 - 1:00 Lunch
1:00 - 1:45 Tour of Bldg. 860 Labs - Mayes & James
1:45 - 2:30 Tour of Metallurgy & Corrosion Labs - Cieslak
2:30 - 3:15 Tour of NDE Labs - Shurtleff
3:15 - 5:00 Tour of AANC - Shurtleff, Hansche, Meza, & Robinson
6:30 - 8:30 Dinner

July 12 - Bldg. 860, Room 212

8:30 - 9:00 Structural Health Monitoring & Identification - Zimmerman (UH)
9:00 - 9:30 Advanced Modeling and Processing - Hunter (LANL) & Paez (SNL)
9:30 - 10:00 Disassembly, Flexibility, & Wavelets - Park (CU) & Alvin (SNL)
10:00 - 10:30 Time - Frequency Analysis Methods - Farrar (LANL)
10:30 - 10:45 Break
10:45 - 11:00 Advanced Measurements - Hansche (SNL)
11:00 - 12:30 Industry Driven Discussions - All
12:30 - 1:30 Lunch
1:30 - 4:30 Individual Discussions (if desired)

The following amended directions are provided to correct a minor error:

Attachment II

Summary of Presentations by Sandia

Tuesday July 11, 1995

1. Health Monitoring (David Martinez)

   The aging of weapon systems has become increasingly important to the Defense Department. Issues being faced include aging components and materials (seals, etc.), a moratorium on the development of new weapon systems, weapons approaching and exceeding 20-year design lives, etc. Where possible, when modifications are made, they attempt to put intelligent systems into replacement parts. This allows for the continual monitoring of the system "state of health".

   One relevant aspect of this technology is the use of microelectronic sensors to help monitor structures. This includes the identification of optimum locations for the placement of sensors. An additional aspect of this technology is to use sensors to calibrate analytical models with experimentally derived dynamic properties.

2. Modal Calibration of a Large Civil Engineering Structure (Chuck Farrar)

   Los Alamos recently performed a field test of technologies to examine the dynamic behavior of varying degrees of damage on a large highway bridge. Tests were performed on the Interstate 40 bridge over the Rio Grande River, that was being removed and replaced by a wider bridge. The project consisted of first developing an analytical model to determine the dynamic behavior of the bridge. Model calibration was then performed by means of ambient measurements and forced excitation.

   One unique aspect of the dynamic measurements was that many were taken by means of non-contact sensors. The system used a microwave technique that is capable of measuring displacements on the order of ambient structural vibrations at a distance of over 100'.

   The tests then focused on using the sensors to detect changes in the dynamic response of the bridge for varying degrees of induced damage. The damage was induced by first cutting a "crack" at the midpoint of one of the two 10' deep longitudinal girders at the midpoint of the web. The crack was then gradually expanded downward until it reached the lower girder flange. The flange was then gradually cut outward until there was final separation. During this process, dynamic measurements were taken to determine the changing nature of the modal shapes.

   Using standard dynamic model interpretation procedures, it appeared that differences in the modal shapes became apparent when the web cut reached the lower flange. However, more sophisticated damage identification procedures indicated changes for

smaller cuts. In this case, the analytical model used linear FEM approaches. Based on their assessment, they believe that most damage scenarios, with the exception of fatigue crack growth, can be modeled using linear approaches.

3. Interactions With Oil Industry (Dave Northrup)

A presentation was made regarding how Sandia is working with the oil industry. The two main avenues have been via the Advanced Computational Technology Initiative (ACTI) and the broader Oil & Gas Partnership. Presently, it is questionable whether the ACTI funding will be renewed by Congress. However, there is some belief that either it or some other similar program will be funded. The Oil & Gas Partnership has heretofore not had any offshore component. However, this Department of Energy (DOE) program is being restructured and it is believed that it will have an offshore component that might be applicable to programs supporting the offshore industry.

4. ACTI Program With DeepStar (Elaine Gorham)

Sandia is presently supporting the DeepStar project in the area of riser vibration analysis and bonding between composites and metal. For risers, their focus is in the area of fluid/structure interaction.

Unfortunately, Sandia acknowledges that there have been some problems in the riser portion of the workscope due to lack of direction/integration with the DeepStar steering committee. Some of the DeepStar partners are pushing for Sandia to develop a stand-alone program for analyses that would duplicate the technologies in Shell's Cosmos program. Others would prefer that Sandia use their capabilities to enhance the Cosmos routines. Sandia is concerned if they are asked to pursue the former approach since they are under general directives to be "non-competitive" with commercial enterprises.

As a result of these discussions, a special meeting was scheduled on the afternoon of the second day to focus on this specific issue. It was attended by Brad Campbell and Denby Morrison (Shell). Documentation of the resolution of this issue is outside the scope of this memorandum.

5. Non-Destructive Evaluations (Bill Shurtleff)

Sandia administers the Federal Aviation Administration (FAA) aging aircraft Non-Destructive Inspection (NDI) Validation Center. They have a large facility at the Albuquerque airport containing the airframes of an old Boeing 737, DC 9, and Falcon jet. Their program develops and validates technologies that can be used to inspect airframes. Their customers include the FAA, airline industry groups, airplane manufacturers, and third party inspector associations.

The primary motivation for their efforts came as a result of the 1988 Hawaii Air incident where a large section of fuselage came off during a flight as a result of fatigue cracking. Some of the technologies that they have developed for airframe inspection include:

- Non-contact inspection techniques such as coherent optics (measures displacement in a fuselage due to internal vacuum or thermal loading) and shearography (measures derivatives of displacements).

- An area eddy current device that can scan rivet areas rather than lines of rivets (this device is about the size of an electric 1/3 sheet sander and scans a similar size area).

- Representative panel defects that can be used to qualify inspection techniques and personnel.

6. Tour of Vibration Laboratory (Randy Mayes)

This laboratory has a vibration isolation table that is typically used to test the vibration characteristics of weapon payloads. It is composed of a 15 ton block of steel isolated on air bags. Payloads are then placed on the steel block and are excited to determine their dynamic properties. In general, the issue for them is to correlate the measured dynamic response with the analytical models.

7. Tour of Metallurgy and Corrosion Laboratory (Rudy Buchleit)

This laboratory is used to accelerate corrosion and aging effects. One oil industry related study that they have in progress is determining the likely life of concrete lined piping used at the Strategic Petroleum Reserves.

8. Tour of Acoustic Emissions Laboratory (Alan Beattie)

The airline industry association has a contract with Sandia to develop an improved method to inspect Halon fire extinguishing container bottles. The method that they are applying is to use acoustic emissions. This is done by heating the bottle, causing the internal pressure to rise. When the bottle expands, the sound induced by any internal cracks is detected. This technology will save the airline industry approximately $2M/year in inspection costs.

9. Tour of Non-Contact Sensor Laboratory (Bruce Hanche)

We were shown an optical holographic laser system that was being used to visualize operating shapes on a model of a compressor turbine ring. The model was excited with an oscillator and the surface was lighted by a laser. By means of optical

interferometry, the surface displacements caused by the vibrations were measured and global vibration patterns were visually displayed.

10. Tour of the Aircraft Inspection Facility (Bill Shurtleff)

Demonstrations of aging airframe inspection techniques were shown to us at the Albuquerque airport facility (see item No. 5 above). Also, an internally funded research project to develop techniques for damage detection using structural vibration measurements was discussed.

Wednesday July 12, 1995

11. Structural Health Monitoring and Identification (Dave Zimmerman of U of H)

Dr. Zimmerman made a presentation on recent system ID work he is performing at the University of Houston for the NASA space station. His work shows that with approximately 100 sensors, up to 85% of the planned structural inspections would not be required. One relevant structural issue that he did discuss was that sensor placement is important and that sensors placed for damage identification are often not ideally located for model verification and vice-a-versa.

12. Advanced Modeling and Processing (Tom Paez)

This session focused on neural networks, probabilistic pattern recognition, and bootstrapping methods. The neural network methods focus on detecting patterns in data and training the system to recognize these patterns. Probabilistic pattern recognition is a methodology to assess data of unknown origins to judge whether it is consistent with the original system or is an outlier. The bootstrapping techniques are used to determine if sparse data measurements meet statistical bounds related to underlying assumptions, such as whether a structural response is linear or not.

13. Analyses Approaches (K. C. Park of U of C)

Dr. Park made a presentation on analyses approaches he has developed in his program at the University of Colorado (Boulder). He believes that the measurement technology has developed much faster than structural modeling techniques in recent years. Dr. Park also presented material on the use of the force method of structural analysis for determining substructural flexibilities from experimental data, and the use of wavelet transforms for determining impulse response functions from dynamic measurements.

14. Error Localization and Finite Element Model Updating (Ken Alvin)

Dr. Alvin made a short presentation on identifying the locations of modeling errors (or unknown damage) using modal parameters. He also reported on recent results in finite element model updating and the predictive accuracy of the identified models.

15. Time Frequency Analysis Methods (Dan Shevitz)

This presentation presented results of methods being used to interpret dynamic systems. The simple system presented was a plastic block with a crack half way through its thickness. The structural system was then "rung" and dynamic properties were measured. The focus of the effort was to interpret the data via several analytical approaches including power spectral densities, wavelets, spectrograms, and Wigner-Ville. Of the approaches used, the spectrogram method seemed to demonstrate the best capability of indicating the damage (opening and closing of the crack) in the block.

16. Non Contact Sensors (Bruce Hanche)

This presentation was a follow-up to the laboratory visit the day before (see item No. 9 above). One of the areas that Sandia has made great progress in is with non-contact sensors for the measurement of vibrations. The three principal types of devices and their applications are as follows:

a) Optical

Optical devices typically employ lasers. Depending on their design, they can cover a wide array of applications, such as measuring very small deflections at a short distance (as was shown during the laboratory visit described in item No. 9) to measuring larger deflections at a large distance (as would be applied to a civil engineering type structure).

Some of the systems use optical triangulation, which is a method of determining displacements by measuring how much the angle of the reflected light signal changes. Other methods employ the interaction of light fringes. Some methods do not measure displacement directly, but instead measure the derivative of displacement (shearography). Some methods employ holographic images.

As of yet, none of these systems could be directly employed underwater since murky water would interfere with the signals. Although not strictly optical, LIDAR systems, which use a laser radar, could be a system that possibly would work underwater.

b) Acoustic

Acoustic pulse echo technology could be employed underwater. Although Sandia admitted that they are not experts in sonar technology, they believed that sonar type systems could be developed that might be applicable for offshore measurement systems.

c) Microwave

Microwave systems can be used to measure displacements on civil engineering type structures. This was one of the technologies used to measure the displacements on the I40 bridge project (see item No. 2 above). It is capable of measuring over large distances and can resolve displacements on the order of a tenth of a millimeter to meters. In our discussions, we determined that such a system could be applied to measuring vibrations on a structure such as a drilling mast, but it would not work underwater.

17. Down Hole Acoustic Research (Doug Drumheller)

This presentation described work that has been done related to the use of acoustic methods to transmit data along drill strings. In general, the goal is to eliminate the need to place electrical signal wire for the obtaining of down hole pressure and temperature data. As part of their testing program, Sandia has a test facility of several thousand feet of casing laid out horizontally that is used to test acoustic transmission techniques. Essentially, these units would be battery powered and would transmit the data along the pipe to a receiver located at the well head.

Intentionally Left Blank

APPENDIX L

ROBUST MODEL ERROR LOCALIZATION FOR DAMAGE DETECTION AND FINITE MODEL UPDATE

Kenneth F. Alvin

Proceedings of the 1995 International Adaptive Structures Conference,

November, 1995

Intentionally Left Blank

ROBUST MODEL ERROR LOCALIZATION FOR DAMAGE DETECTION AND FINITE ELEMENT MODEL UPDATE

Kenneth F. Alvin

ABSTRACT

A new method for identifying the location of finite element model errors given test-identified frequencies and mode shape data is presented. The new method builds on the concept of the modal force error vector, which is the undamped impedance of the given finite element model at each identified frequency multiplied by the corresponding identified mode shape. In order to mitigate the problems associated with reducing analytical models to the set of measurement degrees of freedom, a mode shape projection algorithm is utilized. The projection algorithm is a linear least-squares method which can be controlled to minimize bias caused by model errors. The localization indicator is then defined by the modal force error and a degree of freedom-dependent normalization based on the variance of the identified frequencies and mode shapes. The performance of the method in localizing structural damage is examined using experimental data.

INTRODUCTION

The development of accurate predictive analytical models for structural dynamics traditionally involves the problem of model reconciliation to dynamic testing. This is because, despite advancements in finite element theory, model construction (e.g. meshing algorithms), visualization and high performance computing, there are still significant modeling errors introduced by assumptions of uniform material behavior, joint compliance, element formulations, etc. In order to address the reconciliation of analytical models to dynamic testing, efficient testing methods and algorithms have been developed to adjust model parameters to "fit" the test identified modal parameters. These algorithms can be interpreted as optimization methods; that is, an objective is minimized or maximized with respect to a set of variable parameters.

When the model being adjusted has the correct mathematical form, but inaccurate parameters, parameter estimation algorithms yield excellent results, with the following caveats. First, there must be a sufficient number of test-identified parameters upon which a least-squares estimate of the parameters can be based. Second, the parameters which are in error must be among those being estimated. Finally, the parameters being varied must be as independent as possible in terms of their sensitivity to the data. Unfortunately, these requirements are at odds with one another. For example, if all primary model parameters are allowed to vary, there will not be a sufficient

Research Fellow, Structural Dynamics and Vibration Control Dept., Sandia National Laboratories, P.O. Box 5800, MS 0439, Albuquerque, NM 87185

number of test-identified parameters available to obtain a least-squares estimate. Furthermore, there will likely be a high degree of correlation between the parameters, further limiting the confidence in the estimate. Therefore, we are usually limited to the variation of a few key model parameters to account for the observable errors. The process of selecting these parameters can be termed *model error localization.* In this context, the problem of updating models is a two-stage iterative approach. The first stage is *localization* or selection of model parameters to be estimated; the second stage is the *estimation* of those parameters to optimize a particular metric.

Similarly, in detecting damage in structures using dynamic response data, these two tasks are generally described as finding the *location* and *extent* of the damage. Damage detection usually involves determining location and extent indicators for a structure relative to some baseline condition of the structure, represented either by a previous set of dynamic response data or by the response parameters of an analytical model of the structure which is assumed to be accurate and reflects a particular condition of health. Using damage localization, problem areas can be identified in order to direct more detailed structural inspections. Similarly, in adaptive structures technology, damage or error localization indicators can be used to monitor adaptive structural systems for health or to identify sensor systems which are no longer functioning properly.

In this paper, a new method for identifying the location of finite element model errors, or equivalently damage, given test-identified frequencies and mode shape data is presented. The present model error localization approach is based on the Sensitivity-Based Element-By-Element (SB-EBE) model update theory (Farhat and Hemez, 1993). This algorithm determines parameter estimates by a minimization of modal force errors for a set of modes. The modal force error vector is the undamped impedance of the given finite element model at each identified frequency multiplied by the corresponding identified mode shape. The minimization leads to both a mode shape projection algorithm and physical model parameter update using the projected mode shapes plus the experimental frequencies and the nominal stiffness and mass matrices of the analytical model.

A key component of this model update procedure is the so-called "zooming" feature, whereby a small number of potential model parameters are chosen for updating based upon the degrees of freedom (d.o.f.) exhibiting the largest modal force errors, and the parameters which are localized to those degrees of freedom. Clearly, the "zooming" feature is an example of model error localization for finite element updating. Kaouk and Zimmerman use a similar approach in defining a "damage vector," which is again the modal force error generalized to utilize the damped modal parameters (Kaouk and Zimmerman, 1994). This common concept of using the modal force error vector for localization was proposed in earlier work (Ojalvo and Pilon, 1988).

The present technique builds on the same concept of the modal force error, but introduces additional algorithmic components to increase robustness of the localization in the presence of model errors, differences in localized stiffness, and uncertainty in the identified parameters. In order to compute the modal force error with respect to the d.o.f. of the model, a mode shape projection algorithm is utilized. The projection is formulated as a least-squares problem using the model and the equations of motion at the identified frequency to solve for the displacements at the unmeasured d.o.f. A key component of the present technique, however, is control of the errors introduced by the projection algorithm. This is accomplished by partitioning out rows of the analytical model matrices associated with the largest modal force errors. An alternative approach investigated is the use of a normalization of the functional underlying the projection algorithm.

The model error localization indicator is then defined by the modal force error vector and a d.o.f.-dependent normalization based on the variance of the identified modal parameters. This normalization is critical to understanding the localization effects caused by random errors in the identification process and the relative dynamic stiffness of the model. That is, areas of the model

at which forces tend to localize due to sensitivity in the model formulation itself will be normalized so that they do not mask errors in less sensitive locations. This normalization allows for statistical confidence in the identified modal properties to be incorporated into the localization analysis, such that model parameters sensitive to the most uncertain test parameters will be de-emphasized. Finally, this paper investigates the trade-off between dynamic model reduction and mode shape projection within the context of model error localization. This is an important consideration as traditional approaches have considered only a choice between these techniques, rather than a judicious combination to minimize the ambiguity of the results.

The remainder of the paper is organized as follows. The general theory for error localization via computation of the modal force error is first presented, followed by details of the projection algorithm and techniques for controlling bias due to localized model errors. The present error localization indicator is then defined using a statistical normalization of the modal force error. The variance of common model correlation measures such as the Modal Assurance Criteria are also examined, so that the variance measures for the indicator normalization can be properly interpreted. Finally, the performance of the present method is examined using experimental data.

THEORETICAL DEVELOPMENT

We define the modal force error vector R_i for mode i as

$$R_i = (K - \omega_{E_i}^2 M)\begin{Bmatrix} \phi_{m_i}^E \\ \phi_{o_i} \end{Bmatrix} \tag{1}$$

where K and M are the stiffness and mass matrices from the model, respectively, ω_{E_i} is the identified radial frequency for mode i (rad/s), $\phi_{m_i}^E$ is the identified mode shape at the sensor d.o.f., and ϕ_{o_i} is the partition of the mode shape corresponding to the unmeasured d.o.f. in the model. If the correct stiffness and mass matrices are given as

$$\begin{aligned} K_c &= K + \Delta K \\ M_c &= M + \Delta M \end{aligned} \tag{2}$$

we have

$$((K + \Delta K) - \omega_{E_i}^2 (M + \Delta M))\begin{Bmatrix} \phi_{m_i}^E \\ \phi_{o_i} \end{Bmatrix} = 0 \quad \Rightarrow \quad -R_i = (\Delta K - \omega_{E_i}^2 \Delta M)\begin{Bmatrix} \phi_{m_i}^E \\ \phi_{o_i} \end{Bmatrix} \tag{3}$$

Thus, the modal force error vector R_i contains information on both magnitude and location of the model errors $[\Delta K, \Delta M]$.

Unfortunately, the d.o.f. at which the mode shape is sampled in test is typically much smaller than the number of d.o.f. in the finite element model which defines K and M. Therefore, to apply Eqn. 1, either the model must be reduced to the measured d.o.f., or the measured portion of the mode shapes must be expanded to the displacement d.o.f. basis of the model.

PROJECTION OF EXPERIMENTAL MODE SHAPES

There have been many algorithms proposed for expanding experimental mode shapes into the d.o.f. of a finite element model (see Imregun and Ewins, 1993, for reviews of various techniques). The algorithm presented in this paper is based on the Sensitivity-Based Element-By-Element (SB-EBE) model update theory (Farhat and Hemez, 1993), which incorporates a mode shape projection theory based on a minimization of the modal force error given in Eqn. 1.

PROJECTION ALGORITHM

We seek a estimate of the unmeasured partition of the mode shape ϕ_{o_i} which minimizes the magnitude of the impedance residual, viz.

$$\min_{\phi_{o_i}} R_i^T R_i \quad \Rightarrow \quad \min_{\phi_{o_i}} (\phi_{m_i}^T Z_{mi}^T Z_{mi} \phi_{mi} + \phi_{o_i}^T [2 Z_{oi}^T Z_{mi} \phi_{mi} + Z_{oi}^T Z_{oi} \phi_{oi}]) \tag{4}$$

where $Z_i = K - \omega_{E_i}^2 M$ is the impedance of the model for experimental mode i. This leads to the following least-squares solution for ϕ_{oi}:

$$\begin{gathered} \phi_{oi} = -(Z_{oi}^T Z_{oi})^{-1} Z_{oi}^T Z_{mi} \phi_{mi} \\ \begin{Bmatrix} \phi_{mi} \\ \phi_{oi} \end{Bmatrix} = \begin{bmatrix} I \\ -(Z_{oi}^T Z_{oi})^{-1} Z_{oi}^T Z_{mi} \end{bmatrix} \phi_{mi} = P_i \phi_{mi} \end{gathered} \tag{5}$$

where P_i is the mode shape projection for mode i.

It is known, however, that when the model is in error, R_i should be nonzero even when ϕ_{o_i} is correctly determined; in fact, R_i should hopefully have a small number of (possibly) large nonzero entries. We can partition Eqn. 1 as

$$\begin{bmatrix} Z_{m_i}^A & Z_{o_i}^A \\ Z_{m_i}^B & Z_{o_i}^B \end{bmatrix} \begin{Bmatrix} \phi_{m_i}^E \\ \phi_{o_i} \end{Bmatrix} = \begin{Bmatrix} R_i^A \\ R_i^B \end{Bmatrix} \tag{6}$$

where A and B refer to a partitioning of the equations into the highest and lowest magnitudes of the entries of R_i. Then, a least-squares estimate for ϕ_{o_i} is given by

$$\phi_{o_i} = -((Z_{o_i}^B)^T (Z_{o_i}^B))^{-1} (Z_{o_i}^B)^T (Z_{m_i}^B) \phi_{m_i}^E \tag{7}$$

so long as the number of B equations is greater than the number of unmeasured d.o.f. in Z. The choice of the equation set B upon which the least-squares solution is defined is not trivial. The primary motivation for partitioning the equations is to improve the solution for ϕ_{o_i} over that obtained using the full set of equations, given the assumption that the errors in the model are not distributed uniformly among the d.o.f. but rather are localized. It should be noted that delegating the equilibrium equation for a particular d.o.f. to set A does not impede our ability to find model errors associated with that d.o.f. Indeed, it will tend to enhance the modal force error at those d.o.f. in set A since the projection matrix will not be "designed" to minimize those errors.

A generalization of the above partitioning can be obtained by introducing a weighting function

to the optimization given by Eqn. 4. In the spirit of statistical estimation, we can select an inverse weighting by the variance of the modal force error R_i. This variance reflects the uncertainty of the modal force error as a linear function of the errors in the identified modal parameters used to compute R_i. If we define the covariance matrix of R_i as Q_i, and the covariance matrix of the measured mode shape ϕ_{mi} as $Q_{\phi_{mi}}$, then

$$Q_i = Z_i P_i Q_{\phi_{mi}} P_i^T Z_i^T \tag{8}$$

Using Eqn. 8 and Eqns. 4 and 5, we obtain

$$\min(R_i^T Q_i^{-1} R_i)$$

$$\therefore P_i = \begin{bmatrix} I \\ -(Z_{oi}^T Q_i^{-1} Z_{oi})^{-1} Z_{oi}^T Q_i^{-1} Z_{mi} \end{bmatrix} \tag{9}$$

Note that a nonlinearity has been introduced, because the modal force error covariance matrix Q_i is a function of the projection matrix P_i. This can be handled in a cursory manner by predicting Q_i based on only the measured partition of Z_i, computing an estimate of P_i, correcting Q_i, and finally computing a new projection P_i based on the corrected covariance matrix.

MODEL REDUCTION

An alternative to the mode shape projection algorithm detailed above is to condense the model d.o.f. down to the set of measured d.o.f. There are a number of established techniques for model reduction, such as Guyan reduction (Guyan, 1965) and the Improved Reduced System (IRS) model (O'Callahan, 1989). The difficult trade-off in model reduction, given that the set of reduced d.o.f. are given as a consequence of the experiment design, is between the accuracy of the reduction and the sensitivity of the transformation to model errors.

A reasonable compromise is to reduce the model to the measurement d.o.f., assess the accuracy of the reduced model in terms of its ability to predict the modal parameters of the full-order model, and then add a minimum number of additional d.o.f. to the reduction in order to ensure that the reduced model predicts the analytical modes to within the uncertainty of the experimental parameters. The best choices of additional d.o.f. are either other displacements which would be useful in localizing model errors, or generalized d.o.f. such as the fixed interface modes (FIM) of the Craig-Bampton component mode synthesis technique (Craig and Bampton, 1968).

COMPUTATION OF THE LOCATION INDICATOR FOR MODEL ERROR

The computation of the impedance residual can now be written as

$$R_i = Z_i P_i \phi_{m_i}^E \tag{10}$$

and an estimate of the variance of the entries in R_i due to assumed zero-mean gaussian noise on each of the entries of $\phi_{m_i}^E$ is given by

$$\sigma_\phi^2(R_i) = Z_i P_i \Sigma_\phi P_i^T Z_i^T \tag{11}$$

where the noise covariance matrix for the elements of the measured mode shape $\phi_{m_i}^E$ is given by

. In addition, we can consider additional variance due to uncorrelated frequency uncertainty, although the frequency uncertainty is typically smaller than the mode shape uncertainty, relative to their nominal values. It can be reasonably expected (subject to the noise models assumed above and knowledge of the modal parameter variances) that an accurate analytical model will have impedance residuals $R_i < 3\sigma(R_i)$.

We define the indicator as the impedance residual estimate vector R_i normalized by the standard deviations of the estimates $\sigma(R_i)$,

$$\hat{R}_i(j) = \frac{R_i(j)}{\sigma(R_i(j))} \qquad \sigma(R_i(j)) = \sqrt{Z_i(j,:)P_i\Sigma_\phi P_i^T Z_i(j,:)^T} \tag{12}$$

Therefore, $\hat{R}_i$ can be viewed as a normalized modal force error vector, which indicates degree to which the estimated modal force error from the actual modal data exceeds the normal level of force error due to uncertainty in the modal parameters.

MODAL PARAMETER VARIANCE BASED ON RECONCILIATION CRITERIA

Since we have accepted standards for model update convergence (e.g. level of Modal Assurance Criteria, error in frequency estimates), these can be used to determine the modal variances which in turn are used to arrive at the Model Error Localization Indicator $\hat{R}_i$.

We can determine the variance of the mode shape error Σ_ϕ by determining the expected value of the Modal Assurance Criteria (MAC) as a function of Σ_ϕ. The MAC is defined as

$$MAC(\phi_i, \phi_j) = \frac{(\phi_i^T \phi_j)^2}{(\phi_i^T \phi_i)(\phi_j^T \phi_j)} \tag{13}$$

Now assume that the two mode shapes are identical, except for added noise to ϕ_j. It can be shown that, if the noise is random and of equal magnitude across the measured d.o.f. such that the covariance matrix of the mode shape is $\Sigma_\phi = \sigma_{n(i)}^2 I$ and the dimension of ϕ is N_m, then

$$E[MAC] \approx 1 - \frac{(N_m - 1)\sigma_{n(i)}^2}{\phi^T \phi} \tag{14}$$

This relation can then be used in reverse, by supposing the expected value of the MAC given an ensemble of tests, each of which yields an estimate of the mode shapes. For example, if we assume the expected value of the MAC is 0.99, then

$$\sigma_{n(i)}^2 = \frac{0.01\phi^T\phi}{N_m - 1} \Rightarrow \Sigma_\phi = \left(\frac{0.01\phi^T\phi}{N_m - 1}\right) I \Rightarrow \sigma(R_i) = \sqrt{\left(\frac{0.01\phi^T\phi}{N_m - 1}\right) \text{diag}(Z_i P_i P_i^T Z_i^T)} \tag{15}$$

EXPERIMENTAL RESULTS: INTERSTATE 40 RIO GRANDE BRIDGE

The model error localization algorithm detailed in the present paper has been implemented and checked on numerical data. Due to space considerations, those results will not be given here. Instead, the results below detail the application of the algorithm to damage detection of a highway bridge. The bridge in question is one span of Interstate 40 over the Rio Grande in Albuquerque, New Mexico. As part of a research effort by Los Alamos National Laboratory and New Mexico

State University, with the support of Sandia National Laboratories, an older section of the bridge, slated for destruction, was instrumented and modal tests performed while one of the supporting beams of the roadbed was intentionally damaged. A total of 5 modal tests were performed, with the bridge in its "pre-damage" condition and at progressively stages of damage. In each test, the first 6 modes of the bridge were identified using 26 accelerometers equally spaced on the roadbed above the two I-beams which provide the longitudinal bending support.

The corresponding modes of a finite element model of the bridge are shown in Figure 1. This model, composed of beam and plate elements, has 2027 displacement degrees of freedom. Because the number of model d.o.f. exceeds the test measured d.o.f. by almost two orders of magnitude, a significant amount of model reduction and/or mode shape projection is necessary to compute an error indicator. In this case, model reduction alone will not suffice. This can be seen in Table I. Here the modes of two reduced-order models are compared to the full-order model. The Guyan-reduced model, which includes just the 26 measured d.o.f., exhibits considerable errors, to the point where some modes of the full-order model are not present in the reduced model. A second model, using a Craig-Bampton d.o.f. basis comprised of the 26 measured d.o.f. augmented by 50 fixed-interface modal displacements (modes of the full-order model with the measured d.o.f. fixed-to-ground), is sufficient to capture the lower modes of the full-order model. To utilize this model, however, mode shape projection must be employed, to determine the displacements of the experimental modes for the unmeasured fixed interface d.o.f.

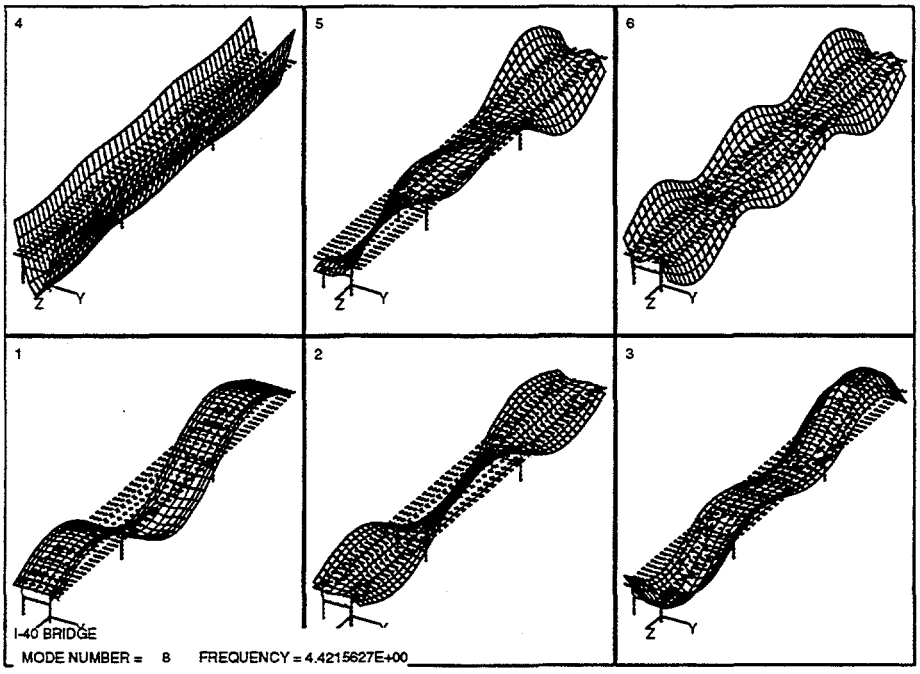

Figure 1: I-40 Rio Grande Bridge: Finite Element Modes

The results of the mode shape projection analysis for the undamaged modal test vectors is given in Table II. These tables compare and contrast the basic mode shape projection and the generalized weighted least-squares projection proposed in a preceding section of this paper. These results are determined for both the full-order model (i.e. projecting the 26 sensor d.of. to the 2027 model d.o.f.) and for the reduced-order Craig-Bampton (C-B) model using the 50 fixed interface

TABLE I: COMPARISON OF MODEL MODES FOR TWO LEVELS OF MODEL REDUCTION

Full-Order Model		Guyan Reduction to Sensor d.o.f.				C-B Model to Sensor d.o.f. + 50 FIM			
Mode #	Freq (Hz)	Mode #	Freq (Hz)	% Freq Error	MAC	Mode #	Freq (Hz)	% Freq Error	MAC
1	2.384	1	2.419	1.46	1.0000	1	2.384	0.01	1.0000
2	2.914	2	2.980	2.28	1.0000	2	2.918	0.16	1.0000
3	3.483	5	4.499	29.14	0.9848	3	3.483	0.00	1.0000
4	3.523	3	3.680	4.45	1.0000	4	3.523	0.02	1.0000
5	3.910	4	4.118	5.31	1.0000	5	3.919	0.23	1.0000
6	4.046	3	3.680	-9.06	0.9993	6	4.046	0.00	1.0000
7	4.358	5	4.499	3.23	1.0000	7	4.359	0.03	1.0000
8	4.422	6	4.812	8.83	0.9999	8	4.433	0.26	1.0000
9	5.077	1	2.419	-52.36	0.9283	9	5.077	0.00	1.0000
10	5.504	6	4.812	-12.57	0.9132	10	5.504	0.01	1.0000

TABLE II: MAC: MODEL VS. PROJECTION OF UNDAMAGED VECTORS

Mode #	Measured MAC	Full-Order Model n=2027		C-B Model (n=67)	
		Basic Projection	Weighted Projection	Basic Projection	Weighted Projection
1	0.9974	0.0002	0.8454	0.0001	0.9975
2	0.9928	0.0141	0.9146	0.0314	0.9931
3	0.9933	0.0101	0.7415	0.0315	0.9942
4	0.9778	0.0190	0.0665	0.2887	0.0806
5	0.9855	0.0185	0.9842	0.0165	0.9756
6	0.9823	0.0536	0.9882	0.0158	0.9853

modal displacements (i.e. projecting the 26 sensor d.o.f. to 76 total model d.o.f.). One problem in evaluating the projections using experimental data is that we do not know the correct responses for the unmeasured d.o.f. One method of evaluation, however, is to compare the MAC between the projected experimental mode shape and model mode shape to the MAC determined by just the measured portions of the two mode shapes. It can be supposed that, if the measured d.o.f. of the model are a reasonable sample of the full mode shape, then the MAC determined by the measured partition will be representative of the MAC between the full mode shapes. Based on this supposition, we can make the following observations.

First, note that the weighted projection is crucial in determining projected mode shapes which are reasonable with respect to the analytical mode shapes. Furthermore, the mode shapes projected into the d.o.f. of the C-B model are more reliable than the projection into the full-order finite element model. This can be seen particularly with the undamaged vector case. Here the MAC between the measured partition of the model's modes and the test modes are quite high, indicating that the model can accurately predict the experimental mode shapes, at least from the point of view of the measured d.o.f. The projected mode shapes for the full-order model, how-

ever, have significantly lower modal assurance criteria, which would be indicative of either significant modeling error or significant error in the experimental mode shape. The C-B model, on the other hand, retains the higher MAC of the measured partitions. Since both models are equivalent in terms of their ability to predict these modes (as was seen in Table I) it is reasonable to attribute these differences to our ability to project the mode shapes into these different displacement sets. Finally, note that the project of mode 4 for all of the models is significantly in error. The cause of these errors is not evident in either the data or the model, but it is likely these is some model form error which is not observable from the measured d.o.f.

The results of the model error localization are shown in Figures 2 through 4. In Figure 2, a comparison of the modal force error vector and the error indicator, which is the force vector normalized by its standard deviation, is shown for the undamaged and full damage cases for mode 1. The measured d.o.f. showing large force errors for both cases are at sensors 1 and 14, which are at the supported ends of the bridge and far away from the actual damage. The error indicator, on the other hand, shows that none of the d.o.f. have a significant level of error in the undamaged condition, while in the damaged condition many d.of. exhibit indications of damage. In fact, d.o.f. 20, associated with sensor 20, shows the highest error indicator and is directly above the location on the support beam where the structural damage was introduced. Figure 3 shows a composite error indicator (root-sum-square of the 6 modess) for the undamaged condition and for damage cases 2 through 4. Note again the clear error indicator associated with d.o.f. 20 in damage case 4. Also, there is a consistent indicator of damage or model error associated with d.o.f. 10-12 for all of the cases. This is associated with the undamaged support beam and is not in the same area of the bridge as the damage. Finally, Figure 4 shows the composite model error indicator for the 4 damage cases divided by the pre-damage error indicator. This gives the best indicator for the damage, and shows that the damage is not detectable in any of the prior partial damage conditions.

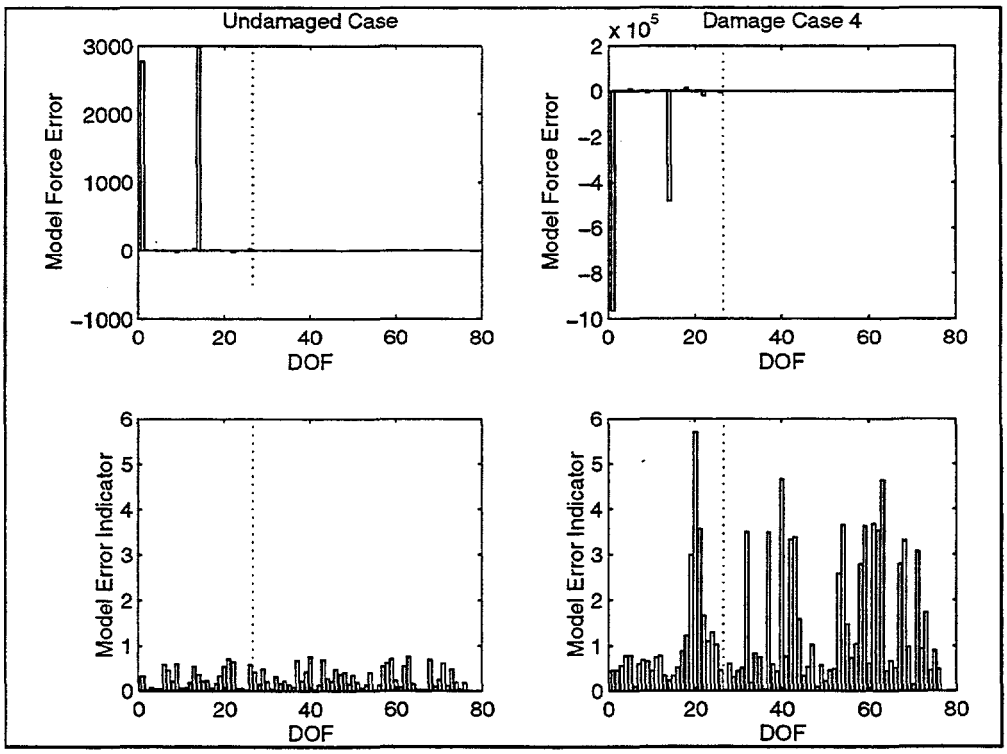

Figure 2: Comparison of Modal Force and Indicator: Results for Mode 1

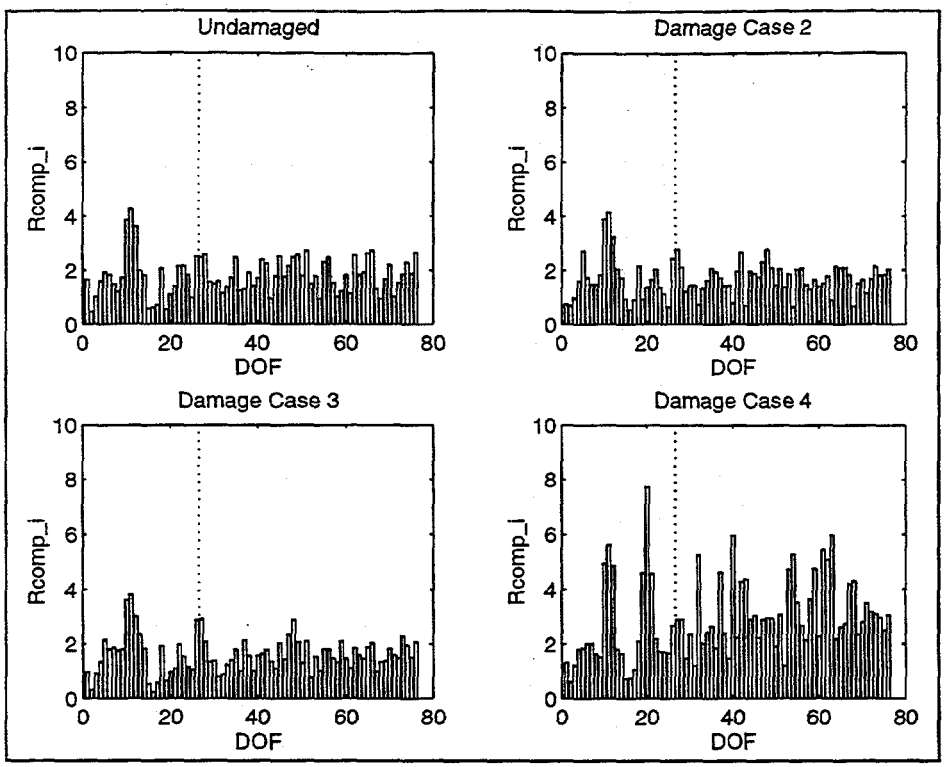

Figure 3: Composite Error Indicator

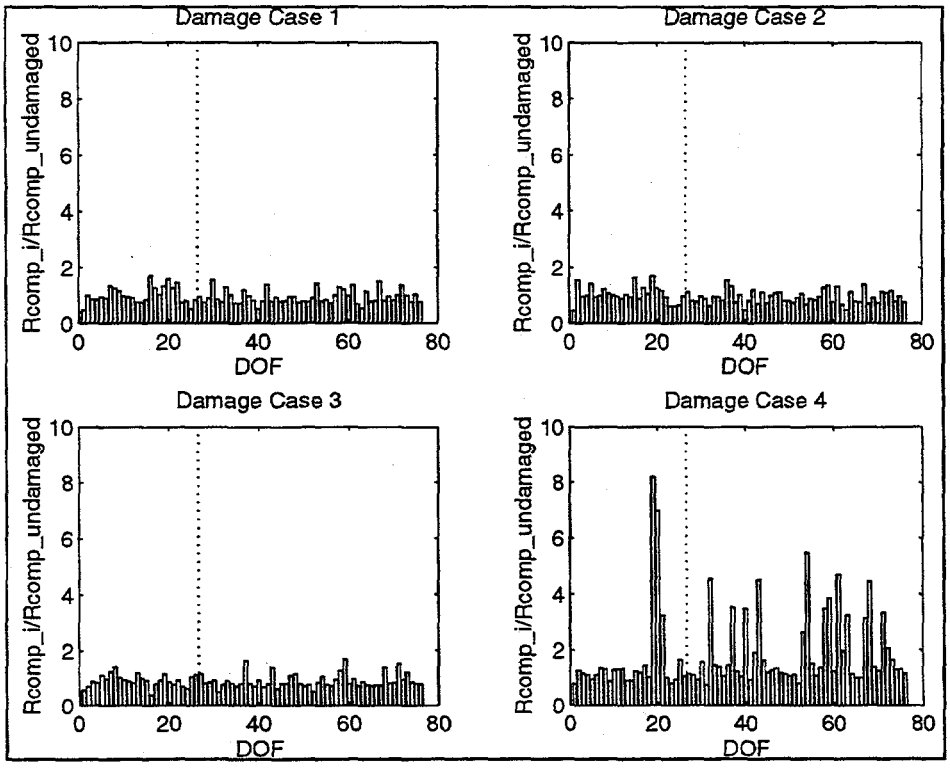

Figure 4: Damage Indicator: Ratio of Error Indicators for Damage Levels

CONCLUSIONS

A method for localizing modeling errors using experimental modal parameters has been presented. The method is robust in the sense that it incorporates the variance of the experimental data used in the localization indicator, and can find errors which would otherwise be masked by stiff areas of the structure. The method can utilize a mix of model reduction and mode shape projection, and a new mode shape projection algorithm is derived which also incorporates statistical measures to reduce bias caused by imperfect experimental data. The method has been successfully applied to damage detection in a highway bridge and is currently being implemented for use as a pre-processor in test-analysis model reconciliation.

ACKNOWLEDGMENTS

This work was supported by the Department of Energy under contract DE-AC04-94AL85000. The author wishes to thank Dr. John Red-Horse of Sandia National Laboratories and Prof. Francois Hemez of Ecole Centrale Paris for their help and encouragement.

REFERENCES

Craig, R. and M. Bampton. 1968. "Coupling of Substructures for Dynamic Analyses," AIAA Journal, Vol. 6, No. 7, pp. 1313-1319.

Farhat, C. and F. M. Hemez. 1993. "Updating Finite Element Dynamic Models Using an Element-By-Element Sensitivity Methodology," AIAA Journal, Vol. 31, No. 9, pp. 1702-1711.

Guyan, R. J. 1965. "Reduction of Mass and Stiffness Matrices," AIAA Journal, Vol. 3, No. 2.

Imregun, M. and D. J. Ewins. 1993. "An Investigation into Mode Shape Expansion Techniques," Proceedings of the 11th International Modal Analysis Conference, Kissimmee, FL, pp. 168-175.

Kaouk, M. and D C. Zimmerman. 1994. "Structural Damage Assessment Using a Generalized Minimum Rank Perturbation Theory," AIAA Journal, Vol. 32, No. 4, pp.836-842.

O'Callahan, J. 1989. "A Procedure for an Improved Reduced System (IRS) Model," 7th International Modal Analysis Conference, Las Vegas, NV.

Ojalvo, I. U. and D. Pilon. 1988. "Diagnostics for Geometrically Locating Structural Math Model Errors from Modal Test Data," Proceedings of 29th AIAA/ASME/ASCE/AHS/ASC Structures, Structural Dynamics and Materials Conference, Paper No. AIAA-88-2358-CP, Williamsburg, VA, pp. 1774-1186.

BIOGRAPHY

Kenneth Alvin received his B.S. in Aerospace Engineering from Iowa State University in 1983. From 1983 to 1989 he was a project engineering in Structural Analysis at Harris Corporation Aerospace Systems Division. He received his M.S. in 1990 and Ph.D. in 1993 in Aerospace Engineering Sciences from University of Colorado at Boulder. Since 1994 he has been a Research Fellow in Structural Dynamics at Sandia National Laboratories. His research interests are in system identification, structural dynamics and finite element methods.

Intentionally Left Blank

APPENDIX M

ISSUES RELATED TO RESONANT FATIGUE TESTING OF A COMPOSITE WIND TURBINE BLADE

Tom Rice, Tom Carne, George James, and Paul Veers

Presented at the Wind Energy '96 Conference
Houston, TX

January 29-31, 1996

Intentionally Left Blank

Issues Related to Resonant Fatigue Testing of a Composite Wind Turbine Blade

Sandia National Laboratories

Thomas M. Rice, Thomas G. Carne, George H. James & Paul S. Veers
Sandia National Laboratories
Albuquerque, New Mexico 87185-0557
Phone: 505-845-9846
Fax: 505-844-0078
Email: tmrice@sandia.gov

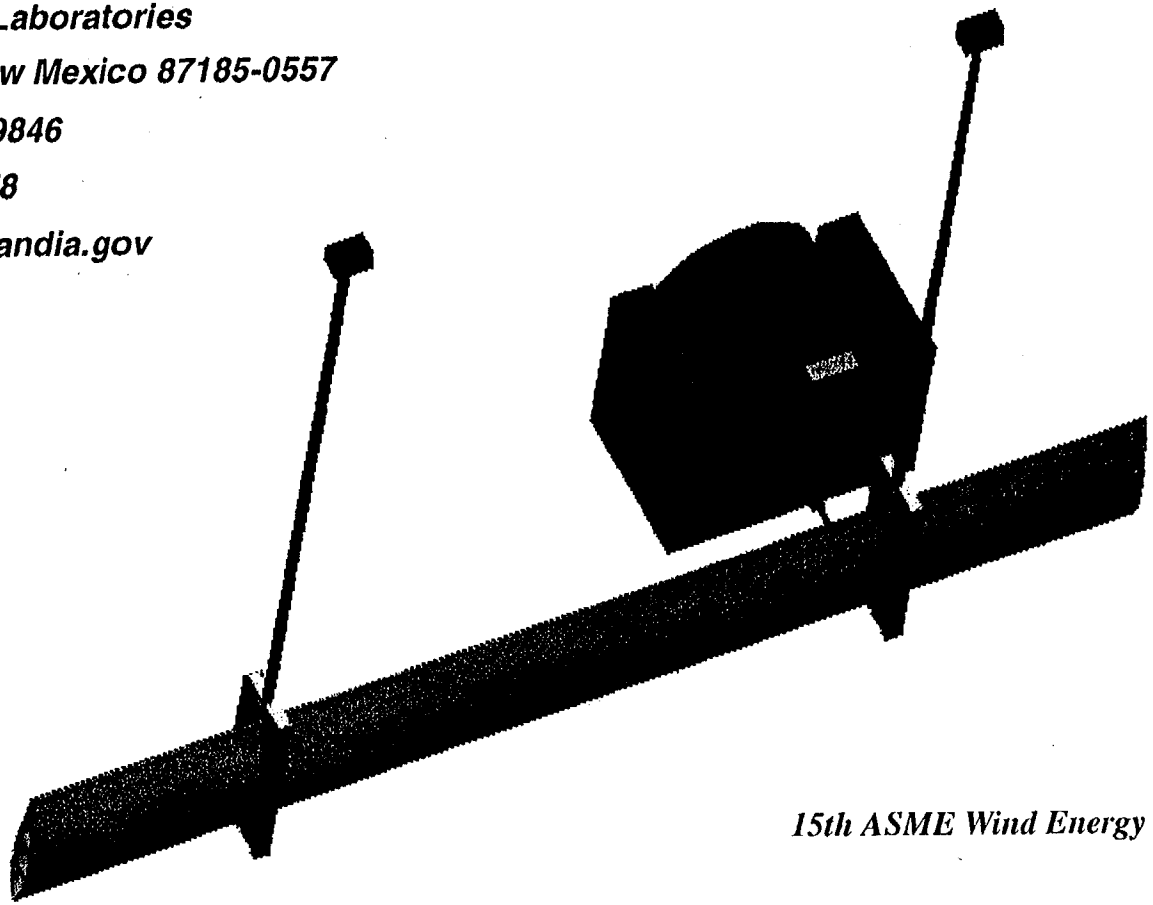

15th ASME Wind Energy Symposium

Objectives

Sandia National Laboratories

- **Develop Resonant Fatigue Testing**
- **Fatigue FloWind Blade**
- **Data for Health Monitoring Project**
- **Successful Test**

Resonant Fatigue Testing

Sandia National Laboratories

- **Blade Test**
- **Dynamic Force**
- **Light Damping → High Q**
- **Input → Stress**
- **Stinger Design**

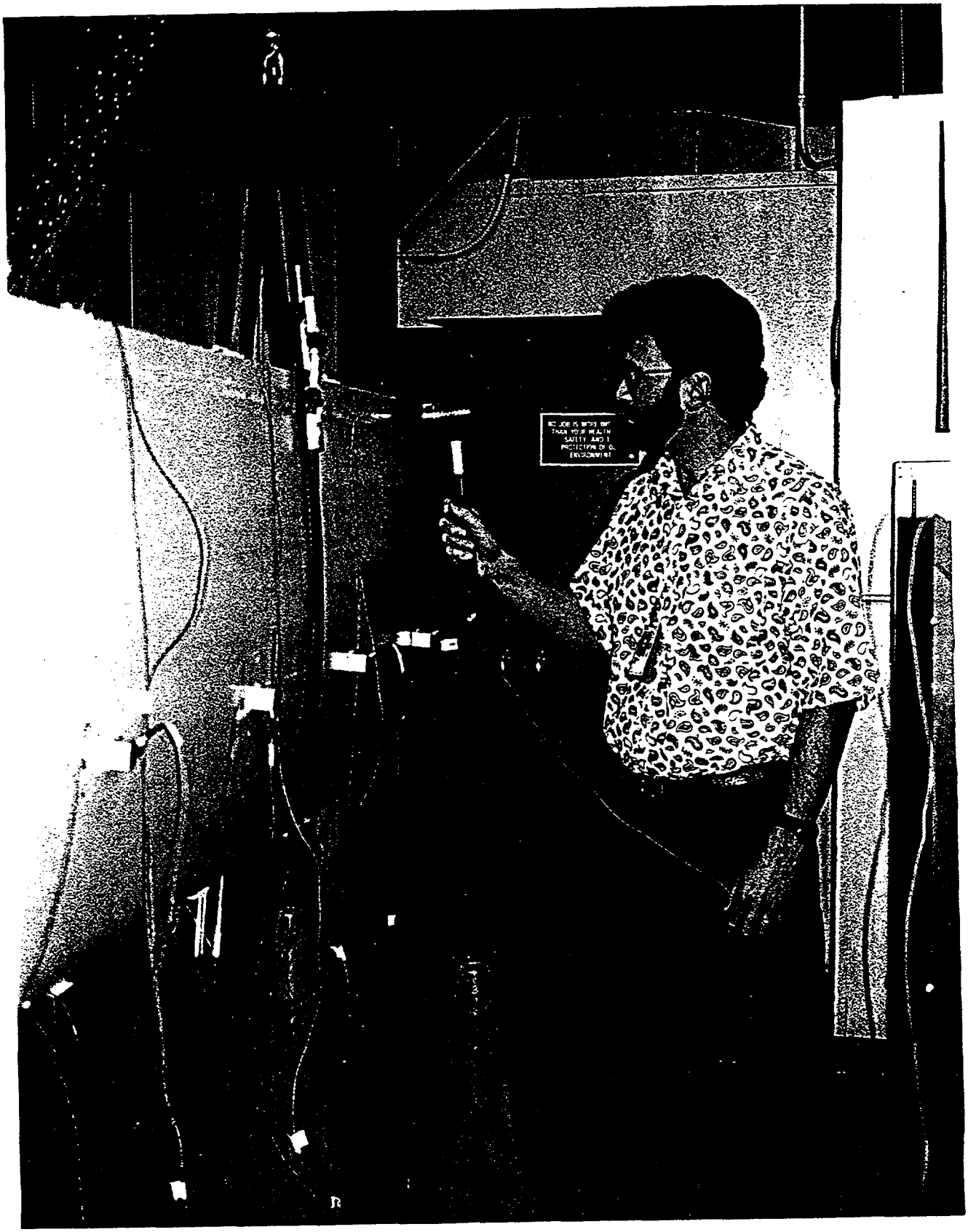

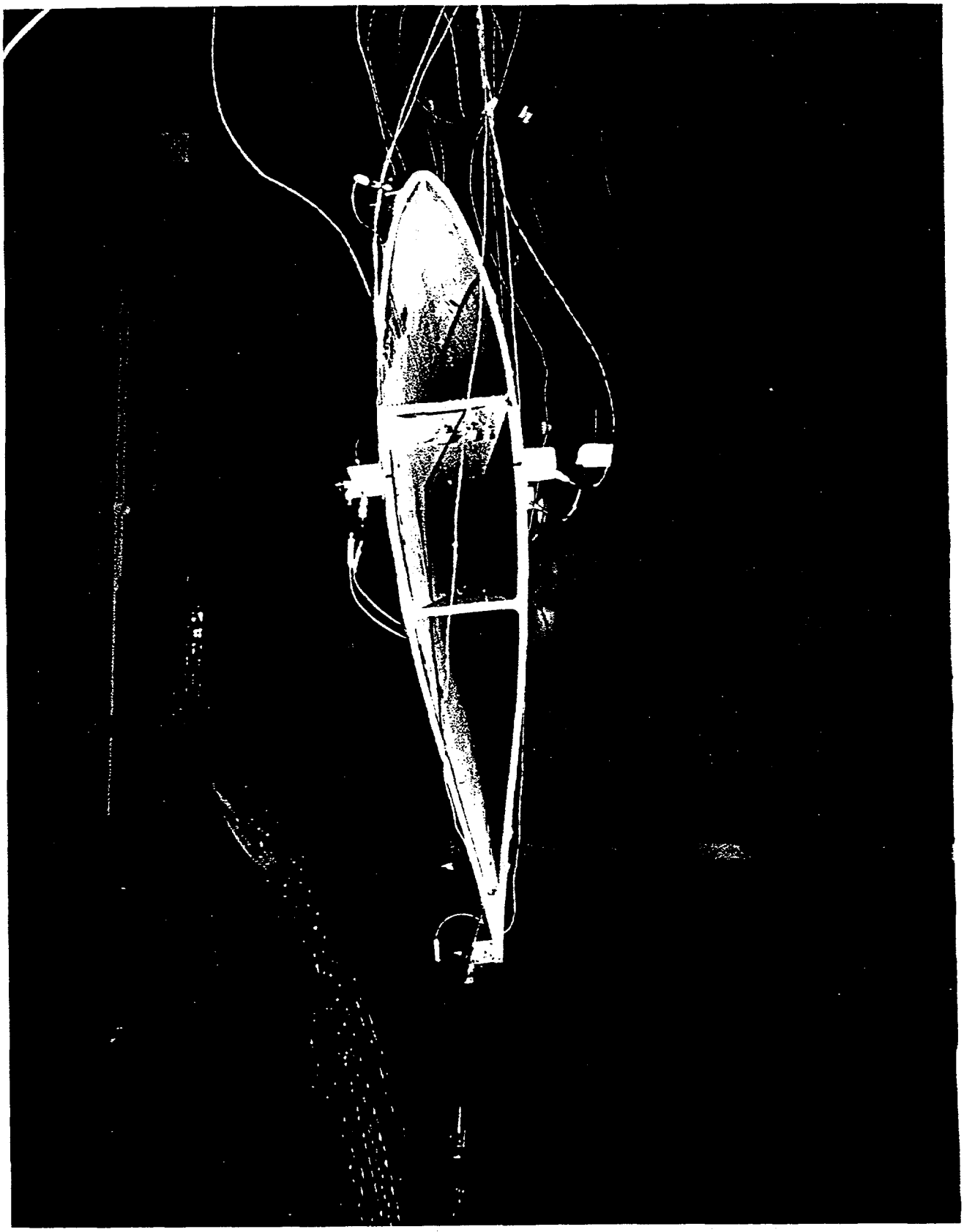

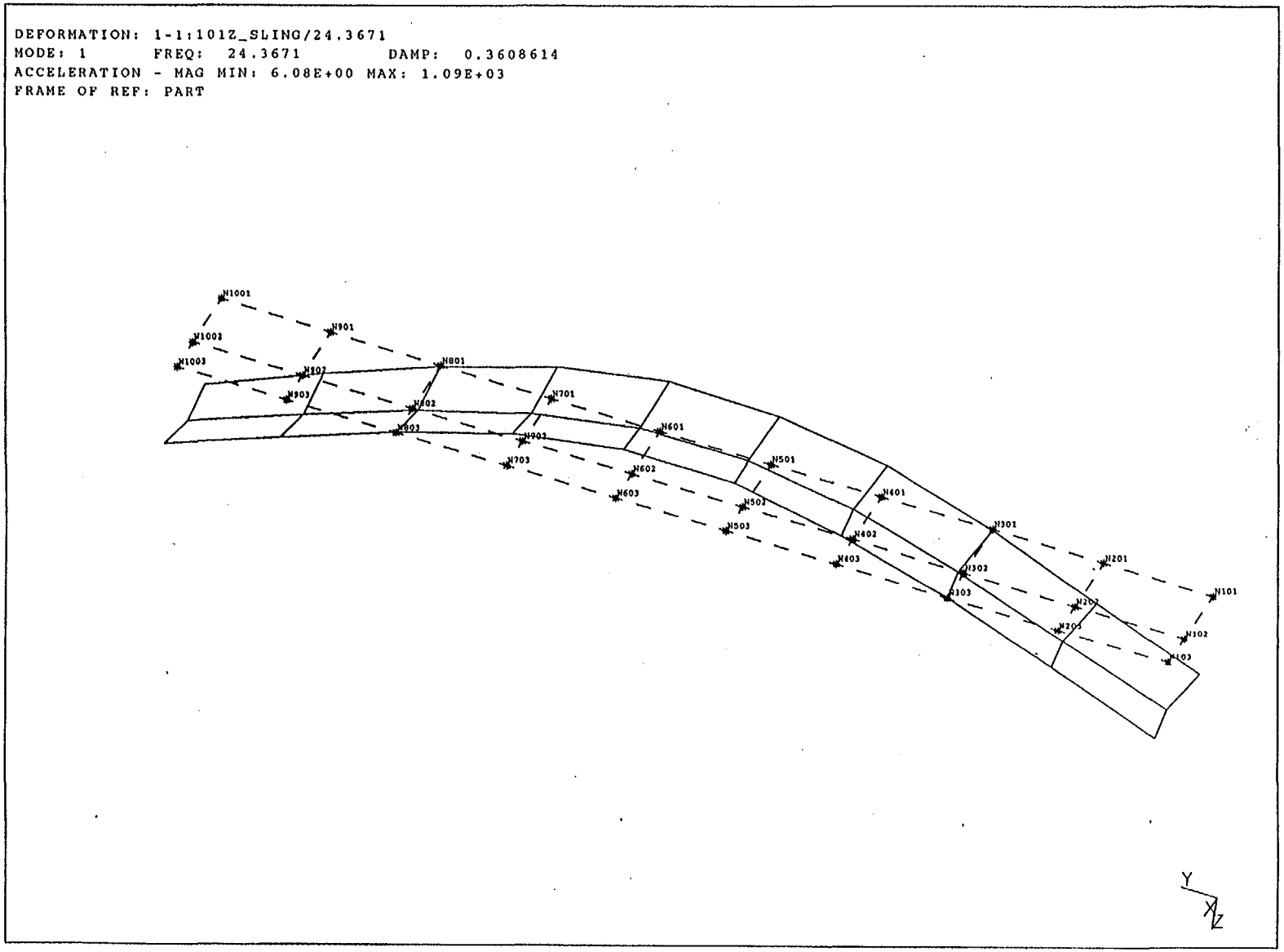
DEFORMATION: 1-1:101Z_SLING/24.3671
MODE: 1 FREQ: 24.3671 DAMP: 0.3608614
ACCELERATION - MAG MIN: 6.08E+00 MAX: 1.09E+03
FRAME OF REF: PART
N1001
N901
N1003
N801
N701
N601
N501
N401
N301
N201
N101
N102
N103
N203
N303
N403
N503
N603
N703
N803
N903
N1003
Y
X
Z

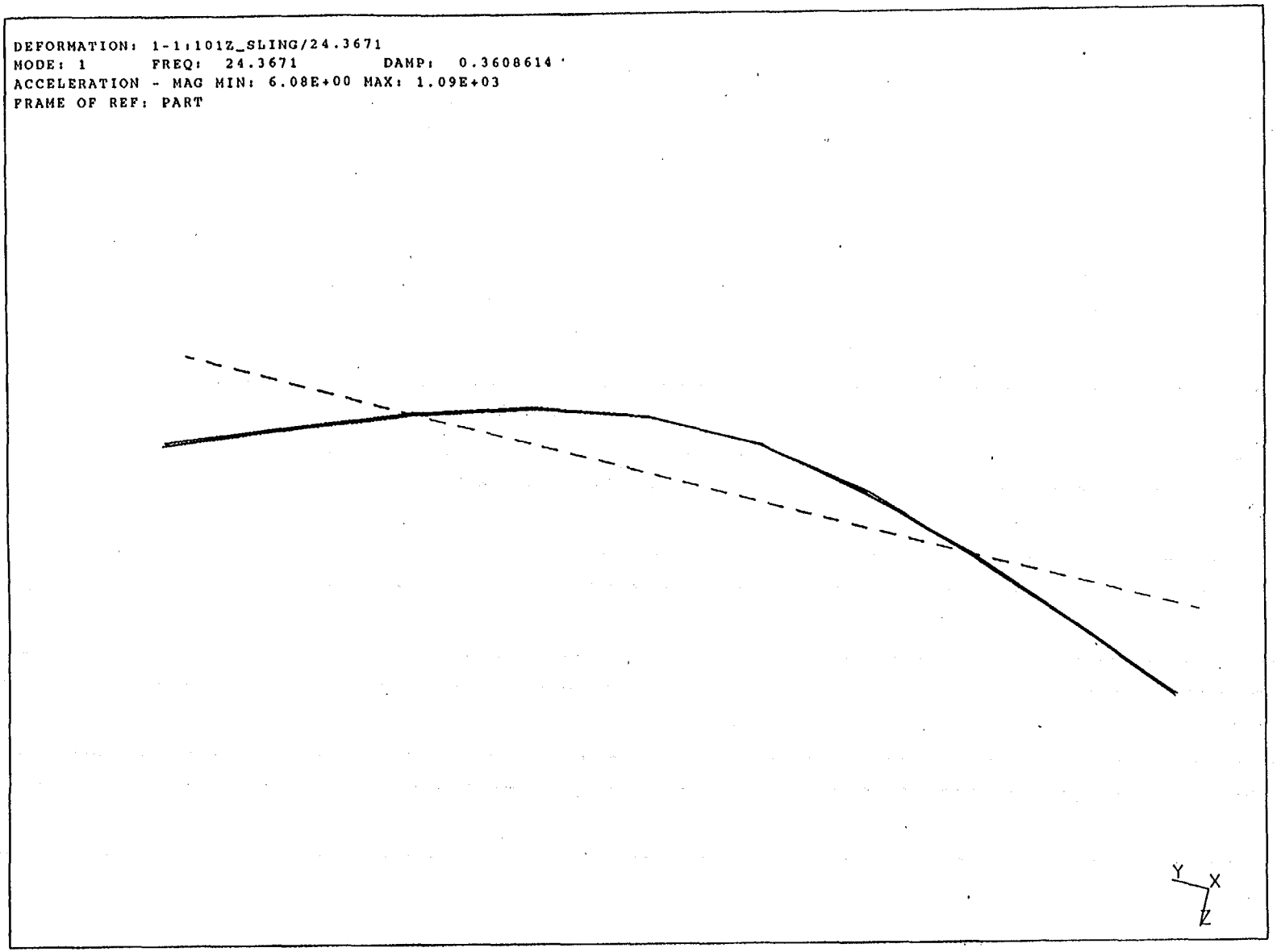
DEFORMATION: 1-1:101Z_SLING/24.3671
MODE: 1 FREQ: 24.3671 DAMP: 0.3608614
ACCELERATION - MAG MIN: 6.08E+00 MAX: 1.09E+03
FRAME OF REF: PART
Y
X
Z

Resonant Fatigue Testing

Sandia National Laboratories

- **Blade Test**
- ☞ **Dynamic Force**
- ☞ **Light Damping → High Q**
- **Input → Stress**
- **Stinger Design**

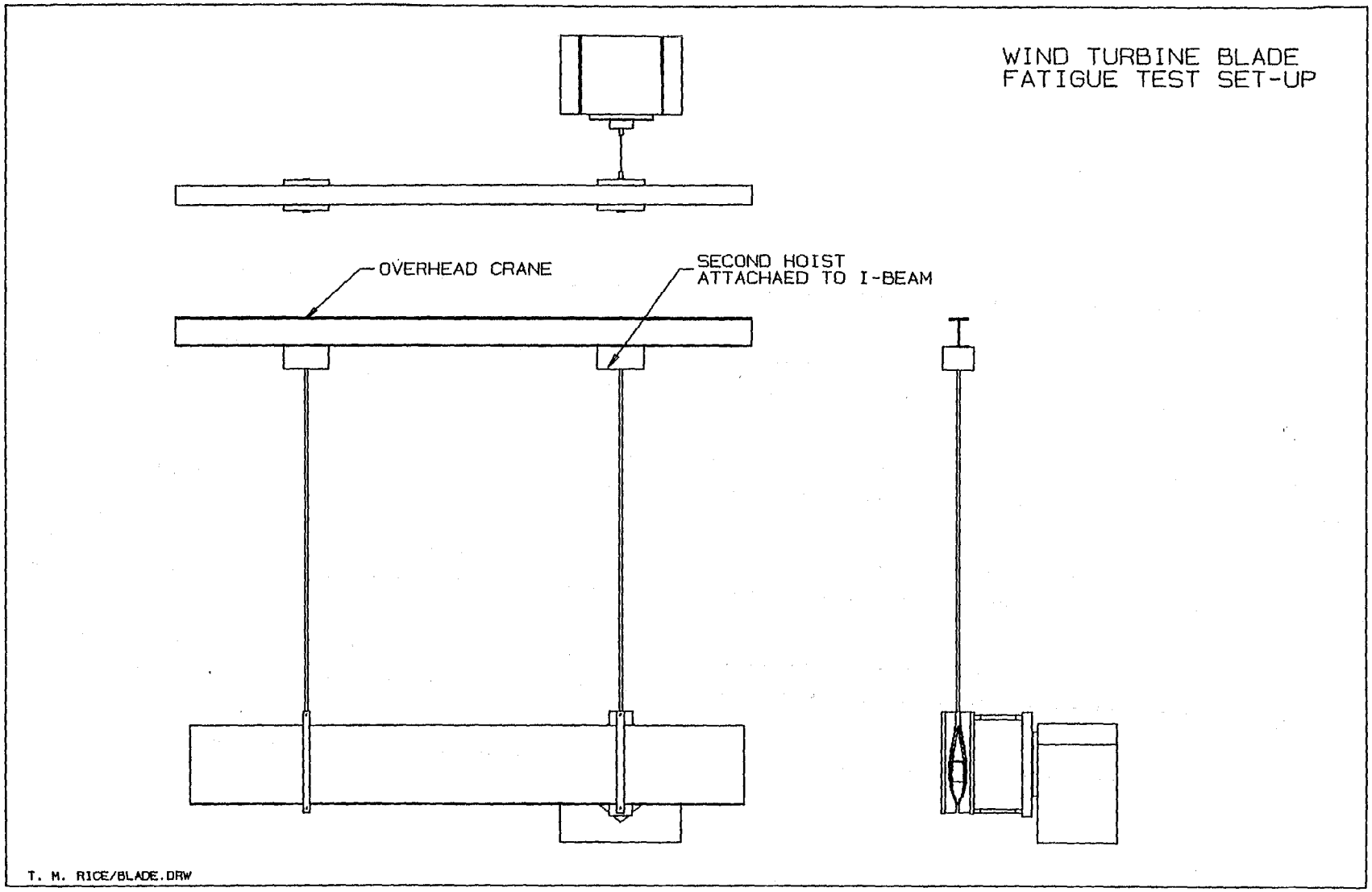
WIND TURBINE BLADE
FATIGUE TEST SET-UP
OVERHEAD CRANE
SECOND HOIST
ATTACHAED TO I-BEAM
T. M. RICE/BLADE.DRW

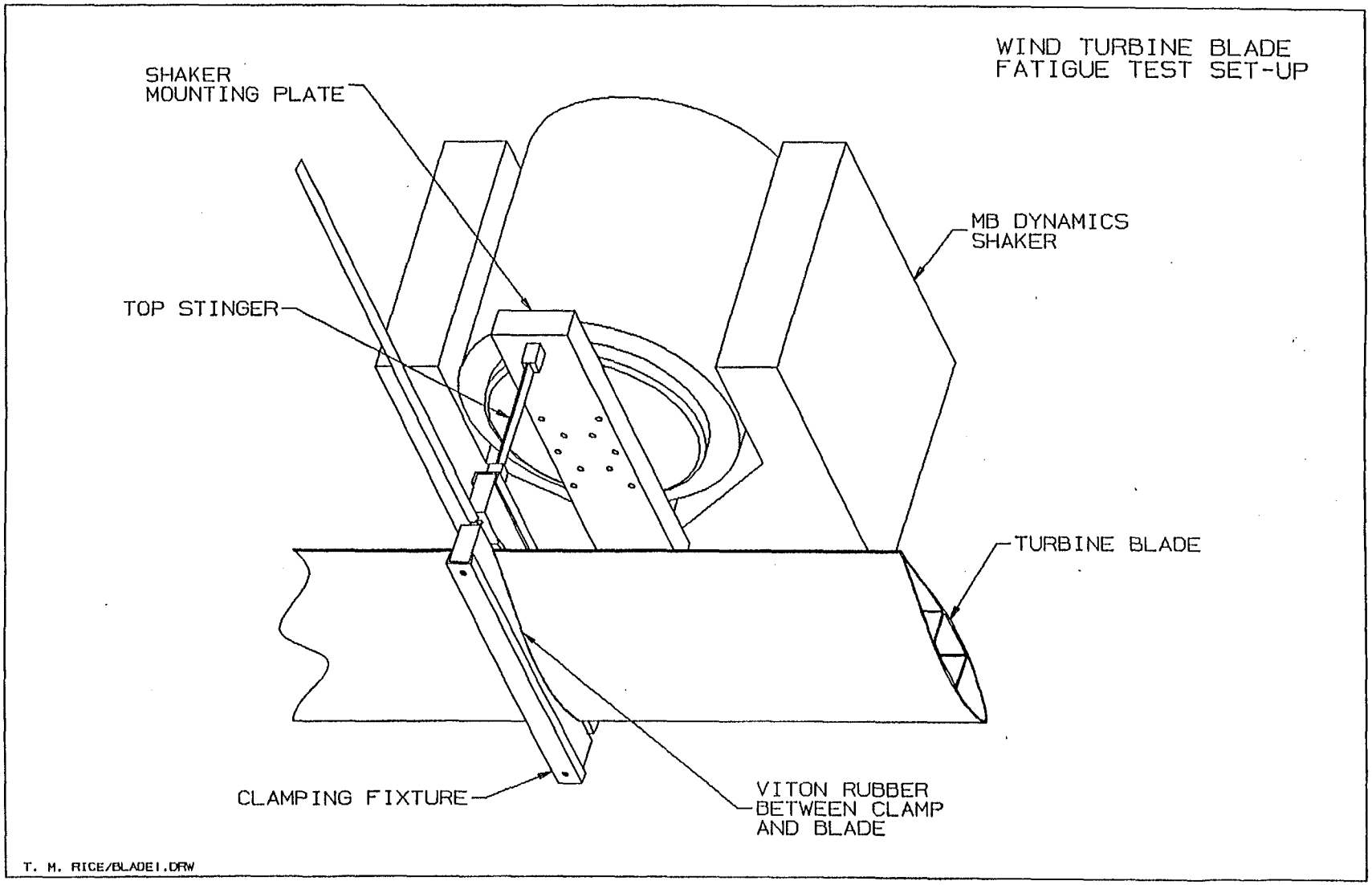
WIND TURBINE BLADE
FATIGUE TEST SET-UP
SHAKER
MOUNTING PLATE
MB DYNAMICS
SHAKER
TOP STINGER
TURBINE BLADE
CLAMPING FIXTURE
VITON RUBBER
BETWEEN CLAMP
AND BLADE
T. M. RICE/BLADE1.DRW

Resonant Fatigue Testing

Sandia National Laboratories

- Blade Test
- Dynamic Force
- Light Damping → High Q
- ☞ Input → Stress
- Stinger Design

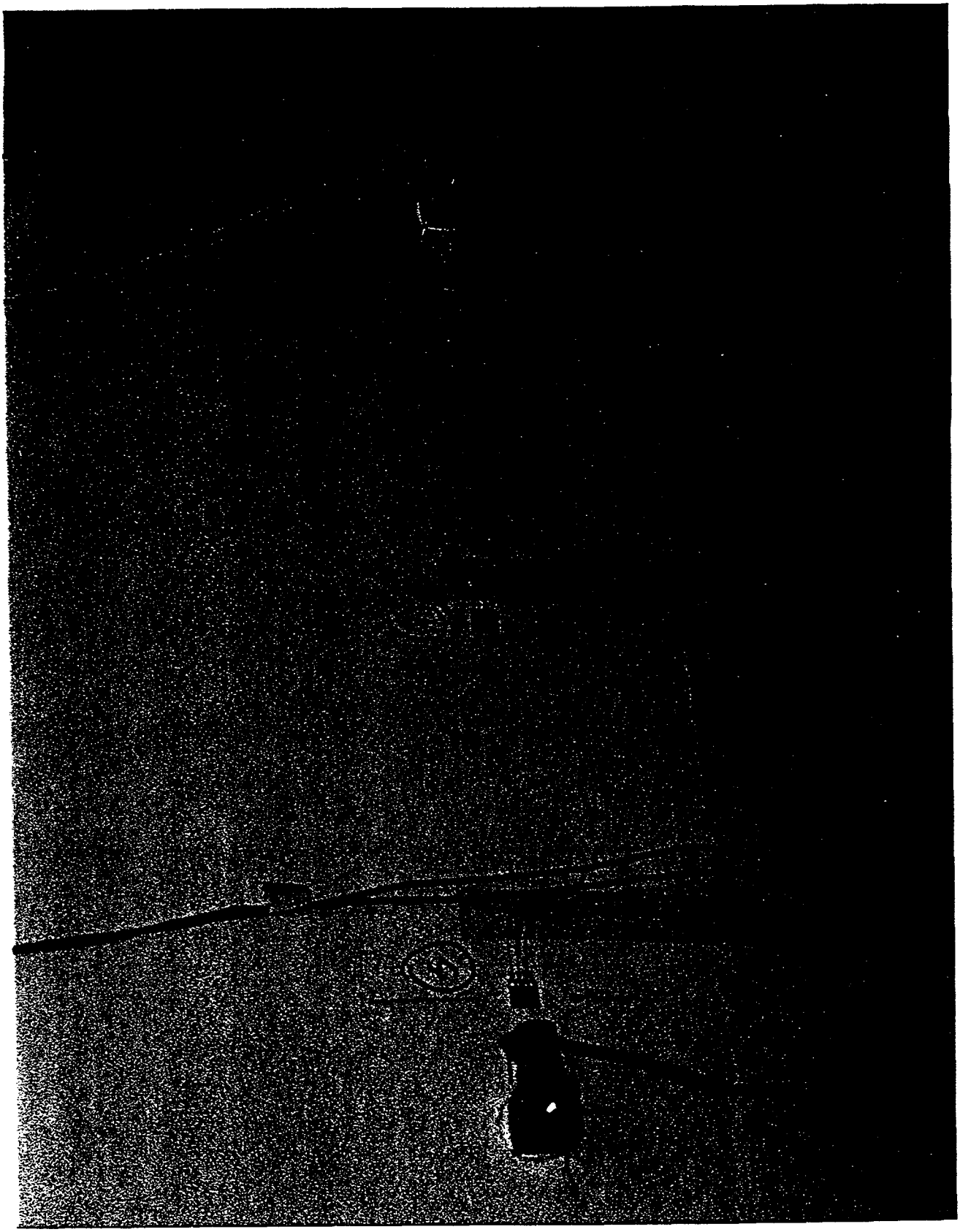

Resonant Fatigue Testing

Sandia National Laboratories

- **Blade Test**
- **Dynamic Force**
- **Light Damping → High Q**
- **Input → Stress**
- ☞ **Stinger Design**

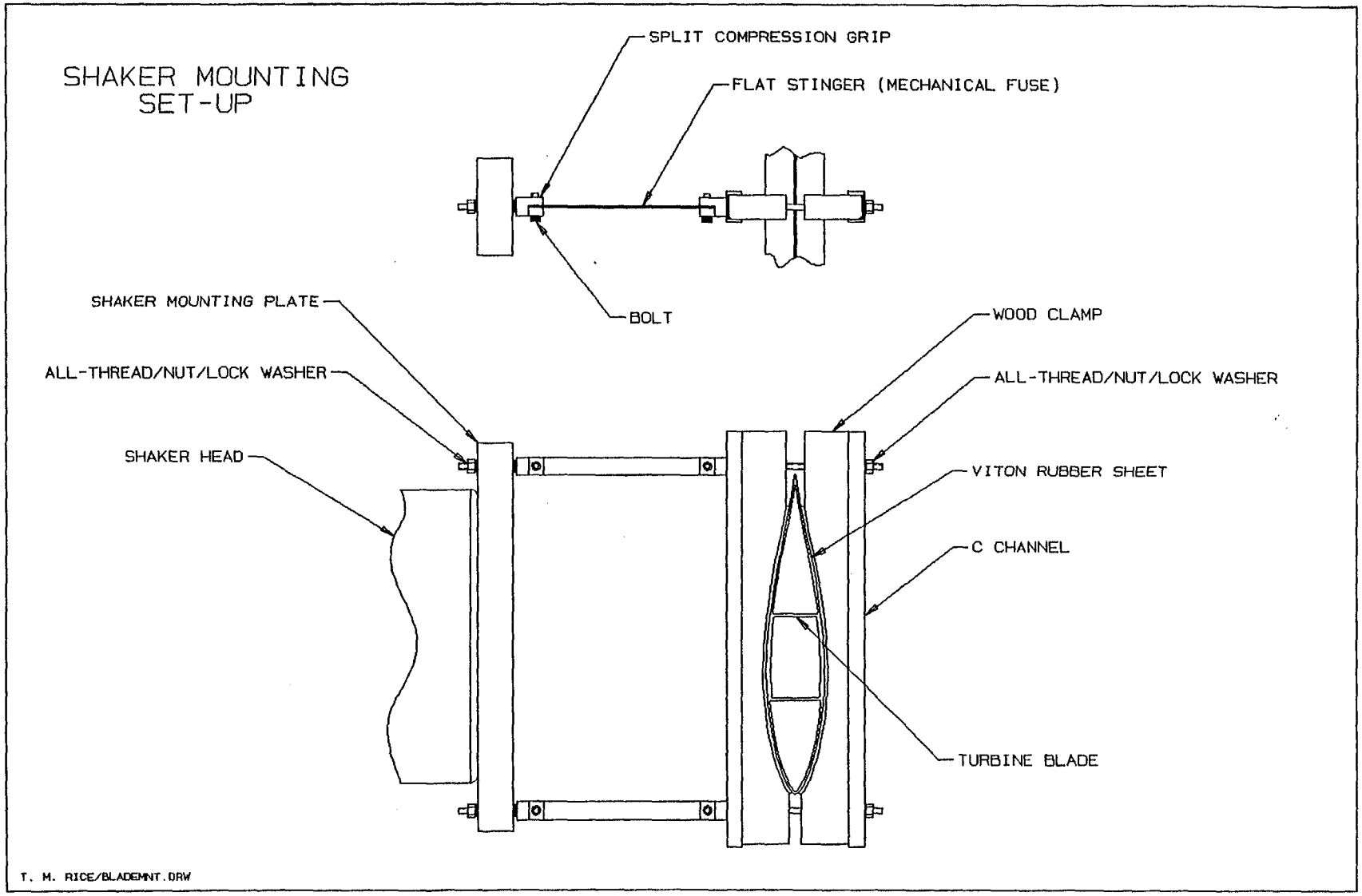
SHAKER MOUNTING
SET-UP
SPLIT COMPRESSION GRIP
FLAT STINGER (MECHANICAL FUSE)
BOLT
SHAKER MOUNTING PLATE
ALL-THREAD/NUT/LOCK WASHER
SHAKER HEAD
WOOD CLAMP
ALL-THREAD/NUT/LOCK WASHER
VITON RUBBER SHEET
C CHANNEL
TURBINE BLADE
T. M. RICE/BLADEMNT.DRW

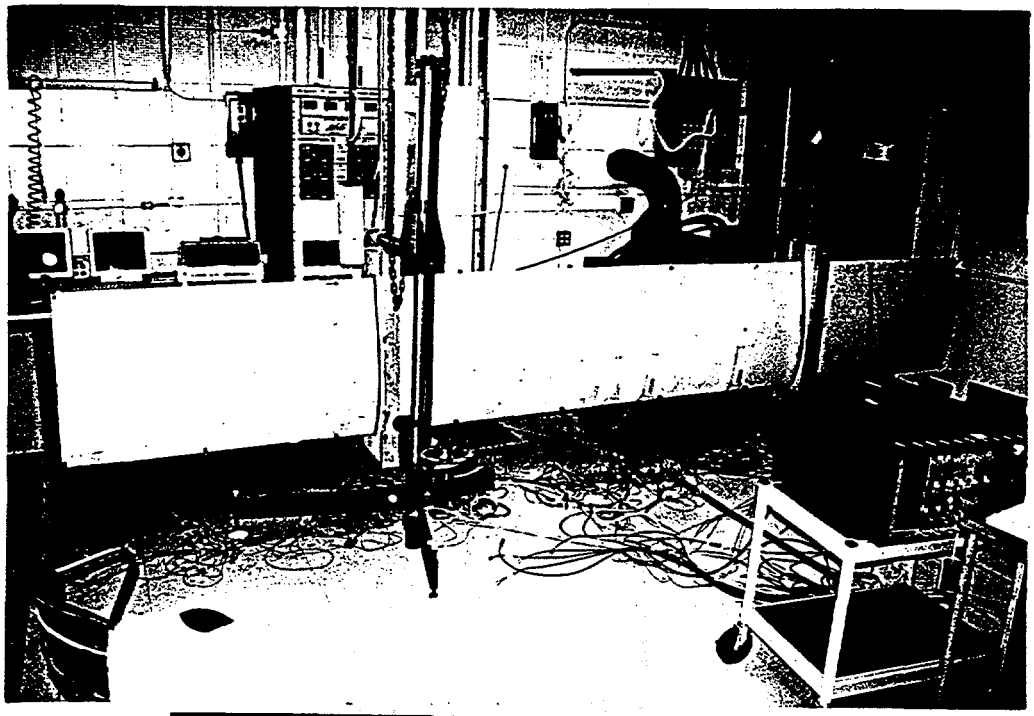

Health Monitoring

Sandia National Laboratories

- **Monitor Structural Health**
- **Develop Predictive Failure Tool**

62.5k cycles → Modal Test
62.5k cycles → Modal Test
125k cycles → Modal Test
250k cycles → Modal Test
500k cycles → Modal Test

Health Monitoring (cont.)

Sandia National Laboratories

Cycles	Total	Strain	Test
62.5k	62.5k	1700με	Modal
62.5k	125k	1700με	Modal
125k	250k	1700με	Modal
250k	500k	1700με	Modal
500k	1000k	1700με	Modal
125k	1125k	2200με	Modal
125k	1250k	2200με	Modal
74.8k	1325k	2200με	Failure

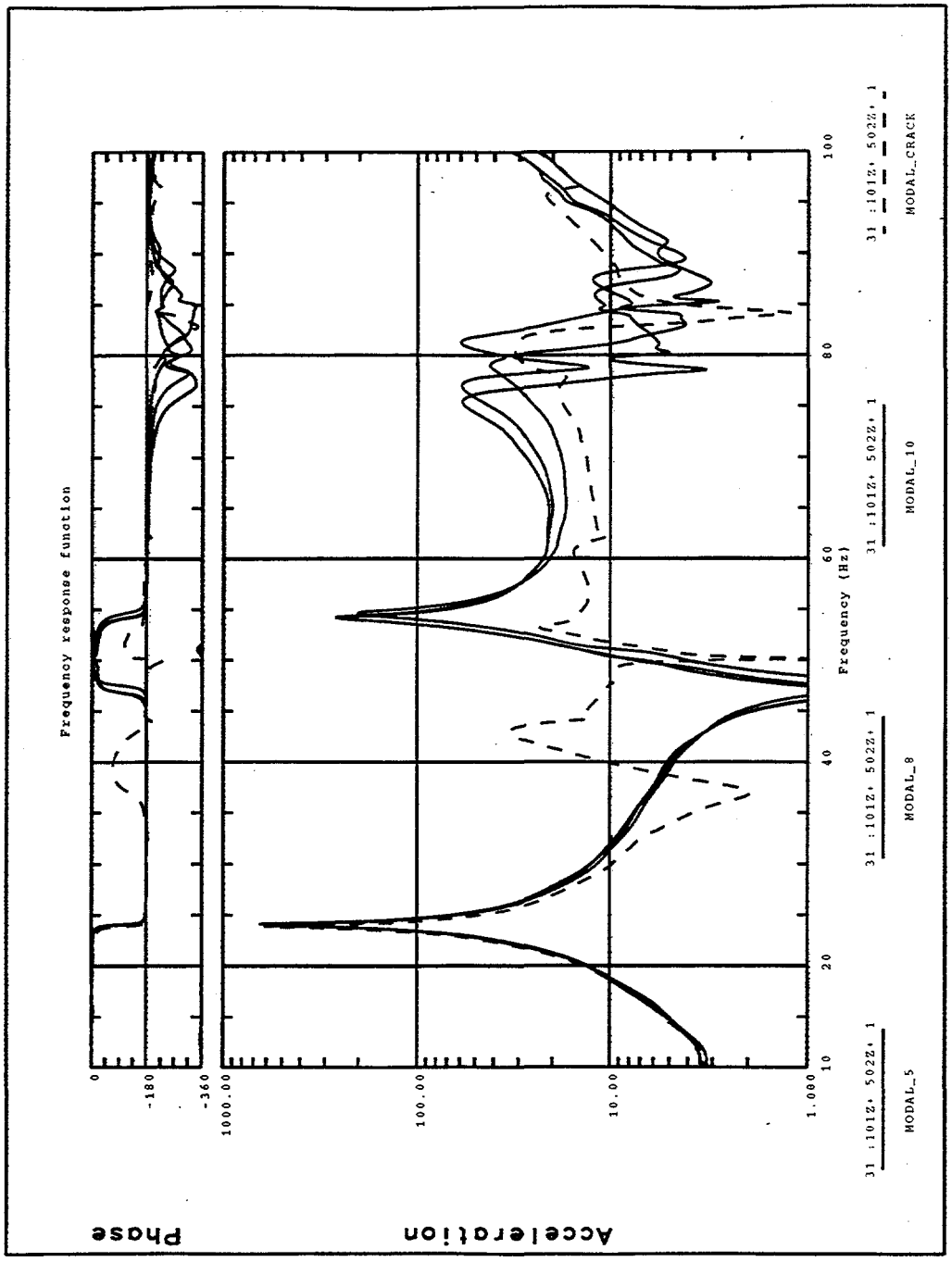
Frequency response function
Phase
Acceleration
0
-180
-360
1000.00
100.00
10.00
1.000
10
20
40
60
80
100
Frequency (Hz)
31 :101Z, 502Z, 1
MODAL_5
31 :101Z, 502Z, 1
MODAL_8
31 :101Z, 502Z, 1
MODAL_10
31 :101Z, 502Z, 1
MODAL_CRACK

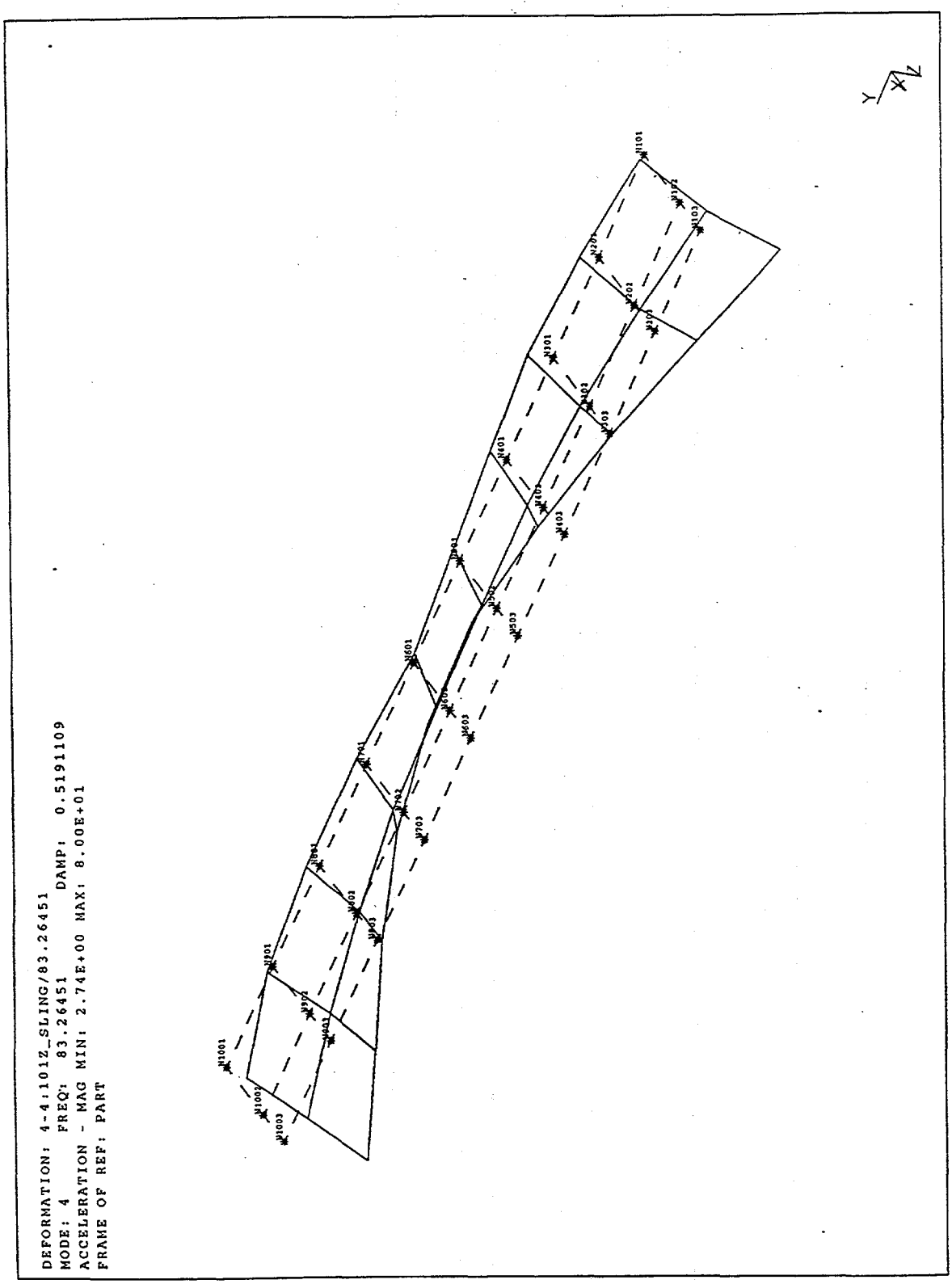
DEFORMATION: 4-4:1012_SLING/83.26451
MODE: 4 FREQ: 83.26451 DAMP: 0.5191109
ACCELERATION - MAG MIN: 2.74E+00 MAX: 8.00E+01
FRAME OF REF: PART
Y
Z
X

DEFORMATION: 4-4:101Z_SLING/83.26451
MODE: 4 FREQ: 83.26451 DAMP: 0.5191109
ACCELERATION - MAG MIN: 2.74E+00 MAX: 8.00E+01
FRAME OF REF: PART

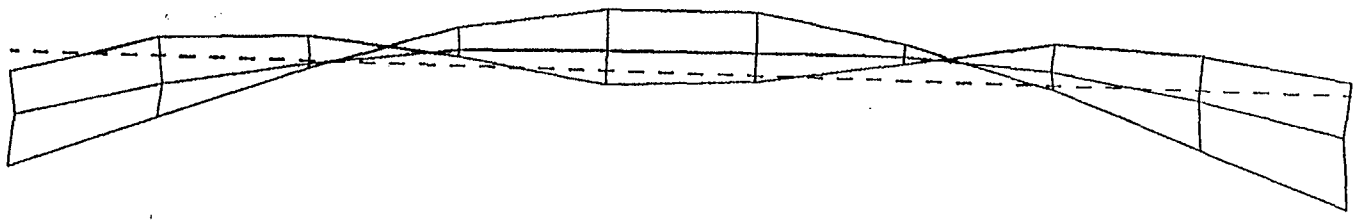

Test Success (Blade Failure)

Sandia National Laboratories

- **Axial Crack**
  - **Few Cross Plies**
  - **Not in Highest Stress/Strength Location**
  - **1,325,000 Cycles**

- **Rapid Testing**
  - **15.5 Total Hours to Fatigue Blade (1,325,000 cycles)**

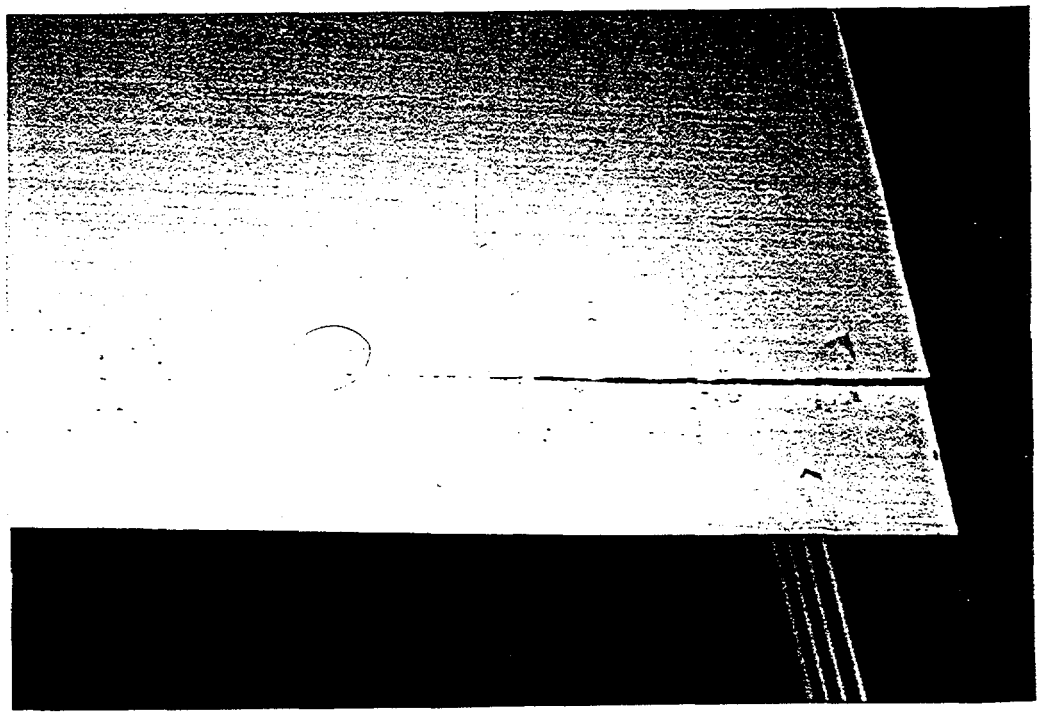

Conclusions

Sandia National Laboratories

- **Blade Failure**
- **Resonant Fatigue Testing Works**
- **Lessons Learned**
- **Health Monitoring Continuing - Initial Results Look Promising**
- **Field Testing**

APPENDIX N

DAMAGE DETECTION IN AIRCRAFT STRUCTURES USING DYNAMICALLY MEASURED STATIC FLEXIBILITY MATRICES

Nikki Robinson, Lee Peterson, George James, and Scott Doebling

Proceedings of the 12th SEM International Modal Analysis Conference
Dearborn, MI

February 12-15, 1995

Intentionally Left Blank

DAMAGE DETECTION IN AIRCRAFT STRUCTURES USING DYNAMICALLY MEASURED STATIC FLEXIBILITY MATRICES

N.A. Robinson[1], L.D. Peterson[2]
University of Colorado
Center for Aerospace Structures and
Department of Aerospace Engineering Sciences
Boulder, Colorado 80309-0429
G.H. James[3]
Sandia National Laboratories
Experimental Structural Dynamics Department
Albuquerque, New Mexico 87185-0557
S.W. Doebling[4]
Los Alamos National Laboratory
Engineering Analysis Group
Engineering Sciences and Applications Division
Los Alamos, New Mexico 87545

ABSTRACT

Two methods for detecting the location of structural damage in an aircraft fuselage using modal test data are presented. Both methods use the dynamically measured static flexibility matrix, which is assembled from a combination of measured modal vectors, frequencies, and driving point residual flexibilities. As a consequence, neither method requires a mode-to-mode correlation, and both avoid tedious modal discrimination and selection. The first method detects damage as a softening in the point flexibility components, which are the diagonal entries in the flexibility matrix. The second method detects damage from the disassembled elemental stiffnesses as determined using a presumed connectivity. Vibration data from a laser vibrometer is used to measure the modal mechanics of a DC9 aircraft fuselage before and after induced weakening in a longitudinal stringer. Both methods are shown to detect the location of the damage, primarily because the normal stiffness of the reinforced shell of the fuselage is localized to a few square centimeters.

INTRODUCTION

In the development and maintenance of aerospace and civil structures, the ability to evaluate the integrity of the structure is an increasingly important technology. Commercial aircraft, for instance, are remaining in service long past their designed lifetime because replacement costs are impractical. For this reason, structural inspection must be done at regular intervals but with minimal impact on the operation of the aircraft. Consequently, inspection techniques which require little or perhaps no dissection of the aircraft are important to maintaining their safety.

Assessing the structural condition without removing the individual structural components is known as non-destructive evaluation (NDE) or non-destructive inspection (NDI). Many NDE methods have been developed, and a good overview of the various techniques is presented by Witherell [1]. Examples of these techniques include visual inspection of cracks and dye-penetrant inspection of cracks. While techniques such as these directly detect damage as discontinuities in the physical properties of the structure, they are time consuming and labor intensive because they are highly localized measurements. To address these problems, researchers have been recently developing an entirely different set of techniques based on the interpretation of measured changes in the global mechanical properties of the structure. These more global methods of damage detection can potentially reduce the required number of locations which must be inspected by the highly localized direct NDE methods.

The use of modal test data to locate structural damage is one approach for determining changes in the global mechanical properties of a structure. This is primarily because modal techniques for data re-

1. Graduate Research Assistant
2. Associate Professor
3. Senior Member Technical Staff
4. Postdoctoral Research Associate

duction and analysis are well developed for other applications, so existing modal test facilities and methods can be utilized for NDE. Also, modern data acquisition systems allow the acquisition, processing, storage, and analysis of hundreds or thousands of channels of data. Since it is desirable to assess the condition of a structure in its operating environment, the ability to make modal measurements remotely and quickly minimizes the impact on the operation of the structure.

One particular method for detecting damage using optimal matrix update is called Minimum Rank Perturbation Theory (MRPT). This technique models the changes to the structure as rank-one updates of the mass, damping and stiffness matrices. This method was developed by Zimmerman and Kaouk [2], [3], [4], and has been used extensively for damage detection, primarily in truss structures. For examples of applications of this technique to NDE problems, see Zimmerman and Simmermacher [5], Zimmerman, et. al. [6], and Kim and Bartkowicz [7].

Another class of methods for FEM update which has been used for NDE is known as sensitivity-based matrix update. A sensitivity-based method which computes the sensitivity of the global structural mass and stiffness matrices at the structural element level has been developed by Hemez and Farhat [8], [9] and applied by Doebling, et. al. [10], [11]. Also, a method that was originally developed for control design, known as the eigenstructure assignment approach, has also been applied to NDE using modal test data. This technique has been applied to the damage detection problem by Zimmerman and Kaouk [12] and Lim and Kashangaki [13], [14], [15].

The above techniques share a common problem in that in some form they all require the correlation of modal vectors from one damage condition to another. This can sometimes lead to ambiguous results, especially when the damage causes very large changes in the modal vectors. The research described in this paper is attempting to avoid this problem through the use of the measured static flexibility matrix. By combining all of the measured modes, frequencies, and residual flexibility coefficients, it contains a complete set of data to describe the static behavior of the structure. Thus, there is no need to find a correspondence between the measured modes of different data sets, since all the modes are used in each case. The theoretical basis for this approach to measuring flexibility is presented in References [16] and [17].

In this paper, the dynamically measured static flexibility matrix is used with two different techniques to find damage in a stringer of a DC9 aircraft fuselage. In the first method, damage is indicated by changes in the point flexibility of the structure. Point flexibilities are the diagonal components of the flexibility matrix, and they are physically the deflection in a measured degree of freedom (DOF) due to a unit force at the same DOF. The second method uses an algebraic disassembly of the flexibility matrix along a presumed finite element connectivity pattern. Both of these techniques are shown to indicate the location of the damage in the aircraft fuselage structure.

This paper is organized into three additional sections. The theoretical development section explains how the measured flexibility matrix and the calculated residual flexibility are collected into a complete flexibility matrix. Then, the experimental configuration and procedures are explained, followed by a presentation and discussion of the results.

THEORETICAL DEVELOPMENT

Experimental Measurement of Static Flexibility

The flexibility matrix, $[G]$, relates the static displacement vector, $\{u\}$, of a structure to the static force loading vector, $\{F\}$, according to

$$\{u\} = [G]\{F\}. \tag{1}$$

For a restrained structure, the columns of $[G]$ represent the displacements of the structure under a static unit load applied at that column's DOF. For an unrestrained structure, the columns of $[G]$ are inertia relief modes of the structure due to a static unit load at the corresponding DOF.

Measuring the flexibility matrix using static test methods is impractical because of difficulties applying static loads under the proper boundary conditions. It has long been recognized that modal data can be used to form an approximation to the static flexibility using the measured modes. In this manner, $[G]$, may be approximated as,

$$[G] = [\Phi_n][\Lambda_n]^{-1}[\Phi_n]^T + [G_r] \tag{2}$$

where $[\Lambda_n]$ and $[\Phi_n]$ represent the measured eigenvalue and mass-normalized eigenvector matrices, respectively, and $[G_r]$ is the residual flexibility of modes outside the test set. In some situations, $[G_r]$ will be small. However, as shown in [16] and [17], this depends on the richness of the test set and also the subspace spanned by the input locations. When the residual flexibility is significant, References [16]

and [17] provide several methods for approximating $[G_r]$.

Damage Detection Using Measured Point Flexibilities

Once the complete flexibility matrix is approximated, the point flexibilities can be used to find damage locations. Point flexibilities are the diagonal of the flexibility matrix:

$$\{G_p\} = diag[G]. \tag{3}$$

Physically, point flexibilities are the static deflection in a measured DOF caused by a unit force input at the same DOF. Damage is located by a "softening" in the point flexibility of a DOF. This method is most applicable to plate-like structures with simple (i.e. localized) connectivity.

Damage Detection Using Disassembled Elemental Flexibilities

Another method for finding the damage in the aircraft is to use the algebraic disassembly of the flexibility matrix. A connectivity must be assumed to apply this method, and its success largely depends on the accuracy of that presumed connectivity. The flexibility matrix is disassembled using the algebraic direct disassembly formulation given in Reference [18]. In this approach, the following linear algebra problem is solved for unknown elemental stiffnesses:

$$\sum_{\beta=1}^{n} p_\beta(\{A_\alpha\}^T[G]\{A_\beta\}\{A_\beta\}^T[G]\{A_\alpha\}) = \{A_\alpha\}^T[G]\{A_\alpha\} \tag{4}$$

in which A_α are elemental stiffness eigenvectors corresponding to elemental stiffness parameters p_α. Damage is detected by averaging the disassembled p_α over individual elements and then compared before and after damage. Again, a "softening" of the averaged stiffness of an element indicates damage.

EXPERIMENTAL CONFIGURATION AND PROCEDURE

Test Article and Data Acquisition System

The forward fuselage of a DC9 aircraft was used as the test article for a series of induced damage tests on an actual structure. This test article contains many of the experimental uncertainties and nonlinearities seen in practical field modal testing (see Figure (1)). A Zonic LAZON system was used to acquire and process the test data for all tests. This system consisted of two major hardware components: an Ometron Scanning Laser Vibrometer and a Zonic Workstation 7000. The Workstation 7000 is a multichannel, real time, FFT-based analyzer and data acquisition system. The system also included the following software: Zonic A&D Engineering and Test Analysis (ZETA) and LSI. Zeta is a general data acquisition and real time analysis package. LSI is a user interface to ZETA written specifically for use with the scanning laser vibrometer.

The Workstation 7000 used three analog output channels. Channels one and two were used to drive the x and y position of the laser beam. Channel three provided a random output signal to drive a 50lb electrodynamic shaker. An accelerometer and load cell were place at the force input location to allow a driving-point Frequency Response Function to be measured. Three analog input channels were also used. The first channel acquired data from the load cell. The second acquired all driving-point accelerometer data. Redundant driving-point data sets were acquired for each laser scan point. The third input channel acquired all laser data.

The force was input to the skin of the DC9 fuselage through an aluminum pad and dental cement. The force was continuous, random excitation with a lower frequency bound of 50Hz and an upper frequency bound of 1250Hz. The maximum force inputs were 5 pounds or less. Data was acquired from a grid of 38 inches by 14 inches on a 1 inch spacing for a total of 585 measurement points. The laser head was positioned on a tripod at a working distance of 75 inches from the surface. The System 7000 calculated FRF's and coherence functions in real-time and saved these functions for detailed post-test analysis at a later time. A Hanning window was used in the band of 0-1250 Hz with 10 measurements ensembles and a block-size of 1024. The acquisition mode was continuous with a 50% overlap. The data acquisition took approximately 1.5 hours for a complete scan.

The laser scan area covered a stringer which had been previously cut, as shown in Figure (2). For the "undamaged" data collected in this paper, the stringer was "repaired" using metal plates as shown in Figure (3).

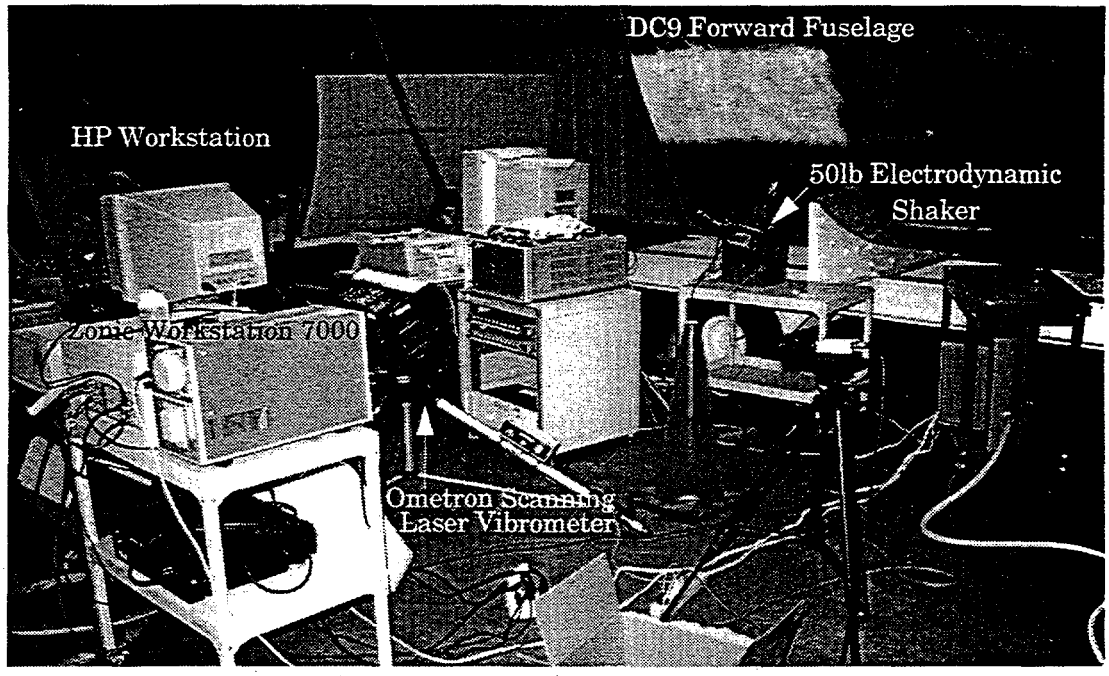

Figure 1. Photograph of DC9 Test Article and Data Acquisition System

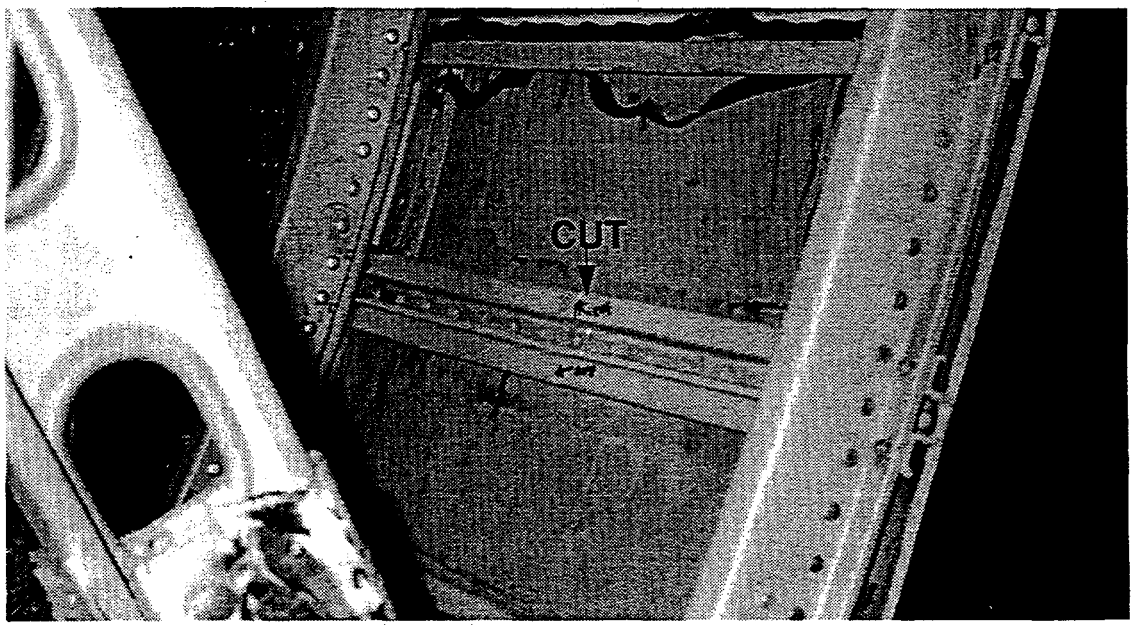

Figure 2. Photograph of Damaged Stringer

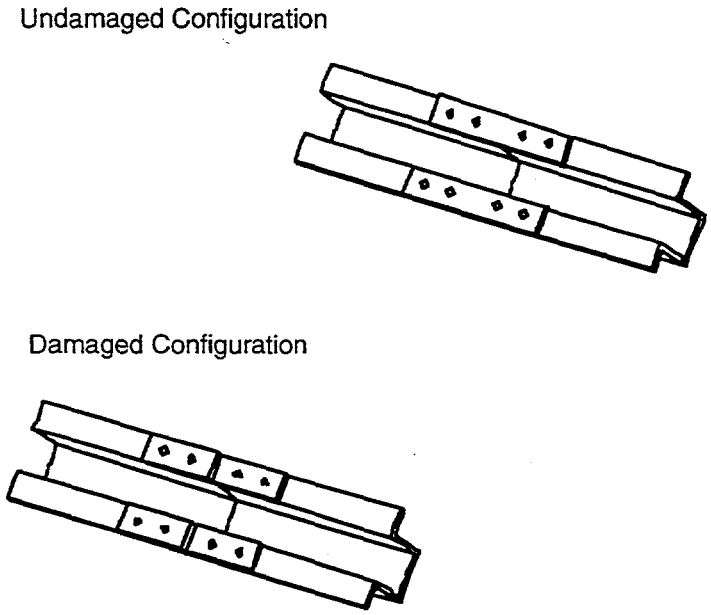

Figure 3. Repair of Previously Damaged Stringer to Simulate Damaged and Undamaged Configuration

RESULTS

Modal Analysis Procedure

The FRF's were estimated using IDEAS. The ERA/DC method of analysis was applied to a 23,400 x 500 Hankel matrix. Details of the particularly efficient algorithm used in this procedure can be found in Reference [19]. A frequency domain curve fit was performed on the data, as described in Reference [20]. The curve fit obtained for the undamaged driving point FRF is shown in Figure (4). The model includes approximately 80 modes, which means that the data is "over identified," meaning there are more modes identified than actually exist in the measured frequency spectrum. This was done to save time on modal identification, and to demonstrate the insensitivity of the measured flexibility matrix to spurious noise modes remaining in the modal set. Total modal analysis time was less than twenty minutes.

Damage Detection Using Point Flexibilities

The flexibility matrix was calculated from the data as explained above. In the first method examined in this research, damage was indicated by a local softening of the aircraft skin as measured by the point flexibilities. The damage is located on a horizontal stringer midway between two vertical frames. Figure (5) shows that the point flexibilities found the damaged area of the aircraft structure. Frames are located on the right and left sides and also down the middle of the test section. Stringers are located on the top, bottom, and middle of the test section. Notice that the reduced flexibility over the stringers and frames reflects the geometry of the structure. Also note that the skin between stringers and frames is much more flexible. The two plots on the right side of Figure (5) plot the point flexibility as a vertical displacement. In both figures, the vertical scale is the same, and the measurement DOF over the skin panels have been omitted for clarity.

Damage Detection Using Disassembled Elemental Flexibilities

In this approach, only nodes along the damaged stringer were used for the connectivity. Nineteen six piece spring elements were used (see Figure (6)). The damage is located at element ten. As shown in Figure (7), the element stiffness of element ten is much lower for the damaged case than for the undamaged case.

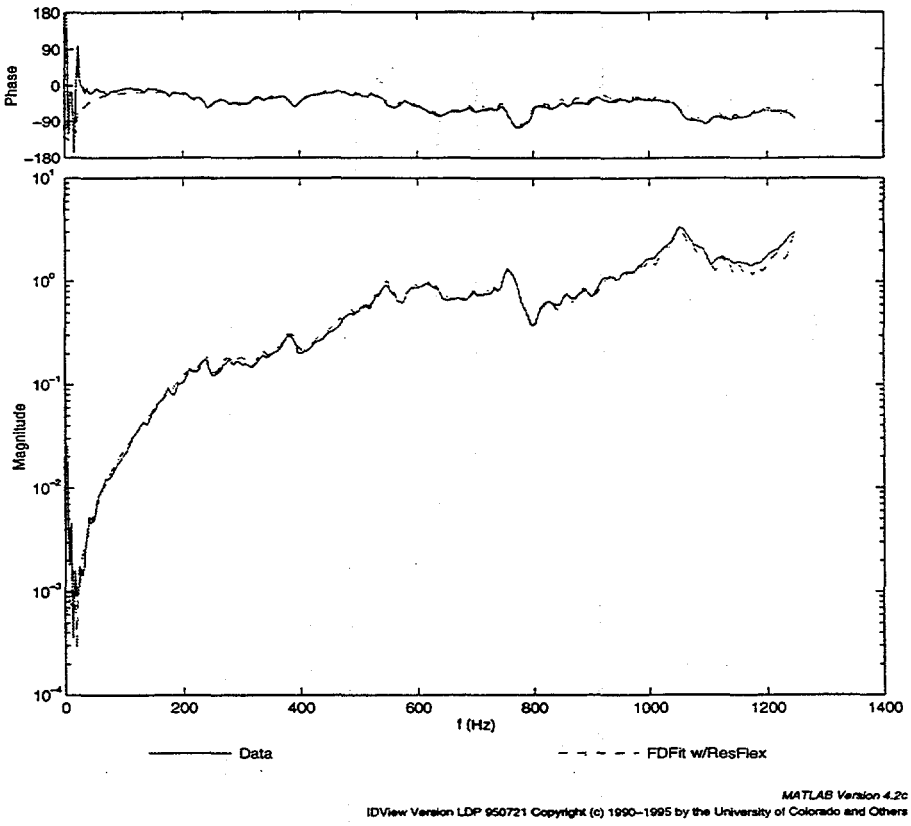

Figure 4. FRF for the Undamaged Driving Point Curve Fit

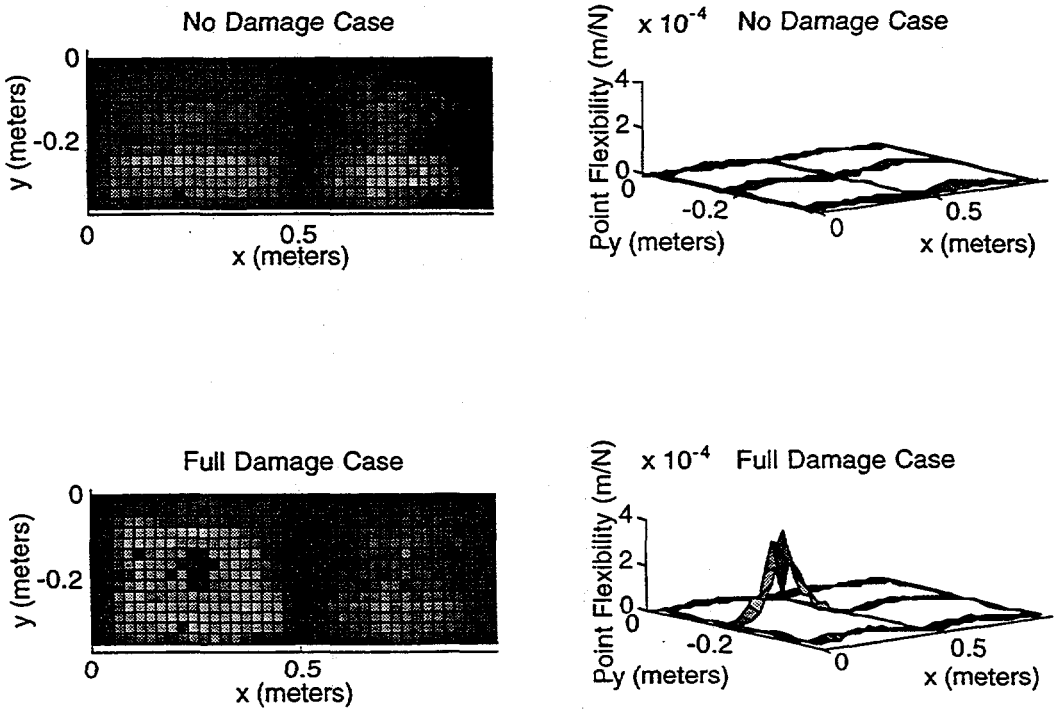

Figure 5. Point Flexibility Plots for Undamaged and Full Damaged Cases

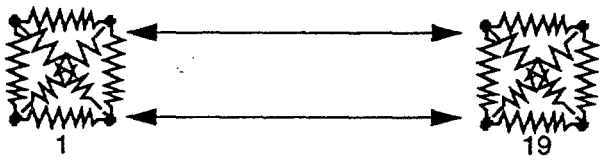

Figure 6. Six-Piece Spring Element Connectivity Distributed Along Damaged Stringer

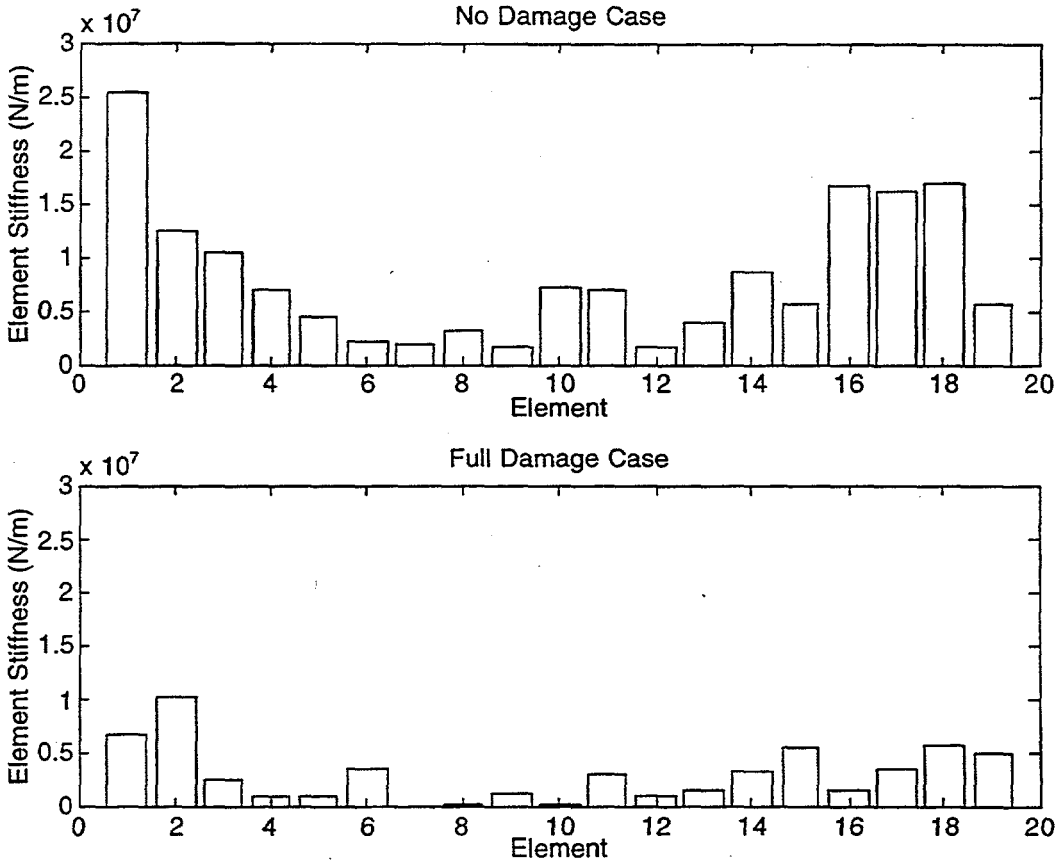

Figure 7. Element Stiffness Plot for Undamaged and Damaged Data

CONCLUSIONS

Two methods for damage detection in aircraft fuselages using modal test data have been introduced and experimentally applied. Both methods use the dynamically measured static flexibility matrix, which is assembled from a combination of measured modal vectors, frequencies, and driving point residual flexibilities. As a consequence, neither method requires a mode-to-mode correlation, and both avoid tedious modal discrimination and selection. This leads to a tremendous savings in modal analysis time, because semi-automated modal discrimination can be applied. Any remaining noisy or numerical modes apparently have little impact on the final flexibility matrix.

The first damage detection method detects damage as a softening in the point flexibility components, which are the diagonal entries in the flexibility matrix. The second method detects damage from the disassembled elemental stiffnesses as determined using a presumed connectivity. Vibration data from a laser vibrometer was used to apply these methods to a DC9 aircraft fuselage in which damage was artificially induced in a longitudinal stringer. In these results, the point flexibility method successfully and unambiguously locates the damaged stringer. The disassembly results are less successful. This is largely due to the

inadequacy of the presumed elemental connectivity used in applying the disassembly method, and because the measured flexibility is not statically complete.

ACKNOWLEDGMENTS

The authors would like to specifically acknowledge the invaluable perspective of Dr. Kenneth F. Alvin of Sandia National Laboratories. In addition, the authors are grateful for the contributions of Mr. Raul Meza, a graduate research assistant from the University of Texas at El Paso, for conducting all of the laser velocimetry tests. This research was sponsored at University of Colorado by Sandia National Laboratories under contract AJ-4223. It was also sponsored by the United States Department of Energy under Contract DE-AC04-94AL85000.

REFERENCES

[1] Witherell, C.E., *Mechanical Failure Avoidance: Strategies and Techniques*, McGraw-Hill, New York, 1994.

[2] Zimmerman, D.C. and Kaouk, M., "Structural Damage Detection Using A Subspace Rotation Algorithm," AIAA-92-2521-CP, Proceedings of the 33rd Structures, Structural Dynamics and Materials Conference, Dallas, TX, April 1992.

[3] Kaouk, M. and Zimmerman, D.C., "Structural Damage Assessment Using a Generalized Minimum Rank Perturbation Theory," AIAA-93-1483-CP, Proceedings of the 34th Structures, Structural Dynamics and Materials Conference, La Jolla, CA, April 1993.

[4] Kaouk, M. and Zimmerman, D.C., "Evaluation of the Minimum Rank Update in Damage Detection: An Experimental Study," Proceedings of the 11th International Modal Analysis Conference, Orlando, FL, February 1993.

[5] Zimmerman, D.C. and Simmermacher, T., "Model Refinement and System Health Monitoring Using Data From Multiple Static Loads and Vibration Tests," AIAA-94-1714-CP, Proceedings of the 35th Structures, Structural Dynamics and Materials Conference, April 1994.

[6] Zimmerman, D.C., Smith, S.W., Kim, H.M., and Bartkowicz, T.J., "An Experimental Study of Structural Damage Detection Using Incomplete Measurements," AIAA-94-1712-CP, Proceedings of the 35th Structures, Structural Dynamics and Materials Conference, April 1994.

[7] Kim, H.M. and Bartkowicz, T.J.,"Damage Detection and Health Monitoring of Large Space Structures," AIAA-93-1705-CP, Proceedings of the 34th Structures, Structural Dynamics and Materials Conference, La Jolla, CA, April 1993.

[8] Hemez, F.M., *Theoretical and Experimental Correlation Between Finite Element Models and Modal Tests in the Context of Large Space Structures*, Ph. D. Dissertation, University of Colorado, Boulder, CO, 1993.

[9] Farhat, C. and Hemez, F.M., "Updating Finite Element Dynamic Models Using an Element-by-Element Sensitivity Methodology," AIAA Journal, Vol. 31, No. 9, September 1993.

[10] Doebling, S.W., Hemez, F.M., Barlow, M.S., Peterson, L.D., and Farhat, C., "Damage Detection in a Suspended Scale Model Truss via Modal Update," Proceedings of the 11th International Modal Analysis Conference, Orlando, FL, February 1993.

[11] Doebling, S.W., Hemez, F.M., Barlow, M.S., Peterson, L.D., and Farhat, C., "Selection of Experimental Modal Data Sets for Damage Detection via Model Update," AIAA-93-1481-CP, Proceedings of the 34th Structures, Structural Dynamics and Materials Conference, La Jolla, CA, April 1993.

[12] Zimmerman, D.C. and Kaouk, M., "Eigenstructure Assignment Approach for Structural Damage Detection," AIAA Journal, Vol. 30, No. 7, July 1992.

[13] Lim, T.W., "Structural Damage Detection of a Planar Truss Structure Using a Constrained Eigenstructure Assignment," AIAA-94-1715-CP, Proceedings of the 35th Structures, Structural Dynamics and Materials Conference, April 1994.

[14] Lim, T.W. and Kashangaki, T. A.-L., "Structural Damage Detection of Space Truss Structures Using Best Achievable Eigenvectors," AIAA Journal, Vol. 32, No. 5, May 1994, pp. 1049-1057.

[15] Kashangaki, T. A.-L., *Damage Location and Model Refinement for Large Flexible Space*

Structures Using a Sensitivity Based Eigenstructure Assignment Method, Ph. D. Dissertation, University of Michigan, Ann Arbor, MI, 1992.

[16] Doebling, S.W., Peterson, L.D., and Alvin, K.F., "Measurement of Static Flexibility Matrices for Experiments with Incomplete Reciprocity," Proceedings of the 36th AIAA/ASME/ASCE/AHS/ASC Structures, Structural Dynamics and Materials Conference, April, 1995, AIAA-95-1092.

[17] Doebling, S.W., "Measurements of Structural Flexibility Matrices for Experiments with Incomplete Reciprocity," CU-CAS-95-10, Center for Aerospace Structures, University of Colorado, Boulder, Colorado, April, 1995.

[18] Peterson, L.D., Alvin, K.F., Doebling, S.W., "Experimental Determination of Local Structural Stiffness by Disassembly of Measured Stiffness Matrices", AIAA-95-1090-CP, Proceedings of the 36th Structures, Structural Dynamics and Materials Conference, New Orleans, LA, April 1995.

[19] Peterson, L.D. "Efficient Computation of the Eigensystem Realization Algorithm" *J. Guidance, Control and Dynamics*, Vol. 18, No. 3, May-June 1995, pp 395-403.

[20] Peterson, L.D. and Alvin, K.F., "A Time and Frequency Domain Procedure for Identification of Structural Dynamic Models" AIAA-CP-94-1731 Proceedings of the *35th AIAA/ASME/ASCE/AHS/ASC Structures, Structural Dynamics and Materials Conference*, Hilton Head, April 1994.

Intentionally Left Blank

APPENDIX O

HEALTH MONITORING STUDIES ON COMPOSITE STRUCTURES FOR AEROSPACE APPLICATIONS

George James, Bruce Hansche, Raul Meza, and Nikki Robinson

Proceedings of the 5th ASCE International Conference on Engineering, Construction, and Operations in Space - SPACE '96
Albuquerque, NM

June 1-6, 1996

Intentionally Left Blank

Health Monitoring Studies on Composite Structures for Aerospace Applications

George James, Dennis Roach, Bruce Hansche, Raul Meza, Nikki Robinson
Sandia National Laboratories
Albuquerque, NM 87185-0557

Abstract

This paper discusses ongoing work to develop structural health monitoring techniques for composite aerospace structures such as aircraft control surfaces, fuselage sections or repairs, and reusable launch vehicle fuel tanks. The overall project is divided into four tasks: operational evaluation, diagnostic measurements, information condensation, and damage detection. Five composite plates were constructed to study delaminations, disbonds, and fluid retention issues as the initial step in creating an operational system. These four square feet plates were graphite-epoxy with nomex honeycomb cores. The diagnostic measurements are composed of modal tests with a scanning laser vibrometer at over 500 scan points per plate covering the frequency range up to 2000 Hz. This data has been reduced into experimental dynamics matrices using a generic software package developed at the University of Colorado at Boulder. The continuing effort will entail performing a series of damage identification studies to detect, localize, and determine the extent of the damage. This work is providing understanding and algorithm development for a global NDE technique for composite aerospace structures.

Introduction

Composite materials are used in a variety of aerospace applications including aircraft control surfaces, fuselage sections and repairs, and reusable launch vehicle fuel tanks. Composite structures offer numerous advantages over metallic structures including light weight, high strength, corrosion resistance, elimination of rivets, and time savings in installation. While composite structures are used extensively in military applications, their use in commercial aviation has encountered design difficulties associated with application, subsequent inspection, and long-term endurance. Also, it has been generally accepted that composite fuel tanks will be a critical element in the development of reusable launch vehicles, however rapid and reliable field-inspection techniques will be required to verify the flight status of these structures. This determination of the current state of health and/or assurance of installation requires that flaws such as disbonds, interply delaminations, fluid ingress, and adhesive failure must be located and evaluated. Because of the increasing use of composites on commercial aircraft and the potential economic impact of reusable launch systems, it appears that the demand for composite health monitoring techniques will increase.

Most composite inspections are performed with the human eye or using the non-scientific tap test. Inconsistencies in these inspection results have prompted industry to look at more advanced NonDestructive Inspection (NDI) techniques. Also, the desire to revolutionize the efficiency of these inspections has driven the recent work to develop wide area or global inspection techniques which can rapidly monitor large structures in the field. Structural dynamics provides a well understood and global set of properties to utilize in such a development. The field of Structural Health Monitoring utilizes structural dynamics properties to inspect, monitor, and assess operational structures for continued service. Development work is being performed in four areas: operational evaluation, diagnostic measurements, information condensation, and damage identification. The current status of this work and its specific application to a set of composite test articles will be the subject of this paper.

Operational Evaluation

Operational Evaluation is the process of evaluating the expected damage types, determining realistic accumulation models, and developing the appropriate test procedures for the operational structure and its environment throughout the service life. Engineered-flaw specimens, resonant fatigue testing, and ambient excitation testing have been the major developments for this aspect of the work. Only engineered-flaw specimens have been used to date in the work reported herein. Final application of structural health monitoring to structures in the will require damage accumulation studies from fatigue tests and operational evaluation tools such as ambient exciation testing.

For this work, a series of five plates have been designed and built with a series of flaws engineered into the construction. The effects of these flaws can then be studied by comparing the response of different plates. The plates are 24 inches by 24 inches constructed of a .5 inch thick Nomex honeycomb core sandwiched between four ply T300 plain weave graphite cloth panels. The graphite lay-up is [-45,0,90,45]. A layer of hysol film adhesive bonds the graphite panels to the honeycomb core. Plate #1 has no engineered flaw and is considered the undamaged specimen. Plate #2 has a four inch diameter disbond (created with a teflon disk) in the geometric center of one graphite panel. Plate #3 has a four inch diameter region of the honeycomb core (located in the geometric center of the plate) filled with fluid. The individual honeycomb cells surrounding the fluid are potted to contain it. Plate #4 uses a teflon insert to produce a four inch diameter delamination between plies 2 and 3 at the geometric center of one graphite panel. Plate #5 contains two of the four inch diameter disbonds located at the geometric centers of opposing quadrants of a graphite panel. A four inch diameter delamination, and a four inch diameter fluid ingress section are at the geometric centers of the two remaining quadrants. Figure 1 shows a schematic for plate #2. Initial results from this plate will be shown in a later section. These three types of flaws in the plates represent common flaws seen in composite aerospace structures.

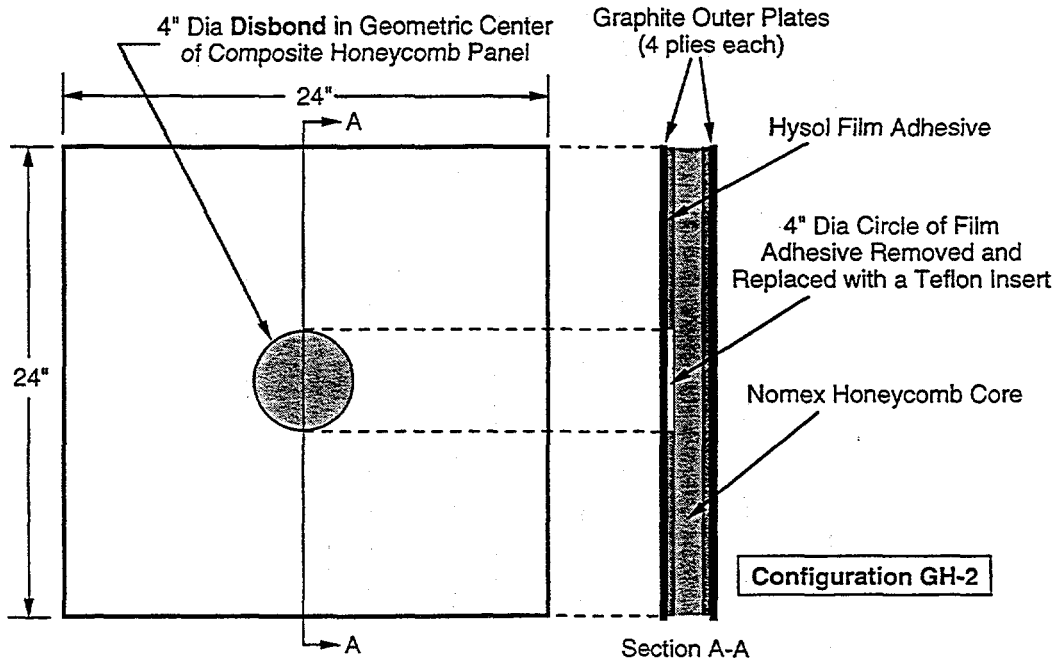

Figure 1. Plate #2 with Four Inch Diameter Disbond in Center

Diagnostic Measurements

Diagnostic Measurements which can monitor large areas (from several to hundreds of square feet) on realistic structures (such as aircraft fuselages) with a large number of measurement points (up to 2000) over a large frequency band (up to 2000 Hz) are required for performing structural health monitoring via dynamics. Non-contact techniques such as scanning laser vibrometry and laser holography have been used to perform these functions. Zonic A&D's LAZON system was used as the data acquisition system for the diagnostic measurements discussed in this work. This system consists of two major hardware components: an Ometron Scanning Laser vibrometer and a Zonic Workstation 7000. The Workstation 7000 is a multichannel, real time, FFT-based analyzer and data acquisition system. The System 7000 uses three analog output channels. Channels one and two are used to drive the horizontal and vertical positions of the laser beam. Channel three provided a random output signal to drive a Wilcoxin hybrid piezoelectric/electro-mechanical shaker. Force was input to the panel via an acrylic stinger, a 5 lb load cell, an aluminum pad, dental cement, and aluminum tape. Three analog input channels were also used on the Workstation

7000. The first channel acquired information from the load cell. The second channel acquired information from a driving point accelerometer. And the third channel acquired all velocity data from the vibrometer.

A measurement grid of 23 by 23 scan points (529 total points) on one inch centers and a .5 inch border was used on the plate. The scanning vibrometer allows an order of magnitude increase in the number of measurement points over traditional discrete sensors with a marked decrease in set-up time. This makes it a unique device for obtaining high density (both spatial and frequency) measurements for structural health monitoring applications. A velocity over force Frequency Response Function (FRF) and the associated coherence function were calculated and saved for each scan point. The data set discussed herein utilized a bandwidth of 0-2500 Hz which is much broader than is typically acquired by traditional accelerometers. A block size of 1024 with 10 averages and 50% overlap were used for FRF calculations. The data acquisition for each plate takes about 1.5 hours. Figure 2a provides a photograph of the test setup used for the composite plates as seen from the side. The plate is seen suspended in a free-free fashion and covered with white dye penetrant to enhance the laser reflectivity. The shaker and stinger are also seen. Figure 2b shows the same configuration as seen from the rear. The scanning laser vibrometer is seen facing the plate.

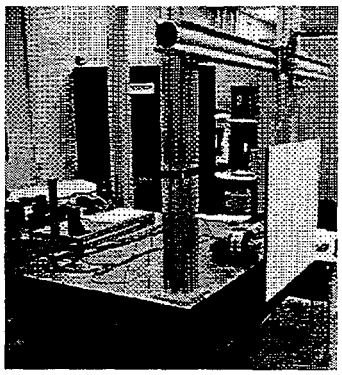

Figure 2a. Experimental Configuration for Composite Plates (Side View)

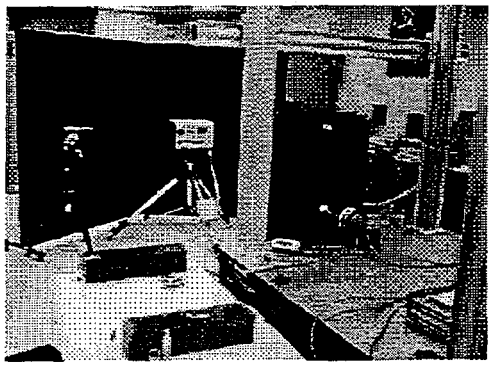

Figure 2b. Experimental Configuration for Composite Plates (Rear View)

Information Condensation

The amount of data which is generated from 530 measurement points (counting the driving point accelerometer) in the range of 0 to 2500 Hz with up to 100 significant modes is staggering when conventional processing techniques are applied. Therefore, more automated and robust techniques are needed to process the data and provide the necessary parameters to perform damage identification. Also, techniques which use mode-to-mode comparisons for damage identification are not inherently automatable. Hence, numerical manipulations which combine all the modal information are most useful. One such manipulation entails collecting the modal information into experimental dynamics matrices (mass, damping, and stiffness matrices) [1,2]. These entities combine the modal information into a form which is amenable to more detailed analyses by damage identification algorithms as will be mentioned in the next section. The data is currently being processed into such forms.

Another class of mathematical entities have proven extremely useful for rapid visualization of changes due to damage and have been applied to this data set. Flexibility shapes are a linear combination of all modes in the data and are more robust and sensitive to the damage than individual mode shapes [3]. This idea has been expanded to create a full flexibility matrix [4] which is an inverse of the stiffness matrix. Such an approach provides a robust reduction of the data which maintains the local shape information in a frequency-independent form. Hence mode-to-mode comparisons before and after damage are not required. Also, the system can be "over-identified" meaning that such anomalies as split modes, noise modes, or false modes due to nonlinearities have much less effect on the final data form [5]. Hence, the procedure becomes much more automatable. This processing has been completed for the plate data and is discussed next.

Figure 3a shows the diagonal values of the flexibility matrix (called driving-point flexibilities) for plate #1 (undamaged) plotted as a mesh (z axis) over the geometric location (x and y axis) on the plate. Physically, these values represent the displacement which would result for a unit force at each scan location. This is an enlightening and rapid method for visualizing the information available in the flexibility matrix. The processing needed to obtain this plot was approximately 20 minutes. In general, the flexibilities of the plate are uniform. Figure 3b shows the driving point flexibilities for plate #2 (disbond). The plate is seen to be much more flexible than plate #1. However, specific location of the damage is not available with this level of processing. The asymmetric nature of the response is due to boundary condition effects, specifically the stiffening which results from the stinger attachment. It should be noted that these plots represent only the diagonal values of the flexibility matrix. Much more information is available on the off-diagonal terms which relate displacement at each scan point to a unit input force at another scan point. Part of the on-going work is to interpret the entire flexibility matrix and will be mentioned in the next section.

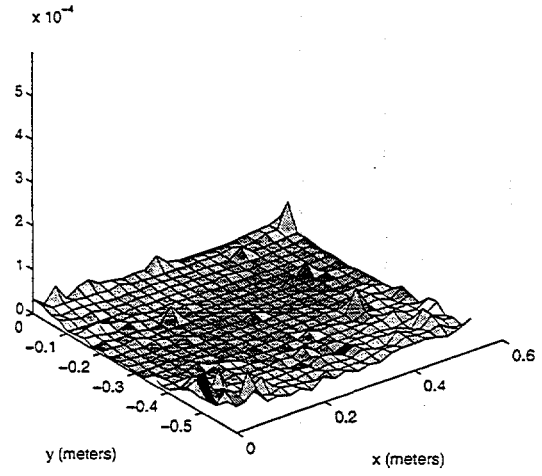

Figure 3a. Driving-Point Flexibilities for Plate #1 (Undamaged)

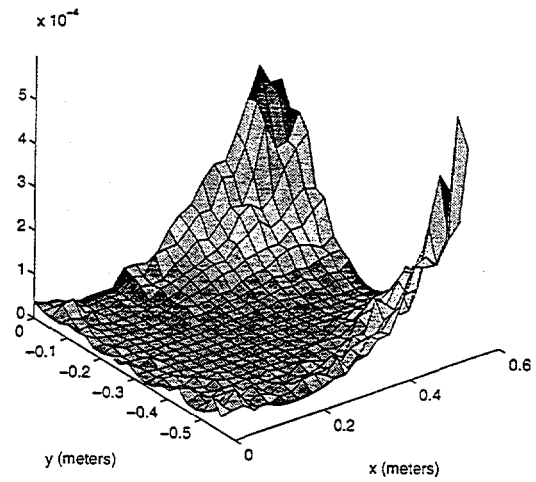

Figure 3b. Driving-Point Flexibilites for Plate #2 (Disbond in Center)

The driving-point flexibilites for the plate #3 (fluid-filled section) show a change in the flexibility when compared to plate #1. Since the mass properties changed, the mode shapes (and the reconstructed flexibility matrix) which changed as well. The driving-point flexibilities for plate #4 (delamination) shows the least change from plate #1. This suggests that the delamination flaw provides less of an impact on the stiffness properties of the plate than the disbond (at least in the frequency band measured). It could be expected that this flaw would provide a greater effect on some of the higher modes. In fact, it is presumed that the detached section of the outer plies should have a local resonance. The driving-point flexibilities for plate #5 (all damage cases) show flexibility changes that are not as great as with plate #2. However, the center of this plate is intact as opposed to plate #2. Hence, location of the flaw has an impact on the results at this level of processing. Both plate #3 and plate #5 contain a fluid filled section and both show an increase in the magnitude of the flexibility values at the corner nearest the driving point. This is opposite of what is seen in the other three plates. This suggests that mass property changes may contain a unique signature. Again, it must be noted that this is only the initial cursory survey of the data. More advanced processing is required to determine specific information about the different flaw scenarios. This processing is underway and will be discussed in the next section.

Damage Identification

Damage Identification is the process of operating on the experimental data reduced using techniques described in the previous section to detect, localize, and calculate the extent of the damage. Current work is underway to disassemble the stiffness (or flexibility) matrix to determine localized stiffness parameters. The magnitudes of these parameters will then be compared before and after damage [6]. This takes into account all off-diagonal terms which were ignored in the previous driving-point flexibility analysis. Other damage detection techniques which are under consideration

include the Minimum Rank Perturbation Theory (MRPT) [7], Structural Translation and Rotation Error CHecking (STRECH) [3], or Strain Energy Comparisons [8].

Conclusions

The development of a structural health monitoring capability using dynamics involves four tasks: operational evaluation, diagnostic measurement, information condensation, and damage identification. This process has begun for composite aerospace structures. The initial work in operational evaluation has centered around the creation of five composite plates with engineered flaws. Diagnostic measurements using a scanning laser vibrometer have been performed using 529 scan points and a frequency range of 0 to 2000 Hz. This information has been condensed into experimental flexibility matrices. An initial study of the flexibility shapes reveals detectable changes in the plates for disbonds and fluid retention. Continuation of this work will use damage identification techniques to obtain more quantitative information on the existence, location and extent of damage. Follow-on work will use accelerated tests such as resonant fatigue testing to study damage accumulation followed by development of field testing procedures.

Acknowledgments

Two individuals are providing much insight and direction to this work: Professor Roberto Osegueda of the Civil Engineering Department at the University of Texas at El Paso and Professor Lee Peterson of the Aerospace Sciences Department at the University of Colorado at Boulder. These individuals are thesis advisors for the fourth and fifth authors and are having a significant impact on this work. This work has been supported by the United States Department of Energy under contract DE-AC04-94AL85000.

References

1. K.F. Alvin, "Second-Order Structural Identification via State Space-Based System Realizations", CU-CSSC-93-09, Ph.D. Dissertation, Aerospace Engineering Sciences, University of Colorado at Boulder, Boulder, CO, April, 1993.

2. G.H. James, T.G. Carne, B.D. Hansche, R.L. Mayes, G.M. Reese, and T.W. Simmermacher, "Health Monitoring of Operational Structures - Initial Results", Proceedings of the 1995 Adaptive Structures Conference, New Orleans, LA, April 13-14, 1995.

3. R.L. Mayes, "An Experimental Algorithm for Detecting Damage Applied to the I-40 Bridge Over the Rio Grande", Proceedings of the 13th International Modal Analysis Conference, Nashville, TN, January 31, 1995.

4. S.W. Doebling, "Measurement of Structural Flexibility Matrices for Experiments with Incomplete Reciprocity", CU-CAS-95-10, Ph.D. Dissertation, Aerospace Engineering Sciences, University of Colorado at Boulder, Boulder, CO, April, 1995.

5. N.A. Robinson, L.D. Peterson, G.H. James, and S.W. Doebling, "Damage Detection in Aircraft Structures Using Static Flexibility Matrices", Proceedings of the 14th International Modal Analysis Conference, Dearborn, MI, February 12-14, 1996.

6. L.D. Peterson, K.F. Alvin, and S.W. Doebling, "Experimental Determination of Local Structural Stiffness by Disassembly of Measured Stiffness Matrices", Proceedings of the 36th SDM Conference, New Orleans, LA, April, 1995.

7. M. Kaouk and D.C. Zimmerman, "Structural Damage Assessment Using a Generalized Minimum Rank Perturbation Theory", Proceedings of the 34th SDM Conference, La Jolla, CA, April, 1993.

8. C.J. Carrasco, "Damage Detection in Beams using Modal Energy Estimates", M.S. Thesis, Civil Engineering Department, The University of Texas at El Paso, El Paso, TX, May, 1992.

Intentionally Left Blank

Distribution:

5 Chuck Farrar and Staff
MS P946
Los Alamos National Laboratory
PO Box 1663
Los Alamos, NM 87545

1 Walt Musial
Wind Technology Division
National Renewable Energy Laboratory
1617 Cole Boulevard
Golden, CO 80401-3393

1 K.C. Park
Center for Aerospace Structures
Department of Aerospace Engineering Sciences
University of Colorado at Boulder
Boulder, CO 80309-0429

1 Lee Peterson
Center for Aerospace Structures and
Department of Aerospace Engineering Sciences
University of Colorado at Boulder
Boulder, CO 80309-0429

1 Nikki Robinson
Center for Aerospace Structures and
Department of Aerospace Engineering Sciences
University of Colorado at Boulder
Boulder, CO 80309-0429

1 David Zimmerman
Department of Mechanical Engineering
University of Houston
Houston, TX 77204-4792

1 Todd Simmermacher
Department of Mechanical Engineering
University of Houston
Houston, TX 77204-4792

Distribution (cont.):

1 Robert West
Dept. of Mechanical Engineering
VPI&SU
Blacksburg, Virginia 24061-0238

1 Roberto Osegueda
Department of Civil Engineering
University of Texas at El Paso
El Paso, TX 79968-0516

1 Raul Meza, Jr.
Department of Civil Engineering
University of Texas at El Paso
El Paso, TX 79968-0516

1 Kenneth R. White
Department of Civil, Agricultural, and Geological Engineering
Dept. 3CE
New Mexico State University
P.O. Box 30001
Las Cruces, NM 88003-0001

1 Norris Stubbs
Department of Civil Engineering
Texas A&M University
College Station, TX 77843-3136

1 David Allen
Department of Aerospace Engineering
Texas A&M University
College Station, TX 77843-3141

1 John Junkins
Department of Aerospace Engineering
Texas A&M University
College Station, TX 77843-3141

1 Ephrahim Garcia
Vanderbilt University
Department of Mechanical Engineering
Box 4, Station B
Nashville, TN 37235

Distribution (cont.):

1 Wiede Cutshall
Mechanical and Fluids Engineering Division
Southwest Research Institute
P.O. Drawer 28510
San Antonio, TX 78228-0510

1 Hyoung-Man Kim
McDonnell Douglas Aerospace
M/S: MDC-2-3353
13100 Space Center Blvd.
Houston, TX 77059

1 Ted Bartkowicz
McDonnell Douglas Aerospace
M/S: MDC-2-3353
13100 Space Center Blvd.
Houston, TX 77059

1 Chris Doktor
McDonnell Douglas Aerospace
M/S: MDC-2-3353
13100 Space Center Blvd.
Houston, TX 77059

1 Edward White
McDonnell Douglas Aerospace
Mailcode: 1021310
P.O. Box 516
St. Louis, MO 63166-0516

1 Lisa Emery
Lockheed Martin
MS 4300
P.O. Box 29304
New Orleans, LO 70189

1 Charles R. Larson
Rockwell-Space Systems Division
Mail Stop AD88
12214 Lakewood Blvd.
Downey, CA 90241

Distribution (cont.):

1 Chuck Wilkerson
NASA-MSFC
Mail Code: EH13
Huntsville, Alabama 35812

1 Michael Grygier
NASA-JSC
Mail Code: ES43
Houston, TX 77058

1 Dimitris A. Saravanos
Ohio Aerospace Institute
c/o Structures Division
NASA Lewis Research Center
M/S 49-8
21000 Brookpark Road
Cleveland, OH 44135

1 Mike Fisher
Code 8220.1
Naval Research Laboratory
Washington, D.C. 20375-5355

1 Charles E. Smith
Minerals Management Service
Technology Assessment and Research Branch
381 Eldon Street
MS 4700
Herndon, Virginia 22070-4817

1 Brian Hornbeck
Department of the Army
Mobility Technology Center - Belvoir
ATTN: AMSTA-RBBC (B. Hornbeck)
10115 Gridley Rd.
Suite 128
Ft. Belvoir, VA 22060-5843

1 Sreenivas Alampalli
New York Department of Transportation
1220 Washington Ave.
Albany, NY 12232

Distribution (cont.):

1 Benjamin Bell
FloWind Corporation
990 A Street
Suite 300
San Rafael, CA 94901

1 John Webster
Holographics, Inc.
4401-11th St.
Long Island City, NY 11101

1 Tim Hasselman
ACTA
23430 Hawthorne Blvd.,
Suite 300
Torrence, CA 90505-4723

1 Greg B. Hale
Ride & Show Engineering
Walt Disney World, Co.
P.O. Box 10,000
Lake Buena Vista, Florida 32830

1 Ward Turner
c/o EPRCO
P.O. Box 2189
Houston, TX 77252-2189

1 Brad Campbell
c/o EPRCO
P.O. Box 2189
Houston, TX 77252-2189

1 Dan Dolan
PMB Engineering, Inc.
500 Sansome Street
San Francisco, CA 94111

1 Denby Grey Morrison
Ocean R&D Department
Shell Development Co.
P.O. Box 481
Houston, TX 77001

Distribution (cont.):

1	0457	H.W. Schmitt, 2000
1	1436	LDRD office, 4523
1	0766	D.E. Ellis, 5500
1	0767	S.C. Roehrig, 5504
1	0706	D.A. Northrop, 6112 (see Appendix K)
1	1322	L.D. Hurtado, 6121
5	0708	H.M. Dodd, 6214 for 6214 library
1	0708	T.D. Ashwill, 6214
1	0708	H.J. Sutherland, 6214
1	0708	P.S. Veers, 6214
1	0151	G. Yonas, 9000
1	0828	E. Gorham, 9104 (see Appendix K)
1	0437	C. Lo, 9118
18	0439	D.R. Martinez, 9234 and staff
1	0507	K.G. McCaughey, 9700
1	0555	R.A. May, 9706
1	1392	V. Gabbard, 9719
1	0555	D.B. Davis, 9732
1	0865	J.L. Moya, 9735
1	0557	J.S. Cap, 9735
1	0557	W.N. Dunn, 9735
1	0557	D.O. Smallwood, 9735
20	0557	T.J. Baca, 9741 and staff
50	0557	G.H. James, 9741
1	0557	T.M. Rice, 9741
1	0557	MSD-1.30, 9741
1	0555	M.S. Garrett, 9742
1	0555	D.L. Gregory, 9742
1	0555	B.D. Hansche, 9742
1	0555	M.E.F. Shields, 9742
5	0615	W.W. Shurtleff, 9752 for 9752 library
1	0615	A.G. Beattie, 9752
1	0615	J.H. Gieske, 9752
1	0615	D.P. Roach, 9752
1	0615	M.T. Valley, 9752
1	1135	J.R. Garcia, 9761
1	9103	D. Andaleon, 8111
1	9018	Central Technical Files, 8523-2
5	0899	Technical Library, 4414
1	0619	Print Media, 12615
2	0100	Document Processing, 7613-2 for DOE/OSTI